

# **Hemodynamic Monitor for Rapid, Cost-effective Assessment of Peripheral Vascular Function**



**By: Elham Shabani Varaki**

**Supervisor: A/Prof. Paul Breen**

**Co-supervisor: Dr. Gaetano Gargiulo**

*A thesis submitted in fulfilment of the requirements for the degree of Doctor of Philosophy*

Biomedical Engineering and Neuromorphic Systems (BENS)  
The MARCS Institute for Brain, Behaviour and Development  
Western Sydney University

2019

## **Statement of Authentication**

The work presented in this thesis is, to the best of my knowledge and belief, original except as acknowledged in the text. I hereby declare that I have not submitted this material, either in full or in part, for a degree at this or any other institution.

(Elham Shabani Varaki)



*Dedicated to my parents, and Hossein*

## **Acknowledgements**

First and foremost, thanks to God for the endless graces and blessings. I am truly grateful for giving me the power to believe in my passion and the strength to pursue my dream especially during the challenging moments in completing this thesis. I cannot thank you enough for your exceptional love during this entire journey.

I would like to express immeasurable and deepest gratitude to my supervisor, A/Prof. Paul Breen for his kindness, patience, guidance, tireless support, encouragement, valuable suggestions and constructive criticisms during this journey. It has been a privilege to be Paul's student and I am indebted to Paul for sharing his knowledge and wisdom. I would like to sincerely thank my co-supervisor Dr. Gaetano Gargiulo for his kindness, extensive support, streams of ideas and encouragement to pursue my research goals. I have been extremely lucky for the opportunity to study under supervision of Paul and Gaetano who both cared so much about my work.

I wish to express my gratitude to Professor André van Schaik and Professor Kate Stevens for their support and encouragement. It has been an honour to be a member of BENS and study at The MARCS Institute.

Special thanks to Mr. Colin Symons and Mr. Grahame Andrews for their technical help. I also would like to thank the members of BENS group who all made my time so enjoyable at The MARCS Institute in Western Sydney University.

Words cannot express how grateful I am to my family. My deepest gratitude to my beloved parents, Tahereh and Bakhtiar, and my siblings, Kosar and Yasin for their endless love, care, support, helpful suggestions, encouragement and prayers. I am extremely grateful to my father and mother in law, Mahdi and Farahnaz, and my sister and brother in law, Elham and Hojat for their never-ending love, encouragement and prayers. My heartfelt gratitude to my loving husband, Hossein, whose unwavering love, support, encouragement and wisdom inspired me to see this light of day. Thanks for never stopping to believe in me.

## **Abstract**

Worldwide, at least 200 million people are affected by peripheral vascular diseases (PVDs), including peripheral arterial disease (PAD), chronic venous insufficiency (CVI) and deep vein thrombosis (DVT). These diseases have considerable socioeconomic impacts due to their high prevalence, cost of investigation, treatment and their effects on quality of life. PVDs are often undiagnosed with up to 60% of patients with PVD remaining asymptomatic. Early diagnosis is essential for effective treatment and reducing socioeconomic costs, particularly in patients with diabetes where early endovascular treatment can prevent lower extremity amputation. However, available diagnostic methods simply do not meet the needs of clinicians. For example, duplex ultrasound or plethysmography are time-consuming methods, costly and require access to highly trained clinicians. Due to the cost and time requirements of such methods, they are often reserved for symptomatic patients. On the other hand, the Ankle Brachial Index (ABI) test is cheap but has poor sensitivity for those patients with diabetes and the elderly, both growing high-risk populations.

There is an urgent need for new diagnostic tools to enable earlier intervention. Researchers at the MARCS Institute have developed a novel hemodynamic monitor platform named HeMo, specifically for the assessment of peripheral blood flow in the leg. This development aimed to provide a fast and low-cost diagnosis of both peripheral arterial disease and chronic venous insufficiency.

This work first provides a comprehensive literature review of the existing non-invasive diagnostic devices developed since 1677 to highlight the need of development of a new blood monitoring tool. Second, it presents the simplified circuit of the HeMo device and provides series of pilot experiments with HeMo demonstrating its potential for diagnosis of both peripheral arterial disease and chronic venous insufficiency. Third, it presents a quantitative

characterisation of the electrical behaviour of the electro-resistive band sensors with the development of an expansion/contraction simulator rig and using spectral analysis. The characterisation of the electro-resistive band was essential to understand the nonlinear electrical behaviour of such sensors and would be of interest for other users and uses of the electro-resistive band sensors. However, in another perspective this sinusoidal linear stretching movement and the presented method shows an example for the application of the presented rig, highlighting that the same technique could be used for characterisation of similar stretchable sensors. Fourth, it shows data from a healthy population, assessing the performance of HeMo compared to light reflection rheography (LRR sensor-VasoScreen 5000) for the assessment of venous function. Fifth, it presents human study data where the performance of HeMo is compared to photoplethysmography (PPG sensor-VasoScreen 5000) for the evaluation of the arterial function. Overall, the presented work here, steps toward development of the final version of a novel hemodynamic monitoring device, and its validation.

# Table of Contents

Table of Contents.....	vi
List of Figures.....	ix
List of Tables.....	xv
List of Abbreviations.....	xvii
Chapter 1 Introduction.....	1
1.1 Literature Review.....	2
1.1.1 Peripheral Vascular Diseases.....	2
1.1.2 Invasive methods.....	4
1.1.3 Non-invasive Plethysmographic Methods.....	6
1.1.4 Non-invasive Ultrasound Methods.....	18
1.1.5 Non-invasive Blood Pressure Methods.....	23
1.1.6 Emerging Techniques.....	27
1.2 Research Motivation.....	30
1.3 HeMo.....	32
1.4 Research Aims.....	33
1.5 List of Publications.....	34
1.6 Thesis Organization.....	35
Chapter 2 Pilot Assessment of HeMo.....	37
2.1 Background.....	38
2.2 HeMo System Design.....	40
2.3 Description of use.....	44
2.4 Pilot Experiment 1: Measuring the Arterial Pulse Wave.....	45
2.5 Pilot Experiment 2: Comparison to Photoplethysmography.....	46
2.6 Pilot Experiment 3: Measuring Venous Filling Index.....	48
2.7 Pilot Experiment 4: Comparison to Light Reflection Rheography.....	49
2.8 Conclusion.....	50
Chapter 3 Characterisation of Electro-Resistive Band Sensors.....	52

3.1	Background .....	53
3.2	Methods.....	55
3.2.1	Expansion/Contraction Simulator Machine.....	55
3.2.2	Data Acquisition .....	56
3.2.3	Data Analysis.....	57
3.3	Results.....	59
3.3.1	Total Harmonic Distortion (THD) Comparison .....	60
3.3.2	Signal to Noise Ratio Comparison .....	61
3.3.3	Peak to Peak Comparison .....	63
3.3.4	Correlation Coefficient .....	64
3.3.5	Frequency Response .....	65
3.3.6	Comparison to Rotary Encoder .....	68
3.4	Discussion .....	70
3.5	Conclusions.....	71
Chapter 4	Utility of HeMo for the Assessment of Peripheral Venous Function.....	73
4.1	Background.....	74
4.1.1	Chronic Venous Insufficiency .....	74
4.1.2	Venous Filling Time (VFT).....	74
4.2	Methods.....	76
4.2.1	Subjects.....	76
4.2.2	Experimental Settings and Measurement Protocol.....	76
4.2.3	Data Acquisition .....	78
4.2.4	Data Analysis.....	78
4.2.5	Data Comparison .....	80
4.3	Results .....	81
4.3.1	Subject Classification .....	82
4.3.2	Comparison of Devices .....	83
4.3.3	Inter-rater Reliability of the Annotations .....	86
4.3.4	Repeatability of the HeMo and LRR measurements .....	88
4.3.5	Effect of Five Minute Walk on VFT .....	90
4.4	Discussion and Conclusion .....	92
Chapter 5	Evaluation of HeMo for the Assessment of Arterial Function.....	95
5.1	Background .....	96
5.1.1	Peripheral Arterial Disease (PAD) .....	96

5.1.2	Arterial Pulse Wave (APW) .....	96
5.2	Methods.....	102
5.2.1	Subjects.....	102
5.2.2	Experimental Settings and Measurement protocol.....	103
5.2.3	Data Acquisition .....	104
5.2.4	Data Analysis.....	104
5.2.5	Data Comparison .....	106
5.3	Results.....	107
5.3.1	Qualitative Analysis and Comparison .....	108
5.3.2	Quantitative Analysis and Comparison .....	108
5.3.3	Repeatability of the HeMo and PPG Measurements .....	119
5.3.4	Effect of Five Minutes Fast Walking on APW Features .....	120
5.4	Discussion and Conclusion .....	124
Chapter 6	Discussion and Future Directions.....	128
6.1	Summary of Contributions.....	129
6.2	Future Directions .....	132
References	.....	135
Appendix A	Graphical User Interfaces and User Guidelines.....	A-1
A.1	User Guide for VFT Annotation .....	A-1
A.2	User Guide for APW Annotation.....	A-6
A.3	Venous Filling Time Annotation Graphical User Interface.....	A-12
A.4	Arterial Pulse Wave Annotation Graphic User Interface .....	A-16

# List of Figures

Figure 1. 1. Examples of peripheral vascular function assessment in the lower limb using plethysmography techniques; (a) Strain Gauge Plethysmography [41]; (b) Photo Plethysmography (PPG); (c) quantitative PPG/Light Reflection Rheography (LRR); (d) Impedance Plethysmography [42]; (e) Air Plethysmography [43] .....7

Figure 1. 2. Schematic view of the use of impedance plethysmography for detection of DVT (adapted from [63])..... 14

Figure 1. 3. VOTI system and its sandal shaped measuring probe [168] ..... 30

Figure 1. 4. Advent of milestone technologies for non-invasive diagnosis of PVDs..... 31

Figure 2. 1. Typical arterial pulse volume waveforms from normal healthy, moderate and severe peripheral arterial disease, adapted from [20]. ..... 40

Figure 2. 2. HeMo prototype; (a) A demonstration of HeMo worn on the calf [33]; (b) HeMo cuff (adapted from [33]); (c) Diagram of HeMo worn on the calf (adapted from [33]). ..... 42

Figure 2. 3. ERB front-end block diagram. .... 42

Figure 2. 4. PCB views (not to scale), top layer (red) and bottom layer (blue). Power is supplied via connector JP, signal is presented at connector JO..... 44

Figure 2. 5. Arterial pulse wave comparison; Top: Arterial pulse recorded by HeMo (raw data); Bottom: MP100 pulse piezoelectric transducer ..... 46

Figure 2. 6. Arterial Pulse wave recording; Top: recorded with PPG; Bottom: recorded with HeMo. .... 47

Figure 2. 7. Blood flow variations before (lower left inset), during and after ten tiptoes (lower right inset)..... 48

Figure 2. 8. Venous Filling Index (VFI) measurement using HeMo ..... 49

Figure 2. 9. Venous filling time measurement; (a) is recorded with LRR sensor; (b) is recorded with HeMo ..... 50

Figure 3.1. Top Panel: Picture of the expansion/contraction simulator rig. System elements: (1) rotary encoder; (2) motor; (3) direction of rotation of motor arm; (4) pulley system; (5) string potentiometer; (6) electro-resistive band. Bottom Panel: Diagram of the expansion/contraction simulator rig. Maximum stretch of the ERB and SP sensors occurs when the DC motor arm reaches position (a), minimum stretch occurs at position (b). ..... 56

Figure 3.2. ERB voltage versus SP voltage for one recording. The circled area highlights the ERB contraction nonlinearity. .... 59

Figure 3.3. Normalized ERB voltage versus Normalized SP voltage ..... 60

Figure 3.4. Total Harmonic Distortion of the ERBs and the SP. (1) to (4) refer to the different ERBs ..... 61

Figure 3.5. Signal to noise ratio of the ERBs and the SP. (1) to (4) refer to different ERBs.. 62

Figure 3.6. Peak-to-Peak voltage comparison of the ERBs and the SP. (1) to (4) refer to the different ERBs. .... 63

Figure 3.7. Peak to peak voltage of the band and the SP. The blue lines refer to the first experiment, and the red lines refer to the second experiment. The dashed line represent the peak-to-peak voltage of the SP data and the solid lines represent the peak-to-peak voltage of the ERB data. .... 64

Figure 3.8. Correlation coefficient of the ERB and the SP sensor for 108 recordings. Different colours refer to different bands used in the experiment. .... 65

Figure 3.9. (a1, b1, c1, d1, e1, f1) show the average temporal response calculated for oscillation frequencies of 0.05 Hz, 0.15 Hz, 0.26 Hz, 0.59 Hz, 0.85 Hz, 2.23 Hz. (a2, b2, c2, d2, e2, f2) show the hysteresis behaviour of the ERB sensor for oscillation frequencies of 0.05 Hz, 0.15 Hz, 0.26 Hz, 0.59 Hz, 0.85 Hz, 2.23 Hz. Hysteresis is calculated at the

midpoint of minimum and maximum strain. Gauge factors are also calculated for each oscillation frequency..... 67

Figure 3.10. Average peak to peak voltage plotted versus frequency at which the ERB is expanded/contracted. The points which were actually measured are marked as red. .... 68

Figure 3.11. Blue refers to normalized interpolated sinusoidal wave derived from the rotary encoder data. Red refers to average of 200 SP recordings. The error bar at each point refers to the maximum difference of the SP recordings from the interpolated wave at that point. Maximum upper error is 15.8% and maximum lower error is 17.45%..... 69

Figure 4.1. A typical venous filling curve. (a): the resting value, (b): the lowest point after exercise, (c): the final refilling ..... 75

Figure 4.2. Illustration of the VFT GUI when the LRR data is opened. User selected start and end points are marked with blue crosses. .... 79

Figure 4.3. VFT GUI when HeMo data is opened. User selected start and end points are marked with blue crosses..... 80

Figure 4.4. Threshold based comparison LRR and HeMo VFT values. .... 82

Figure 4.5. Scatter plot of HeMo VFT measurements vs. LRR VFT measurements. Each dot corresponds to the average of the three ratings for a VFT recording. .... 83

Figure 4.6. Box-whisker plots of LRR and HeMo VFT measurements. The horizontal line within the box indicates the median. The bottom and top edges of the box represent the lower (25%) and upper (75%) quartiles. The whiskers of the diagram show the range for each group of VFT data. P value: 0.01; mean difference: -1.66. .... 84

Figure 4.7. Bland-Altman plots of differences between LRR and HeMo VFT measurements versus their mean values. Horizontal lines from top to bottom represent upper limit, bias and lower limit..... 85

Figure 4.8. LRR annotations for all measurements. .... 87

Figure 4.9. HeMo annotations for all measurements..... 87

Figure 4.10. Box-whisker plots of the three annotations for LRR and HeMo. .... 88

Figure 4.11. LRR measurements for each subject. Values are mean of annotated values. .... 89

Figure 4. 12. HeMo measurements for each subject. Values are mean of annotated values... 89

Figure 4.13. Box-whisker plots of the three measurements for LRR and HeMo ..... 90

Figure 4.14. Comparison of before and after walk VFT measurements. Panel (a) refers to LRR measurements; Panel (b) refers to HeMo measurements..... 91

Figure 4.15. Box-whisker plots of before and after exercise VFT measurements. Panel (a) refers to LRR VFT measurements; Panel (b) refers to HeMo VFT measurements. .... 92

Figure 5.1. A typical arterial pulse waveform. (a) systolic peak, (b) dicrotic notch and (c) diastolic peak. .... 97

Figure 5.2. Arterial pulse wave grading system [192]. Grade A is attributed to an APW with a prominent dicrotic notch and sharp systolic peak; Grade B is attributed to an APW in which the dicrotic notch is disappeared; Grade C is attributed to an APW in which the dicrotic notch is absent, the systolic peak is flattened, the upslope and downslope time are decreased and almost equal; Grade D is when the amplitude of pulse is significantly decreased, upslope and downslope times are equal or there is absence of the pulse. .... 98

Figure 5.3. Illustration of crest time/rise time. .... 99

Figure 5.4. Illustration of half pulse width. .... 99

Figure 5.5. APW pulse width ..... 100

Figure 5.6. Illustration of x and y for calculation of augmentation index. x is amplitude of systolic peak and y is amplitude of diastolic peak..... 100

Figure 5.7. Systolic peak to diastolic peak time for calculation of stiffness index. .... 101

Figure 5.8.Three quarters pulse width. .... 102

Figure 5.9. Dicrotic notch to diastolic peak time ..... 102

Figure 5.10. APW GUI when PPG data is opened for annotation of the starting point, systolic peak, dicrotic notch, diastolic peak and the endpoint. User annotations are marked as crosses and colour coded..... 105

Figure 5.11. APW GUI when HeMo data is opened for annotation of the starting point, systolic peak, dicrotic notch, diastolic peak and the endpoint. User annotations are marked as crosses and colour coded. .... 106

Figure 5.12. Box-Whisker plots of PPG and HeMo arterial pulse wave features. The horizontal lines in each box plot represent median, each box itself shows first and third quartiles, and the whiskers indicate the range. .... 112

Figure 5. 13. Three examples of APW recordings with PPG and HeMo from three subjects. The blue printed plots on the left show PPG recording and the red printed plots illustrate the APW of corresponding HeMo recordings. .... 114

Figure 5.14. Scatter plots of HeMo APW features vs. PPG APW features. .... 116

Figure 5.15. Bland-Altman plots of PPG and HeMo arterial pulse wave features. The dashed horizontal lines in each plot from top to bottom represent upper limit, bias and lower limit. .... 117

Figure 5.16. Comparison of before and after walk APW features. PPG APW features are presented in blue and HeMo APW features are depicted in red. The mean of each feature is presented in black. .... 122

# List of Tables

Table 1. 1. Computerized strain-gauge plethysmography reference values for controls and patients with DVT (from [46]) .....	8
Table 1. 2. Sensitivity and specificity evaluation for the use of photo-plethysmography (PPG) in the diagnosis of PVDs. ....	9
Table 1. 3. Selection of studies using plethysmography methods in the diagnosis of PVDs..	16
Table 1. 4. Selected studies using Doppler ultrasound methods in diagnosis of PVDs. ....	22
Table 1. 5. Selected studies using blood pressure measurement methods in diagnosis of PVDs .....	25
Table 3. 1. THD comparison summary .....	61
Table 3. 2. SNR comparison summary .....	62
Table 3. 3. Statistical parameters of motor speed .....	69
Table 4. 1. Summary of VFT measurement protocol with HeMo and the LRR sensor .....	77
Table 4. 2. Demographics of study population.....	82
Table 4.3. Statistical summary of LRR and HeMo VFT measurements (average of three annotations) .....	84
Table 4.4. Summary of the statistics in Bland Altman plots of HeMo and LRR VFT measurements. ....	85
Table 4.5. Inter-rater reliability of annotations.....	86
Table 4.6. Repeatability of measurements.....	89

Table 4.7. Statistical summary of before and after walk VFT measurements of PPG and HeMo. ....	91
Table 5.1. Summary of APW recording protocol for HeMo and PPG sensor. ....	103
Table 5.2. Summary of participant demographics .....	107
Table 5.3. Statistical summary of PPG and HeMo arterial pulse wave features. ....	109
Table 5.4. Summary of the statistics in Bland Altman plots of HeMo and PPG arterial pulse wave features. ....	118
Table 5.5. Repeatability of the APW features. ....	119
Table 5.6. Statistical summary of before and after walk APW features of PPG and HeMo. ....	122

# List of Abbreviations

PVD: Peripheral Vascular Disease

PAD: Peripheral Arterial Disease

CVI: Chronic Venous Insufficiency

DVT: Deep Vein Thrombosis

RVF: Residual Volume Fraction

SGP: Strain-gauge Plethysmography

APG: Air Plethysmography

PPG: Photo Plethysmography

LRR: Light Reflection Rheography

IPG: Impedance Plethysmography

B-mode: Brightness mode

CW: Continuous Wave

PW: Pulsed Wave

DU: Duplex Ultrasound

ABI: Ankle Brachial Index

TBI: Toe Brachial Index

PWV: Pulse Wave Velocity

MRI: Magnetic Resonance Imaging

VOTI: Vascular Optical Tomographic Imaging

ERB: Electro-resistive Band

HeMo: Hemodynamic Monitoring

TI: Texas Instrument

REF200: REF200 Dual Current Source and Current Sink

ICC: intraclass correlation coefficient

CC: correlation coefficient

# Chapter 1 Introduction

This chapter provides an introduction to the research presented in this thesis. First, it provides detailed background information about Peripheral Vascular Diseases (PVDs) and the current relevant diagnostic modalities. It then, discusses the motivation for pursuing the development of a new non-invasive diagnostic tool for PVDs, and introduces the fundamental idea of a new hemodynamic monitoring device, which provides the foundation upon which this thesis is built. Then, an overview of the undertaken research is presented along with a summary of thesis contributions and a list of publications resulting from this thesis. Finally, the thesis structure is presented.

*Some of the work presented in this chapter has been published in:*

*“Shabani Varaki E, Gargiulo GD, Penkala S, Breen PP. Peripheral vascular disease assessment in the lower limb: a review of current and emerging non-invasive diagnostic methods. Biomed Eng Online. BioMed Central; 2018; 17:61.”*

## **1.1 Literature Review**

### **1.1.1 Peripheral Vascular Diseases**

Peripheral vascular disease (PVD) is a major cause of morbidity and mortality, with significant financial burdens on critical healthcare resources [1–10]. Vascular diseases result from circulatory system dysfunction caused by damage, occlusion and/or inflammation of arteries and/or veins [11]. Peripheral Arterial Disease (PAD), Chronic Venous Disease (CVD), which includes Chronic Venous Insufficiency (CVI) and Deep Vein Thrombosis (DVT), are common types of PVDs and are the most prevalent in the lower extremities.

Peripheral arterial disease is typically the result of the build-up of plaque (substances in the blood such as fat or calcium) in the arteries. This mass of plaque gradually narrows the arteries and impedes the flow of blood. The body segment supplied by the blocked or narrowed artery is then deprived of oxygen-rich blood [12], often resulting in pain and numbness [13]. This blockage can increase the risk of infection in the affected area, while severe blockage of blood flow can lead to gangrene (tissue death) and ultimately amputation [14,15]. In addition, PAD increases the risk of severe medical events such as coronary heart disease, heart attack, and stroke [2,13]. PAD affects 10–15% of the general population and about 20% of people aged over 60 years [2], [16]. Worldwide, the incidence of PAD has increased from 164 million in 2000 to 202 million in 2010 [17].

Another common type of peripheral vascular disease is Chronic Venous Insufficiency (CVI), also known as post thrombotic syndrome [18,19]. When standing upright, the blood in the leg veins must move against the force of gravity in order to return to the heart [20]. This venous return is achieved through active compression of the lower limb veins via contraction of muscles of the feet and legs [20]. Retrograde flow is prevented by a system of one-way valves in the veins [20]. However, extended periods of sitting or standing can lead to pooling of blood and an increase in venous blood pressure in the lower limb. Although leg veins are usually able to tolerate increased blood pressure over short periods of time, extended periods of increased venous pressure can lead to stretched vein walls and damaged venous valves,

ultimately leading to CVI [20,21]. CVI symptoms range from a vague feeling of heaviness in lower extremities, swelling of the legs, aching, itching, skin colour changes and ulceration [20]. The overall prognosis of such ulceration is poor, with delayed healing and recurrent ulceration [7,8]. More than half of venous ulcerations require long duration therapy lasting more than one year [8,22]. Disability caused by venous ulceration leads to loss of productive work hours (estimated at 2 million workdays/year) and early retirement [8,23]. In addition, the financial burden of venous ulceration to the healthcare systems in western countries is reported to be more than \$3 billion annually [3,8].

Deep Vein Thrombosis (DVT) is the formation of a blood clot in a vein deep in the body, commonly in the lower limbs [24]. Although the presence of a DVT is not necessarily symptomatic, some patients with DVT suffer from leg pain, swelling, tenderness and redness of the affected area [24]–[26]. The most serious consequence of DVT is a condition known as pulmonary embolism which occurs when blood clots break off and travel through the bloodstream to arteries of the lungs leading to partially/completely block of blood flow, ultimately leading to disability or death [24,25]. Population studies have estimated annual incidence of DVT as 0.5-1 per 1000 in general population [6,24–26]. Approximately one third of patients with DVT may develop a pulmonary embolism of whom about 20% of patients die before diagnosis or on the first day of diagnosis [25,27].

Early diagnosis and management of PVD is crucial to address the high rates of mortality and morbidity, however around 50% of people are asymptomatic and therefore do not necessary seek medical assistance, or are not screened by clinicians in the absence of diagnosed disease. Establishing effective and efficient clinical non-invasive diagnostic tools to determine vascular competence is essential particularly for asymptomatic PVD patients who have the same risk of morbidity and mortality as those with more obvious symptoms [2,28,29]. Given the prevalence and socioeconomic impacts of PVDs, a variety of both invasive and non-invasive diagnostic devices have been developed since the 1670s to facilitate accurate diagnosis and address the prevalence and socioeconomic impacts of PVDs [30,31].

Here, a comprehensive literature review of the available non-invasive methods for the assessment of peripheral hemodynamic function in the lower extremities is presented to provide background information in regards with the area of PVD diagnosis and to

demonstrate the importance of the research question of this thesis. Note that this review is not a systematic review but it is a narrative review, which focuses on a comprehensive critical analysis of the existing knowledge on the topic of interest. Such a review provides a theoretical framework, which can pinpoint trends, and provide information both on the needs and inconsistencies in the research. This could ultimately lead to greater definition of a research question and justify the research being undertaken.

First, the invasive PVD diagnostic methods are briefly examined to emphasize the importance of non-invasive diagnosis. Subsequently, three primary validated non-invasive technologies (Plethysmography, Doppler Ultrasound and Blood Pressure methods) are discussed in detail. Then, emerging diagnostic techniques are presented. Finally, the limitations and strengths of each method are identified to clarify the motivation behind this research.

### **1.1.2 Invasive methods**

The existing tools for peripheral vascular disease diagnosis can be divided into invasive and non-invasive methods. In this section, the three primary invasive methods, Angiography, Venography and Ambulatory Venous Pressure are briefly reviewed.

#### **Angiography**

Angiography, also known as Arteriography, is an imaging technique used to visualize inside blood vessels. With this method, a radio-opaque contrast agent is injected into the blood vessel and imaging techniques are used to provide information about blood vessel abnormalities such as narrowing, blockage, inflammation, abnormal widening and bleeding. A variety of angiography methods exist for the assessment of PAD [32]. Traditional angiography uses X-ray based imaging techniques while computed tomography angiography requires exposure to ionizing radiation and the injection of relatively large volume of contrast agent [33]. Magnetic resonance angiography is a less invasive method, but has limited spatial resolution, leading to reduced sensitivity. In addition to the invasive nature of the angiography test itself, there are risks and complications which may occur following the test

procedure such as seizures, haemorrhage (bleeding), arterial obstruction, nephrotoxicity (kidney poisoning) and acute impairment of renal function [34–36].

## **Venography**

Venography, also known as Phlebography, involves the insertion of a catheter into a foot vein and subsequent injection of a contrast dye. A venogram (X-ray of veins) is taken to examine the functionality of the valves in the deep veins. Although this method is still used for planning treatment, it is rarely performed due to the high associated cost and attendant risks. Venography can cause cellulitis with the potential for the development of tissue ulceration, necrosis (death of cells) and gangrene (death of tissue) [37]. Other complications include development of thrombosis after the venography procedure (reported in up to 13% of patients) [37].

## **Ambulatory Venous Pressure**

Ambulatory Venous Pressure is measured by placing a 21-gauge needle into a dorsal foot vein and connecting it to a pressure transducer [37]. The procedure typically involves an initial measure of venous pressure with the patient in the standing position. The patient is then asked to perform tiptoe exercises while the venous pressure is recorded. Finally, the patient is asked to stand at rest, while the rate at which venous pressure returns to the initial resting value is measured. The change of venous pressure is monitored as an indication of vascular system health. Venous ambulatory pressure measurement requires specialist clinicians, and similar to angiography and venography is not suitable for routine screening or monitoring the progression of therapy due to its invasive nature [37,38].

Although the invasive methods are highly accurate, they are expensive, uncomfortable for patients and carry inherent risks. These methods are typically reserved for instances where highly detailed measurements are required, for example, before surgical planning. However, the level of risk and discomfort is not appropriate for routine screening, but which is crucial for early disease diagnosis when preventative care could have the greatest benefit. Non-invasive methods are an alternative and can be used more routinely for diagnosis and follow-

up of subsequent treatment. However, each method has limitations, which continue to motivate the development of new diagnostic and clinically applied methods.

### **1.1.3 Non-invasive Plethysmographic Methods**

Plethysmography measures blood volume changes in the lower extremities. The principle of plethysmography for limb volume measurement was first introduced by Francis Glissonioin in 1677 using water displacement [30,31]. Later, the classic water plethysmography method was modified to other measures of volume (i.e. strain gauge, photo, impedance and air) to reduce the complexity of the measurement and improve accuracy [30]. Using plethysmographic devices, information such as the venous filling index (VFI), ejection fraction, residual volume fraction (RVF) and arterial pulse wave shape can be determined and used to evaluate peripheral vascular function [39,40]. Strain gauge, photo, impedance, and air plethysmography are discussed further in the following sections. Figure 1.1 represents an example of different plethysmography techniques.

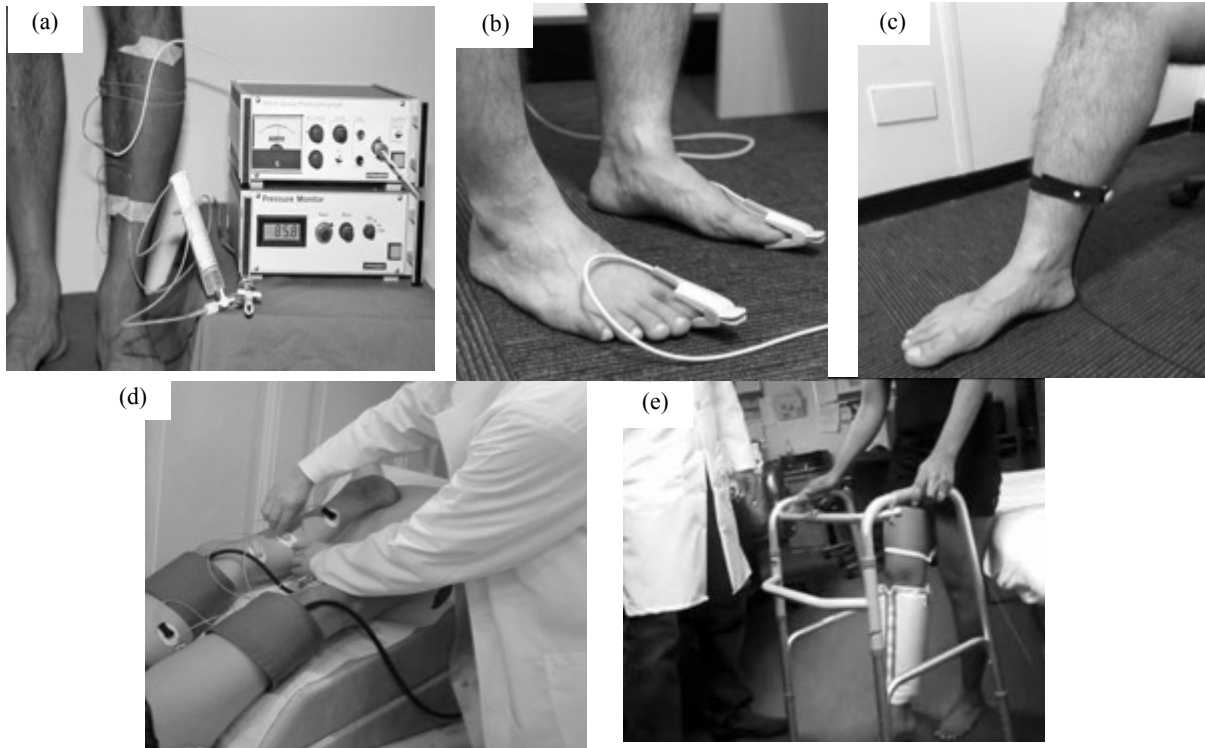


Figure 1. 1. Examples of peripheral vascular function assessment in the lower limb using plethysmography techniques; (a) Strain Gauge Plethysmography [41]; (b) Photo Plethysmography (PPG); (c) quantitative PPG/Light Reflection Rheography (LRR); (d) Impedance Plethysmography [42]; (e) Air Plethysmography [43].

### **Strain Gauge Plethysmography (SGP)**

Strain Gauge Plethysmography (SGP) was first introduced in 1953 and later improved in the 1990s [30,44–46]. SGP can be used to assess both the peripheral arterial and venous systems. The flexible strain gauge is filled with a conductive medium, usually mercury or gallium, and fit snugly around the limb (Figure 1.1a) [31]. Changes in limb blood volume is estimated from proportional changes in the electrical impedance of the strain gauge [31].

SGP reliability has been questioned because of the lack of validation studies [31]. Reference values for computerized SGP were provided in a 2014 study based on data from 63 healthy controls and 56 patients with DVT and post-thrombotic changes [46]. Table 1.1 represents the mean and 95% confidence interval reference values for each variable (venous emptying, venous outflow rate, half refilling time and venous refilling volume) derived from the control

and patient with DVT cohorts [46]. Venous emptying was defined as the blood volume reduction during the first second following cuff release. Venous outflow rate was defined as the expelled volume during the first 4 seconds following cuff release divided by the maximum venous volume and half refilling time referred to the time required for a 50% post exercise volume refilling [45,46]. A right/left side difference of 5-10% was found to be normal for venous emptying and venous outflow rate. A 20-25% side difference for venous refilling volume and venous refilling time was also determined to be normal [46]. However, a reduction in venous emptying and venous outflow rate beyond these inferred a functional outflow obstruction, i.e. the presence of DVT [46].

Parameters indicative of DVT detection (venous emptying and venous outflow rate), muscle pump function (venous refilling volume), and the presence/absence of venous reflux (half refilling time) were tested for disease sensitivity [46]. Combined, these measures had an overall sensitivity of 96% to broadly detect a venous disorder, without the sensitivity to specifically identify the particular component (i.e. the presence of venous reflux and/or DVT)

Table 1. 1. Computerized strain-gauge plethysmography reference values for controls and patients with DVT (from [46]).

<b>Venous Parameter</b>	<b>Control (mean and 95% confidence interval)</b>	<b>Patients with DVT (mean and 95% confidence interval)</b>
Venous emptying (mL/100mL×min)	84 (78-90)	110 (104-116)
Venous outflow rate	0.58 (0.54-0.62)	0.76 (0.74-0.78)
Half refilling time (Seconds)	6 (4-7)	17 (15-18)
Venous refilling volume (mL/100mL)	1.11 (0.95-1.27)	1.65 (1.52-1.78)

[46]. From these results, it is not possible to determine the accuracy of diagnosing specific venous disorders via strain gauge plethysmography. Other limitations that need to be considered with strain gauge plethysmography include temperature sensitivity and chemical hazard [47]. Adoption of indium gallium strain gauges instead of mercury can reduce this hazard [46].

## Photo Plethysmography (PPG)

Photo Plethysmography (PPG), first introduced in the 1930's to assess the vascular system, uses an infrared light source and a light receptor to estimate the variation of blood volume [48]. There are two common PPG sensor designs; one in which the toe or finger is placed between a light source and a light receptor, commonly known as PPG (Figure 1.1b); in the second configuration, known as quantitative PPG or Light Reflection Rheography (LRR) (Figure 1.1c), the light source and receptor are placed beside each other [31]. PPG produces a pulsatile waveform (AC) superimposed on a slowly changing baseline (DC) [49]. The AC component is used to measure changes in the blood volume due to arterial pulsation, and the DC component changes in total blood volume [31,49,50]. The derived arterial pulse wave enables the diagnosis of arterial incompetence [31]. Venous refilling time can also be measured by calculating changes in blood volume between static positioning and post-exercise (usually ten dorsiflexion manoeuvres) [31]. Venous refilling time is the time taken for the PPG curve to return to a stable value for at least five seconds [51]. Table 1.2 provides a summary of the sensitivity and specificity values calculated from evaluations of PPG for the diagnosis of PVDs.

Table 1. 2. Sensitivity and specificity evaluation for the use of photo-plethysmography (PPG) in the diagnosis of PVDs.

Study	Diagnosis Target	Reference Method	N (Control /Patient)	PPG Feature	Sensitivity	Specificity
Allen <i>et al.</i> [52]	PAD	ABI	107 (63/44)	PPG waveform	90.6%,	88.9%
Ro <i>et al.</i> [53]	PAD	Angiography	194* (31/163)	PPG waveform	81.6%	77.4%
Bays <i>et al.</i> [54]	CVI	Duplex Ultrasound	20 (10/10)	PPG refill time (venous refill time)	100%	60%
Sarin <i>et al.</i> [55]	CVI	Duplex Scanning	304* (80/224)	PPG refill time (venous refill time)	74-79%	61%
Mitrani <i>et al.</i>	DVT	Venography	69 (45/24)	Venous	96%	71%

[56]				Emptying (threshold 3mm)	86%	89%
				Venous Emptying (threshold 6mm)	83%	89%
				Venous Emptying Rate (threshold 0.17mm/second)	96%	78%
				Venous Emptying Rate (threshold 0.31mm/second)		
Arora <i>et al.</i> [57]	DVT	Venography	69* (41/28)	Venous Emptying Rate (threshold 0.35mm/second)	96.4%	82.9%
Thomas <i>et al.</i> [58]	DVT	Venography	131* (61/70)	Shape of PPG trace	92%	84%
				Venous refilling time (threshold 20 seconds)	100%	47%
Tan <i>et al.</i> [59]	DVT	Venography or Duplex	103* (66/37)	Venous refilling time (threshold 36 seconds)	100%	35%
					100%	56%

Venous  
refilling time  
and venous  
pump

“\*” denotes the number of the limbs used in the study and not the number of subjects.

“Control” refers to the number of the subjects diagnosed without PVD by the reference method

“Patient” refers to the number of the subjects diagnosed with PVD by the reference method.

---

A study of 63 healthy subjects and 44 PAD patients compared PPG derived pulse wave analysis techniques extracted timing, amplitude and shape characteristics for both toes and for right-to-left toe differences and compared these to diagnosis using the Ankle Brachial Index (Table 1.2). Sensitivity of 90.6%, specificity of 88.9% and accuracy of 90.2% was reported [52]. In a later study, comparing PPG to angiography, a reduced sensitivity (81.6%) and specificity (77.4%) was reported in a cohort of 97 patients (194 legs; Table 1.2) [53]. In this study, a physician visually interpreted the average of PPG waveform during at least 60 heartbeats to diagnose PAD. Qualitative evaluation of the PPG waveform and greater precision of angiography over ABI may account for the lower reported specificity and sensitivity values [2,60,61].

PPG has also been used to evaluate venous reflux, with a reported sensitivity of 100% and specificity of 60%, in a relatively small study of 10 healthy subjects and 10 subjects with deep venous reflux diagnosed using duplex ultrasonography [54]. The venous refill time was calculated following five dorsiflexion manoeuvres with the leg in a dependent position while sitting [54]. The mean venous refill time for the healthy group was  $20.2 \pm 1.1$  seconds and  $6.4 \pm 8.9$  seconds in the patient group [54]. A threshold venous refill time greater than 20 seconds was considered normal, In a larger study of 152 patients (304 legs) using the 20 second venous refill threshold; lower sensitivity 74% (superficial reflux), 79% (deep venous reflux) and specificity (61%) was reported [55].

Examinations of the clinical utility of PPG in the diagnosis of Deep Vein Thrombosis (DVT) have reported sensitivity between 83 and 100% and specificity between 35 and 89% (Table 1.2) [48-51]. In a study of 69 patients with suspected DVT, PPG using LRR was compared with venography for differences in venous emptying rates following 10 ankle dorsiflexion

exercises [56]. A venous emptying threshold ( $\Delta R$ ) of  $\leq 3\text{mm}$  (measured from the LRR tracing) resulted in sensitivity of 96% and specificity of 71% for detecting a DVT. Increasing the  $\Delta R$  threshold to  $\leq 6\text{mm}$  reduced sensitivity to 86% and increased specificity to 89% [56]. Alternatively, using the venous emptying rate to diagnose DVT, a threshold of 0.17mm/second produced sensitivity of 83% and specificity of 89% [56]. Increasing the threshold to 0.31 mm/second, a sensitivity of 96% and a specificity of 78% was achieved [56]. Similarly, in a study of 69 limbs a threshold value of 0.35mm/second for the venous emptying rate, provided a sensitivity of 96.4% and a specificity of 82.9% [57]. Furthermore, the performance of LRR, in comparison to either venography or duplex imaging, in a study of 103 legs with a suspected DVT provided high sensitivity but without high specificity [59]. This study evaluated venous refilling time and venous pump function, defined as the amplitude of the LRR trace during dorsiflexion contraction [59]. A venous refilling time threshold of  $\leq 20$  seconds returned sensitivity of 100% and specificity of 47%. Increasing this threshold to  $\leq 36$  seconds, sensitivity remained the same but specificity reduced to 35%. The combined specificity of venous refilling time and the venous pump was still quite low at 56% [59]. These measures of venous refilling time and venous pump function progressively decrease with age, further leading to less distinction between normal and abnormal groups [59].

Thomas et al. used a different criterion for assessing the performance of LRR versus venography in a group of 131 legs with clinically suspected DVT, classifying a DVT by a flat or a virtually flat LRR trace [58]. Using the shape of the LRR trace as the diagnostic criteria, they achieved a sensitivity of 92% and a specificity of 84% [58]. They reported that false negatives or positives only occurred for patients aged  $\geq 55$  years, suggesting that LRR may not be a good screening tool in the elderly [58].

## **Impedance Plethysmography (IPG)**

In 1939, Nyboer introduced the concept of impedance plethysmography (IPG), and in the 1970's several IPG devices became commercially available particularly for the diagnosis of PVDs [62,63]. IPG uses electrical impedance to derive changes in blood volume to determine hemodynamic functionality. In this method, circumferential electrodes are placed on the leg

(Figure 1.1d), a weak high-frequency alternating current passes through the leg, and voltage changes in the electrodes are monitored to measure blood volume changes in the test area [31]. This plethysmography method is reported to be less cumbersome than fluid displacement based plethysmographic methods [53, 54]. Additionally, as discussed in the following paragraphs, IPG can be employed to detect DVT and to evaluate both arterial and venous competence [63–65].

In a study of 33 legs with arteriography confirmed arterial obstruction greater than 50% diameter, compared to 28 healthy control legs, IPG waveform analysis (resting arterial pulse wave amplitude and maximum systolic slope) provided a sensitivity and specificity greater than 90% [63]. Threshold pulse wave amplitude of 0.06%dR (resistance change due to blood volume change) and 0.60%dR/sec for systolic slope were used [63]. When compared to ABI diagnosed PVD in a study of 66 patients, a sensitivity of 73.2% and a specificity of 96% was reported, using crest time thresholds of 180ms [66].

Anderson evaluated IPG for detecting CVI in 44 subjects compared to Doppler ultrasound [40]. Venous refilling time >11 seconds was chosen to represent a competent set of venous valves, while <11 seconds indicated venous reflux [40]. Reported accuracy was 90%, however, sensitivity and specificity values were not provided [40].

IPG to detect the presence of DVT evaluates the patient in supine position with the leg elevated above the level of the heart (Figure 1.2). A thigh cuff is inflated above venous pressure (50mmHg) with calf impedance monitored until plateau before cuff deflation. The presence of DVT is inferred by measuring maximum venous capacitance (venous volume after 50mmHg pressure application) and venous outflow rate (venous volume decrease in the first 3 seconds of deflation) [63,67]. Six medical centres were cited to independently confirm the accuracy (>94%) of IPG to diagnose a recent DVT proximal to the knee [63]. Sinton et al. compared IPG with venography in 85 legs and reported that IPG was successful in detecting proximal DVT in 20 of 22 subjects [68]. However, IPG was less successful in distinguishing between healthy and pathological groups for distal DVT's [68]. A review of venous disorder diagnosis reported acceptable sensitivity (87–98%) for IPG compared to venography [67,69–74]. In contrast, sensitivity (12-64%) was less acceptable in asymptomatic populations [67,75–78].

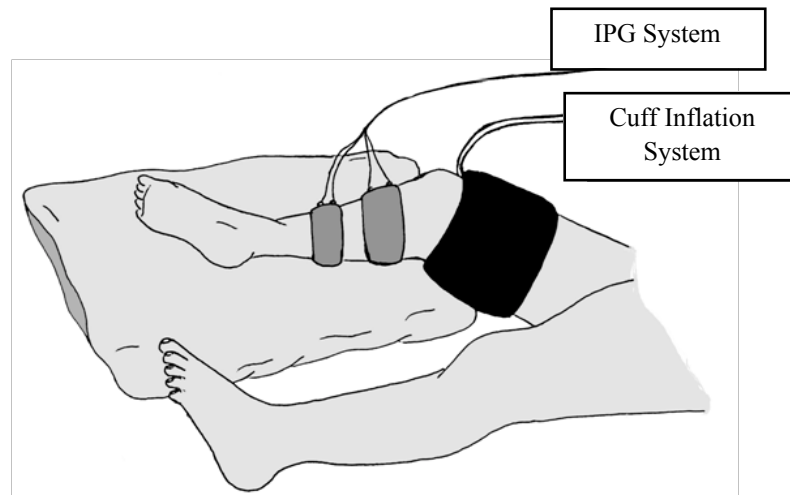


Figure 1. 2. Schematic view of the use of impedance plethysmography for detection of DVT (adapted from [63]).

### **Air Plethysmography (APG)**

Air Plethysmography (APG) was first introduced by Christopoulos et al. in 1987 for evaluation of venous function in the lower extremities [79,80]. An air-filled chamber encloses the lower limb and air displacement is used to measure blood volume changes (Figure 1.1e). The Venous Filling Index (VFI) measurement involves the patient elevating their leg in the supine position, allowing the leg to empty, and then resuming the standing position. The VFI is defined as 90% of the venous volume at rest divided by the time taken for 90% venous refilling following the leg elevation manoeuvre [80]. VFI has been reported to be predictive of venous reflux, with a VFI less than 2 ml/sec demonstrated no reflux, legs with VFI of 2-7 ml/sec demonstrated reflux to above the knee, and a VFI higher than 7 represented venous reflux to below the knee [79]. A VFI threshold greater than 7 had sensitivity of 73%, specificity of 100%, and accuracy of 81% when compared to phlebography for diagnosing venous reflux in 31 limbs [79].

In a study of 186 extremities, APG derived VFI demonstrated sensitivity of 80% and specificity of ~94% for detecting venous reflux when compared to venography and duplex scanning results [39]. The investigators also calculated residual volume fractions - difference between venous volume in the leg elevation position and following ten heel raise exercises, and divided by venous volume at rest [39,80,81]. Another study also showed that using

residual volume fraction can increase the specificity from 90% to 100% compared to VFI [54]. While residual volume fractions can increase specificity, it is not very helpful clinically as only a small subset of patients with symptomatic venous insufficiency have a normal VFI [39]. Due to the relative ease-of-use and reproducibility of APG, it has replaced strain-gauge plethysmography and photo-plethysmography in CVI diagnosis [79].

APG can also be used to detect the presence of venous occlusion. Venous obstruction affects the relationship between venous volume and pressure [79,82]. Harada et al. used APG to measure residual volume fraction and compared it with ambulatory venous pressure [79]. A high correlation ( $r=0.86$ ) between these two factors was found when no venous obstruction was present, while a poor correlation ( $r=0.40$ ) indicated venous occlusion [79]. However, in terms of clinical utility, the measurement of ambulatory pressure is an invasive and uncomfortable procedure, making this diagnostic unsuitable for routine use.

## **Summary and Limitations of Plethysmographic Methods**

Several plethysmography methods have been developed since 1677 for the assessment of peripheral vascular function noninvasively. The oldest plethysmography method, water plethysmography, has been used mostly in clinical research rather than in medical practice, as it is cumbersome to use and difficult to calibrate [31]. Later, strain gauge and photo plethysmography were introduced. Strain gauge plethysmography lacks validation studies [31], is sensitive to temperature variations, and the use of mercury gauges have environmental pollution concerns [47]. On the other hand, while photo plethysmography has acceptable sensitivity and specificity for arterial disease, it has low sensitivity and specificity when detecting venous reflux [55], which further decreases in elderly populations [58]. Impedance plethysmography and air plethysmography were developed later. However, impedance plethysmography has shown to have low sensitivity (12% to 64%) for detecting asymptomatic DVTs [67] and air plethysmography has a relatively low sensitivity (73%) in detecting venous reflux [79]. Additionally, air plethysmography requires associated use of invasive ambulatory venous pressure measurement for diagnosis of venous occlusion. Therefore, although air plethysmography has been reported to have more reproducibility than strain-gauge plethysmography and photo-plethysmography [79], it is not the most popular

technique for peripheral vascular assessment. Photo-plethysmography is generally most popular, however, plethysmography remains cumbersome, requires careful setup by a trained practitioner, and takes considerable time to perform the assessment [14]. While plethysmographic methods have considerable utility in functional assessment, these time and personnel requirements have meant that they have been largely replaced by Doppler ultrasound methods, which will be discussed in the next section [31]. [31]. Table 1.3 demonstrates a summary of the discussed plethysmography studies.

Table 1. 3. Selection of studies using plethysmography methods in the diagnosis of PVDs.

<b>Study</b>	<b>Diagnosis Target</b>	<b>Reference Method</b>	<b>Number of Subjects (Control/Patient)</b>	<b>Plethysmography Method</b>	<b>Sensitivity</b>	<b>Specificity</b>
Harada et al. [79]	CVI	Venography	31* (0/31)	APG	73%	100%
Criado et al. [39]	CVI	Duplex scanning & Venography	186* (61/125)	APG	80%	94%
Bays et al. [54]	CVI	Duplex Ultrasound	20* (10/10)	APG	70%-100%	90%-100%
Rosfors et al. [46]	Venous disorder (CVI,DVT)	Duplex ultrasound	119 (63/56)	SGP	96%-98%	Not given
Allen <i>et al.</i> [52]	PAD	ABI	107 (63/44)	PPG	90.6%,	88.9%
Ro <i>et al.</i> [53]	PAD	Angiography	194* (31/163)	PPG	81.6%	77.4%
Bays <i>et al.</i> [54]	CVI	Duplex Ultrasound	20* (10/10)	PPG	100%	60%
Sarin <i>et al.</i> [55]	CVI	Duplex Scanning	304* (80/224)	PPG	74-79%	61%
Mitrani et al. [56]	DVT	Venography	69 (45/24)	PPG	83%-96%	71%-89%

Arora <i>et al.</i> [57]	DVT	Venography	69* (41/28)	PPG	96.4%	82.9%
Thomas <i>et al.</i> [58]	DVT	Venography	131* (61/70)	PPG	92%	84%
Tan <i>et al.</i> [59]	DVT	Venography or Duplex	103* (66/37)	PPG	100%	35%-56%
Anderson [40]	PAD	Angiography	61* (28/33)	IPG	>90%	>90%
Mašanauskienė <i>et al.</i> [66]	PAD	ABI	62 (21/41)	IPG	73.2%	96%
Hull <i>et al.</i> [69]	DVT	Venography	200 (114/86)	IPG	94%	91%
Toy <i>et al.</i> [70]	DVT	Venography	25* (9/16)	IPG	94%	100%
Flanigan <i>et al.</i> [71]	DVT	Venography	207* (136/71)	IPG	90.4%	75.7%
Cooperman <i>et al.</i> [72]	DVT	Venography	98* (75/23)	IPG	87%	96%
Liapis <i>et al.</i> [73]	DVT	Venography	308* (169/139)	IPG	91%	89%
Peters <i>et al.</i> [74]	DVT	Venography	185(124/61)	IPG	84%	93%
Cruickshank <i>et al.</i> [75]	DVT	Venography	1010*(812/198)	IPG	12.9%	98.1%
Paiement <i>et al.</i> [77]	DVT	Venography	937* (864/73)	IPG	12.3%	99.1%
Agnelli <i>et al.</i> [78]	DVT	Venography	440* (295/145)	IPG	19%	91%

“\*” denotes the number of the limbs used in the study and not the number of subjects.

“Control” refers to the number of the subjects diagnosed without PVD by the reference method

“Patient” refers to the number of the subjects diagnosed with PVD by the reference method.

### **1.1.4 Non-invasive Ultrasound Methods**

Vascular ultrasonography is a non-invasive diagnostic method utilizing a handheld transducer to direct an inaudible sound wave with a frequency of 1-30MHz into the vessel of interest to assess vascular competency [83]. Computer processing converts the data to audible sound waves or graphs, allowing the vascular technician to see and/or hear blood flow through the vessels and is the mainstay of vascular imaging. B-mode, Continuous Wave, Pulsed wave Doppler and Duplex Ultrasound are used to assess the vascular system [28,83–86].

#### **B-mode Doppler Ultrasound**

B-mode (brightness mode) ultrasonography or grey-scale imaging generates a two dimensional real-time picture to visualize the structure of blood vessels and provides information about diameter change in large veins [54,84,87,88].

Dauzat et al. evaluated the clinical value of B-mode for DVT detection in a group of 145 patients and reported a sensitivity of 94% and a specificity of 100% compared to venography [89]. O’Leary et al also used B-mode and found a sensitivity of 88% and a specificity of 96% to detect DVT in 50 subjects compared to venography results [90]. In another study, Sullivan et al. compared B-mode ultrasound with venography for detection of DVT in 23 patients and found a sensitivity of 100% and a specificity of 92% [91]. They also compared the results of B-mode and rheography for detection of DVT in 170 extremities and found an agreement of 82% between the two methods [91]. This study also reported the capability of B-mode in distinguishing an acute DVT from a chronic DVT in 93% of the extremities which underwent venography [91].

#### **Continuous Wave (CW) Doppler Ultrasound**

Continuous Wave (CW) Doppler Ultrasound is routinely used for clinical screening. Venous flow is heard as a low-pitched blowing sound and a normal venous blood flow should be in phase with respiration [83,85]. If manual limb compression is applied distal to the probe, the forward flow (flow towards the heart) will be augmented. The augmentation can be seen as an increase in the amplitude of the CW Doppler signal [83]. If limb compression is applied

proximal to the probe, and valves are competent, the Doppler signal should cease as healthy valves limit retrograde flow [83]. A similar decrease in the blood flow signal can be noted when the patient coughs or performs a Valsalva manoeuvre [83]. Venous reflux can thus be diagnosed by an audible signal during the compression or Valsalva manoeuvre. If the signal lasts for more than 5 seconds, venous reflux is inferred [83,87].

### **Pulsed Wave (PW) Doppler Ultrasound**

Pulsed Wave Doppler mode can be used for categorizing peripheral arterial stenosis [86]. Although PW Doppler overcomes the limitation of CW Doppler in depth discrimination, it is unable to measure high velocities due to the aliasing phenomenon [92]. Aliasing occurs when the velocity of blood flow exceeds one half of the pulse repetition frequency (usually a velocity above 2m/sec) and it affects the velocity waveform such that the velocity and direction of blood flow cannot be interpreted [92].

### **Duplex Ultrasound (DU)**

Duplex ultrasound combines the use of B-mode imaging, PW, CW Doppler modes when evaluation of the anatomy and hemodynamic function of the vascular system is needed [28]. Duplex ultrasound thus is a very sensitive diagnostic method [87], and can be used for detecting venous reflux, arterial stenosis/occlusion and deep vein thrombosis. In one study, 169 limbs were evaluated using duplex ultrasound for diagnosing peripheral arterial disease [34]. Patients rested for 15 minutes before examination. Subsequently, both lower limbs were scanned from the common femoral artery to the pedal arteries and the entire limb was divided into 15 segments [34]. Arterial occlusion was determined by observation of a dampened distal signal in comparison with the proximal signal; presence of a proximal exit collateral; and presence of a distal re-entry collateral. Peak systolic velocity ratio (the peak systolic velocity in the stenosis divided by the peak systolic velocity just proximal to the stenosis) was also measured for those segments with flow velocity increase [34]. Segments with a peak systolic velocity ratio  $\geq 2$ m/sec inferred a diameter reduction  $\geq 50\%$  [34]. Duplex ultrasound was reported to have a sensitivity of 88%, specificity of 79% and accuracy of 95% among 2535 segments (169 limbs  $\times$  15 segments) when compared to angiography (Table 1.4) [34].

In another study of 100 subjects, greater sensitivity 95% and 92% and specificity (99% and 97%) were reported for the diagnosis of arterial occlusion and stenosis respectively when compared to angiography [28,93]. A review of Duplex ultrasound performance for the diagnosis of PAD found the sensitivity values between the range of 79.7%-97% and the specificity ranged from 88.5% to 99% in comparison to angiography [32,94–96]. It also suggested that segment-to-segment comparison possibly increases the number of true negative test results leading to an overestimation of the specificity [32].

Duplex ultrasound is arguably the most important and widely used non-invasive tool for the investigation of chronic venous diseases [97]. It can detect minimal venous reflux even in isolated veins of asymptomatic individuals [87]. Duplex scanning can also determine if the reflux is constrained in veins above or below the knee [87], a limitation of the previously reported IPG diagnosis of venous reflux. Duplex ultrasound scanning is undertaken with the patient in the standing position to allow maximum venous dilation [98]. Several manoeuvres such as foot/calf compression, ankle dorsiflexion and Valsalva can be performed to create physiologic flow [97]. Alternately the patient may be placed in a 15° reversed trendelenburg position and then asked to perform a Valsalva manoeuvre [87]. Nicolaidis argued that both of these examination lead to similar results, and while the second method is more convenient, it does require cooperation from the patient [87]. A reversal of flow during the diagnostic manoeuvres infers venous reflux [97]. Threshold values for the diagnosis of venous reflux are defined as retrograde flow lasting longer than 1000ms in the femoral area or longer than 500ms in the femoral and popliteal veins [98].

At the beginning of the 21st century, the use of duplex ultrasound was extended to detect venous obstruction and its extent [87]. Continuous flow in the femoral veins with little or no change in flow during any manoeuvre infers abnormality [98]. However, the presence of phasic flow does not exclude the potential presence of an obstruction and repeat scans are recommended to confirm or exclude DVT [98]. While duplex ultrasound can detect the presence of venous stenosis by measuring luminal reduction the extent of occlusion is better evaluated with magnetic resonance venography, computed tomography venography or contrast venography [98]. Cronan et al. compared the performance of Duplex ultrasound for detection of DVT in 51 subjects and found 89% sensitivity and 100% specificity [99]. In a

systematic review of diagnostic accuracy of ultrasound for DVT, sensitivity of Duplex ultrasound ranged from 75-96%, and a specificity of 94% depending on the site of DVT [100].

Colour Duplex imaging can also be used to evaluate the direction and velocity of blood flow and thus detect the location of arterial occlusion/stenosis and venous reflux [28,86,101,102]. A study compared colour Doppler imaging with angiography for detection of occlusion and stenosis in one hundred legs of 51 patients [93]. Occlusion detection had a sensitivity of 95% and specificity of 99%, while stenosis detection had sensitivity of 92% and a specificity of 97% [93]. Examination time of 30-45 minutes was reported for each patient [93]. In general, colour Duplex imaging provides better accuracy [101]. However, Doppler transducer positioning (70° to the vessel) is critical and requires highly trained and experienced operators [103].

### **Summary and Limitations of Ultrasound Methods**

Vascular ultrasonography is one of the most commonly used non-invasive methods employed by vascular laboratories to define anatomy, hemodynamic and lesion morphology. Ultrasound examination is considered to be the gold standard and a very powerful tool in establishing diagnosis and aiding therapeutic management of chronic venous insufficiency and peripheral arterial disease, revealing sites of reflux and/or obstruction in the venous system, arterial occlusions and stenosis [98]. However, the use of duplex ultrasound is highly operator dependent [34,87]. Furthermore, 5-20% of patients cannot undergo duplex ultrasound wave exposure because of ulceration, pain, swelling, heavily calcified arteries and obesity [34]. Moreover, duplex ultrasonography can be time-consuming (1-2 hours for full assessment), requires expensive equipment and a highly trained, experienced vascular technician with comprehensive knowledge of the anatomy of the vascular system [97]. Lack of a universally accepted protocols for detection of DVT using the ultrasonic methods is an additional issue [104]. These factors therefore limit the use of ultrasound for routine examination and early diagnosis of PVDs.

Table 1. 4. Selected studies using Doppler ultrasound methods in diagnosis of PVDs.

Study	Diagnosis Target	Reference Method	Number of Subjects (Control/Patient)	Doppler Ultrasound Method	Sensitivity	Specificity
Dauzat et al. [89]	DVT	Venography	145 (45/100)	B-mode	94%	100%
Sullivan et al. [91]	DVT	Venography	23*(12/11)	B-mode	100%	92%
O’Leary et al. [90]	DVT	Venography	50 (25/25)	B-mode	88%	96%
Cronan et al. [99]	DVT	Venography	51(23/28)	Duplex	89%	100%
Aly et al. [95]	PAD	Angiography	177* <sup>†</sup>	Duplex	92%	99%
Linke et al. [94]	PAD	Angiography	46* <sup>†</sup>	Duplex	89%	95%
Bergamini et al. [96]	PAD	Angiography	80*(28/52)	Duplex	80%	95%
Eiberg et al. [34]	PAD	Angiography	169 (0/169)	Duplex	88%	79%
Whelan et al. [93]	Arterial occlusion	Angiography	51 (8/43)	Duplex	95%	99%
Whelan et al. [93]	Arterial stenosis	Angiography	51 (8/43)	Duplex	92%	97%

“\*” denotes the number of the limbs used in the study and not the number of subjects.

“<sup>†</sup>” comparison between limb segments and not control/patients.

“Control” refers to the number of the subjects diagnosed without PVD by the reference method

“Patient” refers to the number of the subjects diagnosed with PVD by the reference method.

## **1.1.5 Non-invasive Blood Pressure Methods**

### **Ankle Brachial Index (ABI)**

In the 1950's, Winsor first described the Ankle Brachial Index (ABI), a simple non-invasive method for assessing arterial perfusion [105]. It remains a primary clinical diagnostic test for PAD [106]. The ABI is measured by calculating the blood pressure at the ankle and dividing by the higher of two brachial systolic blood pressures [28,105]. A normal ABI is between 1 and 1.3 [107] with 0.91 to 0.99 acceptable [106]. An ABI lower than 0.9 indicates the presence of PAD with ratios below 0.4 indicating the presence of severe PAD and problems for healing [28,108]. While an ABI between 0.91 and 0.99 is acceptable, this range and below also indicates increased cardiovascular risk [108], including stroke, coronary diseases or cardiovascular death [109–111]. ABI has a relatively high sensitivity and specificity, but such high accuracy cannot be achieved for all patient types. Arteries of the elderly, patients with diabetes or renal disease are usually calcified and largely incompressible, leading to poor sensitivity in such cases [28]. The poor sensitivity of ABI has been referenced in studies where the ABI appeared to be normal (1-1.3) or even supernormal (above 1.3) for a group of patients with PAD [28,112].

A single ABI measurement may not be sufficient for diagnosis even in symptomatic cases [108]. In such cases, the patient is asked to perform a standardized exercise, after which a ABI is recalculated [108]. Many vascular laboratories use a standardized exercise protocol [113], this may involve treadmill walking at a 12-degree incline, at 2 mph, for at least 5 minutes or graded bike pedalling [108]. Decreases in post exercise ankle pressure of 20 mmHg or more is indicative of severe PAD [108]. While the ABI is a simple test, it can be time consuming and requires training and experience [15]. A recent review highlighted the importance of training by comparing sensitivity and specificity of oscillometric ABI and manual Doppler ABI performed by inexperienced operators [107]. While oscillometric ABI provides sensitivity of 97% and specificity of 89%, manual Doppler ABI has sensitivity of 95% and specificity of just 56% compared to angiography [107,114]. Xu et al reviewed sensitivity and specificity of ABI in detecting/excluding PAD and found the sensitivity values between 61%-96% and the specificity range within 56%-90% [60,61,115–121]. An ABI test

typically takes about 15 minutes [122], and should be preceded by a 30-minute rest period [60]. While ABI is useful as an initial clinical test to assist diagnosis, not all guidelines promote the ABI as a screening tool for PAD in primary care [16]. The ABI is unable to identify the location of arterial stenosis/occlusion [28], is not recommended as a PAD screening tool in primary care by all guidelines [16] and is not capable of diagnosing CVI or DVT.

### **Segmental Blood Pressure Measurement**

Segmental blood pressure measurement, unlike ABI measures, can be used to localize the site of stenosis or occlusion in PAD [28,108,123,124]. Four cuffs are placed around the leg, ankle, calf, lower thigh and upper thigh [123,124] with either handheld Doppler ultrasound, photoplethysmography, strain-gauge plethysmography, or oscillometric blood pressure measurement then used to measure the blood flow/pressure at each of the four leg cuff sites [108,123].

A reference arm blood pressure measure is also taken and normally is at least 30mmHg lower than thigh pressure [108,123,125]. In healthy individuals the pressure difference (gradient) between two adjacent levels in the lower extremities should be 20mmHg or less [86,108]. A pressure gradient of 20-30 mmHg is representative of stenosis with greater pressure reductions indicating occlusion [123,126,127]. A pressure difference  $\geq 20$  mmHg between the bilateral leg segments also indicates arterial occlusion [124].

Limitations of this method include inappropriate cuff sizing resulting in false blood pressure readings [123]. An average error of 8.5mmHg in systolic blood pressure is reported due to inappropriate cuff sizing [123,128]. Accuracy can be improved by including other measures such as arterial pulse wave analysis [108], although no documented accuracy values are available.

### **Toe Brachial Index (TBI)**

Toe blood pressure measurements to evaluate peripheral arterial disease was introduced in 1965 [127,129] and is particularly common for the diagnosis and management of underlying

vascular pathology associated with diabetic foot lesions [129–131]. Similar to ABI, TBI is calculated by dividing the toe systolic pressure by the brachial pressure. TBI is recommended as an alternative to ABI to counter unreliable elevated measures in the presence of medial artery calcification, which is particularly prevalent in people with diabetes and the aged [132–134].

A study of 174 subjects with diabetes and 53 non-diabetic subject found that diabetic patients with an ABI < 1.3 had ABI-TBI differences within the normal ranges for healthy controls, whereas those with an ABI  $\geq$  1.3 had abnormal ABI-TBI differences [132]. The authors suggest that there is no advantage to TBI over ABI where ABI < 1.3 but that the TBI is superior in the presence of calcification, where ABI  $\geq$  1.3 [28,132]. While exact threshold values for TBI are still debated, a TBI  $\geq$  0.7 is generally reported to be normal with a TB < 0.7 associated with claudication and a TBI < 0.2 with pain at rest [28].

Table 1. 5. Selected studies using blood pressure measurement methods in diagnosis of PVDs.

Study	Diagnosis Target	Reference Method	Number of Subjects (Control/Patient)	Blood Pressure Measurement Method	Sensitivity	Specificity
Vega et al. [114]	PAD	Angiography	158* (27/131)	ABI	95%-97%	56%-89%
Wikström et al. [60]	PAD	Angiography	533*(421/112)	ABI	15%-20%	99%
Parameswaran et al. [118]	PAD	Doppler waveform analysis	114* (79/35) type 2 diabetes	ABI	63%	97%
Lijmer et al. [120]	PAD	Angiography	106* (0/106)	ABI	79%	96%
Schröder et al. [115]	PAD	Duplex Ultrasound	216 (103/113)	ABI	68%	99%
Niazi et al. [116]	PAD	Angiography	208*(42/166)	ABI	68%	83%
Guo et al.	PAD	Angiography	298 (277/21)	ABI	91%	86%

[117]

Premalatha et al. [119]	PAD	Duplex Ultrasound	94 (26/68) type 2 diabetes	ABI	70.6%	88.5%
Williams et al. [121]	PAD	Duplex Ultrasound	41* (27/14)	ABI	83%	100%
Williams et al. [121]	PAD	Duplex Ultrasound	32* (25/7) Diabetes	ABI	100%	88%
Williams et al. [121]	PAD	Duplex Ultrasound	57* (41/16) Diabetes with neuropathy	ABI	53%	95%
Williams et al. [121]	PAD	Duplex Ultrasound	41* (27/14)	TBI	100%	81%
Williams et al. [121]	PAD	Duplex Ultrasound	32* (25/7) Diabetes	TBI	91%	65%
Williams et al. [121]	PAD	Duplex Ultrasound	57* (41/16) Diabetes with neuropathy	TBI	100%	61%
Park et al. [135]	PAD	Angiography	30* (17/13) (Diabetes gangrene)	TBI	100%	100%

“\*” denotes the number of the limbs used in the study and not the number of subjects.

“Control” refers to the number of the subjects diagnosed without PVD by the reference method

“Patient” refers to the number of the subjects diagnosed with PVD by the reference method.

---

A review of 22 studies [133] found TBI threshold levels to indicate PAD ranging from 0.54 to 0.75 [121,132,135–155]. Despite this range in TBI threshold values, TBI has high sensitivity (90% to 100%) compared to angiography, with specificity values between 65% to 100% [133]. Several guidelines have suggested using TBI<0.7 as the threshold, however, based on Høyer et al.’s review this cut-off is not necessarily evidence-based. According to Høyer et al.’s findings, there is a lack of agreement on TBI diagnostic threshold in the current literature and more trials are required to recommend the best diagnostic threshold [133]. Test environments and protocols are important to improve test performance. The patient is

required to rest for at least 5 minutes before the measurement, the room temperature should be above 22 °C and toe skin temperature  $\geq 25$  °C [129]. Pre-test limb heating may be required, in order to minimize false positive results [133,156,157].

The measurement of toe blood pressure is technically more complicated than measuring ankle blood pressure [132]. The additional equipment required, such as photo-plethysmography, strain gauge plethysmography and Doppler flowmeter, can limit use in some clinical settings [132,133].

## **Summary and Limitations of Blood Pressure Methods**

Although the ABI is relatively cheap, requiring minimal and inexpensive equipment, and is widely clinically applied, it has a low sensitivity when used in patients with diabetes or the elderly with calcified arteries, where the ABI values are inflated mimicking false negative normal values [28]. This is especially troublesome as these two groups of patients are at higher risk of developing PVDs. TBI can be used as an alternative in cases with the presence of medial artery calcification, but adds an additional time constraint. To assist in pathology site location additional segmental blood pressure measurements can be used. Table 1.5 provides a summary of the discussed blood pressure methods studies.

### **1.1.6 Emerging Techniques**

#### **Pulse Wave Velocity (PWV)**

Pulse wave velocity (PWV) is defined as the velocity at which the arterial pulse wave, generated by heart contraction, propagates through the arteries [158]. The application of pulse wave velocity as a measure of arterial stiffness/elasticity was first predicted by Thomas Young in 1808 [159]. Later, Moens and Korteweg independently presented a mathematical model indicating the relationship between pulse wave velocity and arterial stiffness [160]. Based on the Moens-Korteweg equation,  $PWV = \sqrt{E \cdot h / 2\rho \cdot r}$  (E: intrinsic stiffness of the wall of artery, h: thickness, r: radius,  $\rho$ : blood density), higher PWV is representative of increased stiffness of arteries [160,161]. Patients with PAD are reported to have a higher aortic PWV compared to healthy controls [162]. However, PAD is not the only potential

cause of arterial stiffness, as arteries may become stiffened in the presence or absence of PAD, e.g. hypertension and diabetes [158].

Although the use of PWV as a diagnostic measure is quite old, its use for the diagnosis of PAD is relatively new. In two studies with sample sizes of 105 and 440 healthy subjects and 35 and 38 subjects with PAD, PWV was reduced in the presence of PAD when measured between the heart-feet [163] and femoral-dorsalis [164]. However, increased heart-feet PWV was observed in patients with hypertension, suggesting that PAD and hypertension apply opposing effects on PWV [163]. Even beat to beat blood pressure variability have shown to be correlated with an increase in PWV in the hypertensive population [165]. Additionally, in a study of 101 healthy subjects and 102 patients with diabetes with/without PAD, reduced brachial-ankle PWV (baPWV) was found in people with diabetes and PAD (1221 cm/sec) compared to non-PAD diabetic subjects (1607cm/sec) [166]. The median difference between absolute right-left baPWV was 36 cm/sec in the healthy group, 55 cm/sec in the diabetic/no PAD group and 290 cm/sec in the diabetic/PAD group suggesting the right-left difference may be used as a novel indicator of PAD [166]. However, cautious interpretation is needed when bilateral PAD is present and comparisons to ABI measures which have poor sensitivity in the presence of calcification [166].

The application of PWV as a measure of arterial stiffness has been motivated by the development of new devices to assist measurement. In a recent review PulsePen (DiaTecne, Milan, Italy), Complior (Colson, France), SphygmoCor (AtCor Medical, Sydney, Australia), Photoplethysmography, ultrasound and Magnetic Resonance Imaging (MRI) have been identified for non-invasive PWV measurement [167]. A number of other optical devices are identified but are not commercially available [167]. While a promising area of inquiry, PWV measurement is currently not used for clinical diagnosis of PVD. Limitations include the expense of ultrasound and MRI methods and poor accuracy in more affordable alternatives [167]. As discussed earlier, PAD is not the only parameter that alters PWV. The use of PWV as an indicator of PAD is complicated by the effects of ageing, arterial stiffness, hypertension, beat to beat blood pressure variability, and diabetes. Considering the work to date, it is still possible that PWV could be used for PAD diagnosis. However, no studies have

compared PWV with validated diagnostic techniques; consequently, no values of sensitivity or specificity are reported.

### **Vascular Optical Tomographic Imaging (VOTI)**

Vascular Optical Tomographic Imaging (VOTI) is a new non-invasive imaging system, which can be used to directly measure distal perfusion in the foot by extracting information about haemoglobin concentration [168]. Although VOTI has not been routinely used in vascular clinics yet, this system has the potential to be used as a new diagnostic tool for peripheral arterial disease [168]. The VOTI system has a sandal shaped measuring probe encompassing the foot (Figure 1.3), which uses harmless red, and near infrared light (650 nm <wavelength<900 nm) to illuminate the foot at different points.

The system uses the transmitted lights to construct a cross-section image of haemoglobin concentration at the mid metatarsal region. Lower light intensities are indicative of higher haemoglobin concentration, which is itself representative of better perfusion [168].

The VOTI system was originally introduced in 2007 and in 2015 the system was used to assess PAD in the lower extremities of a group of 40 subjects [168]. Subjects were classified into healthy (n=20), PAD (n=10) and PAD with diabetes (n=10) groups according to a combination of the patients' ABI readings, segmental ultrasound results, physical symptoms, and medical history [168]. Haemoglobin concentration was extracted during staged occlusion and compared with ABI readings and arterial pulse wave recordings. Haemoglobin concentration for healthy subjects was found to be about twice that of patients during 60mmHg venous occlusion, with a faster response to pressure application/release in healthy subjects compared to patients [168]. Despite dissimilar ABI readings from PAD patients and

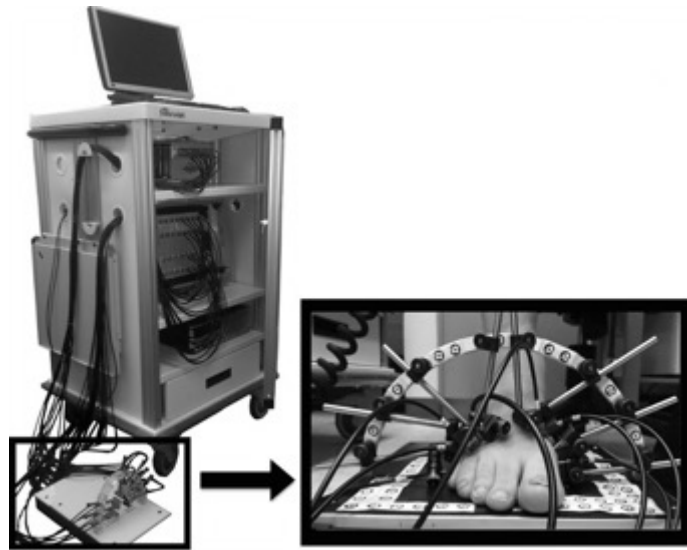


Figure 1. 3. VOTI system and its sandal shaped measuring probe [168].

PAD patients with diabetes, similar haemoglobin time traces were observed in both cohorts, suggesting VOTI may have greater sensitivity in people with diabetes and PAD [168].

## 1.2 Research Motivation

The presented literature review discussed the current non-invasive hemodynamic monitoring techniques and demonstrated their potential for the non-invasive assessment of peripheral vascular function. A summary table including the reviewed methodologies together with their performance (where available) in terms of sensitivity, specificity and accuracy is associated with this thesis as supplementary material.

Considering the prevalence and the adverse impacts of PVDs, it is no surprise that many diagnostic methods have been developed since the 1670s. The timeline in Figure 1.4 shows the advent of milestone technologies for non-invasive diagnosis of PVD. Despite the efforts in the development of an ideal non-invasive diagnostic modality for PVDs, underdiagnosis in the primary care is still an ongoing challenge, which demands development of new unobtrusive monitoring techniques [169–171].

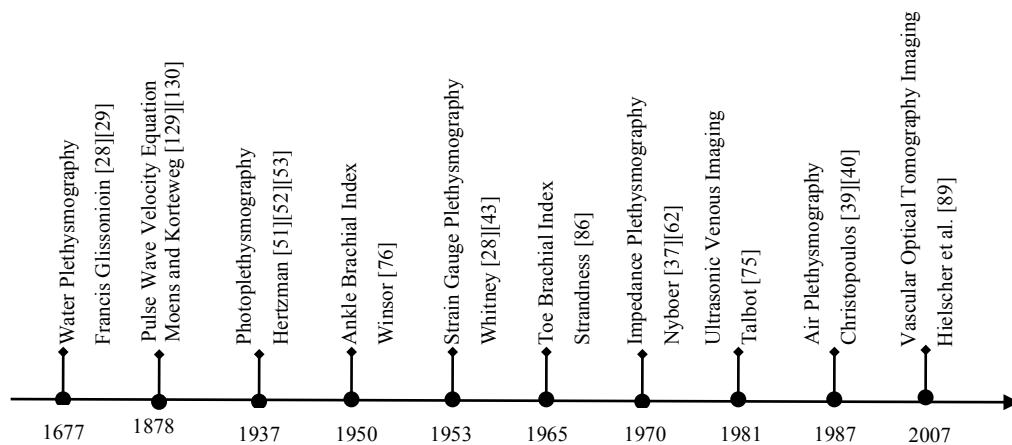


Figure 1. 4. Advent of milestone technologies for non-invasive diagnosis of PVDs

Plethysmographic methods have the best utility to detect both arterial and venous disease including occlusions, chronic venous insufficiency and deep vein thrombosis. However, plethysmography devices are cumbersome and require a highly trained practitioner limiting their use. Plethysmography assessment also takes a considerable amount of time to complete, and typically lacks the potential to localize the site of stenosis/occlusion.

Doppler methods can provide information about the location of vascular dysfunction. Duplex ultrasound is the gold standard method for PVD diagnosis and is the most sensitive non-invasive method that currently exists. However, similar to plethysmographic techniques, expensive equipment and highly trained practitioners are required. Also, Doppler vascular assessment is even more time consuming than plethysmography. As such plethysmography and Doppler methods have limited use for PVD screening or everyday use in the clinic.

In contrast, ABI is relatively simple, fast and cheap and is recommended as an initial diagnostic tool in primary care, however it has poor sensitivity in patients with calcified arteries. Similar to plethysmography, ABI lacks localization capability. Other versions of brachial methods, such as the segmental blood pressure measurement, can assist pathology localization and toe brachial methods can counter medial artery calcification, increasing specificity for people with PAD and diabetes. However, segmental pressure measurement is not reliable and the toe brachial index requires more time than an ABI, and specific environmental conditions.

Many non-invasive methods have been developed to aid the diagnosis of PVDs. However, given the rising number of patients with PVD and the shortcomings of current methods, there is still a need for new non-invasive diagnostic tools. The continuous effort for proposing non-invasive techniques for diagnosis of PVDs over more than three hundred years further highlights the need for developing new diagnostic techniques. While Duplex ultrasound and plethysmography can be excellent means of PVD diagnosis, training requirements limit their more widespread use. Any potential alternative should be intuitive and simple to use, minimizing these training requirements. The high cost of Doppler ultrasound and plethysmography devices is another hurdle against their availability. While asymptomatic patients are also at high risk of morbidity/mortality, the time and cost of such diagnostic methods typically limits their use for symptomatic patients. Ideally, a new solution should provide an early diagnosis of both arterial and venous diseases accurately, easily, cheaply, quickly and without extensive training.

### **1.3 HeMo**

Recently, the use of polymer-based sensors has shown potential for diagnosis of PVDs. Such sensors basically consist of two main components, a highly elastic polymer carrier (e.g. rubber) and an integrated conductive element (e.g. carbon). Typically, deformation of the sensor generates proportional changes in the impedance of the sensor.

Boland et al. introduced two new polymer-based sensors, one created by infusing exfoliated graphene into natural rubber [172] and another, G-putty, made by adding graphene to commercially available silicon polymer (Silly Putty, Crayola, Easton, PA) [173]. Both of these sensors are highly stretchable and capable of capturing arterial pulse waves [172,173]. These graphene polymer composites are low cost and can provide high sensitivity and extensibility (performance beyond 800% strain) [172]. However, neither the graphene-rubber strain sensor nor G-putty is yet commercially available.

In 2014 Breen et al., researchers at the MARCS Institute, used commercially available Conductive Rubber Cord Stretch Sensors (available from Adafruit, NY, USA), also known as Electro Resistive Bands (ERB), to visualize peripheral blood flow [33]. The carbon-black

impregnated rubber ERB sensors, have fixed resistance at rest, with impedance increasing when stretched. The ERB sensors were incorporated in a stretchable piece of fabric to build a novel hemodynamic monitoring device, HeMo. The initial design and testing of HeMo showed its potential for monitoring blood volume changes in the leg, which could potentially be used as measure for diagnosis of peripheral vascular diseases.

## 1.4 Research Aims

The development and validation of any new medical device begins with understanding user needs and then designing a device to meet these needs. User needs are reduced to a set of design inputs, which for the most part describe technical requirements of the device. The design process involves capturing the outputs of design and verifying these meets the device requirements and design inputs. A higher-level validation of the device follows, determining if the medical device meets user needs entirely. The work presented in this thesis is not produced within the framework of a medical device quality management system. However, the research in this thesis investigates several hypotheses to provide a proof of concept and to discover if HeMo is even reasonable prospect.

This thesis investigates the following research hypotheses/questions, which are in fact a set of requirements for the development of HeMo as a new medical device.

- HeMo can measure venous refilling time and provide information about venous competence in the lower leg (Chapter 2 and 4).
- HeMo can reliably capture arterial pulse waves and provide information about arterial function in the lower leg (Chapter 2 and 5).
- The electro-resistive bands used in HeMo have sufficient reliability over time and linearity making them suitable for wearable measurement functions over time (Chapter 3).
- There is an agreement between HeMo and light reflection rheography in measurement of venous filling in healthy volunteers (Chapter 4).
- Exercise has minimal impact on HeMo venous filling measurements (Chapter 4).

- There is an agreement in arterial pulse wave morphology between HeMo and photoplethysmography recordings in healthy volunteers (Chapter 5).
- Exercise has a minimal effect on HeMo arterial pulse wave recordings (Chapter 5).

Overall, the purpose of this research is to step towards providing an intuitive and user-friendly version of the HeMo device for clinical use and validate its performance for the assessment of peripheral vascular diseases. In a similar fashion to how the sphygmomanometer changed the diagnosis and treatment of hypertensive disease by providing a simple means of measuring blood pressure, it is hoped that the results of this research can lead to a similar result for peripheral vascular diseases.

## 1.5 List of Publications

The work presented in this thesis has resulted in two first-author journal articles and three conference papers. A further two research papers comparing HeMo and VasoScreen are in preparation. These publications [174–179] are listed below.

1. Gaetano D. Gargiulo, **Elham Shabani Varaki**, Tara J. Hamilton, Paolo Bifulco, Mario Cesarelli, Maria Romano. A 9-independent-leads ECG system from 10 electrodes: A practice preserving WCT-less true unipolar ECG system. IEEE Biomedical Circuits and Systems Conference; 2015. p. 1–4.

2. **Elham Shabani Varaki**, Paul P. Breen, Gaetano D. Gargiulo. HeMo: Towards an inexpensive wearable peripheral blood flow monitoring device. IEEE Biomedical Circuits and Systems Conference; 2015. p. 1–4.

*Awarded IEEE CAS Charles Desoer Life Science Systems Student Grant, IEEE Biomedical Circuits and Systems Conference 2015, Atlanta, USA.*

3. **Elham Shabani Varaki**, Gaetano D. Gargiulo, Paul P. Breen. Towards Low-Cost Non-Invasive Assessment of Peripheral Vascular Function. Presented at Cardiac Society of Australia and New Zealand Conference, Published in Heart, Lung and Circulation Journal. 2016; 25:S23–S24.

*Awarded Best Commercialization Idea Prize from Capital Markets Cooperative Research Centre, Western Sydney University HDR Showcase 2016, Sydney, Australia*

*Awarded Best Commercialization Idea Prize from Capital Markets Cooperative Research Centre, Western Sydney University HDR Showcase 2017, Sydney, Australia*

4. Gaetano D.Gargiulo, Upul Gunawardana, Aiden O’Loughlin, Mohammad Sadozai, **Elham Shabani Varaki**, and Paul P. Breen. A Wearable Contactless Sensor Suitable for Continuous Simultaneous Monitoring of Respiration and Cardiac Activity. *Journal of Sensors*. 2015; 2015:1–6.

5. **Elham Shabani Varaki**, Paul P. Breen, Gaetano D. Gargiulo. Quantification of a Low-Cost Stretchable Conductive Sensor Using an Expansion/Contraction Simulator Machine: A Step towards Validation of a Non-invasive Cardiac and Respiration Monitoring Prototype. *Machines Journal*. 2017; 5: 22.

6. **Elham Shabani Varaki**, Gaetano D. Gargiulo, Paul P. Breen, Quantification of a Wearable Contactless Sensor Using an Expansion/Contraction Simulator Rig, *International Conference of the IEEE Engineering in Medicine and Biology Society*. 2017.

7. **Elham Shabani Varaki**, Gaetano D. Gargiulo, Stefania Penkala, Paul P. Breen. Peripheral vascular disease assessment in the lower limb: a review of current and emerging non-invasive diagnostic methods. *Biomedical Engineering Online Journal*. 2018;17:61.

## **1.6 Thesis Organization**

*Chapter 1* of the presented thesis provides a comprehensive literature review of the existing non-invasive diagnostic devices developed since 1677. This chapter is formatted as a review article, and has been peer-reviewed and published in *Biomedical Engineering OnLine journal*.

*Chapter 2* discusses the simplified circuit of the HeMo device, and presents pilot data demonstrating the potential of HeMo for diagnosis of peripheral arterial disease and chronic venous insufficiency. Chapter 2 is a combination of two peer-reviewed conference papers.

**Chapter 3** presents characterisation of electro-resistive band sensor behaviour during contraction and expansion. A reformatted version of this chapter is also peer-reviewed and published in the journal *Machines*.

**Chapter 4** presents data from a healthy population, assessing the performance of HeMo compared to light reflection rheography (LRR sensor-VasoScreen 5000) for the assessment of venous function.

**Chapter 5** presents human study data where the performance of HeMo is compared to photo plethysmography (PPG sensor-VasoScreen 5000) for the assessment of arterial function.

**Chapter 6** concludes the thesis by discussing future directions and the overall contribution of the research.

**Appendix A** provides matlab scripts of the graphic user interfaces developed for venous and arterial assessment associating with their corresponding user guidelines.

## Chapter 2 Pilot Assessment of HeMo

This chapter introduces the HeMo device in detail and demonstrates its potential for the diagnosis of peripheral arterial disease and chronic venous insufficiency. First, it provides a brief background, restating the motivation behind the development of HeMo. It then presents the specification of a simplified HeMo embodiment. The remainder of the chapter illustrates a series of experiments that demonstrate the potential of HeMo for assessment of both arterial and venous function.

*Some of the work presented in this chapter has been published in:*

*Shabani Varaki E, Breen PP, Gargiulo GD. HeMo: Towards an inexpensive wearable peripheral blood flow monitoring device. 2015 IEEE Biomed Circuits Syst Conf. IEEE; 2015. p. 1–4.”*

*“Shabani Varaki E, Gargiulo G, Breen P. Towards Low-Cost Non-Invasive Assessment of Peripheral Vascular Function. Hear Lung Circ. Australasian Society of Cardiac and Thoracic Surgeons and The Cardiac Society of Australia and New Zealand; 2016;25:S23-4.”*

## 2.1 Background

Peripheral vascular diseases (PVDs) such as peripheral arterial disease (PAD), chronic venous insufficiency (CVI), and deep vein thrombosis (DVT) are highly prevalent and often go undiagnosed with more than 50% of patients with PAD being asymptomatic [28,180]. Although a variety of techniques are available for the diagnosis of PVDs, some of the existing methods are highly invasive while others require highly skilled operators and expensive equipment. Therefore, there is a need for a new method of PVD diagnosis, ideally one that is non-invasive, fast, cheap and easy to use.

In order to diagnose PVDs, a number of non-invasive tools have been developed (see Chapter 1). For example, the Ankle-Brachial Index (ABI) is a simple non-invasive measure of peripheral arterial perfusion and is measured by dividing the ankle blood pressure by the higher of two brachial pressure [28]. However, ABI measurement may take up to 15 minutes to complete [183] and an additionally 30 minutes rest before the test may be required [60]. Moreover, it has been argued that the ABI may appear normal or even supernormal for patients with diabetes, renal disease or the elderly whose arteries are thickened [28].

Plethysmography is also a non-invasive technique for the evaluation of peripheral vascular competence. Several different types of plethysmography devices exist; impedance, photo, strain gauge and air plethysmography have all been utilized to measure blood flow changes [180]. Plethysmography measures venous and arterial function [39], and as Harada has reported [184], the venous filling index measured by plethysmography has a 100% positive predictive value of diagnosing venous insufficiency. Furthermore, Anderson has argued [40] that impedance plethysmography has a sensitivity and specificity of more than 90% for arterial disease diagnosis. Nevertheless, current embodiments of plethysmography are cumbersome, time consuming and require highly trained practitioners [185], factors that have limited their adoption in clinical practice.

Another non-invasive method for PVD diagnosis is duplex ultrasonography (DU) which allows the anatomy and functionality of vascular system to be defined [186]. DU is a highly sensitive diagnostic tool [87], and it is capable of providing information about the site and

extent of deep vein thrombosis or venous reflux [98]. However, a DU examination takes approximately 45 minutes and the quality of the test results are dependent on operator experience [181], [187]. Some patients cannot undergo DU due to leg swelling, ulceration, pain or heavily calcified arteries [3]. Moreover, DU is an expensive test and in practice is reserved for patients with clear symptoms [180].

A new non-invasive blood flow monitoring technique is required to overcome the limitations of the existing methods. Breen et al. previously reported the development of an inexpensive, wearable, user-friendly device called HeMo for evaluating the peripheral blood flow monitoring non-invasively [33].

In simple terms, the shape of the arterial pulse is a guide to peripheral arterial disease (PAD) diagnosis [185]. A normal arterial pulse wave (Figure 2.1) has a steep upslope, a relatively narrow peak, and a dicrotic notch on the downslope [185]. Any arterial incompetence such as stenosis or occlusion affects arterial pulsation, so PAD can be detected by comparing the arterial pulse waveform of a patient with a grading system [192]. Progress of PAD is evidenced by the disappearance of the dicrotic notch, dampening the wave amplitude and flattening the systolic peak. Threshold values for maximum systolic slope and arterial pulse amplitude exist which may also be used in combination with the HeMo device and which have a reported sensitivity and specificity of more than 90% [40].

To assess venous competence in the lower limb venous Filling Index (VFI) is usually measured and compared to threshold values. The VFI is a parameter, which is defined as 90% of the venous volume at rest divided by the time required for venous refilling to 90% of resting volume after returning to the standing position [8]. A simple manoeuvre is required to measure the VFI. First, the resting venous volume is measured in the standing position. Second, the patient's leg is elevated while supine to reach minimum venous volume. Then, the patient is asked to resume to the upright position. A VFI of less than 2 ml/s is inferred as normal, while presence of venous reflux is evidenced by higher VFI values of 2-7 ml/s [39,184]. A VFI > 7ml/s has been reported to have a 100% positive predictive value for critical venous reflux diagnosis [184]. Similar to VFI, Venous Filling Time (VFT) is also a parameter that is used to assess venous competence in the lower limb. A VFT greater than 20

seconds is reported to represent normal venous function, VFT values less than 20 seconds infer chronic venous insufficiency [49,193].

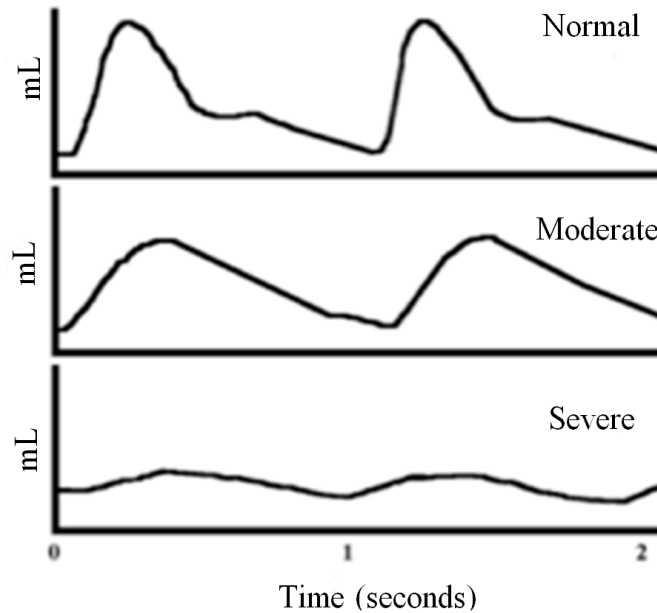


Figure 2. 1. Typical arterial pulse volume waveforms from normal healthy, moderate and severe peripheral arterial disease, adapted from [20].

In the next section, the HeMo device and its simplified circuit are fully described. Then the following sections investigate if HeMo can reliably capture arterial pulse wave and if HeMo can measure venous filling index/time. The work presented in this chapter is a proof of concept as it is the first use of the HeMo device in comparison with validated sensors, which can provide similar information.

## 2.2 HeMo System Design

HeMo is a wearable contactless device (instrumented cuff) worn around the limb (Figure 2.2) and capable of measuring blood volume changes in the limb. The principle of operation is that changes in the blood volume of the limb induce similar changes to the circumference of the cuff. This is captured through measurement of changes in the voltage across the polarised electro-resistive bands (ERBs). Using a calibration equation derived against three known volumes by interpolation, the output signal is translated into blood volume in ml. HeMo is

designed to be unobtrusive and its compression upon the limb is negligible. As a result it may be worn for days without affecting daily routines or activities.

The previous version of HeMo combined volumetric measurements derived from electro-resistive bands worn around the limb with electrical impedance tomography provided by a ring of electrodes worn around the limb in the same region. The previous design incorporated electro-resistive bands and electrodes locating on the lower leg, and accelerometers at the shank and thigh to enable movement detection [33]. Prior development was limited as it only enabled detection of changes in peripheral blood volume with the changes in posture.

In the development of this technology it was discovered that, with an appropriate amplifier arrangement, very small fluctuations in limb volume could be detected using the electro-resistive bands alone. Here, we introduce this new simplified version of the HeMo device in which impedance measurement is excluded.

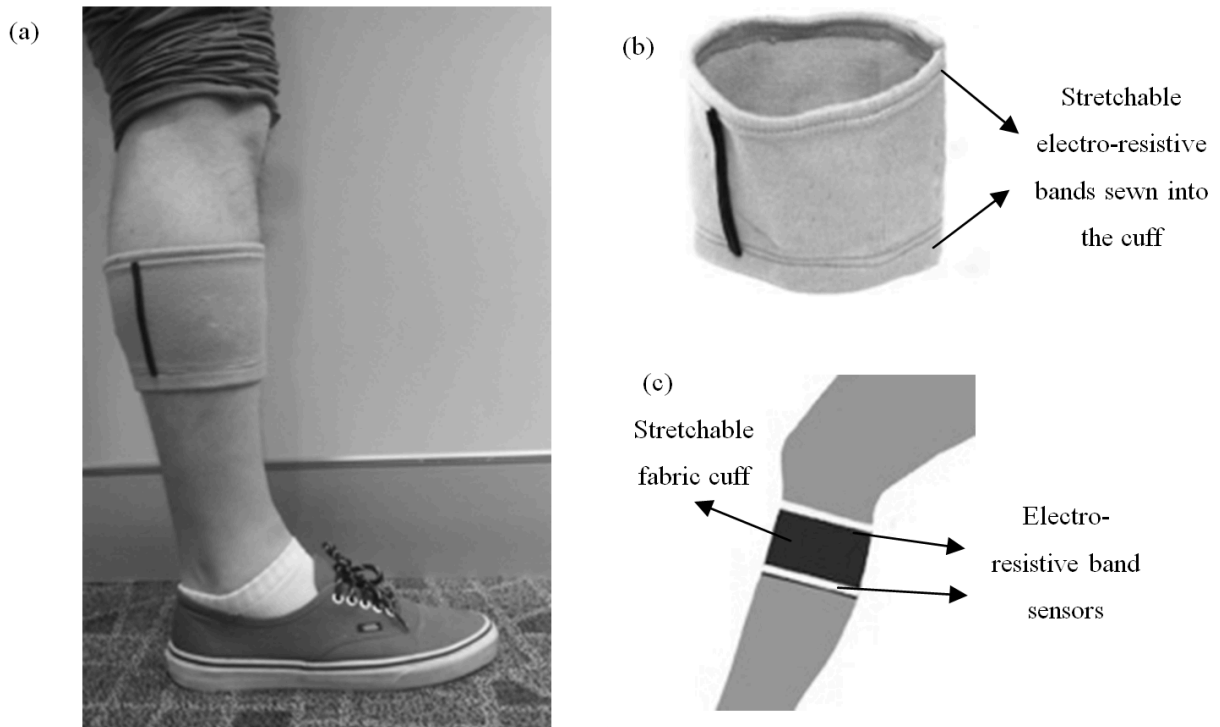


Figure 2. 2. HeMo prototype; (a) A demonstration of HeMo worn on the calf [33]; (b) HeMo cuff (adopted from [33]); (c) Diagram of HeMo worn on the calf (adopted from [33]).

Similar to the previous version, this device incorporates a pair of electro-resistive stretchable bands in a wearable cuff (Figure 2.2). In conjunction with amplification and filtering this wearable, electrode-less system may be used to non-invasively monitor blood volume shifts due to postural changes and arterial inflow into the limb.

The simplified version of HeMo integrates two electro resistive bands made of carbon-black impregnated rubber with a resistance of  $\sim 150$  ohms/cm at rest. The bands are sewn into the top and bottom of a stretchable fabric cuff (Figure 2.2). The electrical block diagram of the circuit is shown in Figure 2.3.

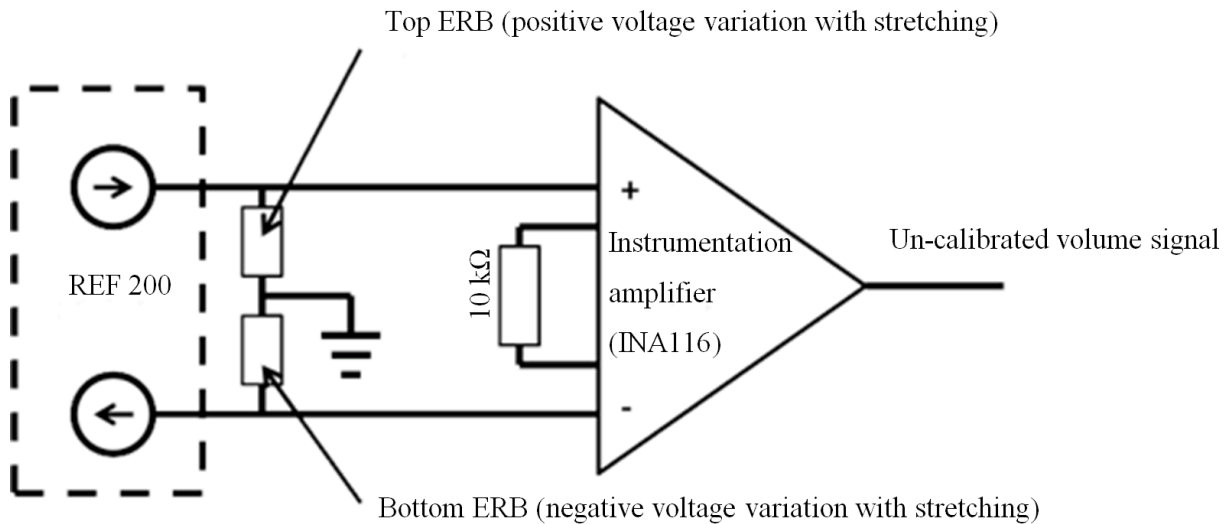


Figure 2.3. ERB front-end block diagram.

The new electro-resistive band (ERB) front-end circuitry is low power, with a measured current consumption of  $1100 \mu\text{A}$  when powered at  $4.5 \text{ V}$ , compared to  $\sim 2.5 \text{ mA}$  in the previous version. It employs only three commercial microchips and can be assembled onto a  $4 \text{ cm}^2$  double-sided PCB (see Figure 2.4).

Similarly to the previous design [1], ERBs are polarized using a small DC current. The required DC current is achieved using the REF200 by TI [188]. Having only two ERBs,

contrary to the previous designs which required adjustable current levels [189], one single REF200 contains two independent  $100\ \mu\text{A}$  current generators which can be used to independently polarize both ERBs. Although HeMo is contactless (the ERBs are assembled on the outside of the cuff), the design is micro-shock safe [190] with the largest DC current that can flow through the body of the patient or operator being  $200\ \mu\text{A}$ .

Summation of the ERB voltages is achieved directly by the analogue circuits using a true differential amplifier (INA116 by TI [191]). In order to achieve summation and not subtraction of voltages, the current was forced through the ERB connected to the inverting input such that it generates a negative voltage with respect to the signal ground. Negative voltage compliance for the current generators is achieved using an isolated DC-DC converter module (DHC10512D by TI) which generates a dual unregulated power supply of up to  $\pm 14\ \text{V}$  from a single power supply of  $4.5\ \text{V}$  ( $5\ \text{V}$  power supply nominal specification). For this application HeMo was powered using the  $5\ \text{V}$  output of the National Instruments NI6009 that was also employed to acquire the data. Although the signal output of the INA116 does not require amplification, in order to accommodate the low dynamic range of the ADC used during our tests (14 bit,  $\pm 5\ \text{V}$ ), a gain of  $6\ \text{V/V}$  is achieved using a single  $10\text{-k}\Omega$  resistor connected between pins 1 and 8 of the INA116.

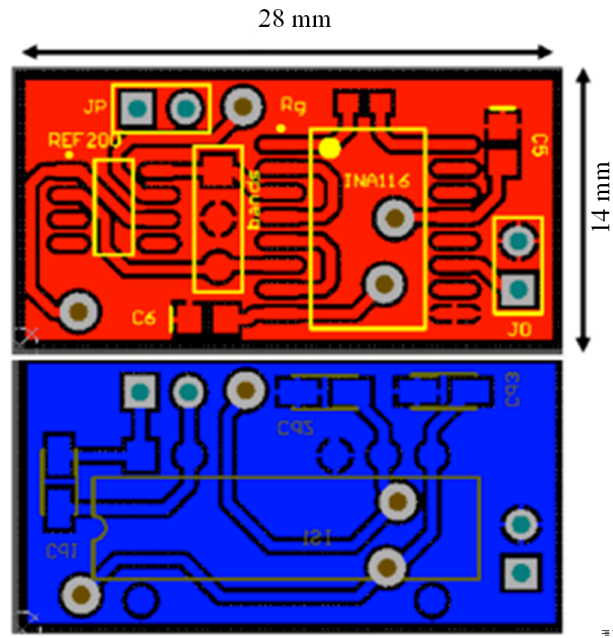


Figure 2. 4. PCB views (not to scale), top layer (red) and bottom layer (blue). Power is supplied via connector JP, signal is presented at connector JO.

The net blood volume inflow is extracted from the raw volume signal using an amplitude compensated software (MATLAB) high-pass IIR filter (50th order) with a cut off frequency at 0.3 Hz. The filter is designed to remove the large DC component due to the large volume of the limb under examination (hundreds of ml) and also removes some unwanted trends in volume due to slow filling of other fluids or relaxation of the muscle due to particular postures (e.g. leg elevated above the heart).

## 2.3 Description of use

To investigate the potential of HeMo for arterial and venous assessment, a healthy volunteer participated in a series of experiments and data were recorded while the volunteer was barefoot and wearing shorts. Two experiments were performed to investigate the potential of HeMo in arterial assessment and two other experiments were performed for investigation of venous assessment with HeMo. To record data from HeMo, the fabric cuff is simply worn around the leg and changes in blood volume in the leg can be recorded. Either postural changes, movement and arterial inflow can induce variations in the inscribed volume of the

HeMo cuff resulting in changes to the length the ERB sensors and so the voltage across the sensor.

Arterial assessment was performed while the subject was sitting relaxed on a chair, HeMo was worn on the leg and a piezo-based pulse sensor was placed on the toe and data were recorded from both simultaneously. In a similar manner and for the same subject, HeMo recording was also compared with a recording from a clinically validated photoplethysmography sensor.

The volume variations due to postural changes were tracked to provide the venous assessment. Data from the volunteer was recorded in multiple positions (standing, lying down with the leg elevated) to measure VFI. Another experiment was done in which the same volunteer was sitting on a chair with HeMo on the leg and a light reflection rheography sensor placed on the inner side of the leg below the HeMo cuff. Data from both HeMo and a clinically validated sensor, light reflection rheography, were recorded simultaneously before, during and after ten consecutive dorsiflexion manoeuvres to compare VFT values measured with HeMo and light reflection rheography.

The experiments for capturing the arterial pulse wave and measurement of VFI/VFT are fully described in the following sections.

## **2.4 Pilot Experiment 1: Measuring the Arterial Pulse Wave**

Arterial data was captured using a toe-worn MP100 pulse transducer from AD Instruments while HeMo simultaneously collected data from the calf of the same limb of a healthy volunteer with no history of peripheral vascular diseases.

A comparison of lower limb arterial inflow as simultaneously measured by a toe-worn pulse transducer and the calf-worn HeMo device is shown in Figure 2.5. A small phase difference is evident between the two recordings; this delay is due to the fact that the HeMo device tracks volume changes while the piezo based pulse transducer is acceleration sensitive. Furthermore, each transducer captured the arterial pulse at different sections of the lower limb.

A dicrotic notch is clearly visible in the HeMo recording (Figure 2.5) indicating a normal healthy arterial system. Additionally, it should be noted that the recorded data using HeMo is calibrated in ml. This capability would potentially allow HeMo to track arterial disease progression or treatment at different time points.

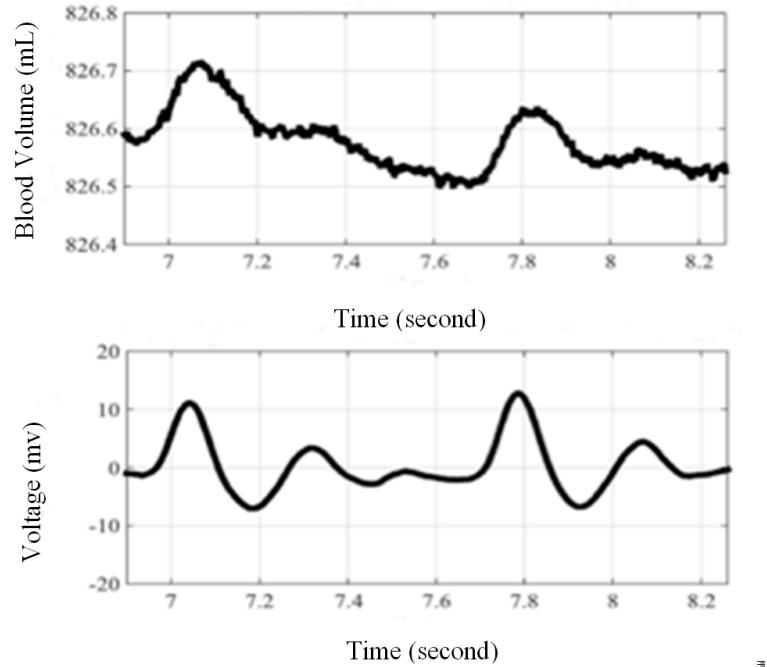


Figure 2. 2. Arterial pulse wave comparison; Top: Arterial pulse recorded by HeMo (raw data): Bottom: MP100 pulse piezoelectric transducer.

## 2.5 Pilot Experiment 2: Comparison to Photoplethysmography

In a second evaluation to investigate the potential of HeMo for arterial assessment, a healthy volunteer with no history of peripheral vascular disease sat upright in a chair while HeMo was worn on the thickest part of the calf. A photoplethysmography sensor (PPG, VasoScreen 5000, Medis) was placed on the subject’s big toe of the same leg. With this setting, we were able to record the arterial pulse wave from HeMo and PPG simultaneously.

A comparison of arterial pulse wave in the lower limb, simultaneously measured by the PPG sensor and the HeMo device is shown in Figure 2.6. A small phase difference is evident

between the two recordings, as each sensor captured the arterial pulse at different sections of the lower limb.

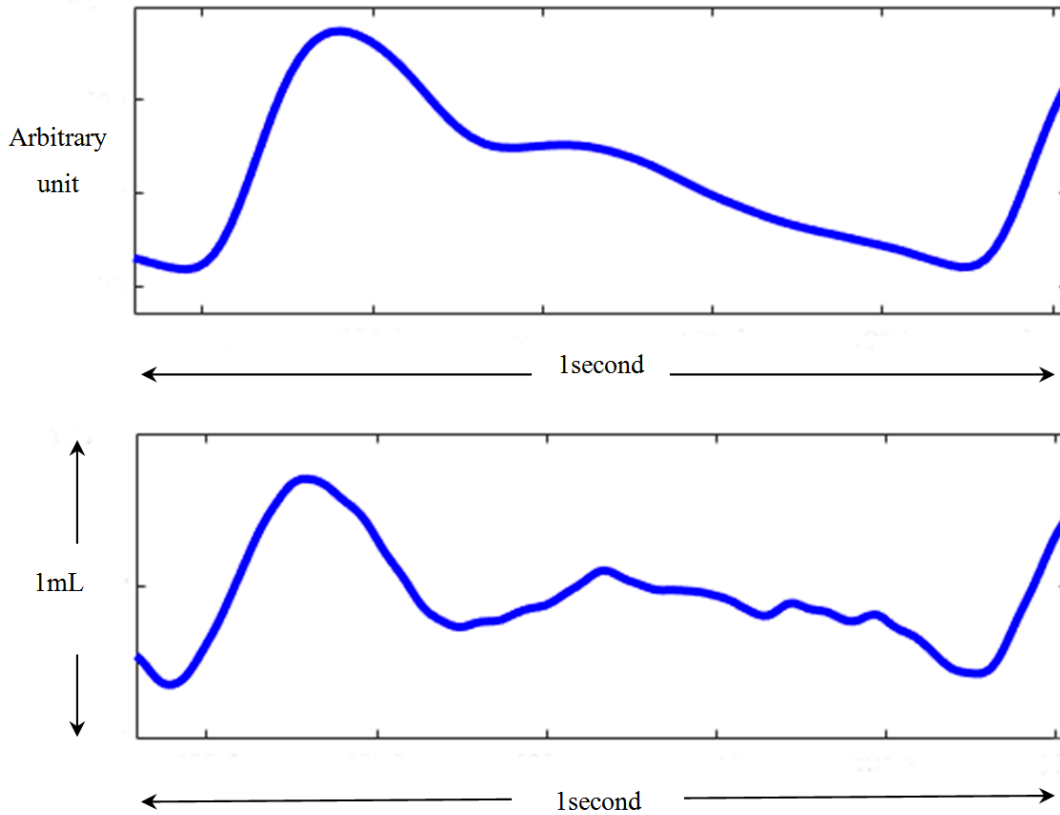


Figure 2. 3. Arterial Pulse wave recording; Top: recorded with PPG; Bottom: recorded with HeMo.

Again, the dicrotic notch is clearly visible with both systems, indicating a healthy arterial system at a cursory level. Moreover, it should be noted that while the recording from photoplethysmography has an arbitrary unit, the HeMo recording can be calibrated in ml.

In a further extension of this work, ten tiptoe manoeuvres were performed while HeMo recorded changes in arterial inflow. Figure 2.7 presents the calibrated data before, during and after the ten tiptoe manoeuvres. The arterial pulse shape changes noticeably following the brief exercise and the pulse volume increases substantially. Data in insets have been extracted using software filters.

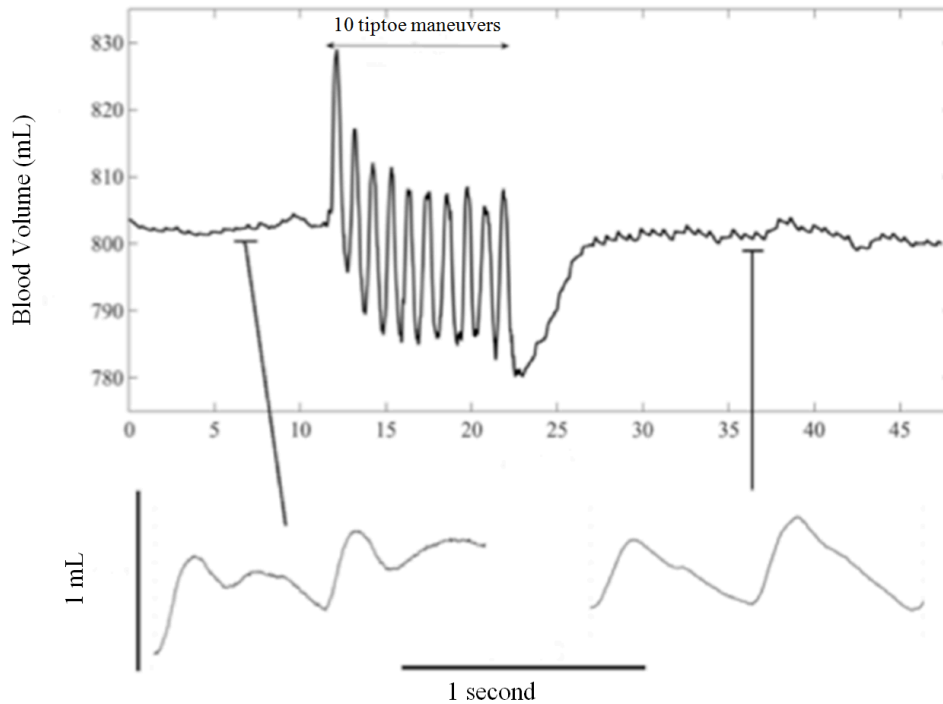


Figure 2. 4. Blood flow variations before (lower left inset), during and after ten tiptoes (lower right inset).

## 2.6 Pilot Experiment 3: Measuring Venous Filling Index

VFI can be easily measured using the HeMo device. The calf volume is measured at rest, with the leg elevated and again in the standing position, using the output voltage of HeMo circuitry and the calibration equation derived from the corresponding output voltages of HeMo when it was placed around three known volumes. After the leg elevation manoeuvre, the time required to reach 90% of the initial venous volume is calculated to find the VFI.

The venous filling index was calculated as described for a healthy volunteer with no history of peripheral vascular disease and it is shown in Figure 2.7. Following venous emptying via leg elevation, the time taken to reach 90% of standing limb volume was calculated. From this data the VFI was easily calculated. In this case it was found to be 0.6 ml/s, which would be classed as normal.

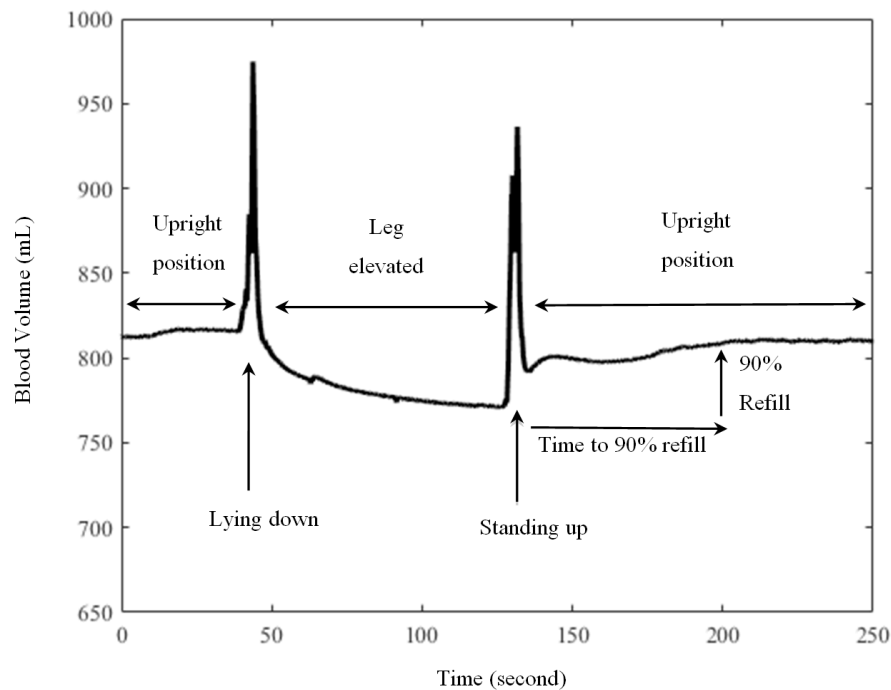


Figure 2. 5. Venous Filling Index (VFI) measurement using HeMo.

## 2.7 Pilot Experiment 4: Comparison to Light Reflection Rheography

The experiments presented in sections 2.5 and 2.6 demonstrated that HeMo is capable of measuring dynamic blood volume shifts due to both postural changes, and arterial inflow into the limb. This experiment compares the performance of HeMo versus a clinically validated device for the assessment of venous refilling using light reflection rheography (VasoScreen 5000, Medis Medizinische Messtechnik GmbH, Ilmenau, Germany).

To examine the capability of HeMo for assessing venous functionality, venous filling time (VFT) measured simultaneously by HeMo and light reflection rheography (LRR) were compared. VFT is defined as the time required for venous filling after exercise [59].

To measure VFT with HeMo and LRR, a healthy volunteer with no history of peripheral vascular disease was asked to sit on a chair and wear HeMo on the thickest part of the calf. The LRR sensor was placed on the inner side of the same leg and about 10 cm above

malleolus as described in the LRR device manual, a small distance below HeMo. The subject was asked to follow ten metronome sounds, which were generated by the reference device, and perform ten consecutive dorsiflexion manoeuvres.

Venous filling simultaneously recorded by HeMo and LRR is shown Figure 2.9. Following venous emptying via repeated dorsiflexion, the venous filling time was calculated from the recorded data. Both devices were closely matched with a calculated venous filling time of approximately 45 seconds indicating normal venous function.

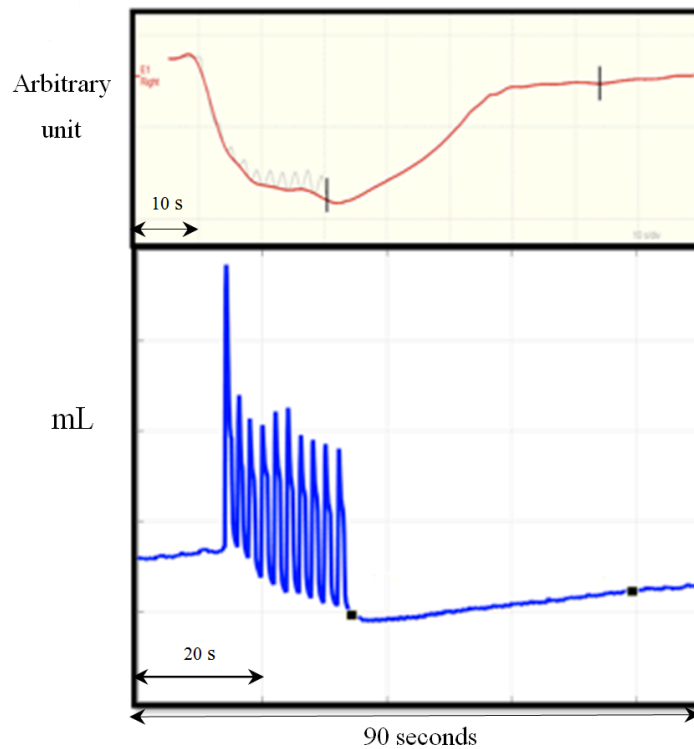


Figure 2. 6. Venous filling time measurement; (a) is recorded with LRR sensor; (b) is recorded with HeMo.

## 2.8 Conclusion

While a previously developed HeMo embodiment for non-invasive monitoring of peripheral blood flow used electrical impedance measurements, in this chapter, a simplified version is presented which is more wearable, easier to use and cheaper to build [33]. As a result, we have a simplified system, which is still capable of measuring dynamic changes in limb blood

volume. The results presented in this chapter also show the sensitivity of HeMo to blood volume fluctuations due to arterial inflow, postural changes and following dorsiflexion.

These pilot comparisons between HeMo and a piezo pulse transducer, photoplethysmography and light reflection rheography in healthy volunteers allowed us to rapidly assess if this embodiment of HeMo is capable in providing the required information for the assessment of arterial and venous perfusion in the lower limb. These preliminary comparisons demonstrated that HeMo measurements and those from validated clinical sensors match closely, proving the concept to be valid. This justified further development and investigations in a larger population.

However, it should be noted that at this point, the electrical behaviour of the electro-resistive band sensors during expansion and contraction is not fully known. In the next chapter, this issue is addressed, presenting an expansion/contraction simulator machine, which enables investigating of the electrical behaviour of the electro-resistive sensors for a range of expansion/contraction frequencies. Using the data collected from this rig we provide characterisation of the electro-resistive band sensors.

## **Chapter 3 Characterisation of Electro-Resistive Band Sensors**

This chapter provides the characterisation of electro-resistive band behaviour during expansion and contraction. First, a brief background, introduces different stretchable electro-resistive band sensors. It then introduces a custom test rig, developed to provide continuous expansion and contraction of the electro-resistive band sensor. Data analysis methods are presented and followed by results quantifying the behaviour of the electro-resistive band sensors. Finally, a discussion is provided to highlight the benefits and limitations of the work described in this chapter.

*Some of the work presented in this chapter has been published in:*

*Elham Shabani Varaki, Paul P. Breen, Gaetano D. Gargiulo. Quantification of a Low-Cost Stretchable Conductive Sensor Using an Expansion/Contraction Simulator Machine: A Step towards Validation of a Non-invasive Cardiac and Respiration Monitoring Prototype. Machines Journal. 2017; 5: 22.*

### 3.1 Background

Wearable sensors have recently attracted a lot of attention as their deployment in biomedical applications has generated new possibilities for health monitoring, treatment assessment, early detection of health disorders, prevention of their complications and ultimately reducing health care costs [194,195].

While traditional health care systems are often limited to use within the clinical environment, wearable sensors can be embedded in ordinary clothing enabling convenient, low-cost implementations in the home and community settings [196]. Stretchable electro-resistive sensors have shown potential for use as wearable strain sensors fulfilling the requirements of future technology, particularly in the monitoring of human activity and personal healthcare [197,198]. Consequently, a great deal of effort has been recently dedicated to the development and characterisation of such sensors. Generally, stretchable electro-resistive sensors incorporate two main components, an integrated conductive component (e.g. carbon-black, graphene, nanowires) and a flexible support material (e.g. silicon-based elastomers, rubber-based elastomers) [197]. These sensors operate through their mechanical deformation, inducing changes in the resistance of the sensor, which ultimately can be monitored as an electrical signal [197]. However, these sensors may respond differently depending on their material and fabrication. For example, stretchable electro-resistive sensors have a diverse range of gauge factors varying by orders of magnitude i.e. 1 [199–202], 10 [172,201,203–206], 100 [207–209], 1000 [210] and up to 1000000 [211]. Other characteristics such as the linearity, hysteresis, and frequency response of the stretchable electro-resistive sensors may also vary from one to another. A careful understanding of these characteristics is crucial for appropriate use of such sensors. For instance, nonlinearity of the sensor may result in requirement of a more complicated calibration process [197]. Two recent reviews have included highly informative details in regards to the performance and applications of different stretchable electro-resistive strain sensors [197,198]. According to the existing literature, several of the recently introduced stretchable sensors can be used for different health monitoring application. For instance, Yamada et al. reported stretchable electro-resistive carbon nanotube sensors which could be used either on skin or clothing such as stockings,

bandages, gloves to detect various types of motions including limb movement, breathing, and speech [199]. Amjadi et al. also reported a highly stretchable electro-resistive sensor made up of silver nanowire and a silicon-based organic polymer (Polydimethylsiloxane) and demonstrated that the sensor could be used in finger motion detection [201]. Blond et al introduced graphene rubber electro-resistive sensors and demonstrated the potential of this sensor in the detection of finger/forearm movement, speech and monitoring of heart rate, breathing and arterial pulse [173]. Stretchable electro-resistive sensors can be used on skin and or clothing providing ubiquitous use and in a wide range of applications. Therefore, many more stretchable electro-resistive have been reported [197,198]. However, these sensors have only recently been developed, and many are not yet commercially available.

Commercially available Conductive Rubber Cord Stretch Sensors, also known as Electro-Resistive Band (ERB) sensors, are normally used for robotic applications and more recently, they have been used as wearable sensors to capture a range of bio-signals [174,175,178,180,189]. The ERB sensors (available from Adafruit, NY, USA) are made of highly elastic carbon-black impregnated rubber and are sold with a length of 1 m and a thickness of 2 mm. The ERBs have a defined resistance at rest ( $\sim 15$  ohms/cm) and their resistance increases as they are stretched. These sensors are cheap, waterproof and are easily sewn into fabric, making them ideal for use as wearable sensors, e.g. embedded in a T-shirt or knee support [175,178]. This chapter focuses on the quantification of the ERB sensors.

The ERB sensors were originally created as electromagnetic field (EMF) gaskets and have been used as displacement sensors in robotic applications [212]. More recently, these sensors have been exploited in several prototype devices with the intention of measuring cardiac stroke volume, respiration tidal volume [178,189], and changes in peripheral blood flow [174,175,180]. This previous work provided some promising results suggesting that these low-cost ERBs were capable of providing valuable clinical information and could lead to a viable solution for continuous and non-invasive measurement of respiration, cardiac function, and peripheral vascular competence. However, characterisation of ERB sensors is necessary to provide a precise pre-calibration of the sensor and/or appropriate post-hoc analysis of the data generated. Investigation of the sensor behaviour during expansion and contraction is a prerequisite to compensate for possible nonlinearities, which may be detrimental to accuracy

and performance. More generally, there is a need for careful quantification of these ERB sensors to fully understand their characteristics and define the possible biases and error that may be associated with their use. This characterisation will be of interest to other users and developers incorporating this type of sensor into their devices.

In the work presented here, an expansion/contraction rig that repeatedly stretches the ERB sensors is described. These bands were tested continuously over the course of four and half days and compared the measurements to a string potentiometer. Our aim was to capture sufficient data from the ERBs over time, compare these to a gold standard measurement and determine if it may be possible to compensate for the predicted non-linearity of the ERBs system.

## **3.2 Methods**

### **3.2.1 Expansion/Contraction Simulator Machine**

In order to investigate the existence of possible nonlinear characteristics of the ERB sensor, a commercially available linear displacement sensor, a string potentiometer (SP), was used as a comparison reference. To have a more informative comparison between the ERB and the SP, simultaneous expansion and contraction of both sensors was required over an extended period of time. Therefore, a rig was developed to enable simultaneous expansion/contraction of both sensors.

This rig was formed on a platform mounted with a DC gear motor (JGY-370-12 v-12 RPM, ASLONG, Shenzhen, China), rotary encoder (E6B2-CWZ6C, OMRON, Osaka, Japan) and string potentiometer (SP1-4, Celesco) with a full stroke range of 120 mm (Figure 3.1). To capture motor position, the rotary encoder and motor were linked together to using a 1:1 timing belt. A metal arm was attached to the shaft of the DC motor. Two pulleys were used to connect the metal arm to the SP and the ERB independently, enabling a smooth periodic expansion/contraction (Figure 3.1). Using this system, the ERB and the SP sensors were expanded when the metal arm reached position (a) and the sensors were fully contracted when the metal arm reached position (b). Therefore, the rotary motion of the metal arm

resulted in sinusoidal stretching pattern for both sensors. Of note, the use of two pulleys prevented both sensors affecting each other and enabled simultaneous but independent expansion/contraction of the two sensors.

The DC motor was directly connected to a DC power supply with a voltage of 10 V and the rotary encoder was powered using the 5 V output of the USB-X-Series NI USB-6343 (National Instruments, Austin, Texas, USA), which also acquired the data. The ERB and the SP were polarized by a small DC current generated using a REF200 by TI [188]. The resultant voltages across the ERB and SP were amplified using two pairs of instrumentation and differential amplifiers (INA118 and OPA129) prior to acquisition.

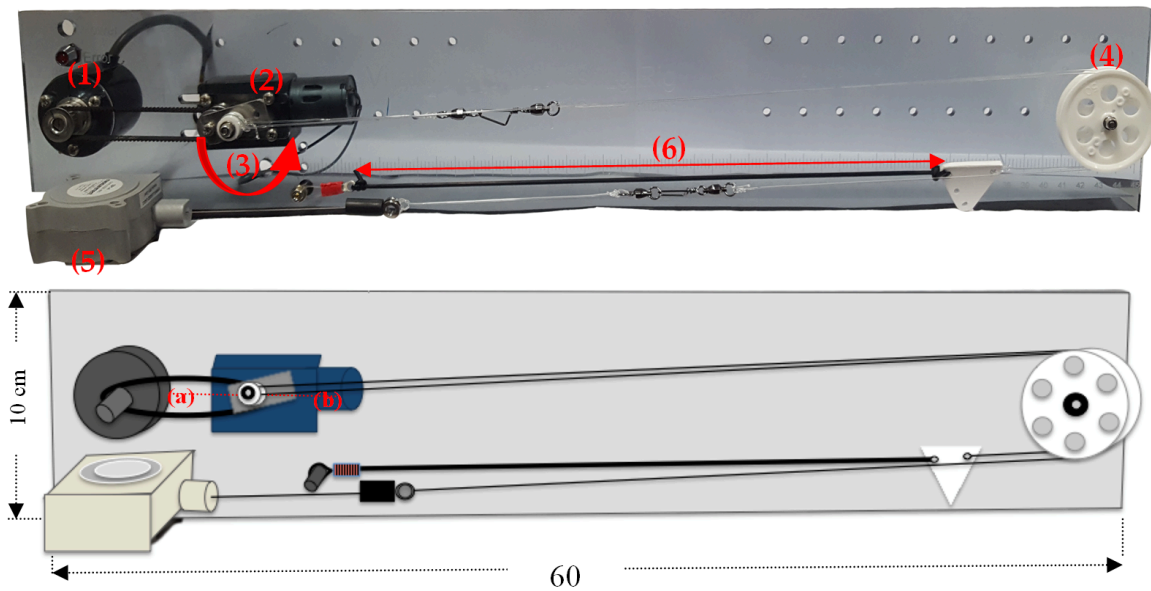


Figure 3.1. Top Panel: Picture of the expansion/contraction simulator rig. System elements: (1) rotary encoder; (2) motor; (3) direction of rotation of motor arm; (4) pulley system; (5) string potentiometer; (6) electro-resistive band. Bottom Panel: Diagram of the expansion/contraction simulator rig. Maximum stretch of the ERB and SP sensors occurs when the DC motor arm reaches position (a), minimum stretch occurs at position (b).

### 3.2.2 Data Acquisition

Four ERBs, all with a length of  $292 \pm 0.5$  mm were used for a comparison against the SP. For each of the four ERBs, the sensor was placed in the rig and pre-stretched  $10 \pm 0.5$  mm to avoid any slack when fully relaxed. The ERB and SP were stretched  $28 \pm 0.5$  mm (13% of its

resting length) when fully expanded by the motor. Of note, the amount of stretch experienced by the ERBs is much more than the required stretch of these sensors when it is used in HeMo. Therefore, the results presented in this work could be used for the use of ERBs in other applications in which greater stretch is required. For example, this stretch is similar to the maximum stretch experienced when the ERB sensor is used for monitoring respiration [21,22].

The rig operated continuously with an average speed of 8.77 rpm for each band over four and half days. An epoch of data was recorded every hour, resulting in one hundred and eight epochs of data collected for each band. All data were acquired with a sampling rate of 20 kHz and acquisition duration of 15 seconds, which guaranteed the capture of at least one full rotation of the motor. A much lower sampling rate would have been sufficient to acquire data from the ERBs and the SP but we required a high sampling rate as we intended to use the rotary encoder data to provide a precise interpolation of the sinusoidal expansion/contraction cycle. This interpolation was required to provide a ground truth for confirming the linearity of the reference sensor (SP) used in our quantification.

### **3.2.3 Data Analysis**

To eliminate high frequency noise, we used a steep low-pass filter derived from modification of a filter which we had earlier implemented for post-processing of physiological signals [175]. Therefore, all acquired data underwent a 50th order software non-causal (zero phase lag) IIR low-pass filter (implemented using Matlab) with a cut-off frequency of 10 Hz. Assuming the bands were linear and the rig was perfect, we would have expected a perfect sine wave as the output voltage of the ERB during a complete expansion/contraction (one full cycle of the motor). This is because, when a mono frequency sinusoidal wave is applied to a linear system, a sinusoidal wave with the same frequency component appears as the output [213]. In contrast, inputting a mono frequency sinusoidal wave to a nonlinear system results in generation of a multi-frequency wave, which contains the fundamental frequency component of the input signal and an associated range of harmonics. The existence of harmonics at the output of a system with a mono frequency input may then be seen as representative of the system's nonlinearity. Total Harmonic Distortion (THD) is widely used

for quantification of the level of nonlinearity due to its sensitivity to the level of harmonics and nonlinear effects in electromechanical systems [213]. Therefore, the THD of each ERB recording was calculated to determine the similarity of the output voltage to a perfect sine wave and so to quantify the level of nonlinearity. However, as no test rig could be perfect and instead could be expected to cause some systemic errors, the THD of the SP recording was also calculated to provide a comparative reference. The THD is calculated by dividing the root sum squared of the harmonics of a waveform by its fundamental frequency.

To extract the fundamental frequency, we found the frequency at which the Fast Fourier Transform (FFT) of the SP data plateaued. The fundamental frequency represents the frequency of the oscillation. The extracted fundamental frequency using FFT was also consistent with the oscillation frequency of the motor. For example, for a recording at which the motor was rotating with a speed of 8.803 rpm, the oscillation frequency of the motor ( $8.803/60=0.1467$  Hz) exactly matched with the fundamental frequency extracted from the FFT signal of the SP data (0.1467 Hz). The fundamental frequency of the band data also matched with the fundamental of the SP data, as they were oscillating at the same speed. Harmonic frequencies are defined as integer multiples of the fundamental frequency. Therefore, to find the harmonics, the first five multiples of the fundamental frequency were extracted. Only the first five harmonics were included in the THD calculation, as these were the dominant harmonics and the rest were negligible. The sum of the power of these five harmonics was used in calculating THD. Therefore, THD was calculated by dividing the power of the first five harmonics by the power of the fundamental frequency.

Additionally, the Signal-to-Noise Ratio (SNR) and the peak-to-peak voltage of the SP and ERB data were also calculated and compared. To calculate the SNR, the maximum frequency component of each recording was considered as the signal and remaining frequency components were considered as noise. In other words, the power of the fundamental frequency was considered as the power of the signal and the sum of the power of the rest of frequency components was considered as the power of the noise. All data were normalized between 0 and 1 before calculating THD and SNR.

### 3.3 Results

A representative single low-pass filtered recording acquired from one ERB and the SP during a full cycle is shown in Figure 3.2. It is immediately clear that the ERB deviates substantially from the SP signal, with a nonlinearity clearly visible in the voltage recording of the ERB during contraction (Figure 3.2). Figure 3.3 demonstrates a comparison of normalized ERB and SP data. A clear difference exists in the shape of both recordings.

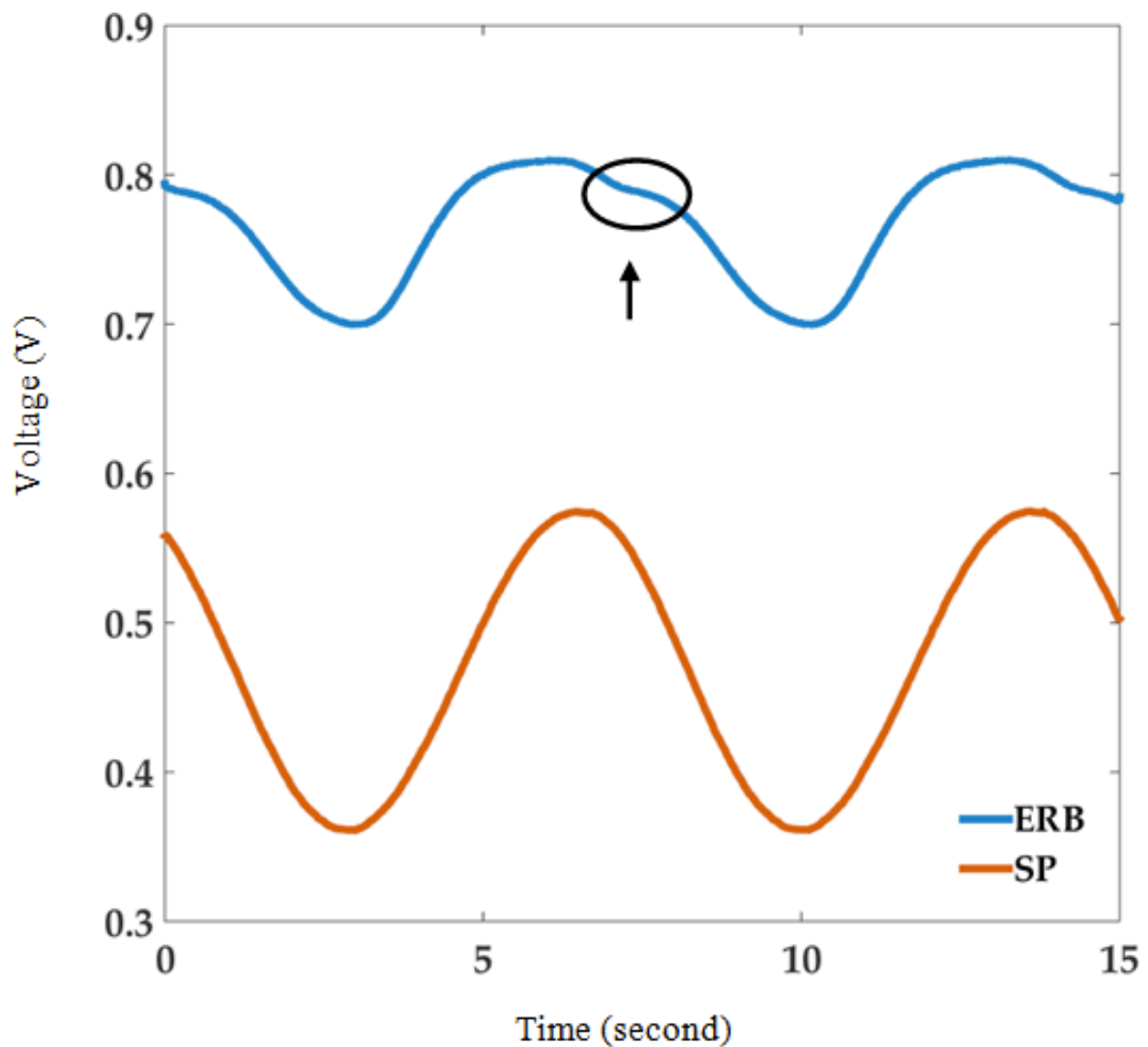


Figure 3.2. ERB voltage versus SP voltage for one recording. The circled area highlights the ERB contraction nonlinearity.

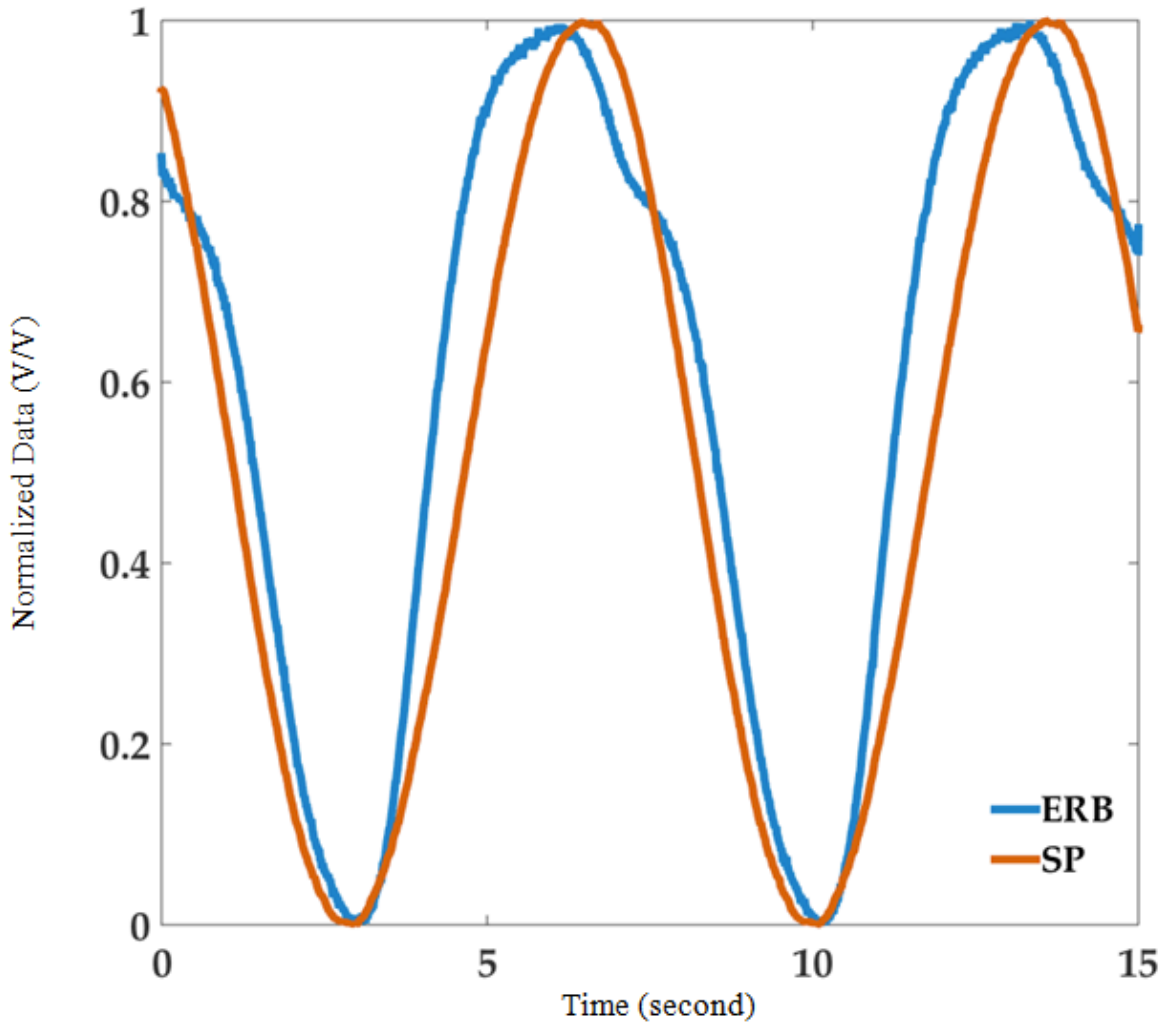


Figure 3.3. Normalized ERB voltage versus Normalized SP voltage.

### 3.3.1 Total Harmonic Distortion (THD) Comparison

The ERB voltage signal (Figure 3.2) clearly demonstrates the ERB sensor nonlinearity. The THD of the band data and THD of the linear sensor (SP) during repeated simultaneous expansion/contraction are shown in Figure 3.4. As the bands and the SP are pulled simultaneously, artefacts during the rotation of the motor affect both sensors. While a THD of both sensors follow a similar trend, higher THD values are observed for the ERBs compared with those of the SP. The difference in THD values may be expected due to the additional distortion during ERB contraction.

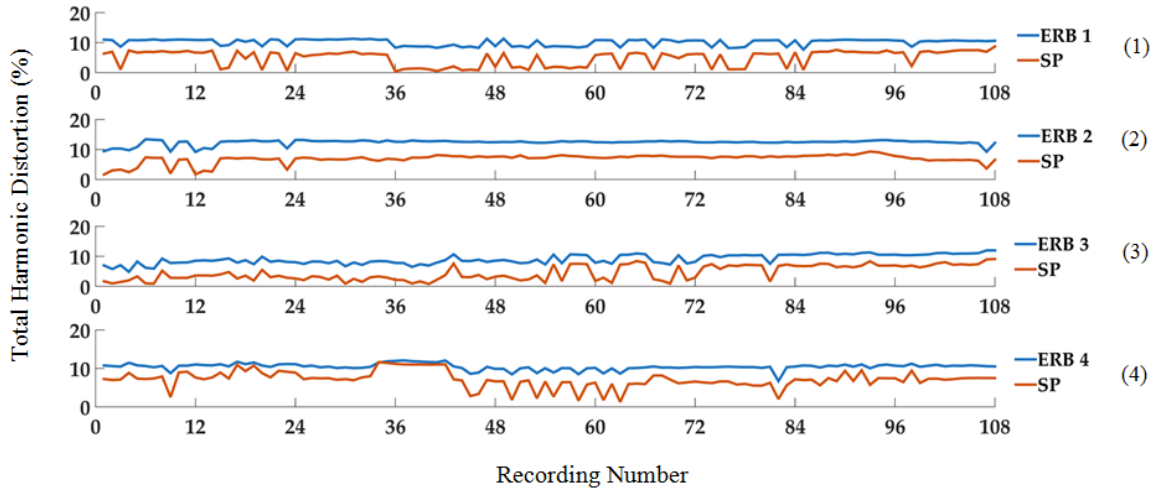


Figure 3.4. Total Harmonic Distortion of the ERBs and the SP. (1) to (4) refer to the different ERBs

Table 3.1 summarizes the THD comparison between the ERBs and the SP. The nonzero values of the SP signals indicate that the rig does not produce a perfect sinusoidal cycle. This emphasizes that the nonlinearity of ERBs can result in more than a 50% increase in the THD calculated over four and half days recording.

Table 3. 1. THD comparison summary.

Experiment	%Mean±SD	%Mean±SD
	ERB THD	SP THD
1	10.11±1.09	4.87±2.57
2	12.36±0.87	6.9±1.53
3	9.07±1.56	4.51±2.47
4	10.45±0.82	7.13±2.17

### 3.3.2 Signal to Noise Ratio Comparison

The signal to noise ratio of all ERBs and the SP are calculated and compared (Figure 3.5). Similar to the visual correlation seen in the trend of the THD of the two sensors, SNR trends of the bands and the SP are quite similar. As expected, the SNR values of the SP are higher

than those of the ERBs, confirming that the ERBs are further affected by additional noise/artefact due to the intrinsic nonlinear behaviour of the bands.

A summary of SNR values of the two sensors is provided in Table 3.2 showing that the mean SNR of the ERBs are from 0.25 dB (Experiment 3) to 0.63 dB (Experiment 1) lower than the SNR values of the SP (in the same experiment). The difference in the SNR values of the two sensors further demonstrates the need for compensation of ERB's nonlinear behaviour, as this would lead to a considerable increase in SNR and ultimately, enabling a more accurate measurement with the ERBs.

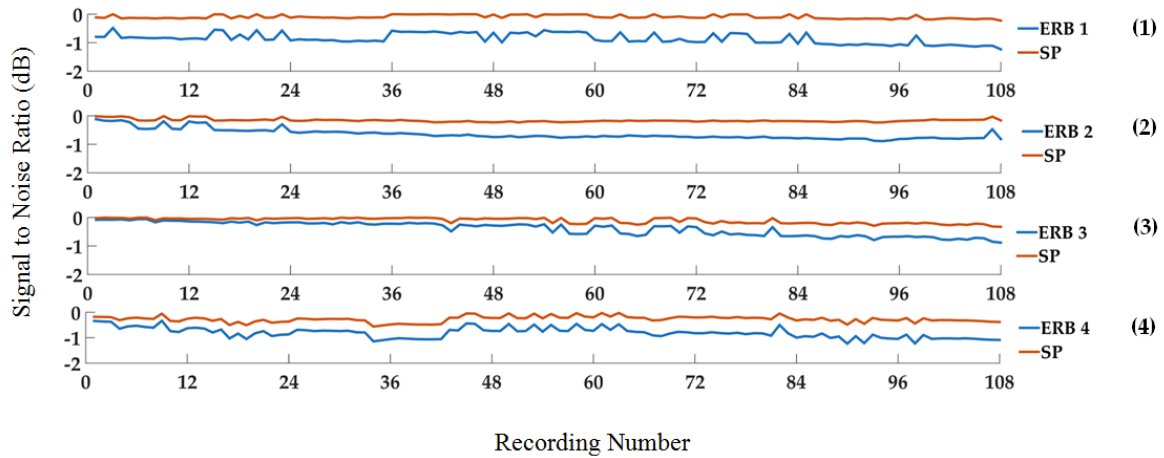


Figure 3.5. Signal to noise ratio of the ERBs and the SP. (1) to (4) refer to different ERBs.

Table 3. 2. SNR comparison summary.

Experiment	Mean±SD	Mean±SD
	(dB) ERB SNR	(dB) SP SNR
1	-0.85±0.18	-0.09±0.06
2	-0.65±0.18	-0.16±0.05
3	-0.4±0.24	-0.11±0.09
4	-0.81±0.21	-0.27±0.12

### 3.3.3 Peak to Peak Comparison

The peak-to-peak voltage of all ERBs and the SP for all recordings are shown in Figure 3.6. While the SP data remained roughly constant during the whole recording for all experiments, a small drift was found in the peak-to-peak voltage of each ERB. The initial drift in the ERB peak-to-peak voltage is small and it disappears after about 40 hours.

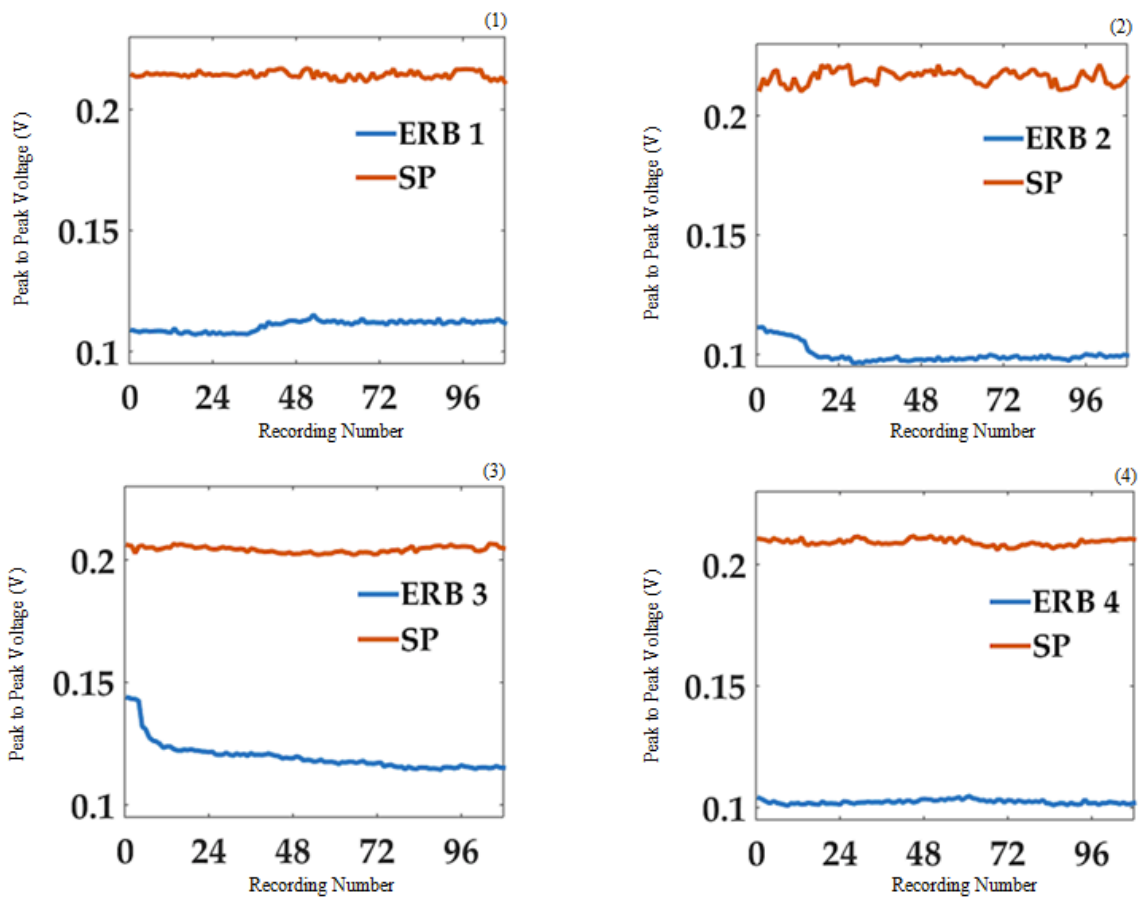


Figure 3.6. Peak-to-Peak voltage comparison of the ERBs and the SP. (1) to (4) refer to the different ERBs.

ERB signal drift during the first 40 hours was suspected to be due to initial use of a new sensor. To explore this further, data were collected from a brand new ERB expanding/contracting for 4.5 days. One epoch of data was saved every hour and again observed drift in the peak-to-peak voltage during the first 40 hours, which then stabilises. Following this experiment, the ERB was left relaxed for 24 hours before repeating the experiment. In the second experiment, the peak-to-peak voltage appeared to be stable and

without drift, confirming that the initial drift was due to the initial use of the ERB sensor (Figure 3.7).

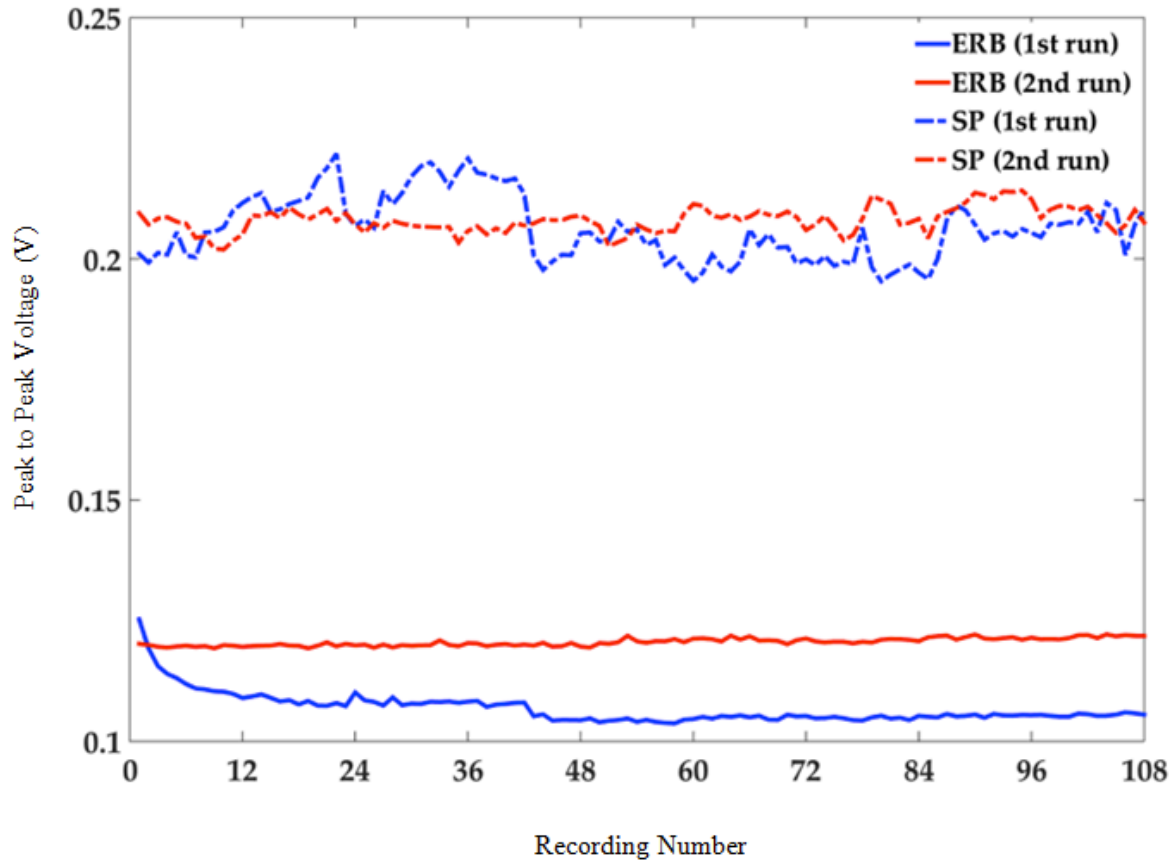


Figure 3.7. Peak to peak voltage of the band and the SP. The blue lines refer to the first experiment, and the red lines refer to the second experiment. The dashed line represents the peak-to-peak voltage of the SP data and the solid lines represent the peak-to-peak voltage of the ERB data.

### 3.3.4 Correlation Coefficient

The band data and the SP data were correlated to quantify the overall similarity of the ERB behaviour to a linear sensor (SP) behaviour. The mean correlation value calculated for the four bands ranged from 0.95 (band 1) to 0.98 (band 3), with an average of 0.97, showing strong similarity between the two sensors. Moreover, the variation of the correlation between the ERB and the SP data was investigated over time (Figure 3.7). For each band, the correlation coefficient was calculated between the recorded band data and the SP data. Since one hundred and eight epochs of data were recorded for each band, one hundred and eight

correlation coefficient values were calculated for each band during its continuous simultaneous expansion/contraction over the course of four and half days. As seen in Figure 3.8, a drift tendency was also found for correlation of the ERB and the SP data over time. The observed drift may refer to the deterioration of the ERB sensors over time.

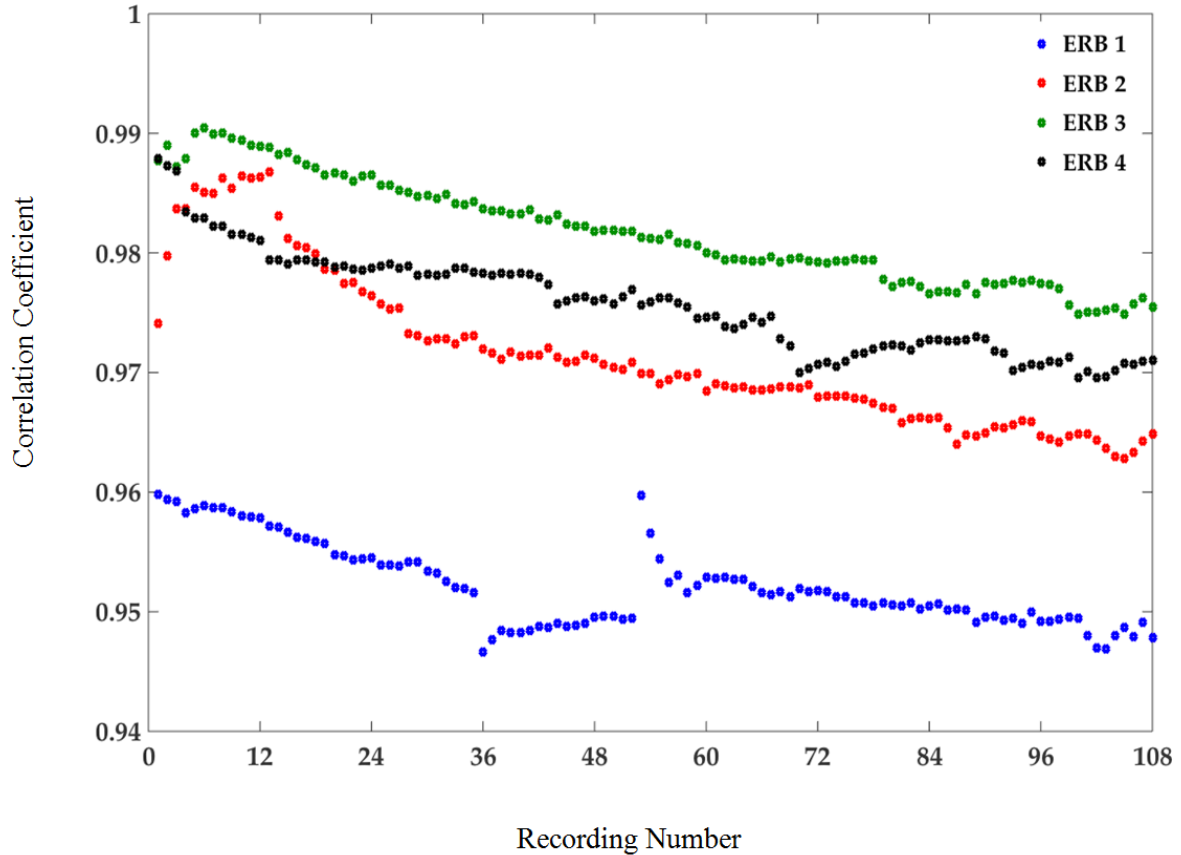
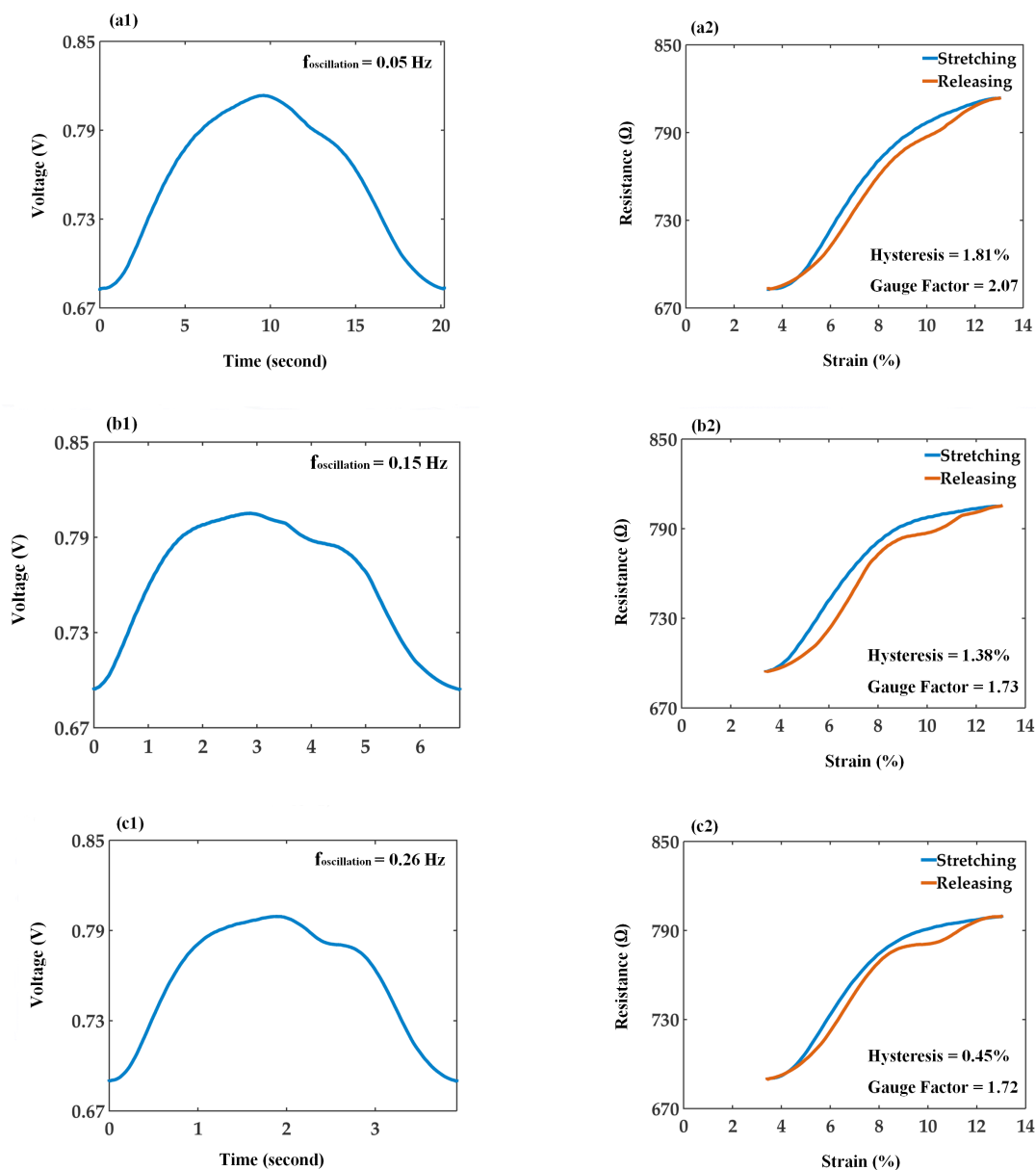


Figure 3.8. Correlation coefficient of the ERB and the SP sensor for 108 recordings. Different colours refer to different bands used in the experiment.

### 3.3.5 Frequency Response

To investigate the behaviour of the ERB sensors for different oscillation frequencies, the speed of expansions/contractions was changed. This change was applied either by changing the voltage of the power supply which fed the DC motor or by replacing the motor with a faster/slower one. Fifty cycles of expansions/contractions were recorded continuously for each oscillation frequency. The average temporal response was calculated for each of the operated oscillation frequencies (Figure 3.9-a1, b1, c1, d1, e1, f1). Then, each average

temporal response was used to measure hysteresis behaviour of the ERB for the operated frequency (Figure 3.9-a2, b2, c2, d2, e2, f2). Generally, electro-resistive type strain sensors have been reported to show hysteresis especially during under large strains [4]. The sensing performance of strain sensors under dynamic loads can become non-reversible when they show large hysteresis behaviour. [4]. Therefore, hysteresis can become an important factor for the use of such sensors in most of the wearable applications where the sensor experiences dynamic loads [4]. Figure 3.9-a2, b2, c2, d2, e2, f2 demonstrates that the hysteresis behaviour and the amount the hysteresis varies for different oscillation.



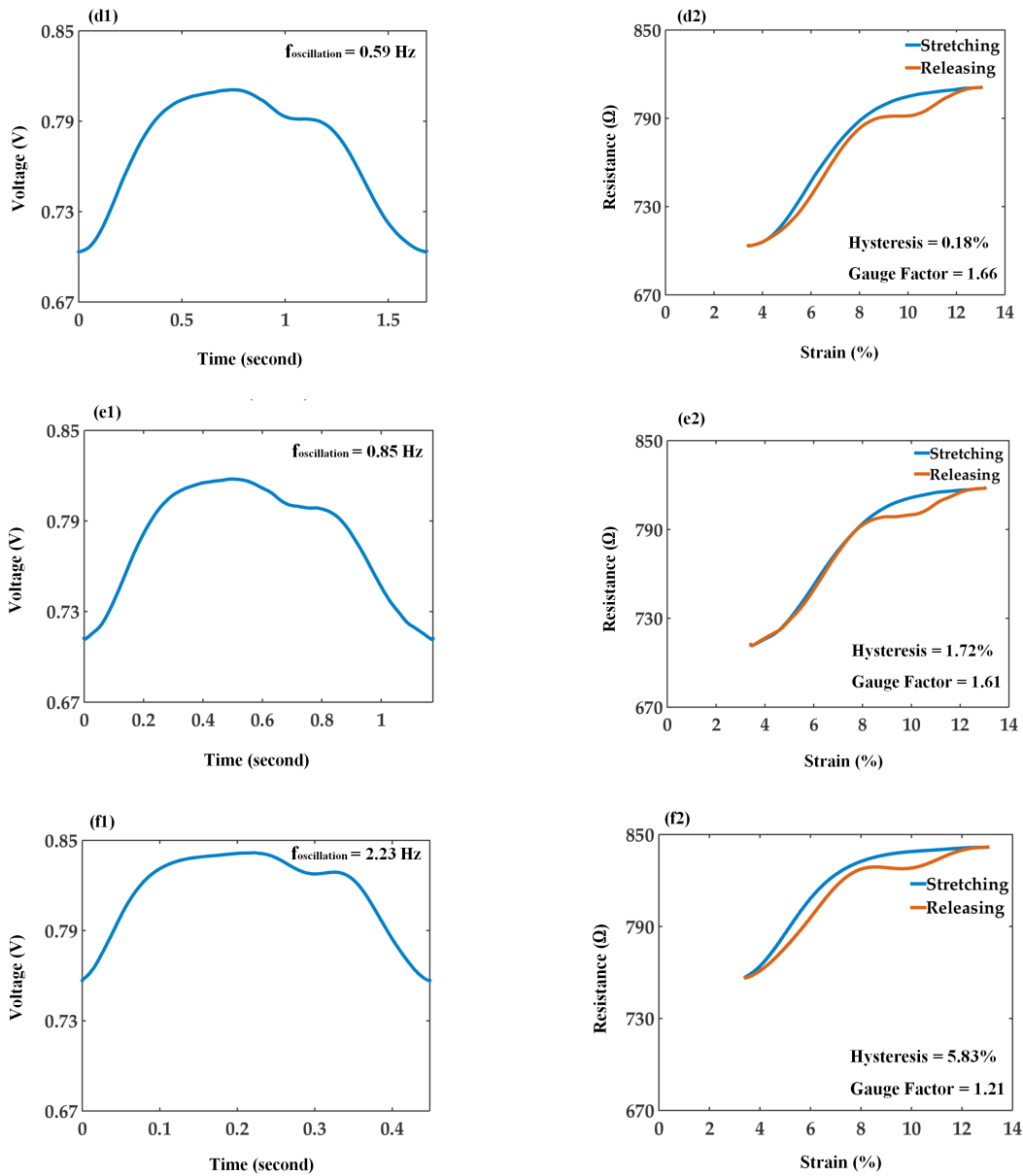


Figure 3.9. (a1, b1, c1, d1, e1, f1) show the average temporal response calculated for oscillation frequencies of 0.05 Hz, 0.15 Hz, 0.26 Hz, 0.59 Hz, 0.85 Hz, 2.23 Hz. (a2, b2, c2, d2, e2, f2) show the hysteresis behaviour of the ERB sensor for oscillation frequencies of 0.05 Hz, 0.15 Hz, 0.26 Hz, 0.59 Hz, 0.85 Hz, 2.23 Hz. Hysteresis is calculated at the midpoint of minimum and maximum strain. Gauge factors are also calculated for each oscillation frequency.

The average hysteresis plots show that the electrical behaviour of the band during expansion and contraction would tend to be more similar when there is a small amount of stretch, and their electrical behaviour of the two modes show more difference as the strain is increased. Moreover, it can be seen that the electrical behaviour of the ERB sensor shows more semi-

sinusoidal response when the ERB sensor is stretched/ contracted with smaller oscillation frequencies.

The sensitivity of strain, known as gauge factor, was also measured for the ERB sensor operated at different oscillation frequencies. This was calculated by using the average temporal responses and simply dividing the relative change in resistance of the ERB sensor by the relative change in the length of the sensor. Figure 3.9-a2, b2, c2, d2, e2, f2 illustrates that the ERB's gauge factor decreases as the oscillation frequency increases. However, the reduction in sensitivity slightly affects the peak to peak voltage of the ERB sensor. Figure 3.10 shows the average peak to peak voltage calculated at six different oscillation frequencies and it emphasizes that the variation of the average peak to peak voltage is negligible when the ERB is expanded/contracted with a frequency ranging between 0.05 Hz to 2.23 Hz.

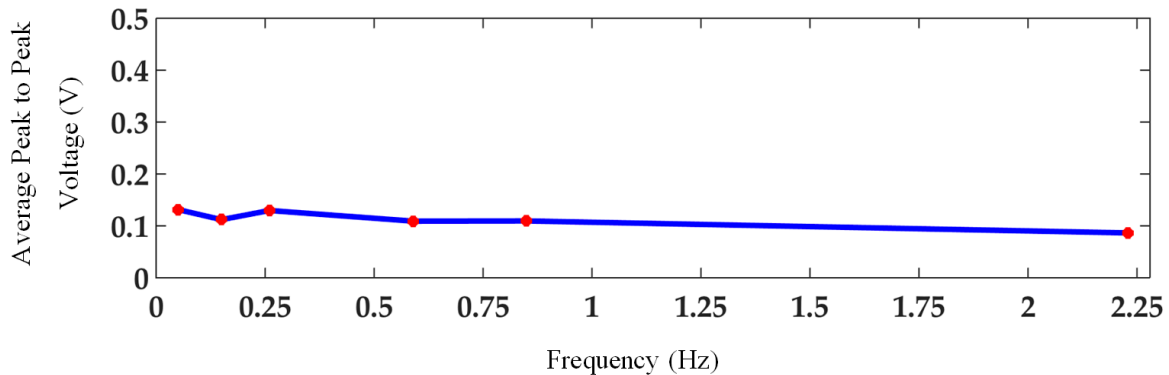


Figure 3.10. Average peak to peak voltage plotted versus frequency at which the ERB is expanded/contracted. The points which were actually measured are marked as red.

### 3.3.6 Comparison to Rotary Encoder

The spring potentiometer was also compared to the rotary encoder. Although the exploited reference sensor (SP) in this work is commercially sold as a linear displacement sensor, we further validated its linearity by comparing two hundred SP recordings with the sinusoidal wave interpolated using the rotary encoder data. The comparison illustrated that the average of two hundred SP recordings differ slightly from the interpolated wave from the rotary encoder. Figure 3.11 presents the sinusoidal wave derived from the rotary encoder data with

maximum error bars from at 30° steps in an interval of 0° to 360°. Although it was intended to have the expansions/contractions of the two sensors at a constant speed during the whole experiment, our rotary encoder data shows that the speed of the motor changed slightly from one recording to another. Table 3.3 summarizes the speed variations of the motor during the data acquisition. Nonetheless as the comparisons of interest were between the ERB and SP, the assessment of these remains valid.

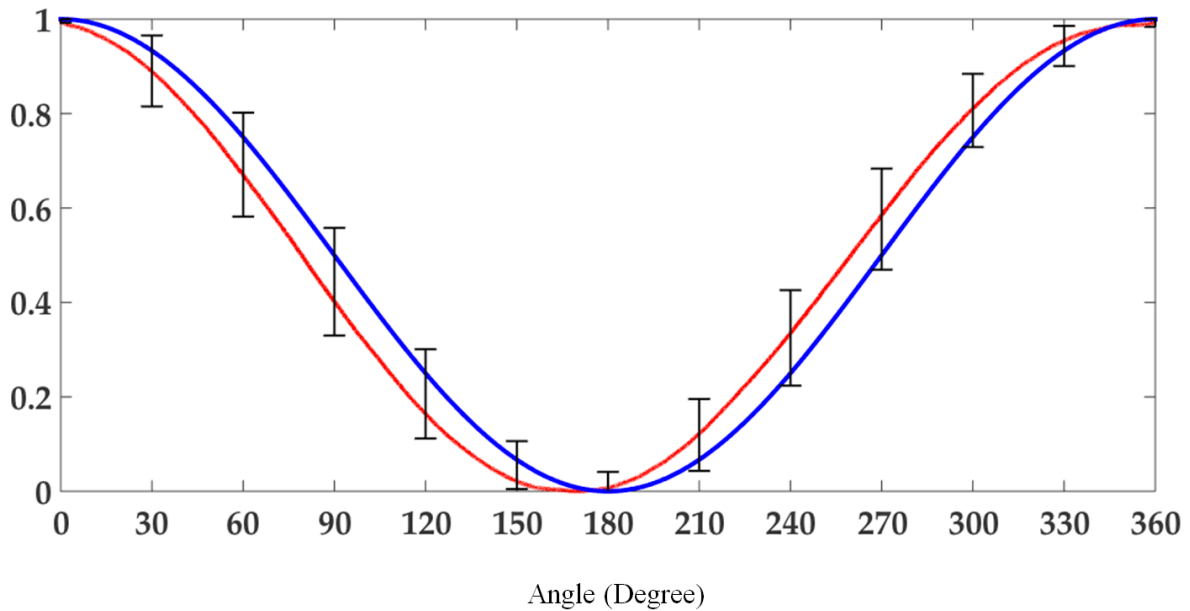


Figure 3.11. Blue refers to normalized interpolated sinusoidal wave derived from the rotary encoder data. Red refers to average of 200 SP recordings. The error bar at each point refers to the maximum difference of the SP recordings from the interpolated wave at that point. Maximum upper error is 15.8% and maximum lower error is 17.45%.

Table 3. 3. Statistical parameters of motor speed.

<b>Experiment</b>	<b>Min</b>	<b>Max</b>	<b>Mean</b>	<b>SD</b>
1	8.33 rpm	8.93 rpm	8.62 rpm	0.10 rpm
2	8.56 rpm	9.32 rpm	8.97 rpm	0.15 rpm
3	8.67 rpm	9.37 rpm	8.95 rpm	0.13 rpm
4	8.75 rpm	9.49 rpm	9.03 rpm	0.14 rpm

### 3.4 Discussion

This work has highlighted a number of important factors that will impact the use of ERB's in wearable devices for accurate measurement of blood volume changes or other bio-signals such as respiration. Primarily, it is evident that the response during expansion and contraction are not the same and substantial nonlinearities exist. Secondly, the presence of baseline drift during the first 40 hours exists; however, this disappears with time hence may be obscured during use.

The ERB sensors consist of conductive fibers coupled to each other. When the sensor is stretched, these fibers decouple, leading to an increase in impedance. A linear stretch-impedance response would require conductive fiber decoupling (and recoupling) to be linear with stretch. It is likely that this is not the case and difference in the rate of coupling/recoupling of fibers is further responsible for the discrepancy in impedance response during stretch and relaxation. Furthermore, the baseline shift over time is likely due to the creation of micro-cracks in the ERB material when first used [197]. The results shown in Figure 3.6 suggest that once the material is repetitively strained over a period of time the baseline stabilizes substantially.

The non-linear behaviour of these ERB's does not exclude their use in the proposed medical applications, but it may need to be accounted for using some transfer function. The difficulty here is the stability of the non-linearity, which would need to be consistent over time for the transfer function to be accurately applied. Should a unique transfer function be required for each sensor then the process may become quite a burden if translated to a commercial device. Similarly, the baseline drift observed may require the ERBs to be cycled in a rig similar to the one described here in order to achieve a stable response. Of note, generally, the nonlinearity of the sensor is not a major impediment as a careful calibration procedure can accommodate all nonlinearities simultaneously.

A number of limitations of this work are evident. Primarily, the rig could be improved as it exhibited minute vibration in both the ERB and SP recording during stretch/relaxation. These appear to be largely due to physical vibration of the sensors and movement of the pulleys over time. However, this rig was sufficient to highlight high-level observations of

nonlinearities. Future work will focus on developing a new, more accurate and reliable system for these purposes and establishing if nonlinear behaviour at all frequencies and lengths of stretch may be removed using a single transfer function.

### **3.5 Conclusions**

An expansion/contraction simulator machine was developed to investigate the characteristics of commercially available Electro-Resistive Band (ERB) sensors. The previous chapter showed that ERBs could be exploited as wearable sensors for measuring blood volume changes in the leg. To assess the linearity/nonlinearity behaviour of the ERBs, the ERB sensor and a linear displacement sensor (string potentiometer) were expanded/contracted simultaneously. The nonlinear response of the ERBs appeared as a notch on its voltage output, and comparison between THD values of the ERBs and the string potentiometer quantified the observed nonlinearity of the ERBs. Further analysis of the ERBs data found decreased SNR values compared to that derived for the spring potentiometer.

However, it should be noted that according to the hysteresis analysis shown in this chapter, the nonlinear behaviour of the ERB sensor would not affect the HeMo recordings, as the stretch experienced by ERB in HeMo is very small. In other words, the HeMo data would be legitimate without the need for compensation as the amount of strain of ERBs small enough so that the nonlinear behaviour of the ERB for this application would be negligible. It was also important to find that the peak-to-peak voltage of the ERB is stable for different frequencies. Additionally, the initial drift observed in their peak-to-peak voltage output of the ERBs may require the ERBs to be cycled before their use to achieve a stable response. Of note, the findings in this chapter impact on future validation of HeMo as the obtained information are parts of the validation process and feed forward to design inputs for the next stage of HeMo development.

The quantification of the ERBs presented in this chapter is a starting point in the development of compensating mechanisms for the nonlinear behaviour of ERBs where required. The results of this characterisation may be of interest of other users and uses of the ERB sensors.

Additionally, the method presented for characterisation of the ERB sensors could be used to characterise the electrical behaviour of similar stretchable sensors.

## **Chapter 4    Utility of HeMo for the Assessment of Peripheral Venous Function**

This chapter describes a simultaneous comparison of HeMo and Light Reflection Rheography (LRR) for the measurement of venous filling time in a group of healthy adults.

## **4.1 Background**

### **4.1.1 Chronic Venous Insufficiency**

The peripheral venous system incorporates an interconnected network of superficial, deep and perforating veins and a series of valves responsible for collecting and returning oxygen-poor blood to the heart [8]. The superficial veins are located above the muscular fascial layer, and are connected to the deep venous system located below the muscular fascial layer via perforating veins [8]. The superficial veins have a primary role in collecting deoxygenated blood, returning the blood to the deep venous system. Muscles in the deep venous system help to pump the blood back to the heart, while the valves prevent the return of blood towards the feet.

Chronic venous insufficiency (CVI) is a condition, characterised by peripheral venous system failure and can cause pathological manifestations such as pain, itching, edema, cramps, skin change, swelling, and venous ulcers [8,87]. Despite the impact of CVI on an individual's quality of life and the resultant financial burden on healthcare systems, CVI is often overlooked in primary care [7,8,22]. Several invasive and non-invasive methods (fully described in the first chapter) have been developed to assist in the diagnosis of CVI. One such method, which HeMo is capable of performing, is to measure venous filling time.

### **4.1.2 Venous Filling Time (VFT)**

Venous filling time is defined as the required time for the venous volume to reach a steady baseline after completion of an exercise [54,67,182,193,214] and is highly correlated with foot vein pressure recovery time, which requires the use of invasive measurements [55]. More accurately, VFT is the time taken from the beginning of post-exercise relaxation until the venous volume reaches an endpoint which is stable for at least five seconds [51]. A typical VFT recording is depicted in Figure 4.1.

Normally, contraction of the calf muscle pump empties blood out of the venous system and results in an immediate reduction in venous pressure. Relaxation of the muscle pump allows

refilling of the venous system via arterial inflow. With valvular dysfunction, refilling of the venous system occurs as a result of both arterial inflow and the retrograde venous flow [8]. Therefore, the refill time will decrease in the presence of CVI. In other words, a shortened venous filling time represents venous incompetence [45,67,103,182,214,215].

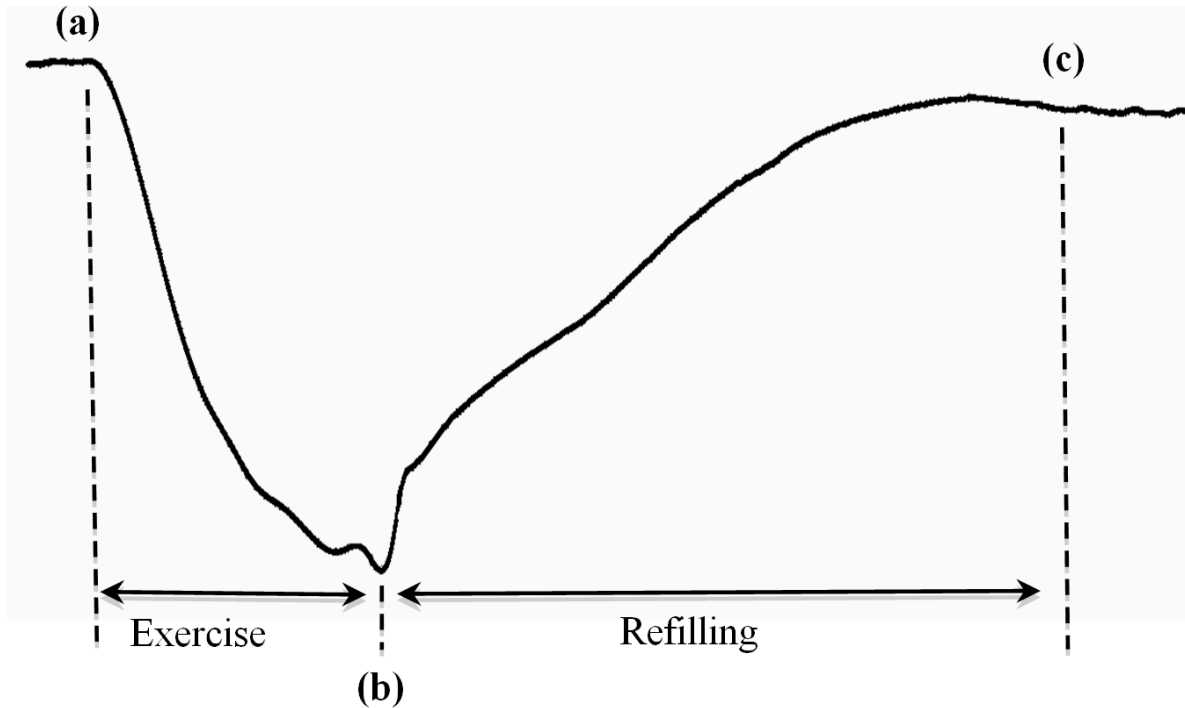


Figure 4.1. A typical venous filling curve. (a): the resting value, (b): the lowest point after exercise, (c): the final refilling.

There is a lack of consensus agreement for VFT threshold value, as a variety of threshold values have been reported (11s [64], 18s [67,103], 19s [67], 20s [54,55,59,87,182], 23s [67] and 25s [51,87]) to detect/exclude venous reflux.

It should be noted that instead of VFT, other parameters such as half refilling time, 90% refilling time, 95% refilling time and the venous filling index could be used for the assessment of venous function [45,54,55,80,87,182,215–217]. Half refilling time is defined as the required time for the venous volume to reach fifty percent of its final volume, and 90% and 95% refilling time are similarly described. The Venous Filling Index (VFI) is measured by dividing venous volume, or a percentage of venous volume, by refilling time [54,80,182,215,217,218].

We previously pilot tested HeMo with a single subject and demonstrated the capability of HeMo to measure venous filling time (chapter 2). In this chapter, HeMo VFT measurements are compared against the VFT values measured simultaneously from an established device in a well-powered study. The hypothesis being tested is that there is agreement between HeMo and LRR VFT measurements in healthy subjects.

## **4.2 Methods**

### **4.2.1 Subjects**

Thirty-six subjects were recruited (Age  $32.53 \pm 10.03$ , Female = 10). All subjects were healthy volunteers with no history of seizures or fainting, cardiovascular disease, chronic venous insufficiency, epilepsy, deep vein thrombosis (DVT), pulmonary embolism or other clotting problems. This study was approved by the Human Research Ethics Committee of Western Sydney University (Approval No: H11268). All subjects were provided with a participant information sheet, and they gave their written consent to participate in the study.

### **4.2.2 Experimental Settings and Measurement Protocol**

All volunteers were asked to participate in the experiment wearing shorts and barefoot. Weight and height of all subjects were measured before the experiment setup, and date of birth was noted. The right leg was examined using HeMo and LRR in all cases.

HeMo was worn on the middle calf (thickest part of the calf). The LRR sensor (VasoScreen 5000, Medis Medizinische Messtechnik GmbH, Ilmenau, Germany) was then attached to the inner side of the same leg, 10 cm above the malleolus as described in the LRR device manual. This positioning was optimal for recordings from HeMo and the LRR sensor and it also allowed simultaneous venous filling time measurement with the two sensors at a minimum distance from each other. Each subject was requested to sit on a chair with the foot relaxed on the floor such that the knee created an angle of about 110 degrees with the chair seat (Figure 4.2).

The participants were instructed to follow an audible metronome generated by the VasoScreen device and perform ten consecutive dorsiflexion manoeuvres in a timeframe of 20 seconds. To reduce the likelihood of signal artefacts, participants were asked to breathe normally and refrain from talking or moving during the experiment which included the pre-exercise, exercise, and post-exercise periods. Venous filling traces were recorded simultaneously from HeMo and the LRR sensor. The experiment was repeated three times for each subject. Table 4.1 shows a summary of our measurement protocol for VFT measurement with HeMo and the LRR sensor:

Table 4. 1. Summary of VFT measurement protocol with HeMo and the LRR sensor.

Step	Task
1	Ask the subject to sit on a chair with the knee flexed at approximately 110-degree angle and the foot relaxed on the floor.
2	Place HeMo around the middle calf of right leg
3	Place LRR sensor on the inner side of the same leg and about 10 cm above malleolus
4	Start Recording and continue recording with no manoeuvres for at least 10 seconds
5	Ask the participant to perform ten consecutive dorsiflexion manoeuvres synchronous with metronome audio
6	Continue recording after the exercise while the subject is asked to breathe normally and to avoid moving and talking, until refilling is complete.
7	Repeat steps 4, 5 and 6 for two more times.

To investigate the effect of activity on venous refilling time, ten of the recruited participants underwent an extended version of the experiment explained above. These ten subjects were asked to walk on a treadmill at a self-selected pace that they considered fast walking. Once they selected their walking speed, they were asked to continue walking for 5 minutes. Both HeMo and the LRR sensor remained attached during the walking phase of the experiment. Subjects sat immediately after completion of the 5-minute walk. The same VFT measurement experiment was then repeated, and VFT of each subject was measured three times.

### **4.2.3 Data Acquisition**

Data from HeMo were acquired using a PowerLab data acquisition unit and LabChart software (AD Instruments Pty Ltd, Dunedin, New Zealand). LRR data were recorded with the inbuilt data acquisition unit of the VasoScreen device and associated VascularLab software. HeMo sampling rate was 1kHz while the VasoScreen device had a sampling rate of 224Hz. Both PowerLab and VasoScreen devices were connected to a laptop via USB.

HeMo recordings were exported from LabChart to “.mat” format. The data from the LRR sensor was saved via VascularLab in a format, which could be only opened with VascularLab. Screenshots of the LRR recordings were converted to an image type dataset for further analysis.

### **4.2.4 Data Analysis**

Although the VascularLab software automatically measured the VFT of LRR recorded venous filling traces, these measurements were not necessarily correct as the software could not detect the starting point or in most cases the endpoint of the venous filling accurately. The VasoScreen device manual noted this issue and suggested manual editing of the auto-selected start and end points of venous refilling.

To ensure fair comparison between devices, we developed a custom Graphic User Interface (GUI), which enabled importing of the LRR and HeMo datasets and manual selection of the venous refilling start and end points. The resulting VFT measurements were automatically calculated and saved based on the selection of these points. Using this GUI, all venous filling traces recorded by the LRR sensor were imported, opened in the GUI window one by one allowing data annotation. Figure 4.2 illustrates the GUI with an example of LRR recording.



Figure 4.2. Illustration of the VFT GUI when the LRR data is opened. User selected start and end points are marked with blue crosses.

Imported HeMo VFT traces underwent a 50<sup>th</sup> order software non-causal (zero phase lag) IIR low-pass filter designed using MATLAB with a cut-off frequency of 10 Hz to eliminate high frequency noise. Filtered HeMo data were then opened one by one, and annotated in a similar manner to the LRR data. An example HeMo recording opened in the GUI window is shown in Figure 4.3. The complete VFT GUI Matlab code and guidelines for use are provided in Appendix A.

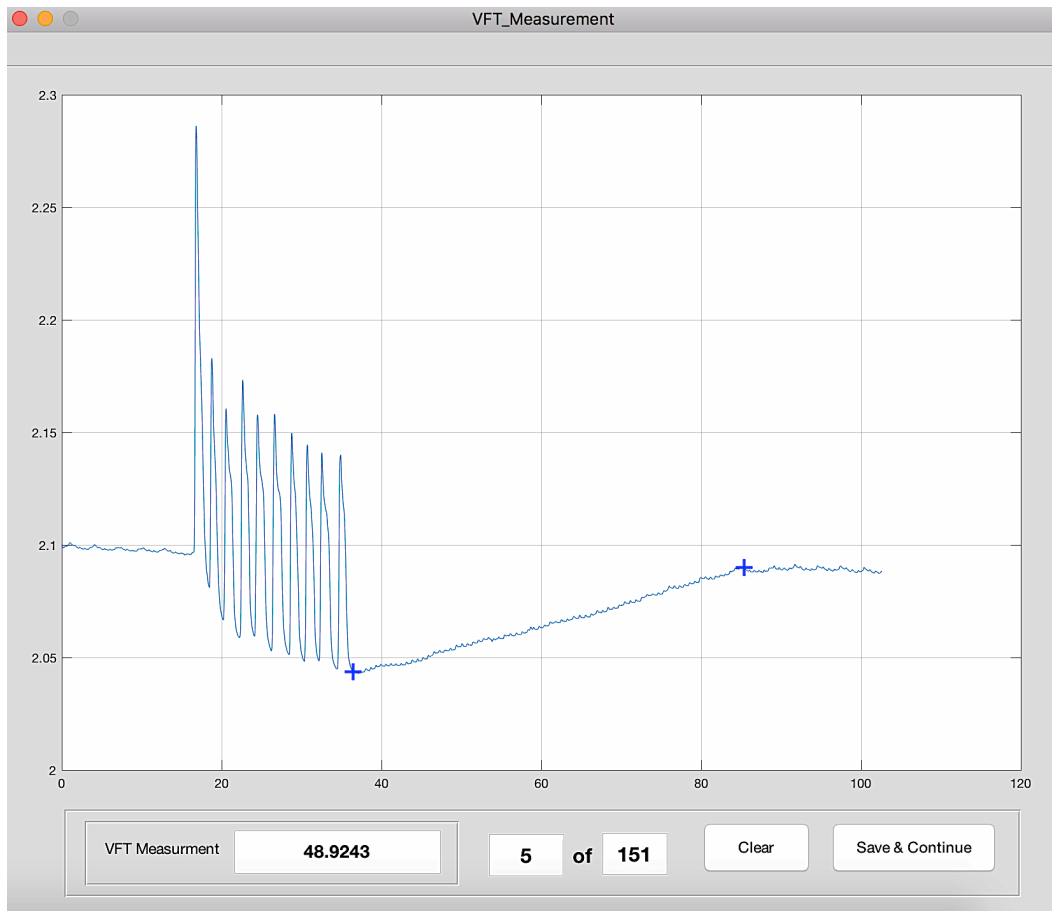


Figure 4.3. VFT GUI when HeMo data is opened. User selected start and end points are marked with blue crosses.

Manual annotation could vary between raters. To assess inter-rater reliability, three individuals were asked to independently annotate the recordings. Each rater was asked to use the developed VFT GUI and mark the starting point and the endpoint of refilling for all HeMo and LRR recordings.

#### 4.2.5 Data Comparison

A VFT threshold value of 25 seconds was used for two reasons: first, this is a strict threshold for healthy subjects; second, this threshold was recommended by the VasoScreen Device's manual. As a cursory comparison we determined if both HeMo and LRR similarly categorise the study participant. Of note, as all subjects were healthy and without any diagnosed

peripheral vascular condition; we anticipated that all subject would be classed as not having venous reflux.

Summary statistics including minimum, maximum, quartiles, mean, and standard deviation of VFT are calculated for both HeMo and LRR recordings. HeMo and LRR VFT measurements were correlated to establish the strength of connection between the two methods. Scatter plots and box-whisker plots of the measured VFT values are presented to visualize the relationship and difference between VFT measurements with the two methods. Paired t-tests are performed to determine if statistically significant differences exist between HeMo and LRR VFT values. A  $p$  value  $< 0.05$  was considered as a statistically significant difference. Bland-Altman plots are used to evaluate the agreement between individual HeMo and LRR measurements.

Intra-class correlation analyses were also applied to investigate the inter-rater reliability of the VFT measurements from the three raters. The repeatability of HeMo and LRR were also assessed by calculating the intra-class correlation coefficient of the VFT measurements.

Finally, to investigate the effect of the five minute walk on VFT measurements, we compared VFT values from before and after walking. In this comparison we used the mean value of the three ratings for each measurement. All statistical analyses were performed using R studio software (version 3.2.1).

### **4.3 Results**

Venous filling traces were collected from thirty-six healthy volunteers (Female = 10) with HeMo and the LRR sensors simultaneously. All recorded data were included in the analysis. Table 4.2 presents a summary of the study population demographics.

Given the three recordings from each participant and three annotations for each trace, our VFT dataset includes 324 VFT values for HeMo and 324 for LRR. Of note, recording time for the LRR sensor was limited to 60 seconds by the manufacturer. Therefore, all VFT values larger than 60 were rounded to 60.

Table 4. 2. Demographics of study population.

Number of Subjects (Female/Male)	Body Weight (Kg) Mean (Range)	Height (cm) Mean (Range)	Body Mass Index (Kg/m <sup>2</sup> ) Mean (Range)	Age (years) Mean (Range)
36 (10/26)	79.4 (49-129)	172.4 (150-193)	26.5 (18.2-40.2)	32.5 (18-56)

### 4.3.1 Subject Classification

Using a VFT of 25 seconds as decision threshold to identify venous reflux, HeMo and LRR were compared. The average of the three ratings for each recording was used for analysis. Using this 25 second cut-off, all 108 LRR recordings (36 subjects x 3 VFT measurements each calculated by averaging the three ratings) were found without venous reflux. This finding was expected, as the data were recorded from a healthy population. Similarly, none of 108 HeMo recordings showed venous reflux. Therefore, the decision of HeMo and LRR matched for all recordings. Figure 4.4 illustrates that all VFT values for both HeMo and LRR are located above the VFT threshold.

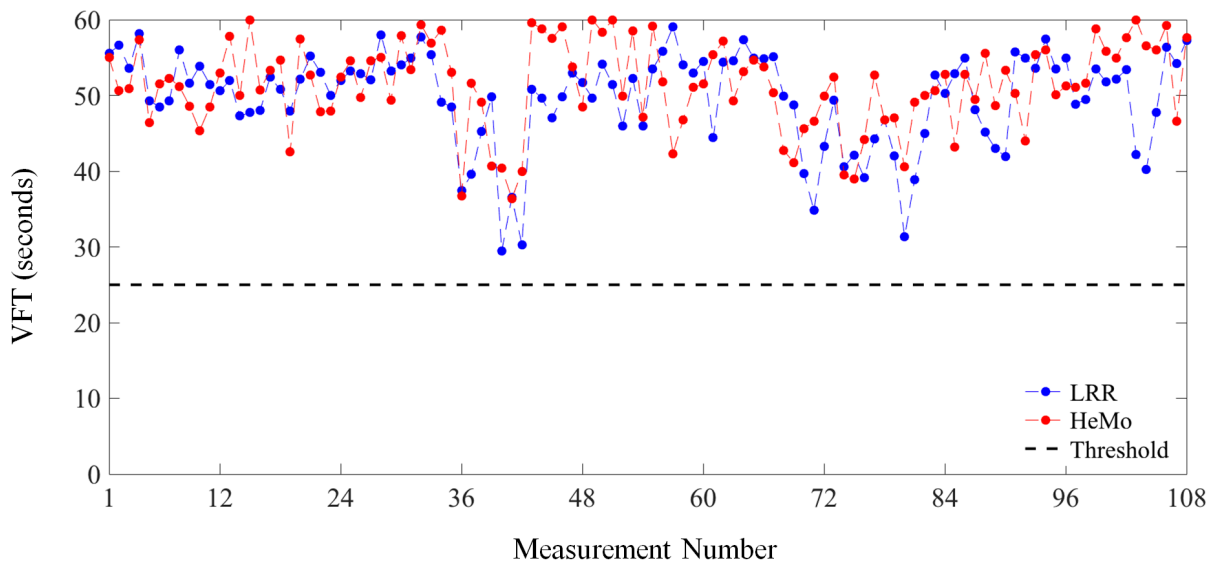


Figure 4.4. Threshold based comparison LRR and HeMo VFT values.

### 4.3.2 Comparison of Devices

A direct comparison of the VFT values measured with LRR and HeMo. Figure 4.5 illustrates the average HeMo VFT measurements versus the average LRR VFT measurements. It should be noted that in this comparison the average of the three ratings was used for each recording.

Correlation coefficients were calculated to examine how strongly the LRR and HeMo VFT measurements are related. A moderate correlation (0.47) was found between the two methods.

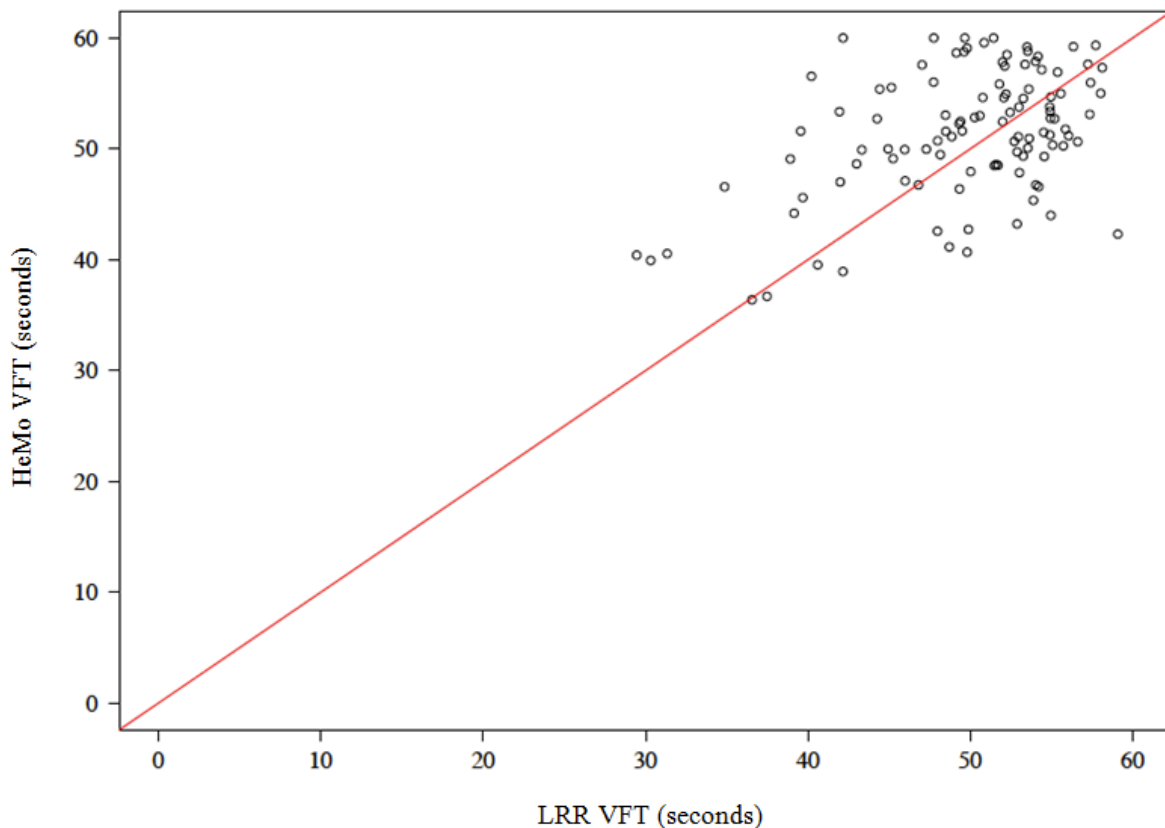


Figure 4.5. Scatter plot of HeMo VFT measurements vs. LRR VFT measurements. Each dot corresponds to the average of the three ratings for a VFT recording.

Table 4.3 demonstrates a statistical summary of the HeMo and LRR VFT measurements (each averaged on the three ratings for each recording). Figure 4.6 provides box-whisker plots of LRR and HeMo VFT measurements to visualize the presented statistical summary by displaying the distribution of HeMo and LRR VFT measurements through their quartiles.

Table 4.3. Statistical summary of LRR and HeMo VFT measurements (average of three annotations)

Method	Minimum	1 <sup>st</sup> quartile	Median	Mean	3 <sup>rd</sup> quartile	Maximum	Standard Deviation
LRR	29.45	47.22	51.53	49.72	54.06	60.00	6.23
HeMo	36.38	48.51	51.60	51.38	55.60	60.00	5.73

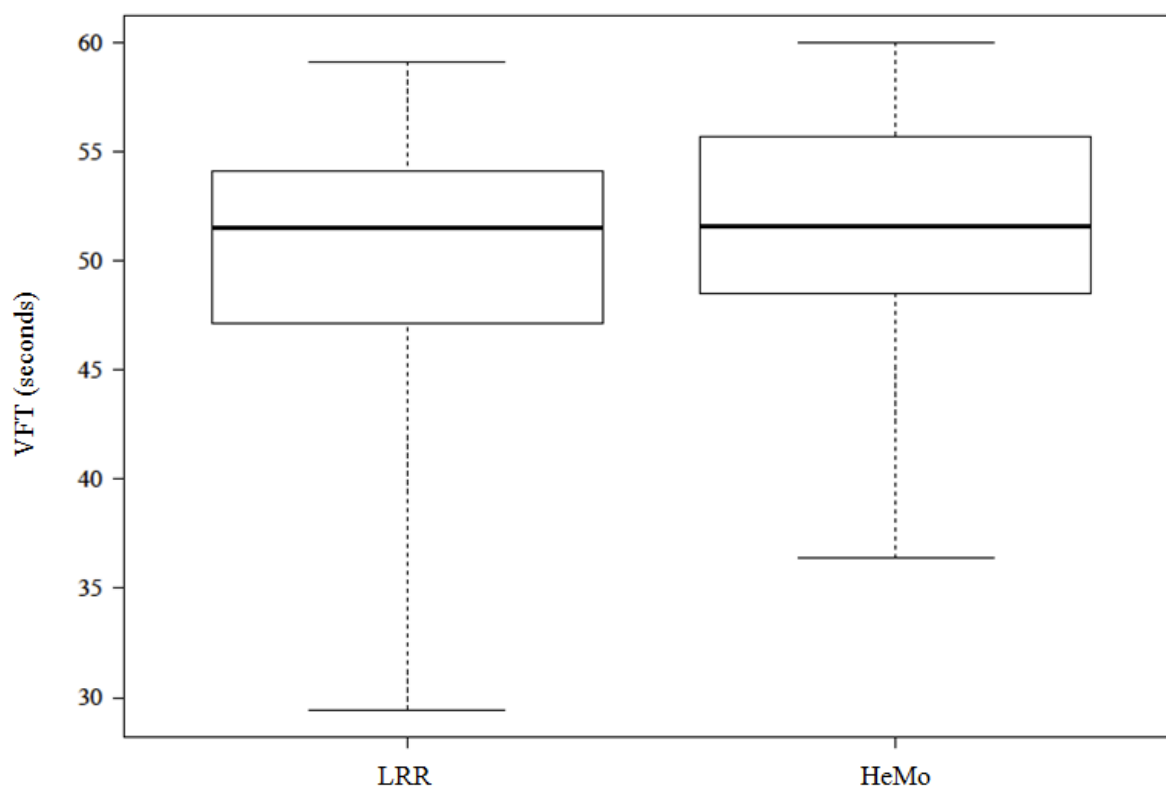


Figure 4.6. Box-whisker plots of LRR and HeMo VFT measurements. The horizontal line within the box indicates the median. The bottom and top edges of the box represent the lower (25%) and upper (75%) quartiles. The whiskers of the diagram show the range for each group of VFT data. P value: 0.01; mean difference: -1.66.

A paired t-test of LRR and HeMo VFT measurements revealed a significant difference between the two devices ( $p = 0.01$ ), with HeMo having longer VFT's (1.66 seconds on average) when compared to LRR.

Agreement between the two methods is graphically presented with Bland-Altman plots in Figure 4.7, where the difference is plotted against the mean of the two measurements. The systematic error is presented by the bias (mean difference of the two measurements) and the limit of the agreement is displayed by the upper (bias+2SD) and lower (bias-2SD) limits.

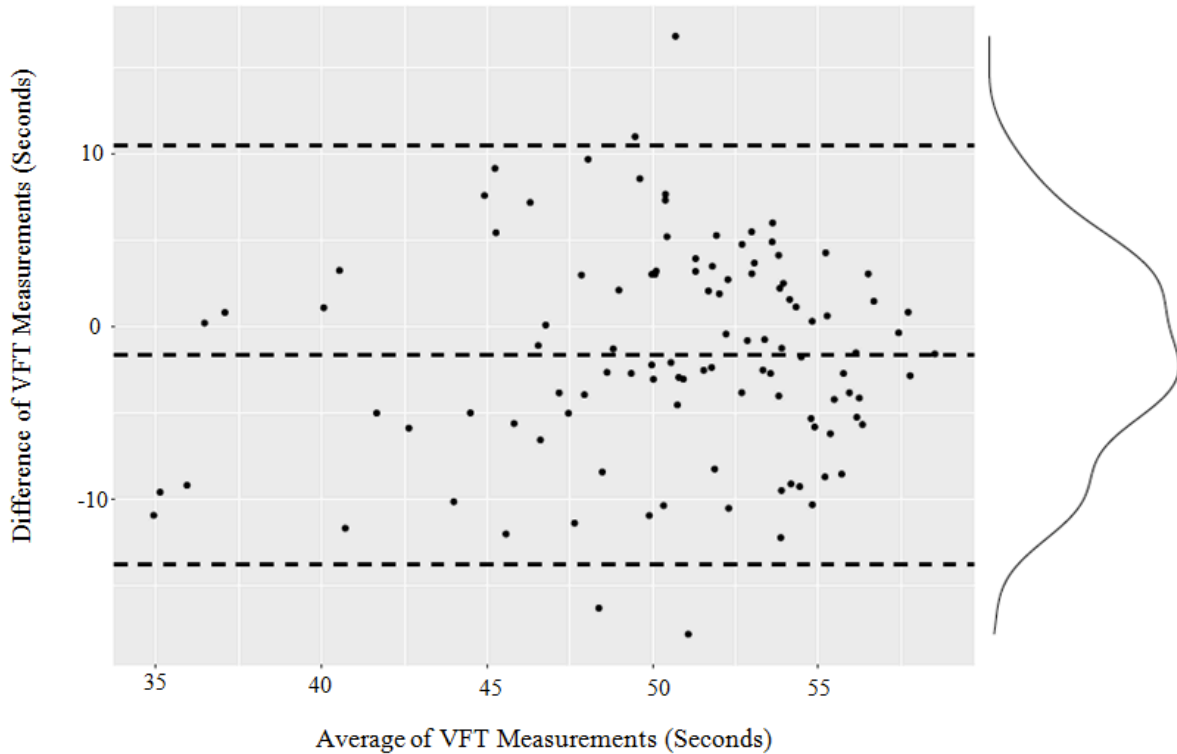


Figure 4.7. Bland-Altman plots of differences between LRR and HeMo VFT measurements versus their mean values. Horizontal lines from top to bottom represent upper limit, bias and lower limit.

Table 4.4 summarizes the systematic error and limits of agreement corresponding to the presented Bland-Altman plots.

Table 4.4. Summary of the statistics in Bland Altman plots of HeMo and LRR VFT measurements.

<b>Bias</b>	<b>SD</b>	<b>Lower limit</b>	<b>Upper limit</b>
-1.66	6.06	-13.78	10.46

As can be seen in Figure 4.7, there is small negative bias showing that the LRR measurements are on average lower than HeMo measurements. Difference points tend to follow an almost normal distribution and 96% of the data points lie within the limits of agreement. Additionally, the difference of the two measurements does not vary with the average values in any significant way highlighting the normality of mean differences.

The limits of agreement are quite wide, raising a question about the degree of agreement between the two measurements. As we showed earlier, all measurements agree in deciding whether or not the subject is healthy. However, we cannot yet make any general claims about the overall agreement of the two devices in patient groups, as this was not the hypothesis under test.

### 4.3.3 Inter-rater Reliability of the Annotations

Three raters independently marked the start and end points of each venous refilling trace. To assess the inter-rater reliability of the three annotations, their intra-class correlation coefficients and 95% confidence intervals were calculated (Table 4.6).

Table 4.5. Inter-rater reliability of annotations.

<b>Method</b>	<b>Intra-Class Correlation of Annotations</b>	<b>95% Confidence Interval</b>
LRR	0.55	0.45 < ICC < 0.65
HeMo	0.39	0.27 < ICC < 0.51

Figures 4.8 and 4.9 visualize the inter-rater reliability of the three annotations for LRR and HeMo. Comparison of mean and quartiles for each annotation are given in Figure 4.10, where box-whisker plots of the three annotations for LRR and HeMo are displayed.

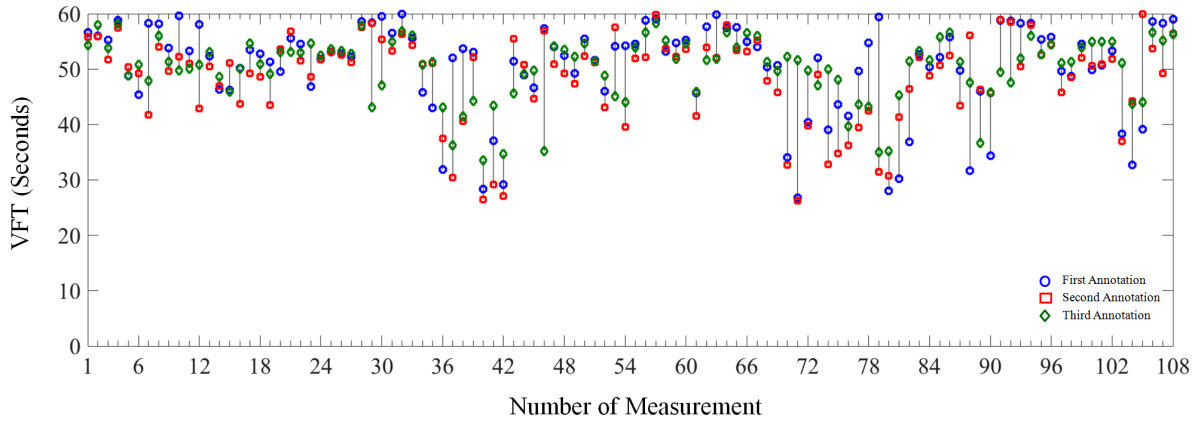


Figure 4.8. LRR annotations for all measurements.

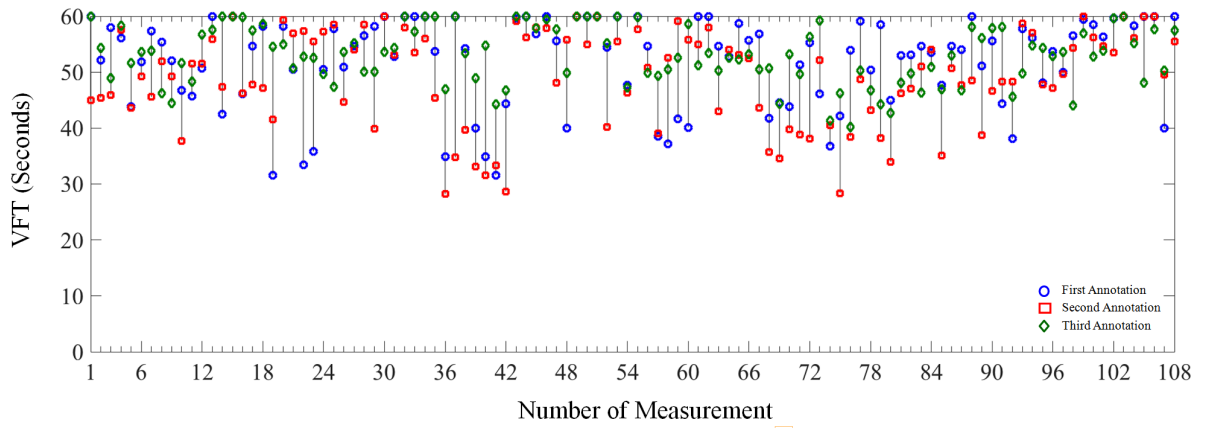


Figure 4.9. HeMo annotations for all measurements.

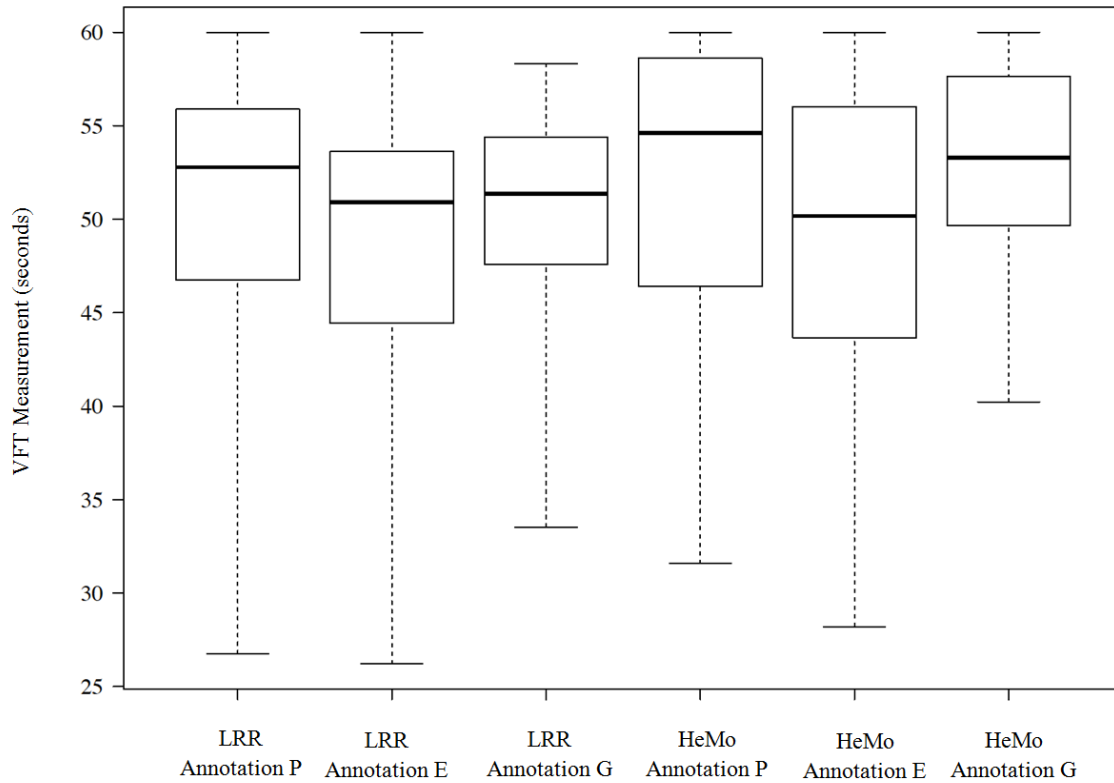


Figure 4.10. Box-whisker plots of the three annotations for LRR and HeMo.

As can be seen in above figures, there is clearly an inter-rater reliability issue for both LRR and HeMo measurements.

#### 4.3.4 Repeatability of the HeMo and LRR measurements

As the LRR and HeMo recordings were repeated three times for each subject, we were able to assess the repeatability of VFT measurement for each device. The average of three annotations was used for each recording and calculated the intra-class correlation coefficient of the three measurements from each subject (Table 4.6). Figures 4.11 and 4.12 visualize the repeatability of the three measurements for LRR and HeMo. Comparison of mean and quartiles for each measurement are given in Figure 4.13 where box-whisker plots of the three measurements for both LRR and HeMo are illustrated.

Table 4.6. Repeatability of measurements.

Method	Intra-class correlation of Measurement1, Measurement2, Measurement3	95%-Confidence Interval for ICC Population Values
LRR	0.72	0.57 < ICC < 0.84
HeMo	0.33	0.13 < ICC < 0.55

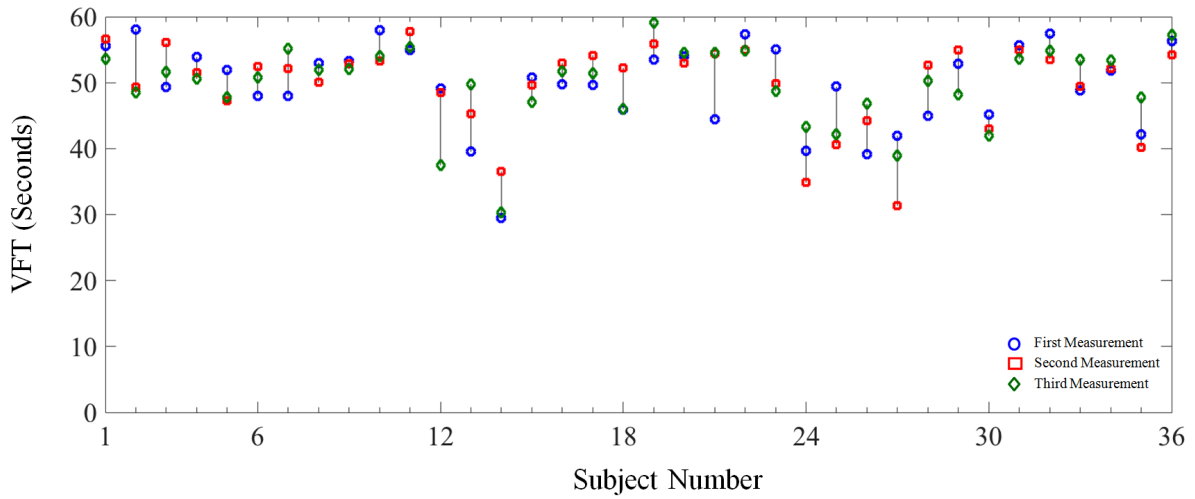


Figure 4.11. LRR measurements for each subject. Values are mean of annotated values.

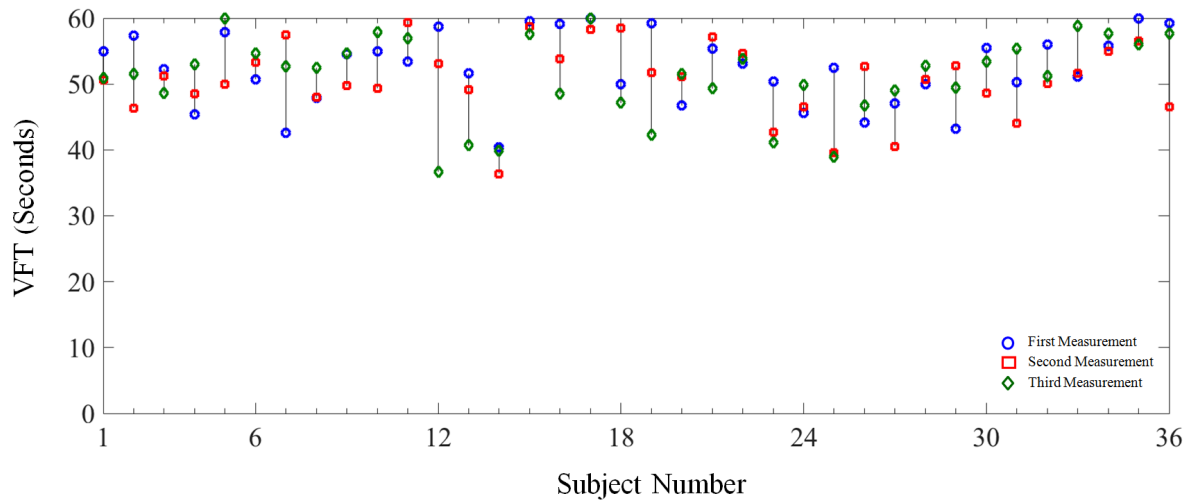


Figure 4. 12. HeMo measurements for each subject. Values are mean of annotated values.

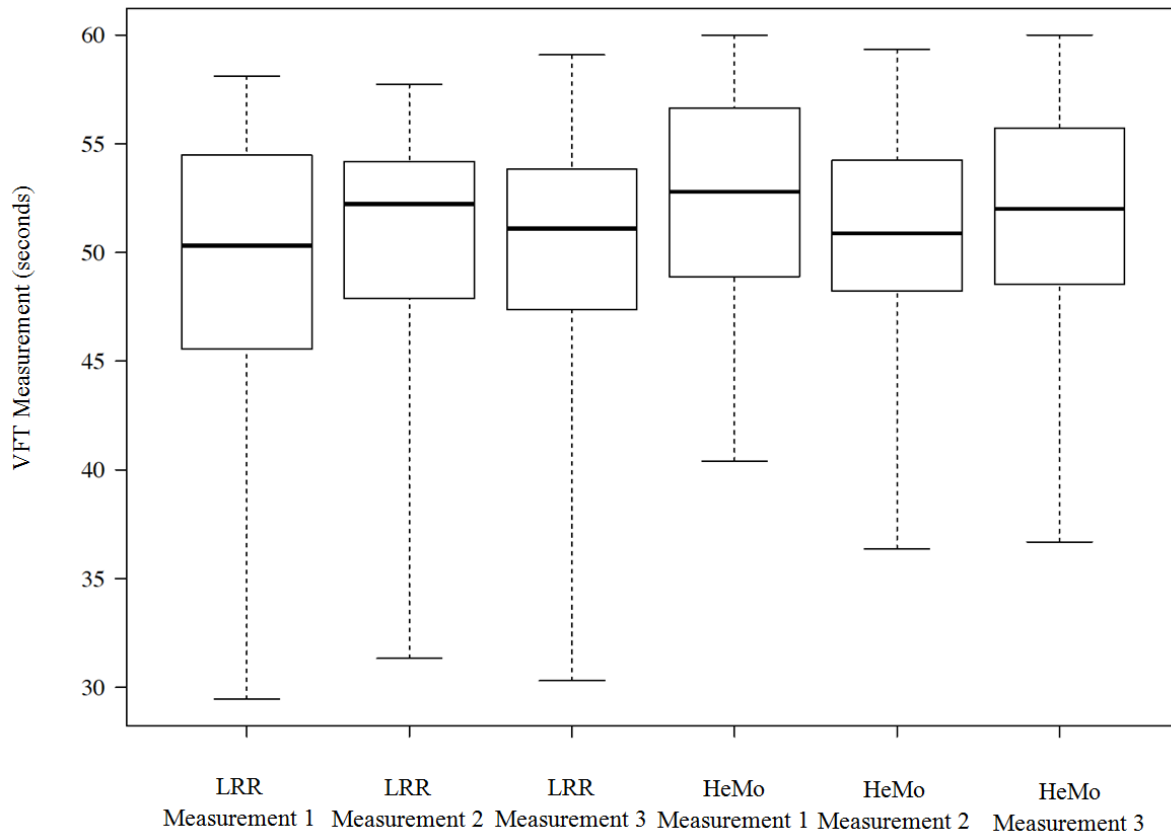


Figure 4.13. Box-whisker plots of the three measurements for LRR and HeMo.

### 4.3.5 Effect of Five Minute Walk on VFT

Ten of the recruited participants underwent an extended version of the experiment, which included three VFT measurements, a five minute walk at a self-selected “fast” speed and a repeat of three VFT measurements. Similar to the previously presented data, three raters marked the start and end points of the venous refilling traces recorded from these ten subjects. The average of the nine VFT values (three measurements each annotated by three raters) was used for each recording.

Figure 4.14 a shows LRR VFT values measured before and after the five-minute walk and Figure 4.15 b provides a similar illustration for HeMo measurements. The mean and standard deviation of both before and after walk VFT measurements with HeMo and PPG are given in Table 4.7.

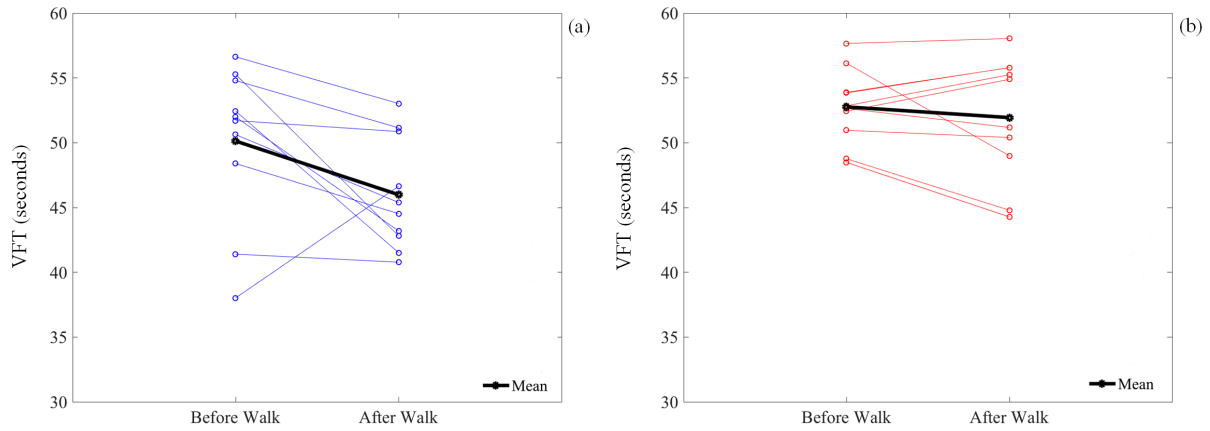


Figure 4.14. Comparison of before and after walk VFT measurements. Panel (a) refers to LRR measurements; Panel (b) refers to HeMo measurements.

Comparison of these two figures infers a better agreement between before and after exercise VFT values for HeMo. To further investigate the legitimacy of the recent cursory conclusion from Figure 4.14 We did a paired t-test between before and after walk VFT measurements for both HeMo and PPG (Table 4.7).

Table 4.7. Statistical summary of before and after walk VFT measurements of PPG and HeMo.

Method	Mean	Mean	Std	Std	P*
	Before Walk	After Walk	Before Walk	After Walk	
LRR	50.13	45.99	6.04	4.32	0.06
HeMo	52.76	51.94	2.90	4.81	0.45

\* Denotes the p value from paired t-test of before and after walk VFT measurements.

The results from paired t-test further highlighted more robustness of HeMo VFT measurements to exercise compared to the LRR VFT measurements.

The box-whisker plots of before/after exercise VFT measurements for HeMo and LRR in Figure 4.15 illustrates a smaller difference of before/after exercise VFT for HeMo measurements compared to the difference for LRR measurements.

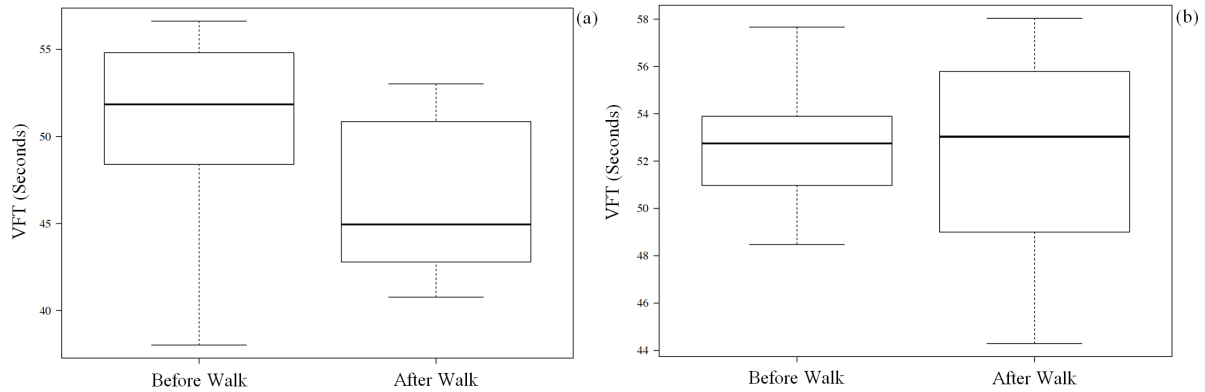


Figure 4.15. Box-whisker plots of before and after exercise VFT measurements. Panel (a) refers to LRR VFT measurements; Panel (b) refers to HeMo VFT measurements.

## 4.4 Discussion and Conclusion

Chronic venous insufficiency is a common condition, which can lead to loss of limb or venous ulcers demanding prolonged therapy. Venous Filling Time (VFT) was measured in thirty-six healthy volunteers using HeMo and a Light Reflection Rheography (LRR) sensor simultaneously. Qualitative comparison of the two measurements revealed similar results, with all subjects classified as healthy based on a threshold VFT of 25 seconds, the borderline selected to distinguish healthy and unhealthy venous systems.

Quantitative comparison of VFT measurements from the two sensors showed only a moderate correlation ( $r=0.47$ ) with a mean difference of  $-1.66$ . A paired t-test of the two measurements highlights a systematic difference between HeMo and the LRR sensor ( $p = 0.01$ ). However, this does not mean one measurement is wrong; LRR is sensitive to only one area of skin whereas HeMo effectively examines the entire part of the leg it encloses.

Bland-Altman plots of HeMo and LRR VFT values demonstrated a small mean bias, 96% of the difference-points within limits of agreement and with a distribution tending to normal.

Limits of agreement were wide, but acceptable for the presented dataset, as it did not affect the decisions of HeMo in classifying a subject as healthy/unhealthy.

The moderate correlation coefficient between devices and the statistical significance difference found between them can be attributed to a variety of factors. The HeMo measurement area on the leg was different from the LRR sensor location. Further, HeMo uses electro-resistive polymer sensors and measures blood volume changes of the area on the leg inscribed by the cuff, whereas, the LRR uses optical-based sensor and measures the amount of blood volume variation underneath the area of skin where the LRR sensor is placed.

Both LRR and HeMo suffer from repeatability and inter-rater reliability issues. As the experiment is quite short, it is feasible to take the mean of multiple measures as we have done here and ameliorate the repeatability issue to some degree. The inter-rater reliability problem is more difficult to solve. Automated computer selection of the start and end points may be the most effective means of ensuring a reliable reproducible measure, as even with extensive instruction the raters were quite different at times.

It should also be noted that the reference method in this experiment is not the gold standard method for venous assessment. This is one of the major limitations of the presented study and comparison of HeMo with the gold standard should be applied in future validation steps of this prototype. Of course, HeMo needs to be studied in clinical settings extending our current VFT dataset to one including both control and patient subjects to define the optimal threshold/ranges to separate healthy and CVI limbs.

This chapter demonstrates acceptable agreement between HeMo and LRR for healthy population. However, it should be noted that HeMo needs improvements in terms of its reliability and of course it needs to be tested in clinical settings against the gold standard for further validation. Although the LRR sensor is cheaper and requires less time and technical skills compared to the gold standard (Duplex Ultrasound) used for venous assessment, HeMo is vastly less expensive by two orders of magnitude and needs less training, which potentially may lead to its widespread use. The results of the exercise experiment showed that HeMo was quite robust to activity, which may eliminate the need for pre-test rest and consequently reduces the required time for diagnosis. Overall, the results suggest that HeMo has good

potential for assessing venous function in the leg. This technology may serve as an important assessment tool in the primary care setting.

## **Chapter 5 Evaluation of HeMo for the Assessment of Arterial Function**

This chapter provides a comparison of HeMo and Photoplethysmography (PPG) arterial pulse wave recordings for the assessment of the peripheral vascular function of healthy volunteers.

## **5.1 Background**

### **5.1.1 Peripheral Arterial Disease (PAD)**

Peripheral arteries are responsible for carrying oxygen-rich blood from the heart to the limbs. The failure of one or more arteries decreases blood flow to the limbs and ultimately, it may lead to morbidity/mortality [4,117,219]. Incompetence of the peripheral arteries is known as peripheral arterial disease (PAD), a condition in which one or more peripheral arteries become narrowed or blocked due to the plaque development in the arteries [220,221]. The most common risk factors for PAD are age, male gender, diabetes, smoking, dyslipidemia (high level of fat in blood), and hypertension [142,222]. PAD is highly prevalent, affecting 10-15% of general population and often underdiagnosed, up to 50% of patients with PAD are asymptomatic [16,66,114,154]. Symptomatic PAD can present with pain at rest, intermittent claudication, skin changes, ischemic ulceration and gangrene [14,147,223]. Both symptomatic and asymptomatic patients with PAD are at high risk of cerebrovascular and cardiovascular events [14,16,28,122,223]. Therefore, a routine screening test is required for risk factor modification and effective treatment which can lead to decreased clinical events, lessen the progression to limb loss, prevent disability/death, and in general to improve quality of life [16]. Various established diagnostic tests (fully described in Chapter 1) have been used for the assessment of arterial perfusion in the leg. The arterial pulse wave has been commonly used for the assessment of arterial perfusion as the arterial pulse becomes distorted in the presence of PAD, appearing damped, delayed and diminished.

### **5.1.2 Arterial Pulse Wave (APW)**

Arterial Pulse Wave (APW) analysis is a non-invasive method to evaluate arterial blood flow and identify peripheral arterial insufficiency in the lower limbs. The arterial pulse signal shows the variation in blood flow with each heartbeat that goes from the heart to the limbs with a wave-like pattern [48]. The APW can be separated into to three main components which, correspond to different phases of a cardiac cycle (Figure 5.1): a steep upstroke and sharp peak occurring during systole (anacrotic phase), the dicrotic notch (reflective wave)

representing the closure of aortic valve, and a gradual downslope occurring during diastole (catacrotic phase) [192].

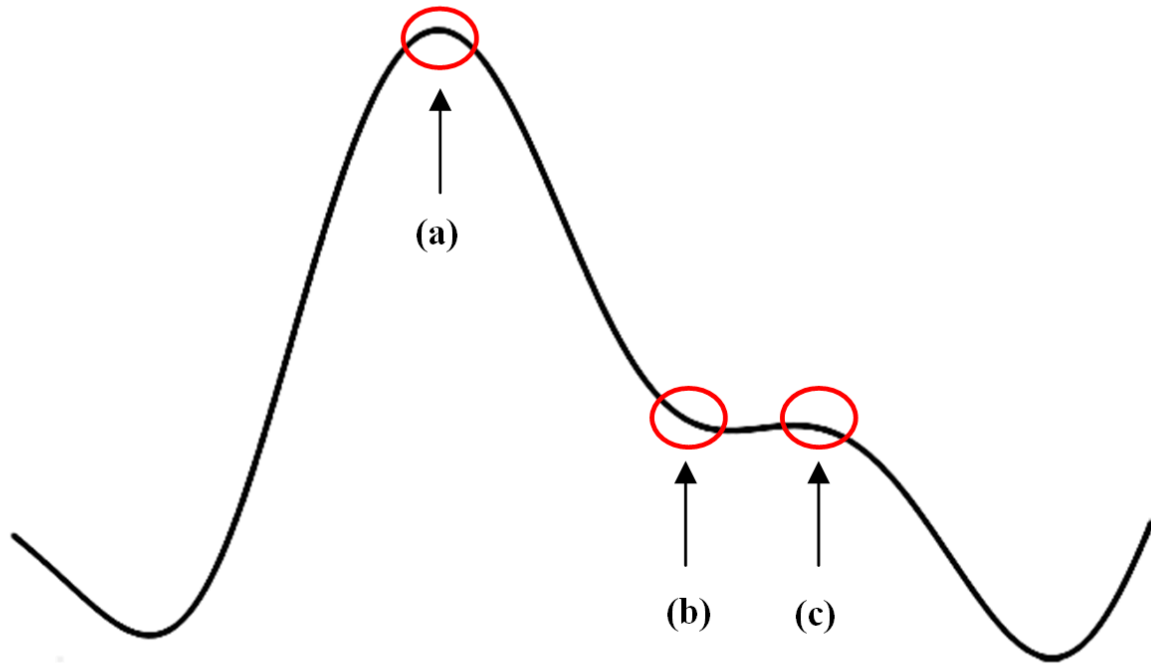


Figure 5.1. A typical arterial pulse waveform. (a) systolic peak, (b) dicrotic notch and (c) diastolic peak.

### **Qualitative Interpretation of the Arterial Waveform**

Normally, the APW appears with a dicrotic notch on the catacrotic phase and the pulse becomes delayed, distorted and diminished in the presence of PAD [52,192,224]. The amplitude of the systolic peak and the shape of the APW are two key aspects, which are commonly considered for a qualitative interpretation of the arterial waveform [185,192]. The disappearance of the dicrotic notch often represents arterial obstruction, while reduced systolic amplitude shows poor local perfusion [185,192]. Qualitative interpretation of the APW is simply done by visually comparing the APW to a four-level grading system (Figure 5.2), which enables the classification of the APW as normal, mild PAD, moderate PAD, and severe PAD [192,225].

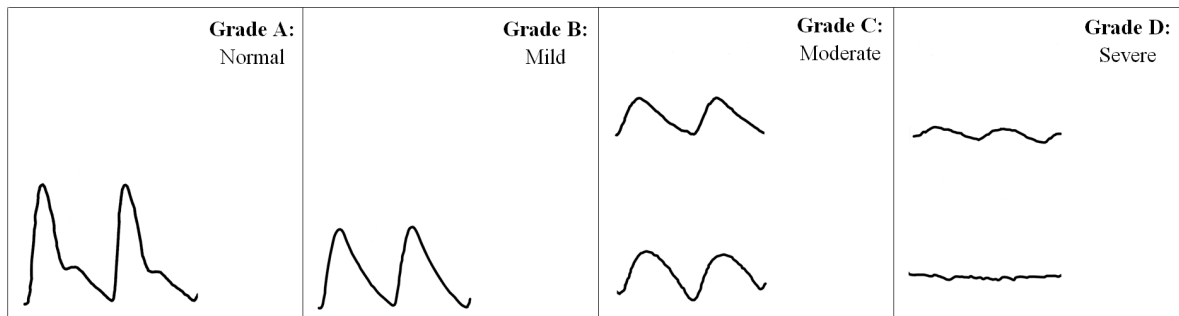


Figure 5.2. Arterial pulse wave grading system [192]. Grade A is attributed to an APW with a prominent dicrotic notch and sharp systolic peak; Grade B is attributed to an APW in which the dicrotic notch is disappeared; Grade C is attributed to an APW in which the dicrotic notch is absent, the systolic peak is flattened, the upslope and downslope time are decreased and almost equal; Grade D is when the amplitude of pulse is significantly decreased, upslope and downslope times are equal or there is absence of the pulse.

### Quantitative Interpretation of the Arterial Waveform

Quantitative interpretation of the APW involves extracting various pulse characteristics such as systolic amplitude, rise time/crest time and half pulse width.

Systolic amplitude represents blood volume changes due to arterial inflow around the measurement site [48,226,227]. Patients with PAD usually have reduced systolic amplitude which can be attributed to blood volume decrease in the microvascular bed resulting from blood pressure reduction across a stenosis [52,228,229].

Crest time or foot-to-peak rise time is defined as the time from the beginning of the APW to its systolic amplitude (Figure 5.3) and has proven to be a useful feature in diagnosis of PAD [48,52]. Delayed rise time is expected in the presence of PAD due to increased vascular resistance and reduced blood pressure as a result of stenosis [52].

Half pulse width is the width of APW at its half height. As the systolic peak reduces and the APW becomes damped with PAD, the half pulse width is expected to become wider. Awad et al. found a positive correlation between the half pulse width and vascular resistance suggesting that the half pulse width is increased with the severity of PAD [230]. It should be also noted that the presence/absence of the dicrotic notch can be investigated by searching for

the inflection point of the APW. The inflection point may be difficult to be found in some APW recordings. However, the first derivative of the APW is helpful as the inflection point appears as a local maximum on the derivative of the APW [48].

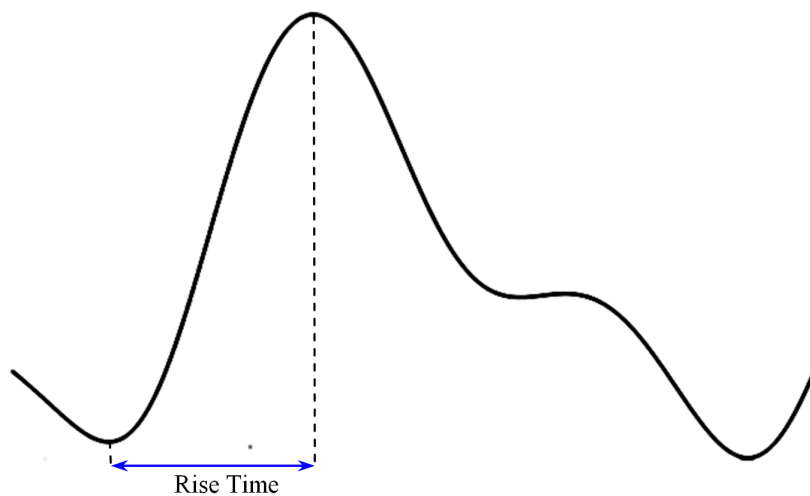


Figure 5.3. Illustration of crest time/rise time.

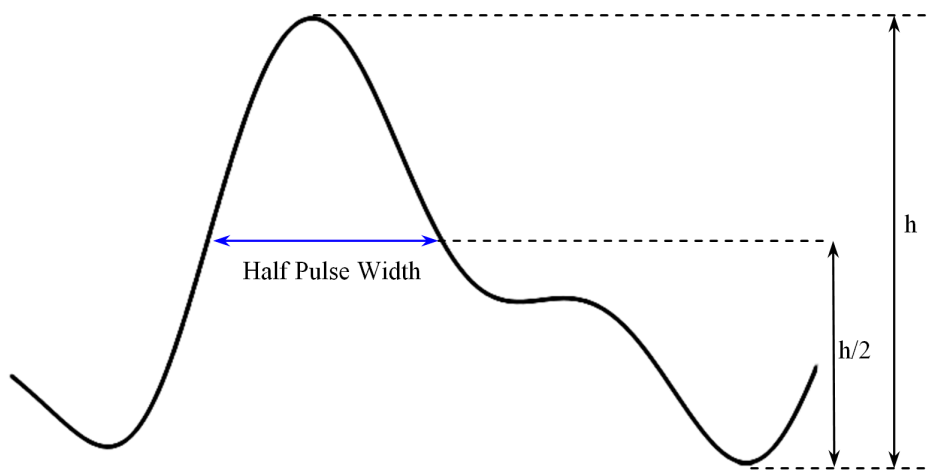


Figure 5.4. Illustration of half pulse width.

Other features of APW such as pulse interval/pulse width, augmentation index and large artery stiffness index (Figure 5.7) can be also extracted from arterial pulse signals and provide meaningful information [48].

Pulse interval or pulse width is the time between the beginning and the end of the APW (distance between two consecutive APW minimums) (Figure 5.5) [48].

Augmentation index is measured by dividing the amplitude of diastolic peak (y) by the amplitude of systolic peak (x) (Figure 5.6):

$$\text{Augmentation index} = \frac{y}{x} \quad (5.1)$$

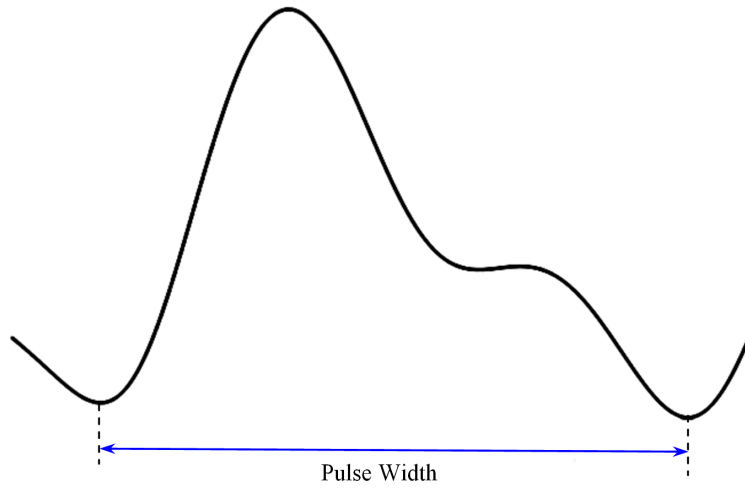


Figure 5.5. APW pulse width

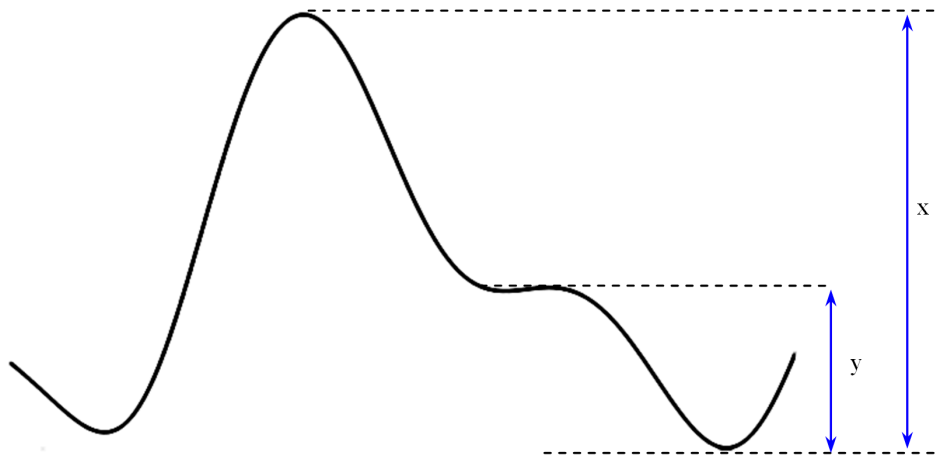


Figure 5.6. Illustration of x and y for calculation of augmentation index. x is amplitude of systolic peak and y is amplitude of diastolic peak.

Large artery stiffness index is defined as the ratio of patients' height to the time interval between the systolic and diastolic peaks (Figure 5.7) [48]:

$$\text{Stiffness index} = \frac{\text{Height of subject}}{\text{Systolic Peak to Diastolic Peak Time}} \quad (5.2)$$

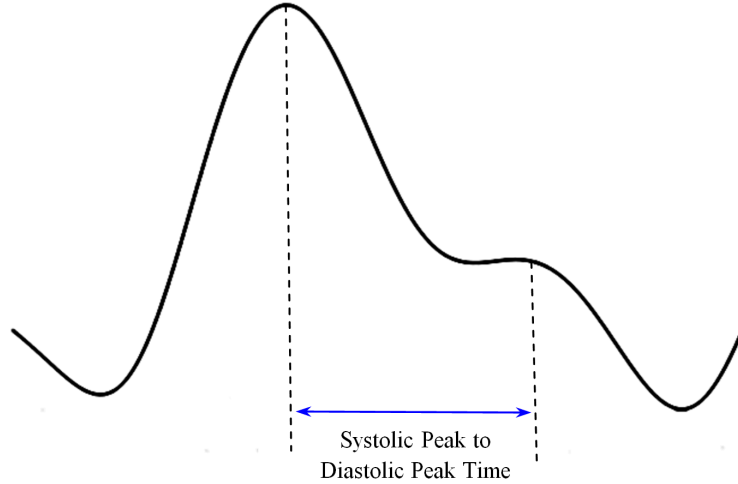


Figure 5.7. Systolic peak to diastolic peak time for calculation of stiffness index.

It is not yet known if these three APW features (pulse width, augmentation index and stiffness index) can reveal information about the presence/absence of PAD. However, each of the mentioned features has been proven to have other diagnostic values. For example, pulse interval represents a complete heart cycle and could be used to monitor heart rate variability [48,231–234]. Augmentation index and large artery stiffness index have been reported to be useful for the assessment of arterial elasticity [48,235]. Additionally, the second derivative of the APW have been reported as a potential candidate for assessment of arterial distensibility [48,236,237].

Other features including three quarters pulse width (Figure 5.8) and dicrotic notch to diastolic peak time (Figure 5.9) can be also extracted from the APW. However, no study has assessed their diagnostic value as of yet.

We previously examined the use of HeMo in a single subject and showed the capability of the device to record arterial pulse waves (chapter 2). In this chapter we expand on this prior work, determining if APW metrics as described may be extracted. We further compare these parameters to arterial pulses recorded from an established device in a well-powered study. Note that the hypothesis under test is - HeMo and PPG produce similar response metrics in healthy subjects.

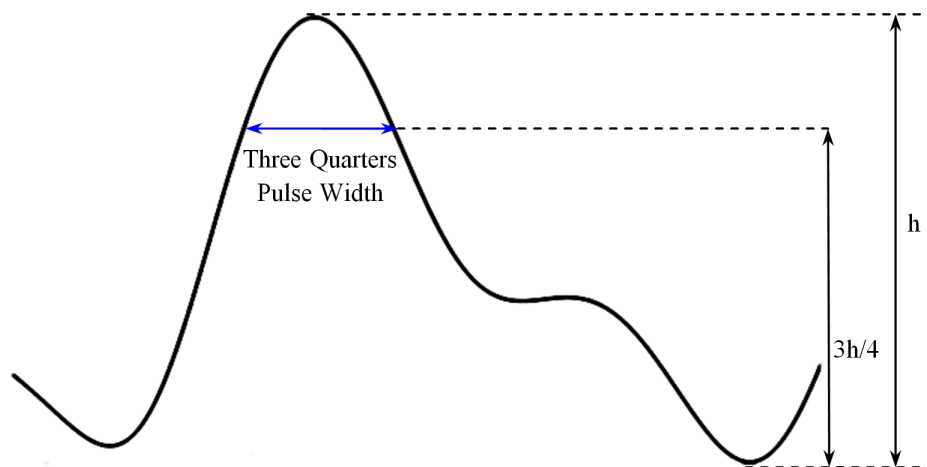


Figure 5.8. Three quarters pulse width.

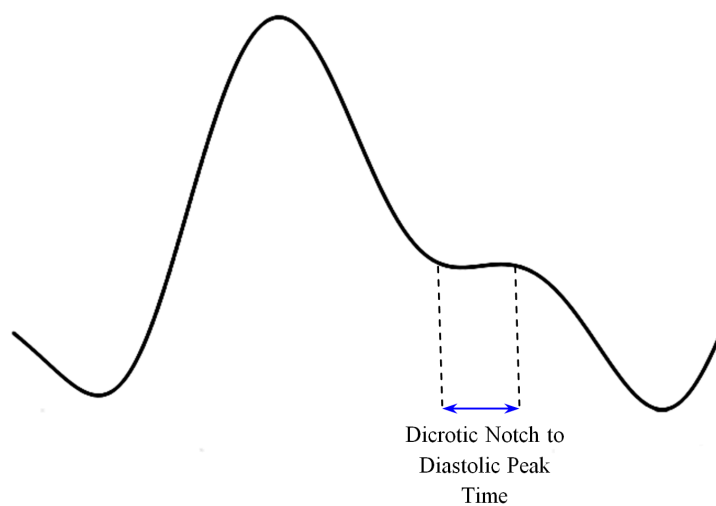


Figure 5.9. Dicrotic notch to diastolic peak time

## 5.2 Methods

### 5.2.1 Subjects

Thirty-six healthy volunteers aged 18-65 were recruited for this study. None of the participants had a history of seizures or fainting, cardiovascular disease, chronic venous insufficiency, epilepsy, deep vein thrombosis (DVT), pulmonary embolism or other clotting problems. All data were recorded from the right leg. This study was approved by the Human

Research Ethics Committee of Western Sydney University (Approval No: H11268). All subjects gave their written informed consent prior to their participation in the study.

## 5.2.2 Experimental Settings and Measurement protocol

All subjects participated in the experiment wearing shorts and barefoot. Height, weight, and age of each participant were recorded. Volunteers were asked to wear HeMo on the thickest part of the calf and the PPG sensor (VasoScreen 5000, Medis Medizinische Messtechnik GmbH, Ilmenau, Germany) was placed on the great toe. Each subject was then asked to sit on a chair with the foot relaxed on the floor. Participants were asked to refrain from talking or moving and asked to breath normally during the experiment to protect the arterial pulse signal from possible artefacts.

Recordings were made simultaneously from both HeMo and the PPG sensor. To synchronize data from the two devices, we asked each participant to perform a single dorsiflexion manoeuvre. The dorsiflexion manoeuvre induced artefact on both recordings providing a marker to synchronize the recordings. Two minutes of data were captured in each instance and participants were asked to perform an additional dorsiflexion to mark the end of the recording. Table 5.1 summarises the experiment protocol.

Table 5.1. Summary of APW recording protocol for HeMo and PPG sensor.

Step	Task
1	Ask the subject to sit on a chair with the foot relaxed on the floor.
2	Place HeMo around the middle calf of right leg.
3	Place PPG sensor on the big toe of the same leg.
4	Start Recording
5	Ask the participant to perform one dorsiflexion manoeuvre and continue recording for two minutes.
6	Ask the participant to perform one dorsiflexion manoeuvre and stop the recording.

An extended version of the experiment was conducted to investigate the effect of activity on the arterial pulse wave. In this experiment, ten of the thirty-six volunteers were asked to rest

while sitting on a chair for fifteen minutes before the experiment to protect the phase one of the APW recording from the effect of walking before the trial. A complete version of the APW experiment (as explained above) was then conducted, and APW was recorded. The experiment continued by asking the subjects to walk on a treadmill with the HeMo cuff on their leg and with a speed at which they could consider fast walking. Of note, the PPG sensor had to be taken off for this phase of the experiment. Once the participant selected their preferred walking speed, they continued walking for five minutes. The subjects were asked to sit immediately following completion of the 5-minute walk and the PPG sensor was then reattached on the great toe for the second phase of APW recording. The same APW recording experiment was then repeated.

### **5.2.3 Data Acquisition**

HeMo APW data were recorded with a sampling rate of 1kHz using a PowerLab data acquisition unit and LabChart software (AD Instruments Pty Ltd, Dunedin, New Zealand). The PPG data were acquired with sampling rate of 224 Hz using the inbuilt data acquisition unit of the VasoScreen device and VascularLab software. The AD instrument box and Vasoscreen device were both connected to a laptop via USB.

HeMo APW traces were exported from LabChart to “.mat” format. PPG APW data were saved with Vascularlab software, exported in “.csv” format and imported into MATLAB for further analysis.

### **5.2.4 Data Analysis**

All HeMo APW recordings underwent a 50<sup>th</sup> order software non-causal (zero phase lag) IIR low-pass filter implemented using MATLAB with a cut-off frequency of 10 Hz to remove high frequency noise. The low-pass filtered data then underwent a Matlab 2<sup>nd</sup> order high pass filter with a cut-off frequency of 1.4 Hz to remove and potential baseline wander. The filtering steps were necessary to clean HeMo recordings and prepare them for comparison with the PPG data. The HeMo and PPG data were then synchronized for each subject using the two dorsiflexion manoeuvre markers visible on both APW recordings. Three arterial beats from HeMo and three corresponding arterial beats from PPG were then selected. We selected

APWs similarly for all participants to create a dataset including 138 HeMo and 138 PPG epochs.

To facilitate the APW feature extraction and comparison of the HeMo and PPG data, we developed a graphic user interface (GUI). The APW GUI enabled importing of the APW dataset, plotting both the APW beat and its first derivative, selecting five key points (the starting and end points, systolic and diastolic peaks and the dicrotic notch) of each beat, and finally saving the coordinates of the selected points for each beat. Of note, since the dicrotic notch is the inflection point of APW, the first derivative of APW can assist finding the dicrotic notch by simply visualizing it as a local maximum (Figure 5.2).

Using this GUI, first, all PPG APW beats were imported and opened sequentially in the GUI window. Figure 5.2 illustrates the GUI with an example PPG recording opened and annotated.

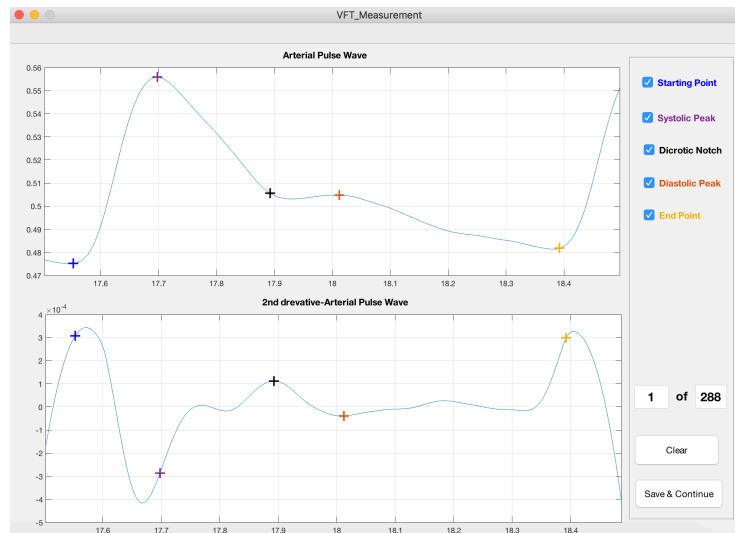


Figure 5.10. APW GUI when PPG data is opened for annotation of the starting point, systolic peak, dicrotic notch, diastolic peak and the endpoint. User annotations are marked as crosses and colour coded.

HeMo data annotated in a similar fashion. Figure 5.3 illustrates the GUI with an example HeMo recording opened in the GUI window and annotated. The complete MATLAB code of the APW GUI associating with the guideline for the use of this GUI is given in Appendix A.

The APW dataset underwent a double-blind annotation. The annotator was asked to use the developed APW GUI and mark five points (APW start and end points, systolic and diastolic

peaks and the dicrotic notch) for all PPG and HeMo recordings. In total, 276 APWs were annotated.

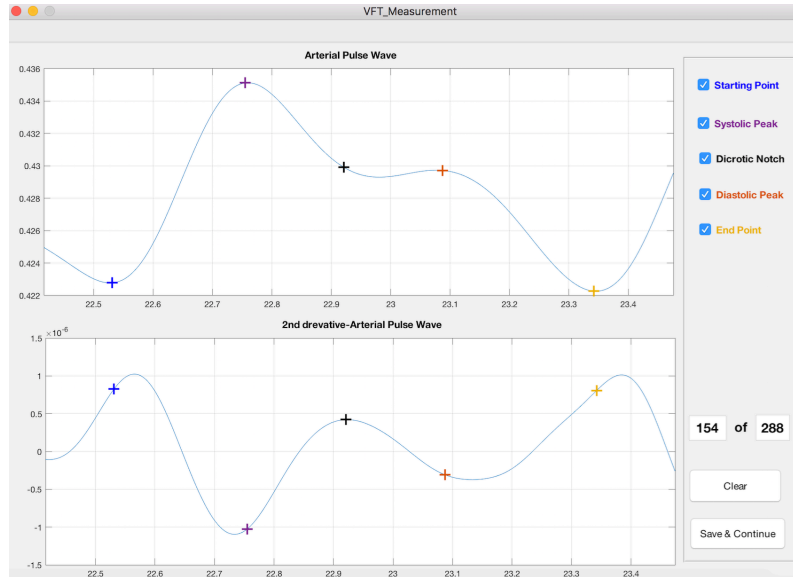


Figure 5.11. APW GUI when HeMo data is opened for annotation of the starting point, systolic peak, dicrotic notch, diastolic peak and the endpoint. User annotations are marked as crosses and colour coded.

## 5.2.5 Data Comparison

### Qualitative Comparison

The presence/absence of the dicrotic notch was investigated in all data by visually checking the point of inflection, the point at where the first derivative of APW appeared with a local maximum. The result of the search for dicrotic notch in HeMo and PPG data were then compared to provide a qualitative comparison of the two sensors.

### Quantitative Comparison

The following features were extracted from each HeMo and PPG APW - rise time, half pulse width, three quarters pulse width, dicrotic notch to diastolic peak time, systolic peak to diastolic peak time, stiffness index, augmentation index and pulse width. All of these metrics are explained in the introduction and are calculated simply using the annotated data points.

HeMo APW and PPG APW features were statistically compared using minimum, maximum, 1<sup>st</sup> and 3<sup>rd</sup> quartiles, median, mean, standard deviation, and confidence intervals. Box-whisker plots of HeMo and PPG features were used to compare the distribution of each feature for the two methods. Correlation coefficients were calculated for each APW feature of HeMo and PPG to assess the strength of the relationship between the two measures. Paired t-tests were also conducted to determine if extracted APW features of HeMo and PPG differ from one another. A *p* value of <0.05 was considered as a statistically significant difference between both methods.

A beat-by-beat comparison of HeMo and PPG APW features was shown using scatter plots to depict the differences between the APW features of the two methods. We used Bland-Altman plots to investigate the limits of agreement for the extracted APW features.

Given that our APW dataset included three arterial beats for each subject, we assessed the repeatability of each APW feature for HeMo and PPG by calculating intra-class correlation coefficients for each of the extracted features.

Finally, APW features from before and after walking we extracted for participants who took part in the exercise study, to determine the effect, if any, of five minutes exercise on the APW features of HeMo and PPG. It should be noted that each APW feature was averaged over the three selected beats for each subject.

All statistical analyses were performed using R studio software (version 3.2.1).

### 5.3 Results

Arterial pulse wave recordings were collected from thirty-six healthy volunteers with HeMo and PPG sensor simultaneously. None of the participants were excluded from the study. Table 5.2 provides a summary of participant demographics.

Table 5.2. Summary of participant demographics

<b>Number of Subjects (Female/Male)</b>	<b>Body Weight (Kg)</b>	<b>Height (cm) Mean (Range)</b>	<b>Body Mass Index (Kg/m<sup>2</sup>)</b>	<b>Age (years) Mean (Range)</b>
---	-----------------------------	-------------------------------------	---	-------------------------------------

	Mean (Range)		Mean (Range)	
36 (10/26)	79.4 (49-129)	172.4 (150-193)	26.5 (18.2-40.2)	32.5 (18-56)

### 5.3.1 Qualitative Analysis and Comparison

A cursory comparison of PPG and HeMo recordings was performed by visually inspecting the APW for the presence of a dicrotic notch. The dicrotic notch was seen in all 108 PPG and HeMo recordings. It should be noted that presence of the dicrotic notch was expected as the arterial pulse waves were recorded from healthy subjects. None-the-less, both HeMo and PPG showed agreement and classified all subjects as healthy.

### 5.3.2 Quantitative Analysis and Comparison

#### Population Distribution of Extracted Features

To provide a quantitative comparison of the two methods, we compared eight features (rise time, half pulse width, three quarters pulse width, dicrotic notch to diastolic peak time, systolic peak to diastolic peak time, stiffness index, augmentation index and pulse width) of both PPG and HeMo arterial pulse recordings. Three APWs were averaged for each of the 36 participants for both PPG and HeMo.

Table 5.3 presents a statistical summary of HeMo and PPG arterial pulse features providing the comparison of minimum (min), maximum (max), 1<sup>st</sup> quartile (1<sup>st</sup> Qu), 3<sup>rd</sup> quartile (3<sup>rd</sup> Qu), mean ( $\mu$ ), median, standard deviation (Std) and 95% confidence interval (95% CI) of HeMo and PPG APW features. The correlation coefficients (CC) and  $p$  value from paired t-test between HeMo and PPG APW features are also given.

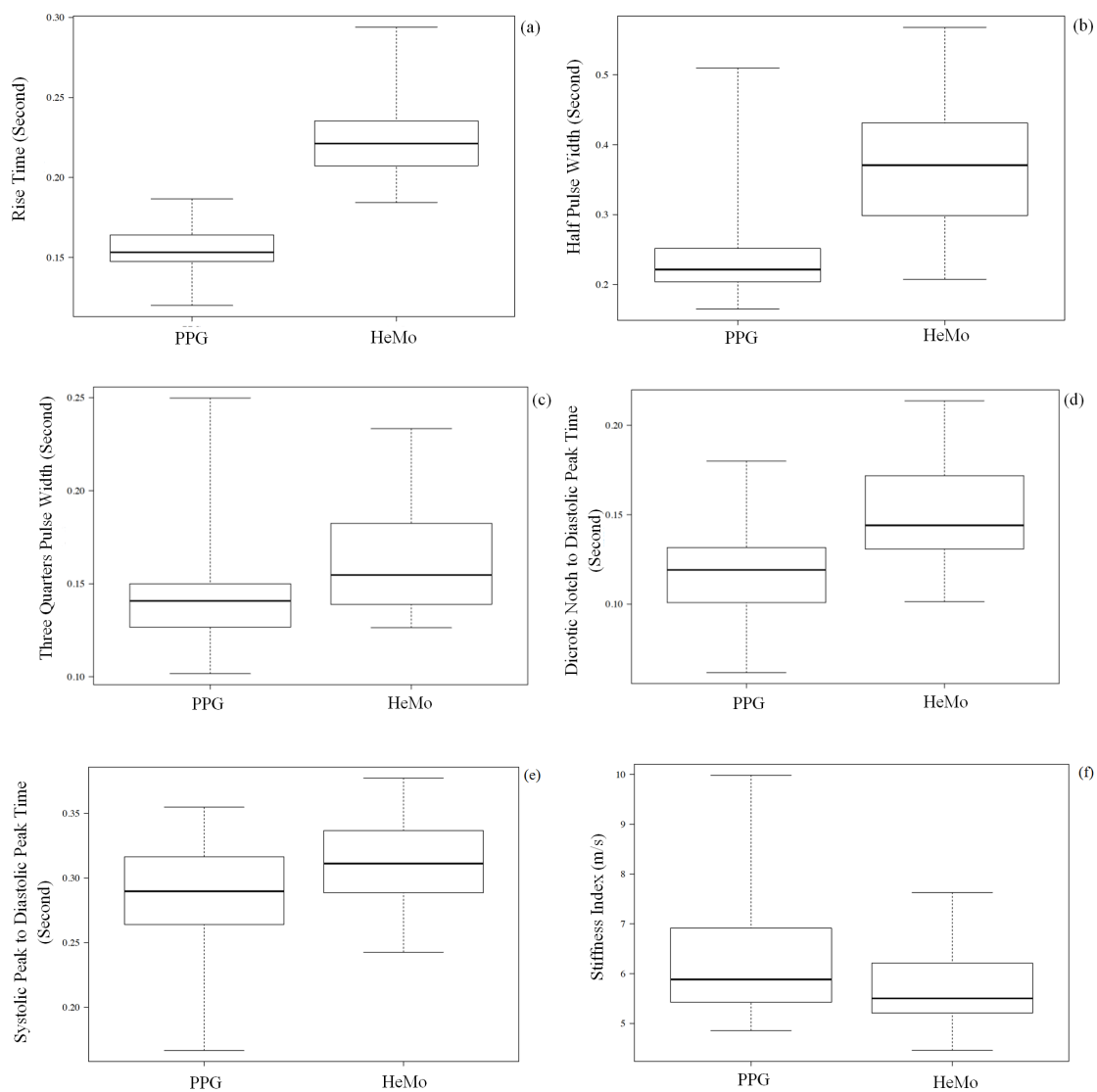
Table 5.3. Statistical summary of PPG and HeMo arterial pulse wave features.

<b>APW Feature</b>	<b>Mi n</b>	<b>1<sup>st</sup> QU</b>	<b>Media n</b>	<b>μ</b>	<b>3<sup>rd</sup> QU</b>	<b>Max</b>	<b>Std</b>	<b>95% CI</b>	<b>CC</b>	<b>p*</b>
Rise Time (PPG)	0.120	0.148	0.153	0.155	0.164	0.187	0.014	0.004	0.152	<0.05
Rise Time (HeMo)	0.184	0.208	0.221	0.224	0.235	0.294	0.022	0.007		
Half Pulse Width (PPG)	0.165	0.204	0.222	0.249	0.251	0.509	0.084	0.027	0.408	<0.05
Half Pulse Width (HeMo)	0.208	0.302	0.371	0.370	0.429	0.568	0.095	0.031		
Three Quarters Pulse Width (PPG)	0.102	0.127	0.141	0.145	0.150	0.250	0.031	0.010	0.190	<0.05
Three Quarters Pulse Width (HeMo)	0.126	0.139	0.155	0.162	0.182	0.233	0.027	0.009		
Dicrotic Notch to Diastolic Peak Time (PPG)	0.062	0.101	0.119	0.117	0.132	0.180	0.026	0.009	0.467	<0.05
Dicrotic Notch to Diastolic Peak	0.101	0.131	0.144	0.150	0.170	0.214	0.028	0.009		

Time (HeMo)										
Systolic Peak to Diastolic Peak Time (PPG)	0.16 7	0.264	0.290	0.286	0.316	0.355	0.041	0.013		
									0.604	<0.05
Systolic Peak to Diastolic Peak Time (HeMo)	0.24 3	0.294	0.311	0.310	0.337	0.377	0.034	0.011		
Stiffness Index (PPG)	4.85 7	5.425	5.881	6.176	6.913	9.986	1.088	0.355		
									0.689	<0.05
Stiffness Index (HeMo)	4.45 7	5.210	5.502	5.686	6.207	7.629	0.706	0.231		
Augmenta tion Index (PPG)	0.17 6	0.350	0.397	0.421	0.452	0.779	0.131	0.043		
									0.588	<0.05
Augmenta tion Index (HeMo)	0.29 5	0.465	0.502	0.519	0.590	0.671	0.086	0.028		
Pulse Width (PPG)	0.63 3	0.745	0.809	0.819	0.891	1.106	0.102	0.033		
									0.987	>0.05
Pulse Width (HeMo)	0.61 7	0.744	0.815	0.817	0.881	1.102	0.098	0.032		

\* Denotes the  $p$  value from paired t-test of HeMo and PPG APW features.

Figure 5.12 provides box-whisker plots for the extracted APW features displaying a comparison of the distributions of HeMo and PPG APW features through their quartiles.



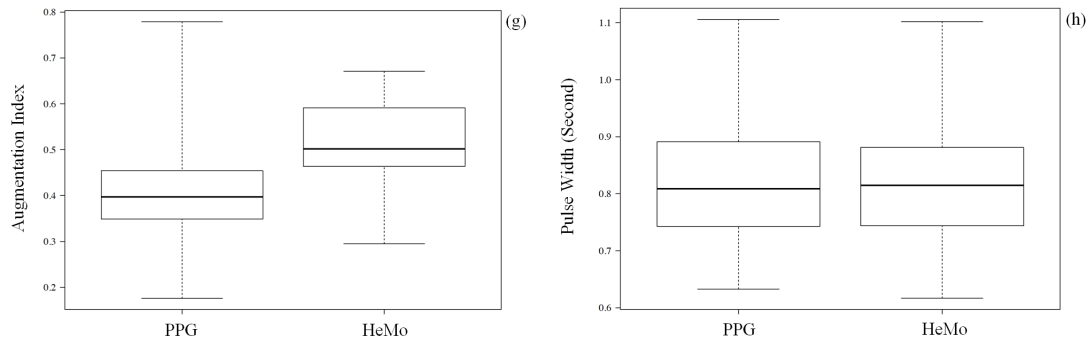


Figure 5.12. Box-Whisker plots of PPG and HeMo arterial pulse wave features. The horizontal lines in each box plot represent median, each box itself shows first and third quartiles, and the whiskers indicate the range.

As can be seen in Figure 5.12 the range of values for HeMo were smaller. This indicates that HeMo has tighter confidence intervals and potentially a more sensitive determination of non-healthy arterial waveforms.

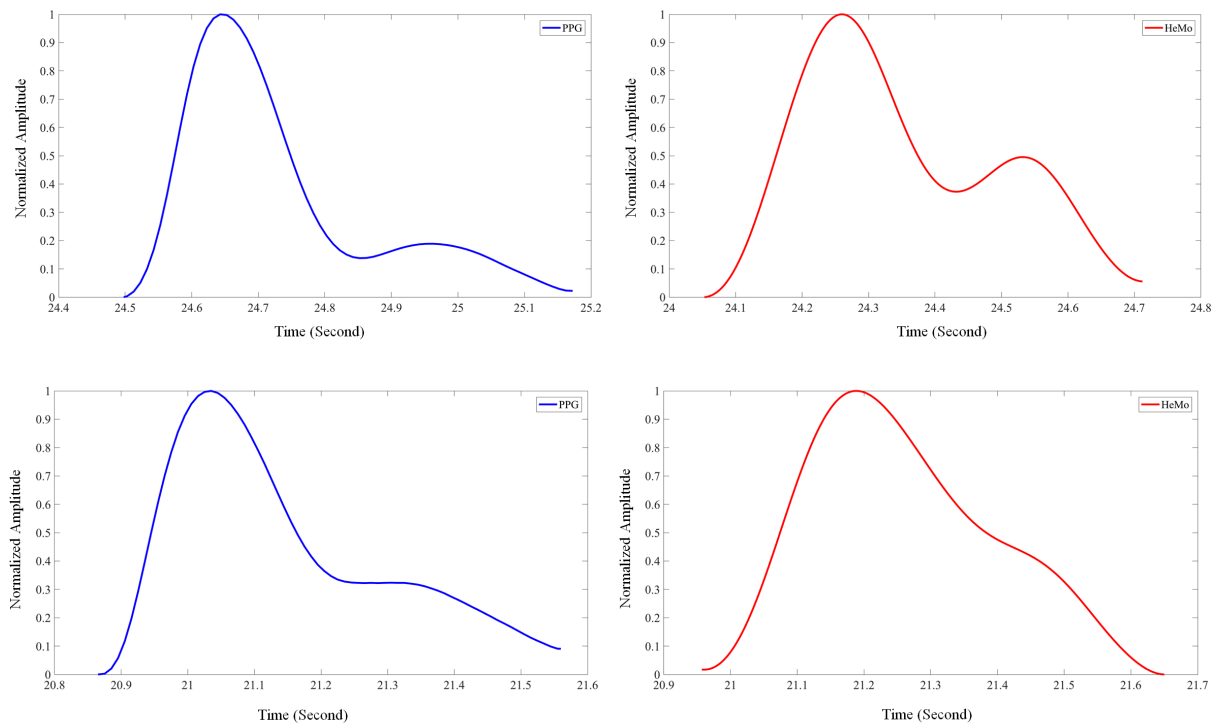
The box plot comparison of HeMo and PPG features shows that the time-based features (rise time, half pulse width, three quarters pulse width, dicrotic notch to diastolic peak time and systolic peak to diastolic peak time) extracted from HeMo form a distribution with higher values compared to the distribution of the same features extracted from PPG. The minimum, maximum and quartiles of HeMo stiffness index values are lower compared to those values from PPG stiffness. It is also evident that the augmentation index measurements of HeMo form a distribution with higher values compared to PPG. Among the extracted features pulse width of the two sensors tend to have a very similar distribution.

The strong correlation found between the pulse width of the PPG and HeMo pulse width was expected as each arterial pulse corresponds to the heartbeat propagating as a wave through limbs and the arterial pulse waves of the two sensors were simultaneously recorded. The poor/moderate correlation of other features can be explained by difference of the contour of arterial pulse wave of HeMo and PPG.

The calculated  $p$  value for pulse width greater than 0.05 further highlights the similarity of pulse widths of HeMo and PPG as expected. The  $p$  values calculated for other extracted APW show statistically significant differences between HeMo and PPG recordings ( $p < 0.05$ ).

### Contours of HeMo and PPG arterial pulse waves

Figure 5.13 illustrates three examples of PPG and HeMo arterial pulse waves recorded for three subjects. Although the overall shape of APW looks similar for PPG and HeMo, we found that the HeMo arterial pulse recording generally look slightly damped compared to PPG arterial pulse recordings resulting in increased rise time values for HeMo recordings. The broadened shape of HeMo APW also explains the difference in time-based features such as half pulse width, three quarters pulse width, dirotic notch to diastolic peak time, systolic peak to diastolic peak time and stiffness index. Another prominent difference is the amplitude of the diastolic peak, which affects augmentation index values.



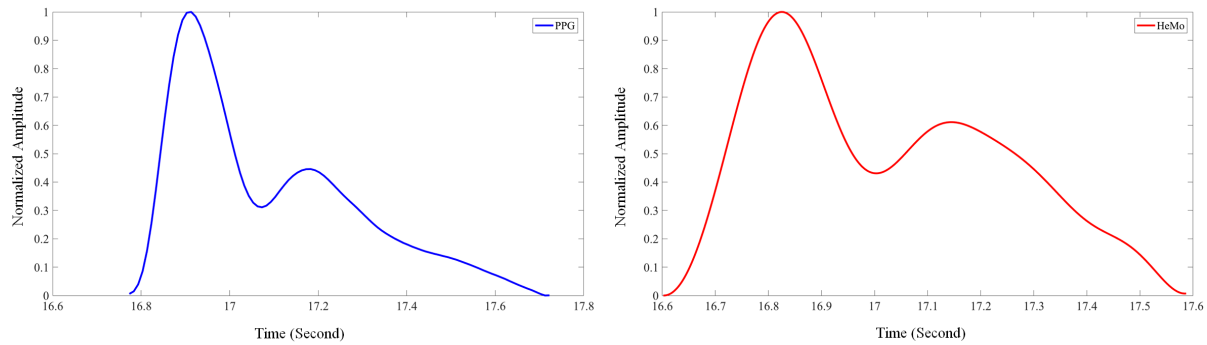
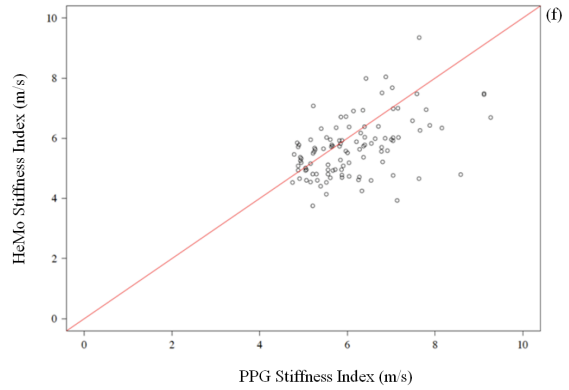
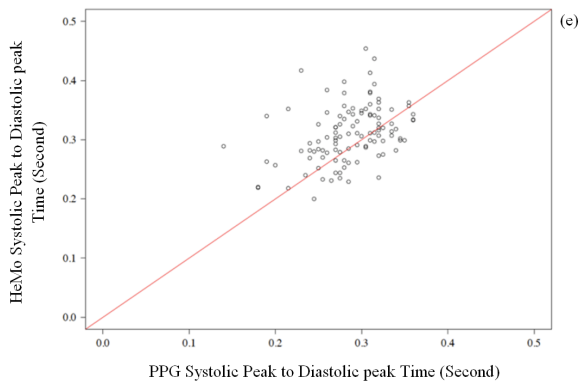
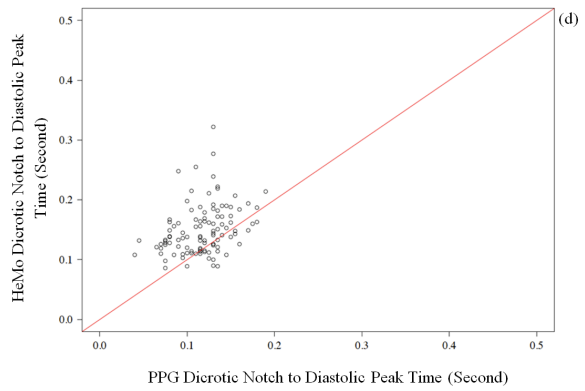
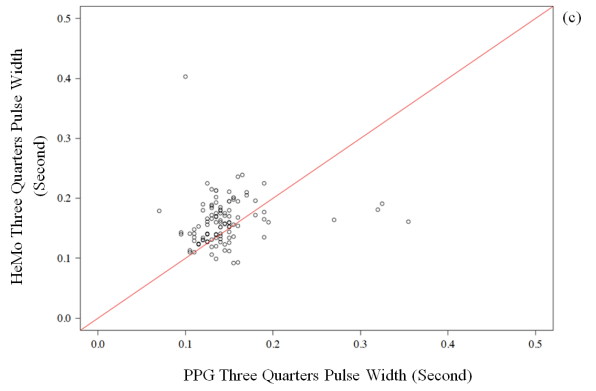
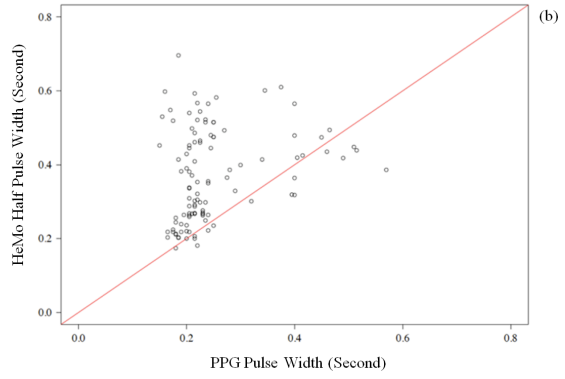
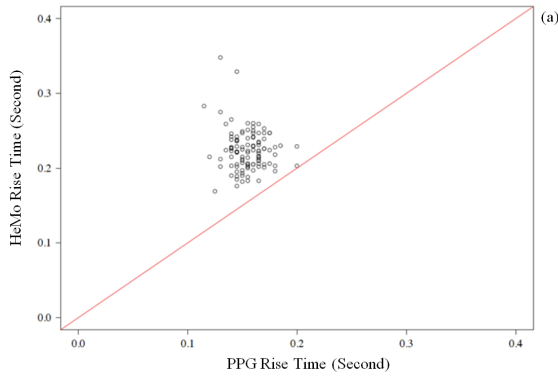


Figure 5. 13. Three examples of APW recordings with PPG and HeMo from three subjects. The blue printed plots on the left show PPG recording and the red printed plots illustrate the APW of corresponding HeMo recordings.

### Beat-By-Beat Comparison of HeMo and PPG

Since our APW dataset contains three APW beats for each participant, the APW features dataset contains 108 values for each of the features of PPG and HeMo. To visualize the relationship between the features of HeMo and PPG arterial pulse waves, we did a direct comparison of HeMo and PPG APW features. Figure 5.14 demonstrates features of HeMo plotted vs. features of PPG. The red line in each plot has a slope of one and passes through the point (1, 1) shown to depict how each features of the two sensors are different from each other.

Figures 5.14 a, b, c, d, e indicate mainly higher values of time-based features (rise time, half pulse width, three quarters pulse width, dicrotic notch to diastolic peak time and systolic peak to diastolic peak time) for HeMo further highlighting steepening of the arterial pulse of PPG compared to HeMo. HeMo appears to have lower stiffness index values (Figure 5.14 f), as stiffness index is inversely related to systolic to diastolic peak time. Figure 5.14 g shows higher values of augmentation index for HeMo, which is explained by higher diastolic peak amplitude seen in HeMo APW recordings. Figure 5.14 h illustrates that pulse width feature for HeMo and PPG closely match as expected.



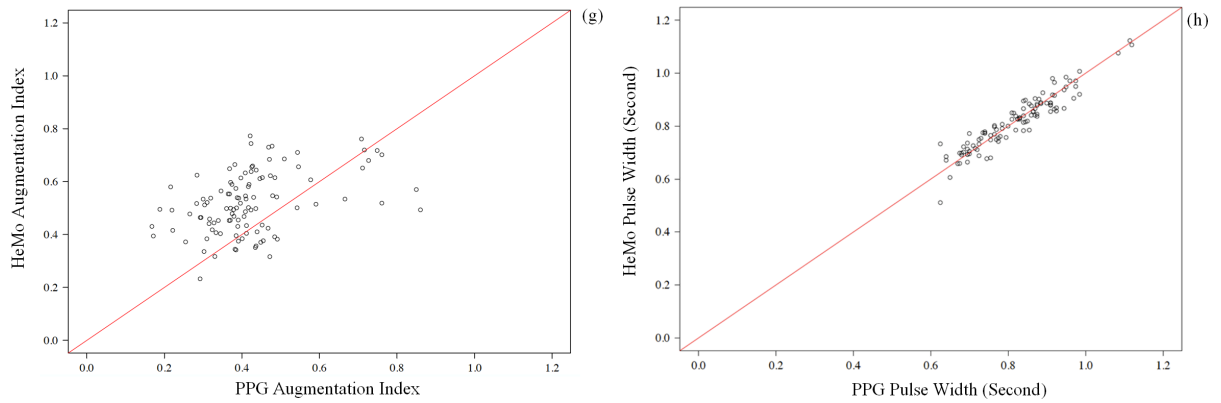
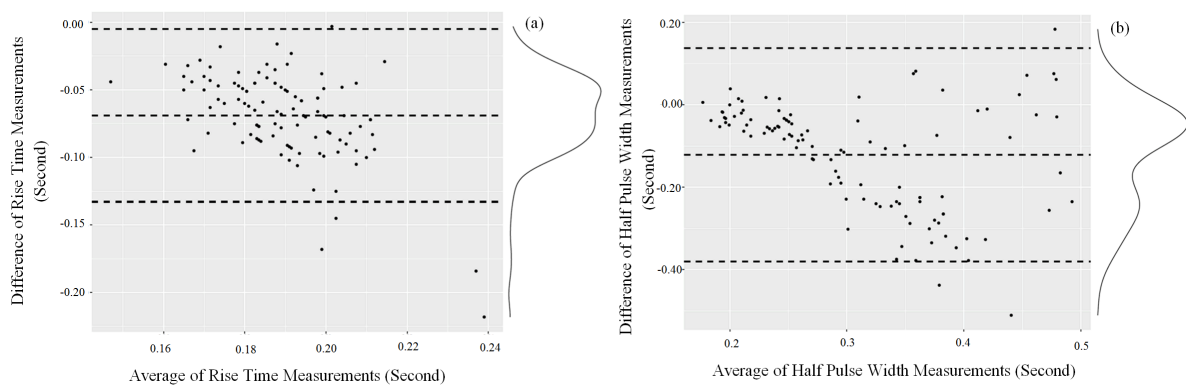


Figure 5.14. Scatter plots of HeMo APW features vs. PPG APW features.

Agreement between the APW features of HeMo and PPG are visualised using Bland-Altman plots, in which the mean differences of each HeMo and PPG APW features is plotted vs. their mean value (Figure 5.15). The bias, mean difference of the two measurements, presents the systematic error between two measurements, and the limits of agreement are shown with the upper (bias+2SD) and lower (bias-2SD) limits. Table 5.4 provides a summary of the bias, SD, upper and lower limits of the presented Bland-Altman plots.



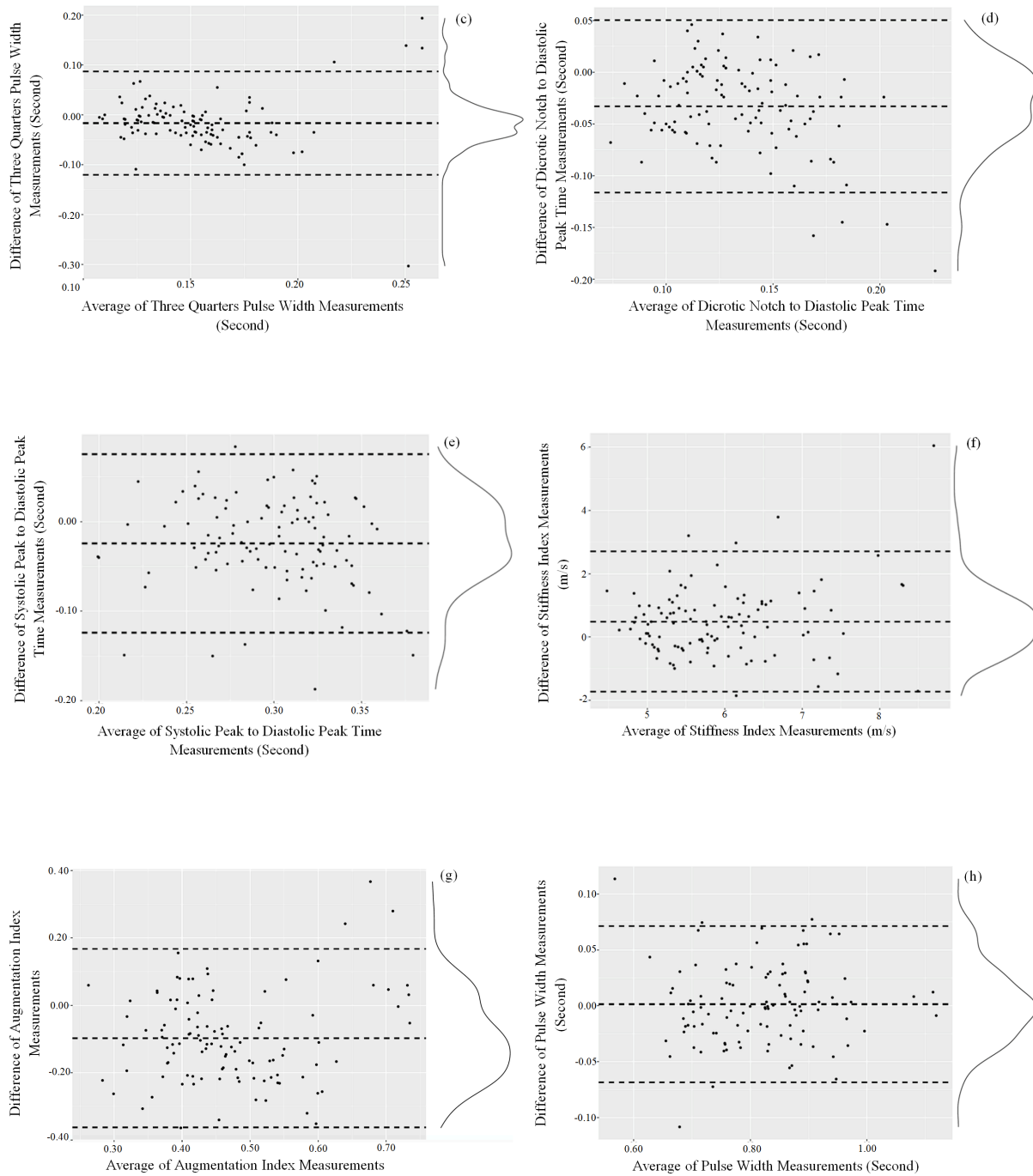


Figure 5.15. Bland-Altman plots of PPG and HeMo arterial pulse wave features. The dashed horizontal lines in each plot from top to bottom represent upper limit, bias and lower limit.

Table 5.4. Summary of the statistics in Bland Altman plots of HeMo and PPG arterial pulse wave features.

<b>APW Feature</b>	<b>Bias</b>	<b>SD</b>	<b>Lower limit</b>	<b>Upper Limit</b>
Rise Time	-0.069	0.032	-0.133	-0.005
Half Pulse Width	-0.121	0.129	-0.380	0.138
Three Quarters Pulse Width	-0.017	0.052	-0.121	0.087
Dicrotic Notch to Diastolic Peak Time	-0.033	0.042	-0.116	0.050
Systolic peak to diastolic peak time	-0.024	0.050	-0.124	0.075
Stiffness Index	0.490	1.109	-1.729	2.708
Augmentation Index	-0.098	0.132	-0.362	0.167
Pulse Width	0.001	0.035	-0.069	0.071

In the presented Bland-Altman plots, at least 94.5% of data for each feature lie within their limits of agreement. No appreciable trend was found for any of the features except for half pulse width. However, due to lack of any reported threshold value for the extracted features we cannot make any claim on the agreement of HeMo and PPG features. This is because making any statement about the agreement of two variable requires the comparison of limits of agreement with a priori defined clinical limit criteria [238].

It should be mentioned that Figure 5.15 b shows the absolute difference increases as the average of measurements increases. Moreover, there can be seen two completely separate local maximums on the distribution of half pulse width differences (Figure 5.15 b) further highlighting the jump of half pulse width values earlier discussed. This effect has resulted to have a wide limit of agreement for half pulse width and in practice would probably exclude it as a potential metric for HeMo. In contrast, a better agreement is found for three quarters pulse width as it has a narrower limit of agreement, a smaller bias, and the distribution of differences looks more similar to a normal distribution.

### 5.3.3 Repeatability of the HeMo and PPG Measurements

We assessed the repeatability of APW features extracted from HeMo and PPG by calculating the intra-class correlation coefficient for each feature. Table 5.5 provides the calculated intra-class correlation coefficients and their 95% confidence interval for the extracted features of HeMo and PPG arterial pulses.

Table 5.5. Repeatability of the APW features.

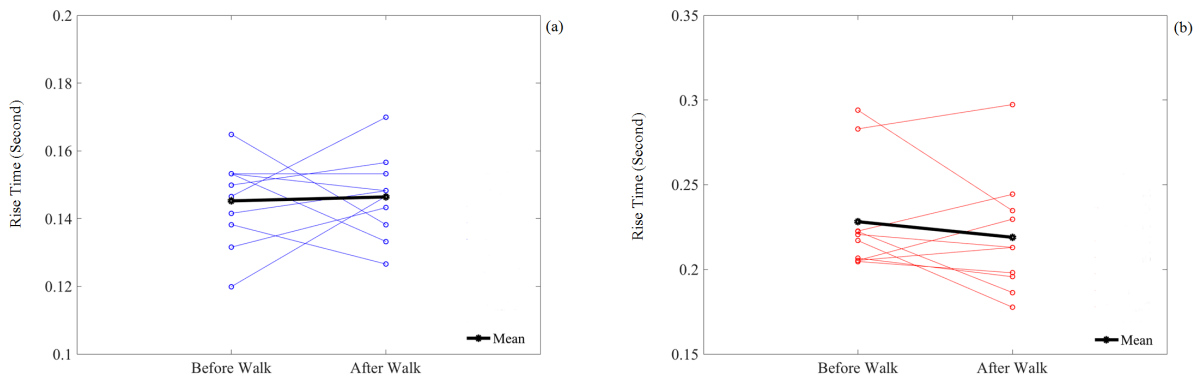
APW Feature	Intra-class correlation of Measurements	95%-Confidence Interval
Rise Time (PPG)	0.747	0.609 < ICC < 0.851
Rise Time (HeMo)	0.479	0.282 < ICC < 0.662
Half Pulse Width (PPG)	0.861	0.774 < ICC < 0.921
Half Pulse Width (HeMo)	0.35	0.144 < ICC < 0.559
Three Quarters Pulse Width (PPG)	0.372	0.169 < ICC < 0.577
Three Quarters Pulse Width (HeMo)	0.188	-0.01 < ICC < 0.414
Dicrotic Notch to Diastolic Peak Time (PPG)	0.667	0.504 < ICC < 0.798
Dicrotic Notch to Diastolic Peak Time (HeMo)	0.181	-0.011 < ICC < 0.405
Systolic peak to diastolic peak time (PPG)	0.881	0.805 < ICC < 0.933
Systolic peak to diastolic peak time (HeMo)	0.209	0.008 < ICC < 0.436
Stiffness Index (PPG)	0.854	0.764 < ICC < 0.917
Stiffness Index (HeMo)	0.294	0.086 < ICC < 0.513
Augmentation Index (PPG)	0.926	0.876 < ICC < 0.959
Augmentation Index (HeMo)	0.324	0.116 < ICC < 0.538
Pulse Width (PPG)	0.879	0.802 < ICC < 0.932
Pulse Width (HeMo)	0.823	0.714 < ICC < 0.899

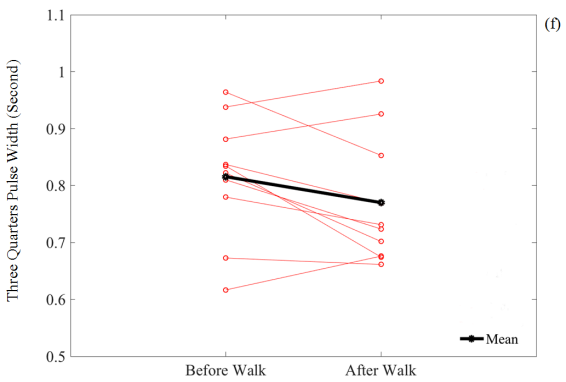
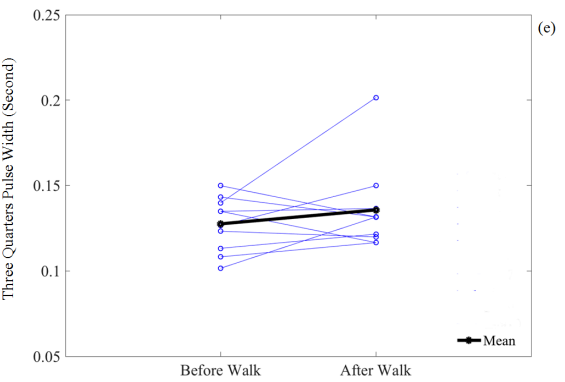
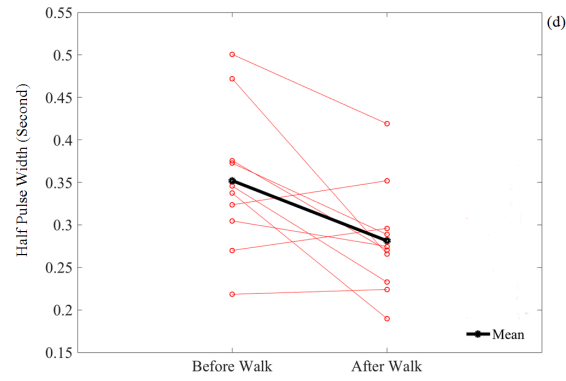
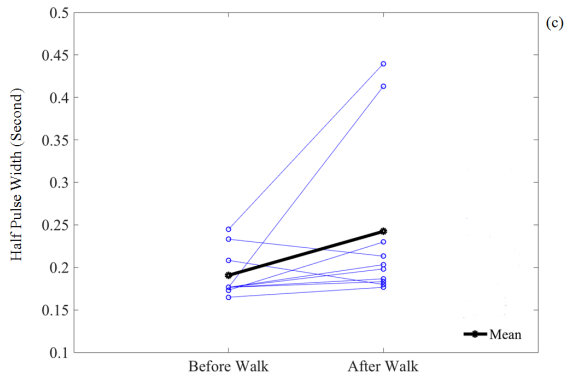
The calculated correlation coefficients show the arterial pulse features extracted from PPG are more repeatable. In contrast, low values of intra-class correlation clearly indicate a repeatability issue for the HeMo measurements.

### 5.3.4 Effect of Five Minutes Fast Walking on APW Features

Ten of the recruited subjects underwent an extended version of the experiment, which included APW recording, five minutes fast walking and re-recording of the APW. Eight arterial pulse wave features were extracted before/after exercise from HeMo and PPG recordings. Each feature was averaged over three beats for each subject.

Figure 5.16 shows the change in each APW feature before and after exercise. Mean and standard deviations of both before and after walk APW features are given in Table 5.6. Correlation coefficients of before and after exercise features were calculated to determine how strongly the measurements before and after exercise are related. A paired t-test between before and after exercise APW features establishes if any of these features changes significantly.





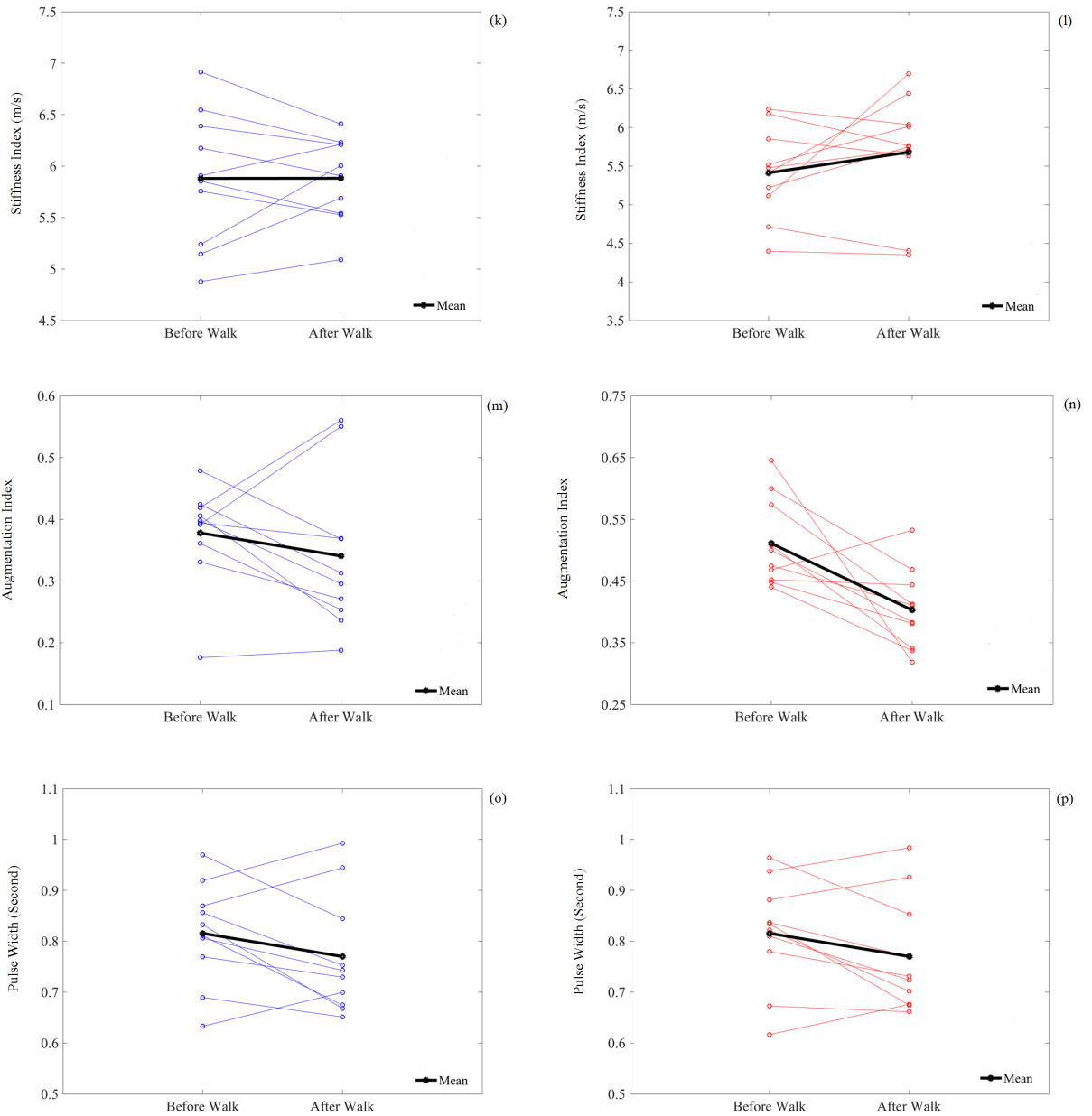


Figure 5.16. Comparison of before and after walk APW features. PPG APW features are presented in blue and HeMo APW features are depicted in red. The mean of each feature is presented in black.

Table 5.6. Statistical summary of before and after walk APW features of PPG and HeMo.

APW Feature	Mean	Std	Correlation	<i>P</i> value from paired t-test PPG/HeMo
	PPG/HeMo	PPG/HeMo	PPG/HeMo	

<b>Rise Time before Walk</b>	0.15	0.23	0.01	0.03	0.04	0.66	0.84	0.33
<b>Rise Time after Walk</b>	0.15	0.22	0.01	0.03				
<b>Half Pulse Width before Walk</b>	0.19	0.35	0.03	0.09	0.43	0.50	0.10	0.02
<b>Half Pulse Width after Walk</b>	0.24	0.28	0.10	0.07				
<b>Three Quarters Pulse Width before Walk</b>	0.13	0.16	0.02	0.03	0.35	0.15	0.33	0.31
<b>Three Quarters Pulse Width after Walk</b>	0.14	0.15	0.03	0.03				
<b>Dicrotic Notch to Diastolic Peak Time before Walk</b>	0.13	0.17	0.02	0.03	0.60	0.23	0.07	0.20
<b>Dicrotic Notch to Diastolic Peak Time after Walk</b>	0.14	0.15	0.02	0.03				
<b>Systolic Peak to Diastolic Peak Time before Walk</b>	0.30	0.33	0.02	0.04	0.32	0.54	0.87	0.24
<b>Systolic Peak to Diastolic Peak Time after Walk</b>	0.30	0.31	0.02	0.04				
<b>Stiffness Index before Walk</b>	5.88	5.41	0.65	0.59	0.77	0.57	0.99	0.22
<b>Stiffness Index after Walk</b>	5.88	5.68	0.41	0.76				
<b>Augmentation Index before Walk</b>	0.38	0.51	0.08	0.07	0.50	-0.16	0.31	0.01
<b>Augmentation Index after Walk</b>	0.34	0.40	0.13	0.07				
<b>Pulse Width before Walk</b>	0.82	0.82	0.10	0.11	0.67	0.76	0.15	0.09

<b>Pulse Width after Walk</b>	0.77	0.77	0.12	0.11
-----------------------------------	------	------	------	------

---

All before and after walk APW features of PPG were not significantly different (paired t-test  $p > 0.05$ ). The same was also the case for HeMo, except for the augmentation index which was significantly lower following exercise ( $p = 0.01$ ).

## 5.4 Discussion and Conclusion

Peripheral Arterial Disease (PAD) is highly prevalent [2,16,17] and can lead to loss of limbs and/or death [2,13–15]. PAD may be symptomatic or asymptomatic, however, both groups are at the same risk [2,28,29]. Early diagnosis of PAD is important as it can help prevent limb amputation and cardiovascular events [50]. Recording arterial pulse wave (APW) and comparing it with a grading system is one means of screening for impaired arterial function [192]. While the lack of an evident dicrotic notch is an initial sign of PAD [192], some APW features have also shown potential in diagnosing PAD [48,52,230]. A variety of features can be extracted from arterial pulse signal [48,52,231–233]. However, not all APW features are proven to have clinical value in diagnosis of PAD. Among APW features, rise time, half pulse width and the amplitude of systolic peak have shown to have diagnostic value for PAD [48,52,230].

APWs from thirty-six healthy volunteers were collected with HeMo and a photoplethysmography sensor simultaneously to compare the HeMo arterial pulse recording with the APW recording of a commercially available sensor. The APW recordings of the two methods were visually compared and the dicrotic notch was found in all HeMo and PPG APW recordings.

To provide a quantitative comparison of recordings of the two methods, eight APW features were extracted from HeMo and PPG arterial pulse recordings and they were statistically compared. The pulse width/pulse interval extracted from the APW of the two sensor were highly correlated ( $r=0.99$ ), and their difference was not statistically significant ( $p = 0.62$ )

showing that HeMo can provide an estimate of heart rate similar to the PPG estimate of heart rate. In contrast, poor or moderate correlation was found between other APW features of HeMo and PPG, and their corresponding  $p$  values showed statistically significant differences between each pair of APW features.

The poor/moderate correlation is due to a difference in the HeMo and PPG APW contours. This is likely due to a variety of factors, however, primary among them are the different recording locations and sensor types. HeMo APWs are recordings of changes in limb blood volume due to the pulse passing through all vessels in the recording region, whereas the PPG APW is a localised recording at the big toe. The difference in the size/lumen of the arterial vessels in these regions can affect the shape of arterial pulse [239]. Furthermore, as HeMo is a summation of all arterial flow in the area, whereas PPG is highly specific to one region, any difference in arterial flow in adjacent vessels in the measurement region of HeMo will lead to temporal dispersion and flattening of the compound signal. The difference seen in the contours of PPG and HeMo may be partially explained by the wave steepening effect, a steepening of arterial pulse and decreasing in mean pressure with distance from the heart [229,240,241]. In other words, the shape of arterial pulse recordings at two different points of body would have looked differently even if they were both recording using the same type of sensor. Further discrepancies may be expected, as the PPG is an optical sensor while HeMo is mechanical, incorporating electro-resistive sensors.

The statistically significant difference found in the APW features of HeMo and PPG does not undermine the potential of HeMo in diagnosing of PAD. It does highlight that APW features may not be used interchangeably. This indicates that if HeMo is to be used to diagnose PAD, its location is important and reference values will need to be calculated as thresholds for diagnosis.

This comparison allowed us to explore the APW features of HeMo and understand how each APW feature of HeMo differs from PPG arterial pulse features. The damped shape and higher diastolic amplitude seen in the arterial pulse of HeMo resulted in higher values for most of the extracted HeMo APW features, except for stiffness index, which was lower than PPG. It should be noted that the half pulse width values for HeMo cluster in two groups. In other words, there seems to be a considerable jump in half pulse width values. This effect

could be explained by the shape of the HeMo APW in which the dicrotic notch mainly occurs at a height close to the half-height of the pulse (Figure 5.13). Therefore, the pulse width values can be divided into two groups; one with smaller values corresponding to the pulses with their dicrotic notch occurring at half height or lower, and the other with higher half pulse width values corresponding to pulses which their dicrotic notch occurs at an amplitude greater than the half-height. The dicrotic notch typically occurred below the half-height of PPG arterial pulses, resulting in a more homogenous dataset for PPG half pulse width. However, some of PPG arterial pulses also appeared with their dicrotic notch occurring at or above the half-height of the pulse. This observed discrepancy makes half pulse width an unsuitable metric in defining a range for normal and PAD subjects. To address this issue, we defined three quarters pulse width, which in contrast is a more homogenous feature. This is because the three quarters height is virtually guaranteed to be greater than the amplitude at which the dicrotic notch typically occurs. Although this alternative metric was found to provide a more homogenous dataset for HeMo, future clinical trials will be required to identify the diagnostic value of this metric.

It should be also mentioned that among the extracted features rise time is the only APW feature which has been used to distinguish limbs with and without PAD [52]. A 95% confidence interval of PPG rise time was previously reported for healthy control subject by Allen et al. (0.172 - 0.278 seconds) [52]. The PPG rise time 95% confidence interval was lower in our study (range). This may be due to our younger population group (age range: 18-56) compared to the age range in Allen et al.'s study (age range: 40-85). HeMo rise time values lied within the reported range by Allen et al.'s study.

None of the PPG APW features showed statistically significant differences before and after exercise (5 minute walk). All HeMo APW features, except half pulse width and augmentation index, were not significant difference between before and after exercise. Augmentation index is dependent on the amplitude of systolic and diastolic peaks. As cardiac output increases with exercise, peripheral resistance decreases due to vasodilatation of the exercised muscle resulting in a rise in systolic peak but the diastolic peak remains largely unchanged [242]. While before and after walk augmentation index values were found not significantly different for PPG, we found the effect of exercise evident on HeMo augmentation index values. This

may be due to the location of HeMo, around the calf muscles. In contrast, PPG measures are localised underneath the skin of the toe where there are no muscles.

There are a number of limitations for the work presented in this chapter. We were not able to make any statement about the agreement between the APW features of the two sensors due to lack of priori defined clinical limit criteria for the extracted features. We also were not able to provide a comparison between the systolic amplitude of HeMo and PPG due to their different measurement units. Among the extracted features only half pulse width and rise time have been shown to correlate with vascular resistance and the clinical value of other extracted features is not yet known for PAD. There is clearly a repeatability issue for HeMo that could be improved, potentially by averaging more pulse waves. Another limitation of the presented study is that the reference method is not the gold standard for diagnosis of PAD. The presented study only provides the comparison of APW features of HeMo and PPG in a group of healthy volunteers and does not include patients in the study population. A clinical trial with patients diagnosed with PAD and age-matched controls is required to have a better understanding of its APW features, to define threshold values for each, and to investigate the diagnostic value of each feature.

Overall, this study highlights the potential of HeMo for low-cost and simplified diagnosis of PAD. However, an extensive clinical trial will be required to assess the legitimacy of this hypothesis. While the available diagnostic methods are expensive and usually reserved for patients with symptoms, HeMo is wearable, low-cost and requires minimal time and training, which may potentially lead to its widespread use as a screening tool for the assessment of arterial function in the leg.

## **Chapter 6 Discussion and Future Directions**

This chapter provides a summary of the work presented in this thesis by briefly discussing the motivation, objectives and achievements of the presented work. It is followed by a list of prospective future work, which could follow as a result of this research.

## 6.1 Summary of Contributions

Despite the ubiquity of peripheral vascular disease (PVD) and the importance of early diagnosis, the available diagnostic methods do not completely meet the need of clinicians for diagnosis in the primary care setting. The need for a new non-invasive diagnostic device was the motivation for the work presented in this thesis. The development of a new medical device requires extensive verification and validation as a key element of the design process. A complete set of user needs is a base requirement to complete this process. This thesis does not attempt to complete this process, but assesses the possibility of a new non-invasive blood-monitoring device and investigates a series of hypotheses to test a proof of concept device.

This thesis demonstrates that HeMo can reliably capture arterial pulse wave and measure venous refilling time. HeMo was compared with LRR in a well-powered group of healthy volunteers and an acceptable agreement between the two devices was found suggesting that HeMo has good potential for assessing venous competence in the leg. It was found that HeMo needs improvements in terms of its reliability when is used for VFT measurement. Comparison of arterial pulse wave recordings from HeMo and PPG revealed information on the APW features of HeMo and helped to understand how each APW feature of HeMo differs from PPG arterial pulse features. This thesis also revealed information on the characteristics of the ERB sensors used in HeMo. Investigation of the electrical behaviour of the ERB sensors showed that the peak-to-peak voltage of ERB sensors is associated with a drift during the first 40 hours of use, which then stabilises. Combined, these findings feed into the design requirements and user needs for the next stage of development in the commercialisation process. The main outcomes of the presented work include:

1. A comprehensive literature review of the available non-invasive diagnostic methods for PVDs was given discussing the advantages and limitations of each method. This review further highlights the need for new diagnostic tools and justifies the overall aim of the thesis.
2. HeMo was introduced as a candidate for hemodynamic monitoring and a simplified version of its embodiment and circuitry is presented. Pilot proof-of-concept

recordings demonstrate the potential to measure the arterial pulse wave and venous filling time. These experiments show that HeMo may be useful for the diagnosis of both arterial disease and chronic venous insufficiency.

3. A simulator rig was introduced and used to compare data from electro-resistive bands sensor and a linear displacement sensor during their simultaneous expansions/contractions. The comparison of the data from the two sensors provided characterisation of the electrical behaviour of the electro-resistive band sensors. HeMo incorporates electro-resistive bands to sense the changes in blood flow. Therefore, the characterisation of the ERB sensors was necessary to provide an understanding of the nonlinear behaviour of the sensor. Of note, the presented characterisation may be of interest for other applications/users of this sensor.
4. Venous filling measurements from HeMo were compared with measurements from an established medical device, a light reflection rheography sensor, in a group of thirty-six healthy volunteers. The VFT measurements of both HeMo and LRR exhibited issues with repeatability. As the VFT measurement experiment is quite short the repeatability issue could potentially be ameliorated by taking the average of multiple measures as we have done. Both HeMo and LRR VFT measurements were further affected by inter-rater reliability problems, highlighting the need for an automated computer framework for the selection of the start and end of venous refilling. Overall, the comparison showed an agreement between the VFT measurements of the two sensors, with all subjects classified as healthy further demonstrating the potential of HeMo for diagnosis of CVI. Additionally, HeMo was more robust to exercise compared to LRR, which could lead to a reduction in examination time. Finally, this work provides a control healthy patient dataset that may be of use in future research as a comparator to clinical data.
5. Arterial pulse wave recordings from HeMo were compared with simultaneous recordings from an established medical photoplethysmography sensor, in a group of thirty-six healthy volunteers. Eight arterial pulse wave features were extracted from

HeMo and PPG and they were statistically compared. A repeatability problem was associated with HeMo APW features, which could be ameliorated by taking the average multiple APW epochs. We found the broader shape of HeMo APW's to be responsible for the differences seen between APW features of HeMo and PPG. This comparison revealed the differences of HeMo arterial recordings compared to PPG pulse recordings, generating a better understanding of the HeMo arterial pulse wave and its features. This comparison also highlighted that the location of APW recording is important. We discovered that HeMo half pulse width values are clustering in two groups, which could be problematic for the diagnosis of PAD. This problem also existed in PPG recordings, albeit less frequently. We introduced an alternative feature, three quarters pulse width, which generated homogenous values. However, the diagnostic value of this metric needs to be investigated in clinical trials. We also found HeMo capable of sensing peripheral resistance changes with exercise, as the effect of exercise was evident in the HeMo augmentation index values. Overall, HeMo and PPG arterial pulse recordings agreed in term of their overall shape and visualising the dicrotic notch, highlighting the potential of HeMo for diagnosis of PAD.

Overall, the work presented in thesis is a step towards the development and validation of new non-invasive monitoring device, which can provide information about arterial and venous function in less time, with less training and at a lower cost compared to the available diagnostic techniques.

## 6.2 Future Directions

There are a number of points, which should be considered in future extension of the presented thesis:

1. The electro-resistive band sensors used in HeMo were sensitive enough to capture both the blood volume variations due to arterial inflow and postural changes. However, testing other stretchable sensors is recommended as this would lead to replace the exploited ERBs with a sensor with better precision, which would lead to have more repeatable VFT measurements/APW features. Of course, replacement of the ERBs will require characterisation of the electrical behaviour of the newly replaced sensor and it also may need modification of HeMo circuit.
2. Future research should examine the performance of HeMo in a clinical setting. Of note, data recorded from patients may require modification of HeMo. For example, disposable stretchable material may be needed to prevent infection. HeMo would also need to become adjustable in size to fit patients with larger legs. Additionally, the current design of HeMo is not suited for patients with active wounds or leg injury. HeMo could be modified such that the wound area is unaffected. Multiple design options could be explored. For example, a single ERB could be used on a narrow piece of stretchable fabric, which could be placed above or below the wound. Another solution could include two or more ERB sensors placed on wound-free sites on the lower leg.

A clinical trial of HeMo would identify whether the HeMo VFT measurements/APW features are accurate in diagnosing venous disease, arterial disease and the presence of both. The comparison of control and patient data would enable the definition of optimum thresholds for VFT and each of the APW features. Moreover, the clinical value of each HeMo APW features could be investigated. This investigation may lead to find the best feature or combination of features for the discrimination of legs with and without PAD.

Future research should also determine the bilateral difference for VFT measurements/APW features using HeMo. This is important as diagnostic information about peripheral circulation can be inferred from the loss of similarity in the measurements of sides and the degree of asymmetry can represent the severity of disease [52]. Additionally, measurements of bilateral differences have been shown better repeatability compared to measurements from single sides [52,241].

Although light reflection rheography and photoplethysmography are not the gold standards for diagnosis of chronic venous insufficiency and peripheral arterial disease, they were chosen as the comparator tools in the presented work in this thesis. Duplex ultrasound is the gold standard, but is expensive and requires clinical experts and so we could not use this for this preliminary development. The next stage of development will require assessing HeMo use with patients diagnoses with peripheral vascular diseases, recruited from a clinic with clinicians performing ABI, TBI, and duplex ultrasound tests, comparing all these with HeMo. Of course, the comparison of HeMo measurements with the gold standard will be required to identify the sensitivity, specificity and accuracy of HeMo, and ultimately validate HeMo as a screening tool for diagnosis of PAD and CVI.

3. A variety of features can be extracted from both the arterial pulse recording and its first and second derivatives, which may have diagnostic value for other clinical applications. For example, pulse width/pulse interval have been shown to be useful for the monitoring of heart rate variability [48]. Augmentation index, stiffness index, and a number of features from the first and second derivatives of APW have been shown to detect arterial stiffness/distensibility [48]. Future research should further develop and confirm these findings for HeMo APW features, which would potentially lead to use of HeMo for convenient heart rate variability monitoring and diagnosis of arterial stiffness.
4. Future research is required to investigate the capability of HeMo for detection of deep vein thrombosis, which is another common type of PVDs with fatal complications. Diagnosis of DVT is complicated as more than two third of patients of DVT do not

show any symptoms [242]. Additionally, while the early diagnosis is crucial, most of the available techniques are reserved for patients with symptoms. Several studies have shown the capability of LRR for detection of DVT [56,57,242]. These studies have shown that the slope of blood emptying during ten-dorsiflexion exercise can be used as marker to detect DVT. They classified LRR trace based on their slope and achieved sensitivity of 92%-96.4% and specificity of 82.9%-84% compared to venography [56,57,242]. In chapter 4, venous filling time were extracted from HeMo and LRR traces. It is evident that venous emptying slope of HeMo and LRR can be also extracted and compared. Comparison of the venous emptying slope of controls and patients can identify the clinical value of HeMo for detection of DVT.

5. VFT values were measured from HeMo and LRR venous filling traces by annotating start and end of refilling. Of course, we now know that there is error associated with this method as we found discrepancy between the VFT values from three annotations. An automated framework instead could improve the repeatability and reliability of VFT measurements. However, no automatic algorithm for detection of the start and end points of VFT has been published to our knowledge. Of note the VasoScreen device does have a semi-automatic inbuilt algorithm to identify the start and end points. However, we found their algorithm requiring manual modification of the automatic selected points in many cases. Additionally, this algorithm has not been published to date.

## References

1. Artazcoz AV. Diagnosis of Peripheral Vascular Disease: Current Perspectives. *Journal of Anesthesia & Clinical Research*. 2015;06.
2. National Clinical Guideline Centre. Lower Limb Peripheral Arterial Disease: Diagnosis and Management. National Clinical Guideline Centre. London: Royal College of Physicians; 2012.
3. Pierce GF, Mustoe TA. Pharmacologic Enhancement of Wound Healing. *Annual review of medicine*. 1995;46:467–81.
4. Regensteiner JG, Hiatt WR. Treatment of Peripheral Arterial Disease. *Clinical Cornerstone* . 2002;4:26–37.
5. Bahr C. CVI and PAD: A Review of Venous and Arterial Disease. *JAAPA: official journal of the American Academy of Physician Assistants*. 2007;20:20–5.
6. Cushman M. Epidemiology and Risk Factors for Venous Thrombosis. *Seminars in Hematology*. 2007;44:62–9.
7. Barron GS, Jacob SE, Kirsner RS. Dermatologic Complications of Chronic Venous Disease: Medical Management and Beyond. *Annals of Vascular Surgery*. 2007;21:652–62.
8. Eberhardt RT, Raffetto JD. Chronic Venous Insufficiency. *Circulation*. 2005;111:2398–409.
9. Malone M, Lau NS, White J, Novak A, Xuan W, Iliopoulos J, et al. The Effect of Diabetes Mellitus on Costs and Length of Stay in Patients with Peripheral Arterial Disease Undergoing Vascular Surgery. *European Journal of Vascular and Endovascular Surgery*. Elsevier Ltd;

2014;48:447–51.

10. Laing W. *Chronic Venous Diseases of the Leg*. London, UK: Office of Health Economics; 1992. p. 1–44.

11. Longo D, Fauci A, Kasper D, Hauser S, Jameson J. *Harrison's Manual of Medicine*. 18th ed. Longo D, Fauci A, Kasper D, Hauser S, Jameson J, editors. McGraw Hill Professional; 2012.

12. Brass EP, Hiatt WR, Green S. Skeletal Muscle Metabolic Changes in Peripheral Arterial Disease Contribute to Exercise Intolerance: A Point-counterpoint Discussion. *Vascular Medicine*. 2004;9:293–301.

13. Gornik HL. Peripheral Arterial Disease. *Circulation*. 2005;111:e169–72.

14. AbuRahma AF, Bergan JJ. *Noninvasive Peripheral Arterial Diagnosis*. AbuRahma AF, Bergan JJ, editors. London: Springer London; 2010.

15. Lin JS, Olson CM, Johnson ES, Whitlock EP. The Ankle–Brachial Index for Peripheral Artery Disease Screening and Cardiovascular Disease Prediction Among Asymptomatic Adults: A Systematic Evidence Review for the U.S. Preventive Services Task Force. *Annals of Internal Medicine*. 2013;159:333.

16. Au TB, Golledge J, Walker PJ, Haigh K, Nelson M. Peripheral Arterial Disease: Diagnosis and Management in General Practice. *Australian family physician*. 2013;42:397–400.

17. Fowkes FGR, Rudan D, Rudan I, Aboyans V, Denenberg JO, McDermott MM, et al. Comparison of Global Estimates of Prevalence and Risk Factors for Peripheral Artery Disease in 2000 and 2010: A Systematic Review and Analysis. *The Lancet*. Elsevier Ltd; 2013;382:1329–40.

18. Persson L, Lapidus L, Lärfars G, Rosfors S. Asymptomatic Deep Venous Thrombosis is Associated with a Low Risk of Post-thrombotic Syndrome. *European Journal of Vascular and Endovascular Surgery*. 2009;38:229–33.

19. Rosales A, Sandbæk G, Jørgensen JJ. Stenting for Chronic Post-thrombotic Vena Cava and Iliofemoral Venous Occlusions: Mid-term Patency and Clinical Outcome. *European Journal of Vascular and Endovascular Surgery*. Elsevier Ltd; 2010;40:234–40.
20. Bergan J, Pascarella L. *Venous Anatomy, Physiology, and Pathophysiology. The Vein Book*. Elsevier Ltd; 2007. p. 39–45.
21. Bundens WP. *The Chronically Swollen Leg: Finding The Cause: Theory and Practice. Venous Ulcers*. Elsevier Ltd; 2007. p. 67–74.
22. Scott TE, LaMorte WW, Gorin DR, Menzoian JO. Risk Factors for Chronic Venous Insufficiency: A Dual Aase Control Study. *Journal of Vascular Surgery*. 1995;22:622–8.
23. DaSilva A, Navarro M, Batalheiro J. The Importance of Chronic Venous Insufficiency: Various Preliminary Data on its Medico-social Consequences. *Phlebologie*. 1992;45:439–443.
24. Rathbun S. The Surgeon General’s Call to Action to Prevent Deep Vein Thrombosis and Pulmonary Embolism. *Circulation*. 2009;119:e480–2.
25. Barker RC, Marval P. Venous Thromboembolism: Risks and Prevention. *Continuing Education in Anaesthesia, Critical Care & Pain*. 2011;11:18–23.
26. Silverstein MD, Heit JA, Mohr DN, Petterson TM, O’Fallon WM, Melton LJ. Trends in the Incidence of Deep Vein Thrombosis and Pulmonary Embolism. *Archives of Internal Medicine*. 1998;158:585.
27. Wells P, Anderson D. The Diagnosis and Treatment of Venous Thromboembolism. *Hematology*. 2013;2013:457–63.
28. Dhaliwal G, Mukherjee D. *Peripheral Arterial Disease: Epidemiology, Natural History, Diagnosis and Treatment*. The International journal of angiology. Berlin, Heidelberg: Springer Berlin Heidelberg; 2007;16:36–44.
29. Tzoulaki I, Fowkes FGR. *Peripheral Arterial Disease*. International Encyclopedia of Public Health. Elsevier Ltd; 2008. p. 53–8.

30. Paulev P-E, Neumann F, Nielsen SL, Keiding N. Strain-gauge versus Water Plethysmography Description of Simplified Systems and Analysis of Differences and Accuracy. *Medical & Biological Engineering*. 1974;12:437–45.
31. Holohan T V. *Plethysmography: Safety, Effectiveness, and Clinical Utility in Diagnosing Vascular Disease*. DIANE Publishing; 1996.
32. Collins R, Burch J, Cranny G, Aguiar-Ibanez R, Craig D, Wright K, et al. Duplex Ultrasonography, Magnetic Resonance Angiography, and Computed Tomography Angiography for Diagnosis and Assessment of Symptomatic, Lower Limb Peripheral Arterial Disease: Systematic Review. *BMJ*. 2007;334:1257–1257.
33. Breen PP, Gargiulo GD. Hemodynamic Monitor for Rapid, Cost-effective Assessment of Peripheral Vascular Function. 2014 Annual International Conference of the IEEE Engineering in Medicine and Biology Society. *IEEE*; 2014. p. 4795–8.
34. Eiberg JP, Grønvall Rasmussen JB, Hansen MA, Schroeder T V. Duplex Ultrasound Scanning of Peripheral Arterial Disease of the Lower Limb. *European Journal of Vascular and Endovascular Surgery*. Elsevier Ltd; 2010;40:507–12.
35. Hessel SJ, Adams DF, Abrams HL. Complications of Angiography. *Radiology*. 1981;138:273–81.
36. Aspelin P, Aubry P, Fransson S-G, Strasser R, Willenbrock R, Berg KJ. Nephrotoxic Effects in High-Risk Patients Undergoing Angiography. *New England Journal of Medicine*. 2003;348:491–9.
37. Krishnan S, Nicholls SC. Chronic Venous Insufficiency: Clinical Assessment and Patient Selection. *Seminars in Interventional Radiology*. 2005;22:169–77.
38. Nicolaides A, Hussein M, Szendro G, Christopoulos D, Vasdekis S, Clarke H. The Relation of Venous Ulceration with Ambulatory Venous Pressure Measurements. *Journal of Vascular Surgery*. 1993;17:414–9.
39. Criado E, Farber MA, Marston WA, Daniel PF, Burnham CB, Keagy BA. The Role of Air Plethysmography in the Diagnosis of Chronic Venous Insufficiency. *Journal of Vascular*

Surgery. 1998;27:660–70.

40. Anderson FA. Impedance Plethysmography in The Diagnosis of Arterial and Venous Disease. *Annals of Biomedical Engineering*. 1984;12:79–102.

41. Stranden EP. STR Teknikk [Internet]. Available from: [http://www.strteknikk.no/Previous\\_products/previous\\_products.htm](http://www.strteknikk.no/Previous_products/previous_products.htm)

42. Chemische Fabrik Kreussler & Co. GmbH. Healthy Veins-Free of Varicose Veins [Internet]. Available from: <http://www.healthy-veins.com/spider-veins-varicose-veins/diagnosis/additional-methods-examination/>

43. ACIMedical. Intro to APG® Air Plethysmography [Internet]. Available from: [https://www.youtube.com/watch?v=PLM3T8l0\\_HU](https://www.youtube.com/watch?v=PLM3T8l0_HU)

44. Whitney RJ. The Measurement of Volume Changes in Human Limbs. *The Journal of Physiology*. 1953;121:1–27.

45. Rooke TW, Hesser JL, Osmundson PJ. Exercise Strain-gauge Venous Plethysmography: Evaluation of a “New” Device for Assessing Lower Limb Venous Incompetence. *Angiology*. 1992;43:219–28.

46. Rosfors S, Persson LM, Blomgren L. Computerized Venous Strain-gauge Plethysmography is a Reliable Method for Measuring Venous Function. *European Journal of Vascular and Endovascular Surgery*. Elsevier Ltd; 2014;47:81–6.

47. Singh M. *Instrumentation, Introduction to Biomedical*. 2nd ed. 2014.

48. Elgendi M. On the Analysis of Fingertip Photoplethysmogram Signals. *Current Cardiology Reviews*. 2012;8:14–25.

49. Allen J. Photoplethysmography and its Application in Clinical Physiological Measurement. *Physiological Measurement*. 2007;28:R1–39.

50. Alnaeb M, Alobaid N, Seifalian A, Mikhailidis D, Hamilton G. Optical Techniques in the Assessment of Peripheral Arterial Disease. *Current Vascular Pharmacology*. 2007;5:53–9.

51. Hershey FB, Barnes RW, Sumner DS, editors. *Noninvasive Diagnosis of Vascular Disease*. revised. Elsevier Ltd; 1984.
52. Allen J, Oates CP, Lees TA, Murray A. Photoplethysmography Detection of Lower Limb Peripheral Arterial Occlusive Disease: A Comparison of Pulse Timing, Amplitude and Shape Characteristics. *Physiological Measurement*. 2005;26:811–21.
53. Ro DH, Moon HJ, Kim JH, Lee KM, Kim SJ, Lee DY. Photoplethysmography and Continuous-Wave Doppler Ultrasound as a Complementary Test to Ankle-Brachial Index in Detection of Stenotic Peripheral Arterial Disease. *Angiology*. 2013;64:314–20.
54. Bays R a, Healy D a, Atnip RG, Neumyer M, Thiele BL. Validation of Air Plethysmography, Photoplethysmography, and Duplex Ultrasonography in the Evaluation of Severe Venous Stasis. *Journal of Vascular Surgery*. 1994;20:721–7.
55. Sarin S, Shields DA, Scurr JH, Coleridge Smith PD. Photoplethysmography: A valuable Noninvasive Tool in the Assessment of Venous Dysfunction?. *Journal of Vascular Surgery*. 1992;16:154–62.
56. Mitrani AA, Gonzalez ML, O'Connell MT, Guerra J, Harwood RB, Gardner LB. Detection of Clinically Suspected Deep Vein Thrombosis Using Light Reflection Rheography. *The American Journal of Surgery*. 1991;161:646–50.
57. Arora S, Lam DJK, Kennedy C, Meier GH, Gusberg RJ, Negus D. Light Reflection Rheography: A Simple Noninvasive Screening Test for Deep Vein Thrombosis. *Journal of Vascular Surgery*. 1993;18:767–72.
58. Thomas PRS, Butler CM, Bowman J, Grieve NWT, Bennett CE, Taylor RS, et al. Light Reflection Rheography: An Effective Non-invasive Technique for Screening Patients with Suspected Deep Venous Thrombosis. *The British journal of surgery*. 1991;78:207–9.
59. Tan YK, da Silva AF. Digital Photoplethysmography in the Diagnosis of Suspected Lower Limb DVT: Is It Useful? *European Journal of Vascular and Endovascular Surgery*. 1999;18:71–9.
60. Wikström J, Hansen T, Johansson L, Lind L, Ahlström H. Ankle Brachial Index <0.9

Underestimates the Prevalence of Peripheral Artery Occlusive Disease Assessed with Whole-Body Magnetic Resonance Angiography in the Elderly. *Acta Radiologica*. 2008;49:143–9.

61. Xu D, Li J, Zou L, Xu Y, Hu D, Pagoto SL, et al. Sensitivity and Specificity of the Ankle Brachial Index to Diagnose Peripheral Artery Disease: A Structured Review. *Vascular Medicine*. 2010;15:361–9.

62. Nyboer J, Kreider MM, Hannapel L. Electrical Impedance Plethysmography; A Physical and Physiologic Approach to Peripheral Vascular Study. *Circulation*. 1950;2:811–21.

63. Anderson FA. Impedance Plethysmography in the Diagnosis of Arterial and Venous Disease. *Annals of Biomedical Engineering*. 1984;12:79–102.

64. Golden JC, Miles DS. Assessment of Peripheral Hemodynamics Using Impedance Plethysmography. *Physical Therapy*. 1986;66:1544–7.

65. Jaffrin MY, Vanhoutte C. Quantitative Interpretation of Arterial Impedance Plethysmographic Signals. *Medical & Biological Engineering & Computing*. 1979;17:2–10.

66. Mašanauskienė E, Sadauskas S, Naudžiūnas A, Unikauskas A, Stankevičius E. Impedance Plethysmography as an Alternative Method for the Diagnosis of Peripheral Arterial Disease. *Medicina*. 2014;50:334–9.

67. Lynch TG, Dalsing MC, Ouriel K, Ricotta JJ, Wakefield TW. Developments in Diagnosis and Classification of Venous Disorders: Non-invasive Diagnosis. *Cardiovascular Surgery*. 1999;7:160–78.

68. Sinton AM, Seagar AD, Davis FM. Automated Venous Occlusion Plethysmograph. *Medical & Biological Engineering & Computing*. 1988;26:295–302.

69. Hull R, Hirsh J, Sackett DL, Powers P, Turpie AGG, Walker I. Combined Use of Leg Scanning and Impedance Plethysmography in Suspected Venous Thrombosis. *New England Journal of Medicine*. 1977;296:1497–500.

70. Toy PT, Schrier SL. Occlusive Impedance Plethysmography. A Noninvasive Method of Diagnosis of Proximal Deep Vein Thrombosis. *The Western Journal of Medicine*.

1978;129:89–93.

71. Flanigan DP, Goodreau JJ, Burnham SJ, Bergan JJ, Yao JS. Vascular Laboratory Diagnosis of Clinically Suspected Acute Deep Vein Thrombosis. *The Lancet* (London, England). 1978;2:331–4.

72. Cooperman M, Martin EW, Satiani B, Clark M, Evans WE. Detection of Deep Venous Thrombosis by Magnetic Resonance Imaging. *Chest*. 1993;104:54–60.

73. Liapis CD, Satiani B, Kuhns M, Evans WE. Value of Impedance Plethysmography in Suspected Venous Disease of the Lower Extremity. *Angiology*. 1980;31:522–5.

74. Peters SH, Jonker JJ, de Boer AC, den Ottolander GJ. Home-diagnosis of Deep Venous Thrombosis with Impedance Plethysmography. *Thrombosis and Haemostasis*. 1982;48:297–300.

75. Cruickshank MK, Levine MN, Hirsh J, Turpie AG, Powers P, Jay R, et al. An Evaluation of Impedance Plethysmography and <sup>125</sup>I-fibrinogen Leg Scanning in Patients following Hip Surgery. *Thrombosis and Haemostasis*. 1989;62:830–4.

76. Heijboer H. Detection of Deep Vein Thrombosis With Impedance Plethysmography and Real-Time Compression Ultrasonography in Hospitalized Patients. *Archives of Internal Medicine*. 1992;152:1901.

77. Paiement G, Wessinger SJ, Waltman AC, Harris WH. Surveillance of Deep Vein Thrombosis in Asymptomatic Total Hip Replacement Patients. *The American Journal of Surgery*. 1988;155:400–4.

78. Agnelli G, Cosmi B, Ranucci V, Renga C, Mosca S, Lupattelli L, et al. Impedance Plethysmography in the Diagnosis of Asymptomatic Deep vein Thrombosis in Hip Surgery. A Venography-controlled Study. *Archives of Internal Medicine*. 1991;151:2167–71.

79. Harada RN, Katz ML, Comerota A. A Noninvasive Screening Test to Detect “Critical” Deep Venous Reflux. *Journal of Vascular Surgery*. 1995;22:532–7.

80. Christopoulos DG, Nicolaides a N, Szendro G, Irvine a T, Bull ML, Eastcott HH. Air-

plethysmography and the Effect of Elastic Compression on Venous Hemodynamics of the Leg. *Journal of Vascular Surgery*. 1987;5:148–59.

81. Katz ML, Comerota AJ, Kerr R. Air Plethysmography (APG): A New Technique to Evaluate Patients with Chronic Venous Insufficiency. *Journal of Vascular Technology*. 1991;15:23–7.

82. Welkie JF, Comerota a J, Katz ML, Aldridge SC, Kerr RP, White J V. Hemodynamic Deterioration in Chronic Venous Disease. *Journal of Vascular Surgery*. 1992;16:733–40.

83. Pellerito JS, Polak JF. *Introduction to Vascular Ultrasonography*. 6th ed. Elsevier Health Sciences; 2012.

84. Yousuf AM, Pai NB, Kaul A, Gerst PH. Noninvasive Evaluation of Vascular Diseases. *Hospital Physician*. 1999;35:48–53.

85. Miller SS, Foote A V. The Ultrasonic Detection of Incompetent Perforating Veins. *British Journal of Surgery*. 1974;61:653–6.

86. Gerhard-Herman M, Gardin JM, Jaff M, Mohler E, Roman M, Naqvi TZ. Guidelines for Noninvasive Vascular Laboratory Testing: A Report from the American Society of Echocardiography and the Society of Vascular Medicine and Biology. *Journal of the American Society of Echocardiography*. 2006;19:955–72.

87. Nicolaides AN. Investigation of Chronic Venous Insufficiency : A Consensus Statement. *Circulation*. 2000;102:e126–63.

88. Eiberg JP, Hansen M a., Grønvall Rasmussen JB, Schroeder T V. Minimum Training Requirement in Ultrasound Imaging of Peripheral Arterial Disease. *European Journal of Vascular and Endovascular Surgery*. 2008;36:325–30.

89. Dautzat MM, Laroche JP, Charras C, Blin B, Domingo-Faye MM, Sainte-Luce P, et al. Real-time B-mode Ultrasonography for Better Specificity in the Noninvasive Diagnosis of Deep Venous Thrombosis. *Journal of Ultrasound in Medicine*. 1986;5:625–31.

90. O’Leary DH, Kane RA, Chase BM. A Prospective Study of the Efficacy of B-scan

Sonography in the Detection of Deep Venous Thrombosis in the Lower Extremities. *Journal of Clinical Ultrasound*. 1988;16:1–8.

91. Sullivan ED, Peter DJ, Cranley JJ. Real-time B-mode Venous Ultrasound. *Journal of Vascular Surgery*. 1984;1:465–71.

92. Kisslo JA, Adams DB. Principles of Doppler Echocardiography and the Doppler Examination# 1. London: Ciba-Geigy. 1987.

93. Whelan JF, Barry MH, Moir JD. Color Flow Doppler Ultrasonography: Comparison with Peripheral Arteriography for the Investigation of Peripheral Vascular Disease. *Journal of Clinical Ultrasound*. 1992;20:369–74.

94. Linke RJ, Davies RP, Giles AJ, Walsh JA, Thompson BW. Colour Duplex Ultrasound: A Screening Modality for Femoropopliteal Disease in Patients with Intermittent Claudication. *Australasian Radiology*. 1994;38:320–3.

95. Aly S, Jenkins MP, Zaidi FH, Coleridge Smith PD, Bishop CC. Duplex Scanning and Effect of Multisegmental Arterial Disease on its Accuracy in Lower Limb Arteries. *European Journal of Vascular and Endovascular Surgery*. 1998;16:345–9.

96. Bergamini TM, Tatum CM, Marshall C, Hall-Disselkamp B, Richardson JD. Effect of Multilevel Sequential Stenosis on Lower Extremity Arterial Duplex Scanning. *American Journal of Surgery*. 1995;169:564–6.

97. Khilnani NM, Grassi CJ, Kundu S, D’Agostino HR, Khan AA, McGraw JK, et al. Multi-society Consensus Quality Improvement Guidelines for the Treatment of Lower-extremity Superficial Venous Insufficiency with Endovenous Thermal Ablation from the Society of Interventional Radiology, Cardiovascular Interventional Radiological Society. *Journal of Vascular and Interventional Radiology*. Elsevier Inc.; 2010;21:14–31.

98. Malgor RD, Labropoulos N. Diagnosis of Venous Disease with Duplex Ultrasound. *Phlebology*. 2013;28:158–61.

99. Cronan JJ, Dorfman GS, Scola FH, Schepps B, Alexander J. Deep Venous Thrombosis: US Assessment Using Vein Compression. *Radiology*. 1987;162:191–4.

100. Goodacre S, Sampson F, Thomas S, van Beek E, Sutton A. Systematic Review and Meta-analysis of the Diagnostic Accuracy of Ultrasonography for Deep Vein Thrombosis. *BMC Medical Imaging*. 2005;5:6.
101. Asbeutah AM, Riha AZ, Cameron JD, Mcgrath BP. Reproducibility of Duplex Ultrasonography and Air Plethysmography Used for the Evaluation of Chronic Venous Insufficiency. *Journal of Ultrasound in Medicine*. 2005;475–82.
102. Gornik HL, Sharma AM. Duplex Ultrasound in the Diagnosis of Lower-Extremity Deep Venous Thrombosis. *Circulation*. 2014;129:917–21.
103. Thrush A, Hartshorne T. *Peripheral Vascular Ultrasound: How, Why, and When*. 2nd ed. Elsevier Ltd; 2005.
104. Crisp JG, Lovato LM, Jang TB. Compression Ultrasonography of the Lower Extremity with Portable Vascular Ultrasonography Can Accurately Detect Deep Venous Thrombosis in the Emergency Department. *Annals of Emergency Medicine*. Elsevier Inc.; 2010;56:601–10.
105. Winsor T. Influence of Arterial Disease on The Systolic Blood Pressure Gradients of The Extremity. *The American Journal of Medical Sciences*. 1950;220:117–26.
106. Gerhard-Herman MD, Gornik HL, Barrett C, Barshes NR, Corriere MA, Drachman DE, et al. 2016 AHA/ACC Guideline on the Management of Patients With Lower Extremity Peripheral Artery Disease: Executive Summary: A Report of the American College of Cardiology/American Heart Association Task Force on Clinical Practice Guidelines. *Circulation*. 2016;135:e686–725.
107. Crawford F, Chappell FM, Welch K, Andras A, Brittenden J. Ankle Brachial Index for the Diagnosis of Lower Limb Peripheral Arterial Disease (Review). Crawford F, editor. *Cochrane Database Systematic Reviews*. Chichester, UK: John Wiley & Sons, Ltd; 2016;
108. Del Conde I, Benenati JF. Noninvasive Testing in Peripheral Arterial Disease. *Interventional Cardiology Clinics*. Elsevier Inc; 2014;3:469–78.
109. Criqui MH, Langer RD, Fronek A, Feigelson HS, Klauber MR, McCann TJ, et al. Mortality over a Period of 10 Years in Patients with Peripheral Arterial Disease. *New*

England Journal of Medicine. 1992;326:381–6.

110. McDermott MM, Guralnik JM, Tian L, Liu K, Ferrucci L, Liao Y, et al. Associations of Borderline and Low Normal Ankle-Brachial Index Values With Functional Decline at 5-Year Follow-Up. *Journal of the American College of Cardiology*. 2009;53:1056–62.

111. Fowkes F, Murray G, Butcher I, Heald C, Lee R, Chambless L, et al. Ankle Brachial Index Combined With Framingham Risk Score to Predict Cardiovascular Events and Mortality. *JAMA*. 2008;300:197.

112. Resnick HE. Relationship of High and Low Ankle Brachial Index to All-Cause and Cardiovascular Disease Mortality: The Strong Heart Study. *Circulation*. 2004;109:733–9.

113. Gardner AW, Skinner JS, Cantwell BW, Smith LK. Prediction of Claudication Pain from Clinical Measurements Obtained at Rest. *Medicine and Science in Sports and Exercise*. 1992;24:163–70.

114. Vega J, Romaní S, Garcipérez FJ, Vicente L, Pacheco N, Zamorano J, et al. Peripheral Arterial Disease: Efficacy of the Oscillometric Method. *Revista Espanola de Cardiologia*. 2011;64:619–21.

115. Schröder F, Diehm N, Kareem S, Ames M, Pira A, Zwettler U, et al. A Modified Calculation of Ankle-brachial Pressure Index is far more Sensitive in the Detection of Peripheral Arterial Disease. *Journal of Vascular Surgery*. 2006;44:531–6.

116. Niazi K, Khan TH, Easley KA. Diagnostic Utility of the Two Methods of Ankle Brachial Index in the Detection of Peripheral Arterial Disease of Lower Extremities. *Catheterization and Cardiovascular Interventions*. 2006;68:788–92.

117. Guo X, Li J, Pang W, Zhao M, Luo Y, Sun Y, et al. Sensitivity and Specificity of Ankle-Brachial Index for Detecting Angiographic Stenosis of Peripheral Arteries. *Circ J*. 2008;72:605–10.

118. Parameswaran GI, Brand K, Dolan J. Pulse Oximetry as a Potential Screening Tool for Lower Extremity Arterial Disease in Asymptomatic Patients with Diabetes Mellitus. *Archives of Internal Medicine*. 2005;165:442–6.

119. Premalatha G, Ravikumar R, Sanjay R, Deepa R, Mohan V. Comparison of Colour Duplex Ultrasound and Ankle-brachial Pressure Index Measurements in Peripheral Vascular Disease in Type 2 Diabetic Patients with Foot Infections. *The Journal of the Association of Physicians of India*. 2002;50:1240–4.
120. Lijmer JG, Hunink MGM, van den Dungen JJAM, Loonstra J, Smit AJ. ROC Analysis of Noninvasive Tests for Peripheral Arterial Disease. *Ultrasound in Medicine and Biology*. 1996;22:391–8.
121. Williams DT, Harding KG, Price P. An Evaluation of the Efficacy of Methods Used in Screening for Lower-Limb Arterial Disease in Diabetes. *Diabetes Care*. 2005;28:2206–10.
122. Hirsch AT, Haskal ZJ, Hertzler NR, Bakal CW, Creager MA, Halperin JL, et al. ACC/AHA 2005 Guidelines for the Management of Patients With Peripheral Arterial Disease (Lower Extremity, Renal, Mesenteric, and Abdominal Aortic): Executive Summary A Collaborative Report From the American Association for Vascular Surgery/Society for Vascular surgery. *Journal of the American College of Cardiology*. 2006;47:1239–312.
123. Kupinski AM. Segmental Pressure Measurement and Plethysmography. *The Journal of Vascular Technology*. 2002;26:32–8.
124. Fronek a, Johansen KH, Dilley RB, Bernstein EF. Noninvasive Physiologic Tests in the Diagnosis and Characterization of Peripheral Arterial Occlusive Disease. *American Journal of Surgery*. 1973;126:205–14.
125. Cutajar CL, Marston A, Newcombe JF. Value of Cuff Occlusion Pressures in Assessment of Peripheral Vascular Disease. *British Medical Journal*. 1973;2:392–5.
126. Allan JS, Terry HJ. The Evaluation of an Ultrasonic Flow Detector for the Assessment of Peripheral Vascular Disease. *Cardiovascular Research*. 1969;3:503–9.
127. Strandness D., Bell J. Peripheral Vascular Disease: Diagnosis and Objective Evaluation Using a Mercury Strain Gauge. *Annals of Surgery*. 1965;
128. Manning DM, Kuchirka C, Kaminski J. Miscuffing: Inappropriate Blood Pressure Cuff Application. *Circulation*. 1983;68:763–6.

129. Orchard TJ, Strandness DE. Assessment of Peripheral Vascular Disease in Diabetes. Report and Recommendations of an International Workshop Sponsored by the American Diabetes Association and the American Heart Association. September 18- 20, 1992 New Orleans, Louisiana. *Circulation*. 1993;88:819–28.
130. Holstein P, Lassen N a. Healing of Ulcers on the Feet Correlated with Distal Blood Pressure Measurements in Occlusive Arterial Disease. *Acta Orthopaedica Scandinavica*. 1980;51:995–1006.
131. Holstein P. The Distal Blood Pressure Predicts Healing of Amputations on the Feet. *Acta Orthop Scand*. 1984;55:227–33.
132. Brooks B, Dean R, Patel S, Wu B, Molyneaux L, Yue DK. TBI or not TBI: that is the Question. Is it Better to Measure Toe Pressure than Ankle Pressure in Diabetic Patients? *Diabetic Medicine*. 2001;18:528–32.
133. Høyer C, Sandermann J, Petersen LJ. The Toe-brachial Index in the Diagnosis of Peripheral Arterial Disease. *Journal of Vascular Surgery*. 2013;58:231–8.
134. Romanos MT, Raspovic A, Perrin BM. The Reliability of Toe Systolic Pressure and the Toe Brachial Index in Patients with Diabetes. *Journal of Foot and Ankle Research*. BioMed Central Ltd; 2010;3:31.
135. Park SC, Choi CY, Ha YI, Yang HE. Utility of Toe-brachial Index for Diagnosis of Peripheral Artery Disease. *Archives of Plastic Surgery*. 2012;39:227.
136. Kallio M, Forsblom C, Groop PH, Groop L, Lepantalo M. Development of New Peripheral Arterial Occlusive Disease in Patients with Type 2 Diabetes During a Mean Follow-up of 11 Years. *Diabetes Care*. 2003;26:1241–5.
137. Makisalo H, Lepantalo M, Halme L, Lund T, Peltonen S, Salmela K, et al. Peripheral Arterial Disease as a Predictor of Outcome after Renal Transplantation. *Transplant International*. 1998;11 Suppl 1:S140-143.
138. Criqui MH, Browner D, Fronek A, Klauber MR, Coughlin SS, Barrett-Connor E, et al. Peripheral Arterial Disease in Large Vessels is Epidemiologically Distinct from Small Vessel

Disease. An analysis of risk factors. *American Journal of Epidemiology*. 1989;129:1110–9.

139. Bird CE, Criqui MH, Fronck A, Denenberg JO, Klauber MR, Langer RD. Quantitative and Qualitative Progression of Peripheral Arterial Disease by Non-invasive Testing. *Vascular Medicine*. 1999;4:15–21.

140. Høyer C, Sandermann J, Petersen LJ. Randomised Diagnostic Accuracy Study of a Fully Automated Portable Device for Diagnosing Peripheral Arterial Disease by Measuring the Toe-brachial Index. *European Journal of Vascular and Endovascular Surgery*. 2013;45:57–64.

141. Weinberg I, Giri J, Calton MA, Hawkins BM, Weinberg MD, Margey R, et al. Anatomic Correlates of Supra-normal Ankle Brachial Indices. *Catheterization and Cardiovascular Interventions*. 2013;81:1025–30.

142. Norgren L, Hiatt WR, Dormandy JA, Nehler MR, Harris KA, Fowkes FGR. Inter-Society Consensus for the Management of Peripheral Arterial Disease (TASC II). *European Journal of Vascular and Endovascular Surgery*. 2007;33:S1–75.

143. Begelman SM, Jaff MR. Noninvasive Diagnostic Strategies for Peripheral Arterial Disease. *Cleveland Clinic journal of medicine*. 2006;73 Suppl 4:S22-9.

144. Chan D, Anderson ME, Dolmatch BL. Imaging Evaluation of Lower Extremity Infrainguinal Disease: Role of the Noninvasive Vascular Laboratory, Computed Tomography Angiography, and Magnetic Resonance Angiography. *Techniques in Vascular and Interventional Radiology*. 2010;13:11–22.

145. Azam SM, Carman TL. Diagnostic Approach to Peripheral Arterial Disease. *Cardiology Clinics*. 2011;29:319–29.

146. Lau JF, Weinberg MD, Olin JW. Peripheral Artery Disease. Part 1: Clinical Evaluation and Noninvasive Diagnosis. *Nature Reviews Cardiology*. 2011;8:405–18.

147. Sahli D, Eliasson B, Svensson M, Blohme G, Eliasson M, Samuelsson P, et al. Assessment of Toe Blood Pressure is an Effective Screening Method to Identify Diabetes Patients with Lower Extremity Arterial Disease. *Angiology*. 2004;55:641–51.

148. Williams DT, Price P, Harding KG. The Influence of Diabetes and Lower Limb Arterial Disease on Cutaneous Foot Perfusion. *Journal of Vascular Surgery*. 2006;44:770–5.
149. Suominen V, Uurto I, Saarinen J, Venermo M, Salenius J. PAD as a Risk Factor for Mortality Among Patients with Elevated ABI - A Clinical Study. *European Journal of Vascular and Endovascular Surgery*. Elsevier Ltd; 2010;39:316–22.
150. Leskinen Y, Salenius JP, Lehtimäki T, Huhtala H, Saha H. The Prevalence of Peripheral Arterial Disease and Medial Arterial Calcification in Patients with Chronic Renal Failure: Requirements for Diagnostics. *American Journal of Kidney Diseases*. 2002;40:472–479.
151. Suominen V, Rantanen T, Venermo M, Saarinen J, Salenius J. Prevalence and Risk Factors of PAD among Patients with Elevated ABI. *European Journal of Vascular and Endovascular Surgery*. 2008;35:709–14.
152. Papanas N, Tziakas D, Maltezos E, Kekes A, Hatzinikolaou E, Parcharidis G, et al. Peripheral Arterial Occlusive Disease as a Predictor of the Extent of Coronary Atherosclerosis in Patients with Coronary Artery Disease with and without Diabetes Mellitus. *The Journal of International Medical Research*. 2004;32:422–8.
153. Morimoto S, Nakajima F, Yurugi T, Morita T, Jo F, Nishikawa M, et al. Risk Factors of Normal Ankle-brachial Index and Low Toe-brachial Index in Hemodialysis Patients. *Therapeutic Apheresis and Dialysis*. 2009;13:103–7.
154. Bonham FP. Measuring Toe Pressures Using a Portable Photoplethysmograph to Detect Arterial Disease in High-risk Patients: An Overview of the Literature. *Ostomy Wound Management*. 2011;57:36–44.
155. Reinhard H, Wiinberg N, Hansen PR, Kjaer A, Petersen CL, Winther K, et al. NT-proBNP Levels, Atherosclerosis and Vascular Function in Asymptomatic Type 2 Diabetic Patients with Microalbuminuria: Peripheral Reactive Hyperaemia Index but Not NT-proBNP is an Independent Predictor of Coronary Atherosclerosis. *Cardiovascular diabetology*. 2011;10:71.
156. Sawka AM, Carter SA. Effect of Temperature on Digital Systolic Pressures in Lower

Limb in Arterial Disease. *Circulation*. 1992;85:1097–101.

157. McCollum PT, Stanley ST, Kent P, Grouden MC, Moore DJ, Shanik GD. Assessment of Arterial Disease Using Digital Systolic Pressure Measurement. *Annals of Vascular Surgery*. 1988;2:349–51.

158. Fleenor BS, Berrones AJ. *Arterial Stiffness: Implications and Interventions*. Cham: Springer International Publishing; 2015.

159. Young T. The Croonian Lecture: On the Functions of the Heart and Arteries. *Philosophical Transactions of the Royal Society of London*. 1809;99:1–31.

160. Boutouyrie P, Briet M, Collin C, Vermeersch S, Pannier B. Assessment of Pulse Wave Velocity. *Artery Research*. 2009;3:3–8.

161. O'Rourke M. Arterial Stiffness, Systolic Blood Pressure, and Logical Treatment of Arterial Hypertension. *Hypertension*. 1990;15:339–47.

162. Catalano M, Scandale G, Carzaniga G, Cinquini M, Minola M, Dimitrov G, et al. Increased Aortic Stiffness and Related Factors in Patients with Peripheral Arterial Disease. *Journal of Clinical Hypertension*. 2013;15:712–6.

163. Simonson E, Koff S, Keys A, Minckler J. Contour of the Toe Pulse, Reactive Hyperemia, and Pulse Transmission Velocity: Group and Repeat Variability, Effect of Age, Exercise, and Disease. Intergovernmental Panel on Climate Change, editor. *American Heart Journal*. Cambridge: Cambridge University Press; 1955;50:260–79.

164. Eliakim M, Sapoznikov D, Weinman J. Pulse Wave Velocity in Healthy Subjects and in Patients with Various Disease States. *American Heart Journal*. 1971;82:448–57.

165. Xia Y, Liu X, Wu D, Xiong H, Ren L, Xu L, et al. Influence of Beat-to-beat Blood Pressure Variability on Vascular Elasticity in Hypertensive Population. *Scientific Reports*. Springer US; 2017;7:8394.

166. Yokoyama H, Shoji T, Kimoto E, Shinohara K, Tanaka S, Koyama H, et al. Pulse Wave Velocity in Lower-Limb Arteries among Diabetic Patients with Peripheral Arterial Disease.

Journal of Atherosclerosis and Thrombosis. 2003;10:253–8.

167. Pereira T, Correia C, Cardoso J. Novel Methods for Pulse Wave Velocity Measurement. *Journal of Medical and Biological Engineering*. 2015;35:555–65.

168. Khalil MA, Kim HK, Hoi JW, Kim I, Dayal R, Shrikhande G, et al. Detection of Peripheral Arterial Disease Within the Foot Using Vascular Optical Tomographic Imaging: A Clinical Pilot Study. *European Journal of Vascular and Endovascular Surgery*. Elsevier Ltd; 2015;49:83–9.

169. Szuba A, Oka RK, Harada R, Cooke JP. Limb Hemodynamics Are Not Predictive of Functional Capacity in Patients with PAD. *Vascular Medicine*. 2006;11:155–63.

170. Lin W-H, Zhang H, Zhang Y-T. Investigation on Cardiovascular Risk Prediction Using Physiological Parameters. *Computational and Mathematical Methods in Medicine*. 2013;2013:1–21.

171. Zhang Y-T, Zheng Y-L, Lin W-H, Zhang H-Y, Zhou X-L. Challenges and Opportunities in Cardiovascular Health Informatics. *IEEE Transactions on Biomedical Engineering*. 2013;60:633–42.

172. Boland CS, Khan U, Backes C, O’Neill A, McCauley J, Duane S, et al. Sensitive, High-Strain, High-Rate Bodily Motion Sensors Based on Graphene–Rubber Composites. *ACS Nano*. 2014;8:8819–30.

173. Boland CS, Khan U, Ryan G, Barwich S, Charifou R, Harvey A, et al. Sensitive Electromechanical Sensors Using Viscoelastic Graphene-polymer Nanocomposites. *Science*. 2016;354:1257–60.

174. Shabani Varaki E, Gargiulo G, Breen P. Towards Low-Cost Non-Invasive Assessment of Peripheral Vascular Function. *Hear Lung and Circulation*. Australasian Society of Cardiac and Thoracic Surgeons and The Cardiac Society of Australia and New Zealand; 2016;25:S23–4.

175. ShabaniVaraki E, Breen PP, Gargiulo GD. HeMo: Towards an Inexpensive Wearable Peripheral Blood Flow Monitoring Device. *2015 IEEE Biomedical Circuits and Systems*

Conference. 2015. p. 1–4.

176. Varaki ES, Breen P, Gargiulo G. Quantification of a Low-Cost Stretchable Conductive Sensor Using an Expansion/Contraction Simulator Machine: A Step towards Validation of a Noninvasive Cardiac and Respiration Monitoring Prototype. *Machines*. 2017;5:22.

177. Varaki ES, Gargiulo GD, Breen PP. Quantification of a Wearable Contactless Sensor for Health Monitoring Applications Using an Expansion / Contraction Simulator Rig. 2017 International Conference of the IEEE Engineering in Medicine and Biology Society. 2751:2–5.

178. Gargiulo GD, Gunawardana U, O’Loughlin A, Sadozai M, Varaki ES, Breen PP. A Wearable Contactless Sensor Suitable for Continuous Simultaneous Monitoring of Respiration and Cardiac Activity. *Journal of Sensors*. 2015;2015:1–6.

179. Gargiulo GD, Shabani Varaki E, Hamilton TJ, Bifulco P, Cesarelli M, Romano M. A 9-Independent-leads ECG System from 10 Electrodes: A Practice Preserving WCT-less True Unipolar ECG system. 2015 IEEE Biomedical Circuits and Systems Conference. 2015. p. 1–4.

180. Breen PP, Gargiulo GD. Hemodynamic Monitor for Rapid, Cost-effective Assessment of Peripheral Vascular Function. 2014 36th Annual International Conference of the IEEE Engineering in Medicine and Biology Society. 2014. p. 4795–8.

181. Eiberg JP, Grønvall Rasmussen JB, Hansen MA, Schroeder T V. Duplex Ultrasound Scanning of Peripheral Arterial Disease of the Lower Limb. *European Journal of Vascular and Endovascular Surgery*. 2010;40:507–12.

182. Krishnan S, Nicholls SC. Chronic Venous Insufficiency: Clinical Assessment and Patient Selection. *Seminars in Interventional Radiology*. 2005;22:169–77.

183. Mohler ER, Treat-Jacobson D, Reilly MP, Cunningham KE, Miani M, Criqui MH, et al. Utility and Barriers to Performance of the Ankle-brachial Index in Primary Care Practice. *Vascular Medicine*. 2004;9:253–60.

184. Harada RN, Katz ML, Comerota A. A Noninvasive Screening Test to Detect “Critical”

- Deep Venous Reflux. *Journal of Vascular Surgery*. 1995;22:532–7.
185. Aburahma AF, Bergan JJ. Noninvasive Peripheral Arterial Diagnosis. *Noninvasive Peripheral Arterial Diagnosis*. 2010;1–174.
186. Kundu S, Grassi CJ, Khilnani NM, Fanelli F, Kalva SP, Khan AA, et al. Multi-disciplinary Quality Improvement Guidelines for the Treatment of Lower Extremity Superficial Venous Insufficiency with Ambulatory Phlebectomy from the Society of Interventional Radiology, Cardiovascular Interventional Radiological Society of Europe. *Journal of Vascular and Interventional Radiology*. 2010;21:1–13.
187. Eiberg JP, Madycki G, Hansen M a, Christiansen S, Gronvall Rasmussen JB, Schroeder T V. Ultrasound Imaging of Infringuinal Arterial Disease Has a High Interobserver Agreement. *European Journal of Vascular and Endovascular Surgery*. 2002;24:293–9.
188. BURR-BROWN/Texas Instruments. REF200, Dual Current Source/current Sink. 2009. p. 1–19.
189. Gargiulo GD, O’Loughlin A, Breen PP. Electro-resistive Bands for Non-invasive Cardiac and Respiration Monitoring, A Feasibility Study. *Physiological Measurement*. IOP Publishing; 2015;36:N35–49.
190. Webster JG. *Medical Instrumentation Application and Design*, 4th Edition. 4th ed.
191. Burr-Brown/Texas Instruments. Ultra Low Input Bias Current Instrumentation Amplifier- INA116. datasheet. 1995.
192. Davies JH, Lewis JE, Williams EM. The Utility of Pulse Volume Waveforms in the Identification of Lower Limb Arterial Insufficiency. *EWMA Journal*. 2014;14:21–5.
193. Bermudez K. Fasciotomy, Chronic Venous Insufficiency, and the Calf Muscle Pump. *Archives of Surgery*. 1998;133:1356.
194. Deshmukh SD, Shilaskar SN. Wearable Sensors and Patient Monitoring System: A Review. 2015 International Conference on Pervasive Computing. IEEE; 2015. p. 1–3.
195. Pantelopoulos A, Bourbakis N. A Survey on Werable Sensor-Based Systems for Health

Monitoring and Prognosis. *IEEE Transactions on Systems, Man, and Cybernetics - Part C: Applications and Reviews*. 2010;40:1–12.

196. Zhang T, Lu J, Hu F, Hao Q. Bluetooth Low Energy for Wearable Sensor-based Healthcare Systems. *2014 IEEE Healthcare Innovation Conference*. 2014. p. 251–4.

197. Amjadi M, Kyung K-U, Park I, Sitti M. Stretchable, Skin-Mountable, and Wearable Strain Sensors and Their Potential Applications: A Review. *Advanced Functional Materials*. 2016;26:1678–98.

198. Trung TQ, Lee N-E. Flexible and Stretchable Physical Sensor Integrated Platforms for Wearable Human-Activity Monitoring and Personal Healthcare. *Advanced Materials*. 2016;28:4338–72.

199. Yamada T, Hayamizu Y, Yamamoto Y, Yomogida Y, Izadi-Najafabadi A, Futaba DN, et al. A Stretchable Carbon Nanotube Strain Sensor for Human-motion Detection. *Nature Nanotechnology*. Nature Publishing Group; 2011;6:296–301.

200. Amjadi M, Yoon YJ, Park I. Ultra-stretchable and Skin-mountable Strain Sensors Using Carbon Nanotubes-Ecoflex Nanocomposites. *Nanotechnology*. IOP Publishing; 2015;26:375501.

201. Amjadi M, Pichitpajongkit A, Lee S, Ryu S, Park I. Highly Stretchable and Sensitive Strain Sensor Based on Silver-Elastomer Nanocomposite. *ACS Nano*. 2014;8:5154–63.

202. Muth JT, Vogt DM, Truby RL, Mengüç Y, Kolesky DB, Wood RJ, et al. Embedded 3D Printing of Strain Sensors within Highly Stretchable Elastomers. *Advanced Materials*. 2014;26:6307–12.

203. Lu N, Lu C, Yang S, Rogers J. Highly Sensitive Skin-Mountable Strain Gauges Based Entirely on Elastomers. *Advanced Functional Materials*. 2012;22:4044–50.

204. Jeong YR, Park H, Jin SW, Hong SY, Lee SS, Ha JS. Highly Stretchable and Sensitive Strain Sensors Using Fragmentized Graphene Foam. *Advanced Functional Materials*. 2015;25:4228–36.

205. Mattmann C, Clemens F, Tröster G. Sensor for Measuring Strain in Textile. *Sensors*. 2008;8:3719–32.
206. Gong S, Lai DTH, Su B, Si KJ, Ma Z, Yap LW, et al. Highly Stretchy Black Gold E-Skin Nanopatches as Highly Sensitive Wearable Biomedical Sensors. *Advanced Electronic Materials*. 2015;1:1400063.
207. Xiao X, Yuan L, Zhong J, Ding T, Liu Y, Cai Z, et al. High-strain Sensors Based on ZnO Nanowire/Polystyrene Hybridized Flexible Films. *Advanced Materials*. 2011;23:5440–4.
208. Ding Y, Yang J, Tolle CR, Zhu Z. A Highly Stretchable Strain Sensor Based on Electrospun Carbon Nanofibers for Human Motion Monitoring. *The Royal Society of Chemistry Advances*. 2016;6:79114–20.
209. Roh E, Hwang B, Kim D, Kim B, Lee N. Stretchable, Transparent, Ultrasensitive, and Patchable Strain Sensor for Human–Machine Interfaces Comprising a Nanohybrid of Carbon Nanotubes and Conductive Elastomers. *ACS Nano*. 2015;9:6252–61.
210. Kang D, Pikhitsa P V., Choi YW, Lee C, Shin SS, Piao L, et al. Ultrasensitive Mechanical Crack-based Sensor Inspired by the Spider Sensory System. *Nature*. Nature Publishing Group; 2014;516:222–6.
211. Li X, Zhang R, Yu W, Wang K, Wei J, Wu D, et al. Stretchable and Highly Sensitive Graphene-on-polymer Strain Sensors. *Scientific Reports*. 2012;2:870.
212. Bifulco P, Esposito D, Gargiulo GD, Savino S, Niola V, Iuppariello L, et al. A Stretchable, Conductive Rubber Sensor to Detect Muscle Contraction for Prosthetic Hand Control. *2017 E-Health and Bioengineering Conference*. 2017. p. 173–6.
213. Giner-Sanz JJ, Ortega EM, Pérez-Herranz V. Total Harmonic Distortion Based Method for Linearity Assessment in Electrochemical Systems in the Context of EIS. *Electrochimica Acta*. Elsevier Ltd; 2015;186:598–612.
214. Kuhlmann TP, Siström CL, Chance JF. Light Reflection Rheography as a Noninvasive Screening Test for Deep Venous Thrombosis. *Annals of Emergency Medicine*. 1992;21:513–

7.

215. Neglen P, Raju S. Ambulatory Venous Pressure Revisited. *Journal of Vascular Surgery*. 2000;31:1206–13.

216. Criado E, Farber MA, Marston WA, Daniel PF, Burnham CB, Keagy BA. The Role of Air Plethysmography in the Diagnosis of Chronic Venous Insufficiency. *Journal of Vascular Surgery*. 1998;27:660–70.

217. Lattimer CR, Azzam M, Kalodiki E, Geroulakos G. Venous Filling Time Using Air-Plethysmography Correlates Highly with Great Saphenous Vein Reflux Time Using Duplex. *Phlebology*. 2012;90–7.

218. Criado E, Daniel PF, Marston W, Mansfield DI, Keagy B a. Physiologic Variations in Lower Extremity Venous Valvular Function. *Annals of Vascular Surgery*. 1995;9:102–8.

219. Faxon DP, Creager MA, Smith SC, Pasternak RC, Olin JW, Bettmann MA, et al. Atherosclerotic Vascular Disease Conference: Executive Summary: Atherosclerotic Vascular Disease Conference Proceeding for Healthcare Professionals from a Special Writing Group of the American Heart Association. *Circulation*. 2004;109:2595–604.

220. Kevil CG, Bir SC, Pattillo CB. *Peripheral Arterial Disease: Pathophysiology and Therapeutics*. Morgan & Claypool Life Science Publishers; 2013.

221. Ouriel K. Peripheral Arterial Disease. *The Lancet*. 2001;358:1257–64.

222. Allen J, Murray A. Prospective Assessment of an Artificial Neural Network for the Detection of Peripheral Vascular Disease from Lower Limb Pulse Waveforms. *Physiological Measurement*. 1995;16:29–38.

223. Rumwell C, McPharlin M. *Vascular Technology; An Illustrated Review*. 3rd ed. Davies Publishing, Inc.; 2004.

224. Chua CP, Heneghan C. Continuous Blood Pressure Monitoring Using ECG and Finger Photoplethysmogram. *Annual International Conference of the IEEE Engineering in Medicine and Biology*. 2006;5117–20.

225. Asada HH, Shaltis P, Reisner A, Rhee S, Hutchinson RC. Mobile Monitoring with Wearable Photoplethysmographic Biosensors. *IEEE Engineering in Medicine and Biology Magazine*. 2003;22:28–40.
226. Lax H, Feinberg AW, Cohen BM. Studies of the Arterial Pulse Wave. *Circulation*. 1958;18:1125–30.
227. Nichols WW, O'Rourke MF, Vlachopoulos C. McDonald's Blood Flow in Arteries: Theoretic, Experimental and Clinical Principles. 6th ed. CRC Press; 2011.
228. Awad AA, Haddadin AS, Tantawy H, Badr TM, Stout RG, Silverman DG, et al. The Relationship between the Photoplethysmographic Waveform and Systemic Vascular Resistance. *Journal of Clinical Monitoring and Computing*. 2007;21:365–72.
229. Mat Jubadi W, Aisyah Mohd Sahak SF. Heartbeat Monitoring Alert via SMS. 2009 IEEE Symposium on Industrial Electronics & Applications. 2009. p. 1–5.
230. Linder SP, Wendelken SM, Wei E, McGrath SP. Using the Morphology of Photoplethysmogram Peaks to Detect Changes in Posture. *Journal of Clinical Monitoring and Computing*. 2006;20:151–8.
231. Gil E, Orini M, Bailón R, Vergara JM, Mainardi L, Laguna P. Photoplethysmography Pulse Rate Variability as a Surrogate Measurement of Heart Rate Variability During Non-stationary Conditions. *Physiological Measurement*. 2010;31:1271–90.
232. Lu S, Zhao H, Ju K, Shin K, Lee M, Shelley K, et al. Can Photoplethysmography Variability Serve as an Alternative Approach to Obtain Heart Rate Variability Information? *Journal of Clinical Monitoring and Computing*. 2008;22:23–9.
233. Millasseau SC, Kelly RP, Ritter JM, Chowienczyk PJ. Determination of Age-related Increases in Large Artery Stiffness by Digital Pulse Contour Analysis. *Clinical Sciences*. 2002;103:371–7.
234. Takazawa K, Tanaka N, Fujita M, Matsuoka O, Saiki T, Aikawa M, et al. Assessment of Vasoactive Agents and Vascular Aging by the Second Derivative of Photoplethysmogram Waveform. *Hypertension*. 1998;32:365–70.

235. Miyai N, Miyashita K, Arita M, Morioka I, Kamiya K, Takeda S. Noninvasive Assessment of Arterial Distensibility in Adolescents Using the Second Derivative of Photoplethysmogram Waveform. *European Journal of Applied Physiology*. 2001;86:119–24.
236. Alastruey J, Parker KH, Sherwin SJ. Arterial Pulse Wave Haemodynamics. BHR Group's 11th International Conference on Pressure Surges. 2012;401–442.
237. van de Vosse FN, Stergiopoulos N. Pulse Wave Propagation in the Arterial Tree. *Annual Review of Fluid Mechanics*. 2011;43:467–99.
238. Giavarina D. Understanding Bland Altman analysis. *Biochemica Medica*. 2015;25:141–51.
239. Cohen DL, Townsend RR. Exaggerated Systolic Blood Pressure Response to Exercise. *The Journal of Clinical Hypertension*. 2007;9:291–2.
240. Hall JE, Guyton AC. *Guyton and Hall Textbook of Medical Physiology*. 13th ed. Elsevier Health Sciences; 2015.
241. Jago JR, Murray A. Repeatability of Peripheral Pulse Measurements on Ears, Fingers and Toes Using Photoelectric Plethysmography. *Clinical Physics and Physiological Measurement*. 1988;9:319–29.
242. Thomas PR, Butler CM, Bowman J, Grieve NW, Bennett CE, Taylor RS, et al. Light Reflection Rheography: An Effective Non-invasive Technique for Screening Patients with Suspected Deep Venous Thrombosis. *The British Journal of Surgery*. 1991;78:207–9.
243. Kuhlmann TP, Siström CL, Chance JF. Light Reflection Rheography as a Noninvasive Screening Test for Deep Venous Thrombosis. *Annals of Emergency Medicine*. 1992;21:513–7.

# Appendix A Graphical User Interfaces and User Guidelines

## A.1 User Guide for VFT Annotation

- The Matlab script in section A.3 is named VFT\_Measurement.m.
- Run VFT\_Measurement.m and the GUI will open as shown in Figure A.1:



Figure A.1. VFT annotation GUI opened. A cursor is available for selecting the start point of refilling.

- As can be seen in Figure A.2, once you run the GUI you can select the start of refilling. The start point is where the exercise is completed.

- Once the start point of refilling is selected, a cursor will appear again to allow selection of the end point of refilling. The endpoint is where the recording reaches a stable baseline [45,51,59,87,193,243].

- 

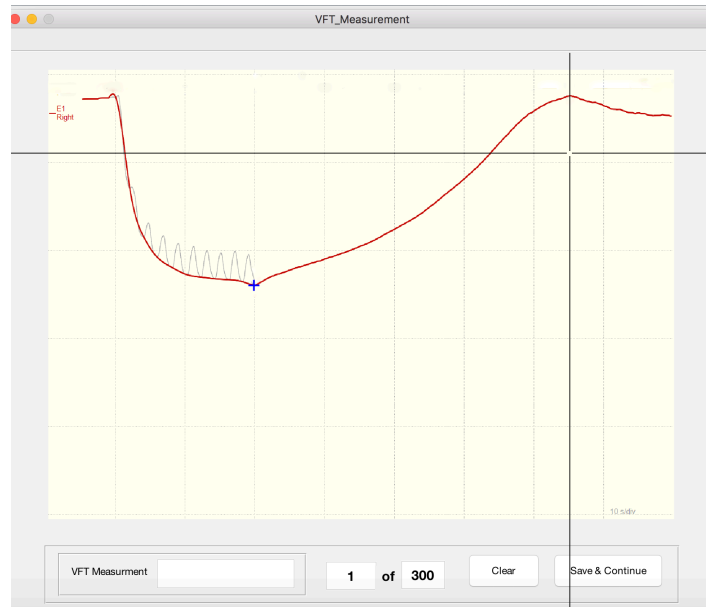


Figure A.2. VFT annotation GUI opened. The start point is shown in blue cross. A cursor is available for selecting the end point of refilling.

- Once both the start and end points are selected (Figure A.3), if you are happy with what you have chosen you can click on save and continue to save what you annotated and continue annotating the rest of the data.
- In the bottom panel of the GUI (Figure A.3), you can see the calculated venous filling time measured based on your chosen points.
- You can also see how many data are remaining to be annotated.
- If you are not happy with what you have annotated (e.g. you marked the start point or the endpoint in a wrong place by mistake), finish annotation for the current data (e.g.

you annotated the start point by mistake, just choose an endpoint to finish the annotation). You then can click on the clear button to clear your previous annotation and annotate the same data again.



Figure A.3. VFT annotation GUI opened. The start and end points are shown in blue crosses. The VFT measurement is shown in the bottom panel.

- Once the data annotation is completed the GUI window can be closed, and all information will be automatically saved as LRR\_VFT\_DB.mat in the folder where the VFT\_Measurement.m file is saved.
- The GUI window can be closed before completing annotation of all the data. In this case, with the re-run of the GUI, the annotation will resume from where it stopped.
- Examples of LLR and HeMo VFT annotation are presented in Figure A.4 and Figure A.5.

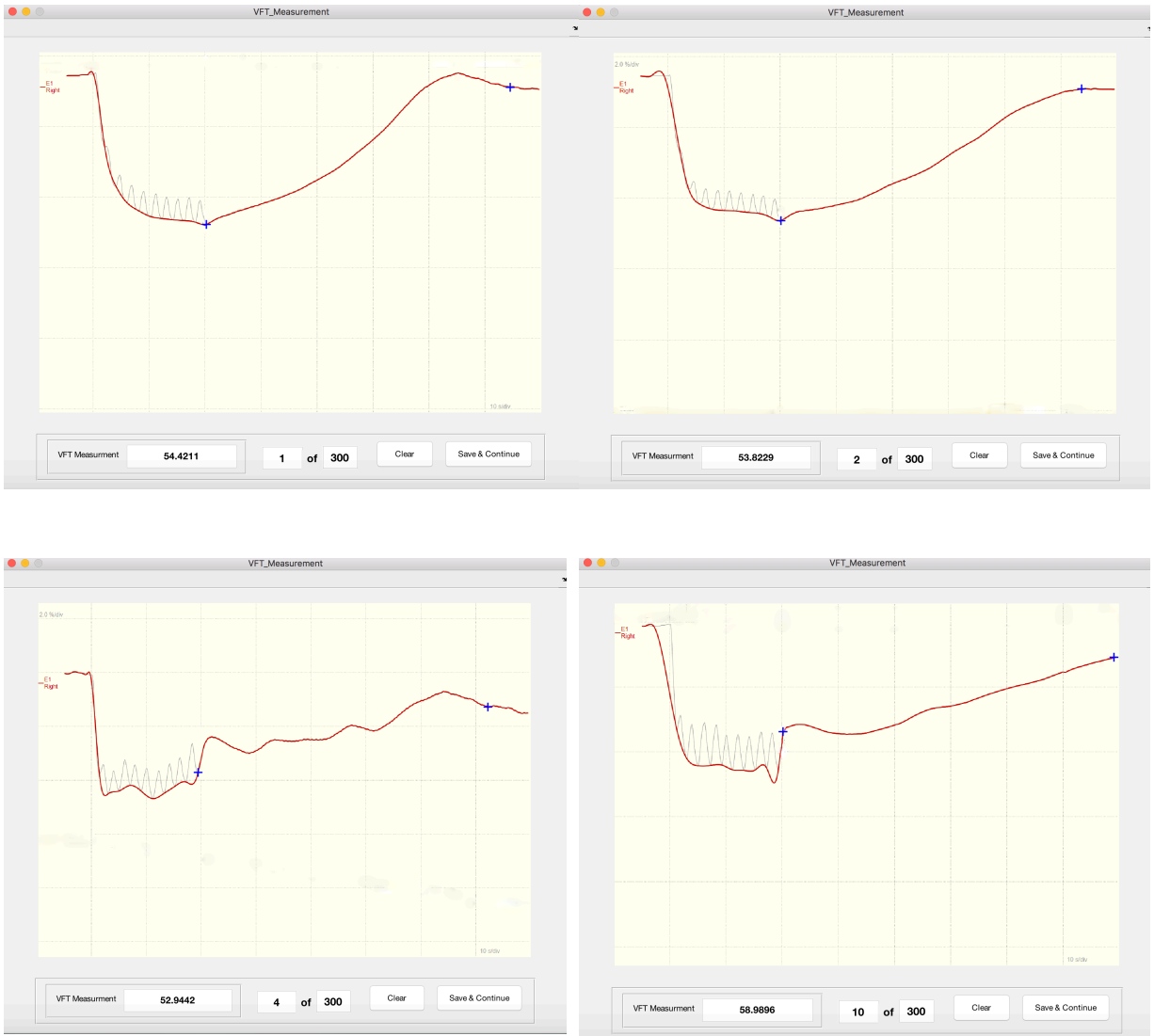


Figure A.4. Examples of LRR VFT annotation.

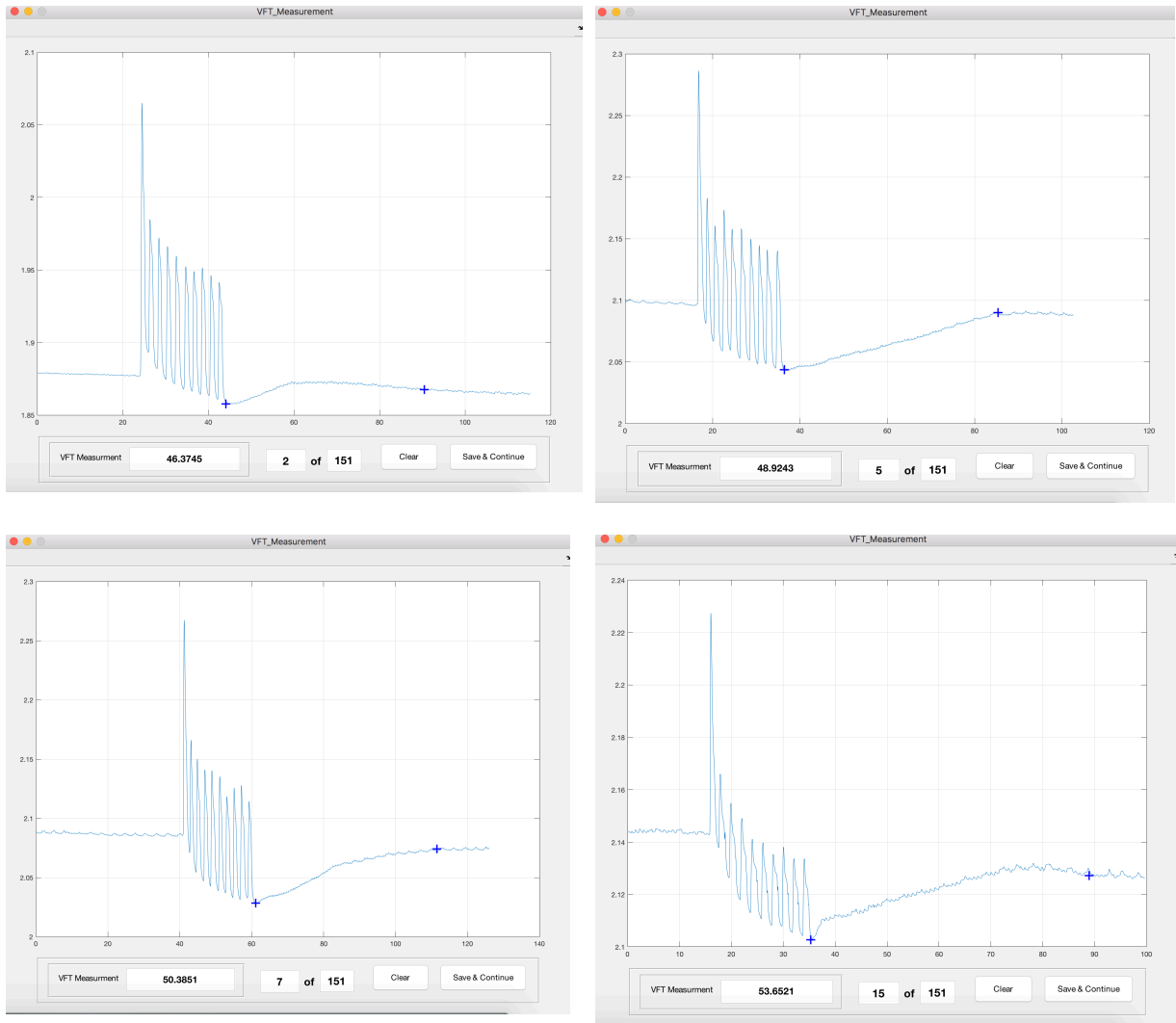


Figure A.5. Examples of HeMo VFT annotation.

## A.2 User Guide for APW Annotation

- The presented Matlab script in section A.4 is named APW\_Measurement.m.
- Run APW\_Measurement.m and you will see the GUI will show up as in Figure A.6.
- As can be seen in Figure A.6, once you run the GUI, two plots will appear. The top plot is the arterial pulse wave and the bottom one is its second derivative. A cursor also becomes available for selection of marker points.

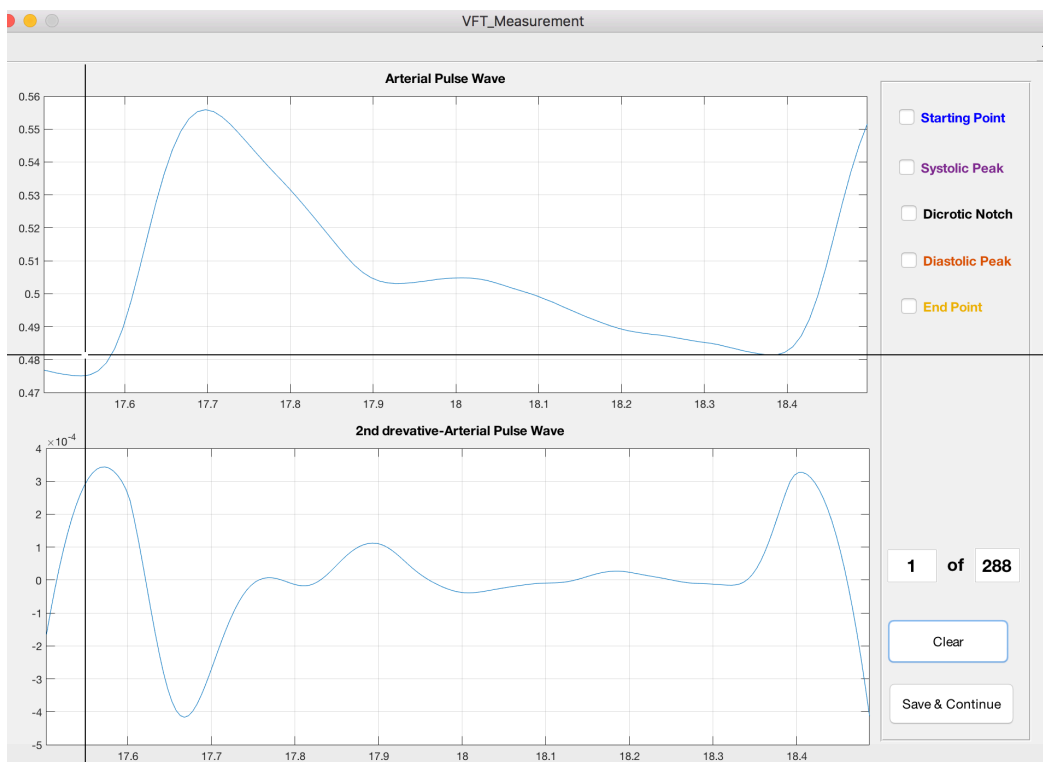


Figure A.6. APW GUI.

- Five points should be selected for each epoch of data. These points include the start point of the arterial pulse, the systolic peak, the dicrotic notch, the diastolic peak and the endpoint.

- Each of the point can be selected either from the top panel or the bottom panel and the marked point on the other panel will be shown automatically. However, it would be easier to select the start point, systolic peak, diastolic peak and the end point using the top panel. As a local maximum appears on the second derivative signal at where the dicrotic notch occurs, using the second derivative will help to annotate the dicrotic notch.
- The start point can be selected by clicking on the point where you think the arterial pulse wave starts.
- Once the start point is selected, a cursor will appear again to allow marking of the systolic peak. The systolic peak is shown in Figure A.7.
- Once the systolic peak is selected, a cursor will appear again to allow marking of the dicrotic notch. The dicrotic notch is shown in Figure A.7.
- Once the dicrotic notch is selected, a cursor will appear again to allow marking of the diastolic peak. The diastolic peak is shown in Figure A.7.
- Finally, once the diastolic peak is selected, a cursor will appear again to allow marking of the arterial pulse wave endpoint.

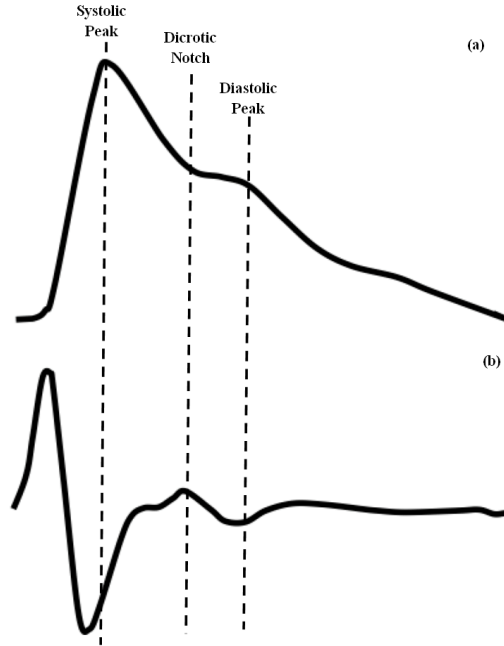


Figure A.7. Illustration of arterial pulse wave and its second derivative. Panel (a) shows the arterial pulse; Panel (b) shows the second derivative of the arterial pulse.

- Once the five points are selected (Figure A.8), if you are happy with what you have chosen you can select the “save and continue” button to save what you have annotated and continue annotating the rest of the data.
- There is a checkbox panel on the top right side of the GUI, which will show the order of the points you need to annotate. Each check box will be checked as you select points (Figure A.8).
- On the right panel, you can also see how many epochs remain to be annotated.
- If you are not happy with any epochs that you have annotated (e.g. you marked any of the of the five points in a wrong place by mistake), finish annotation for the current data (e.g. you annotated the start point by mistake, just choose rest of the points to finish the annotation) and then you can click on the clear button to clear your previous annotation and annotate the same data again.

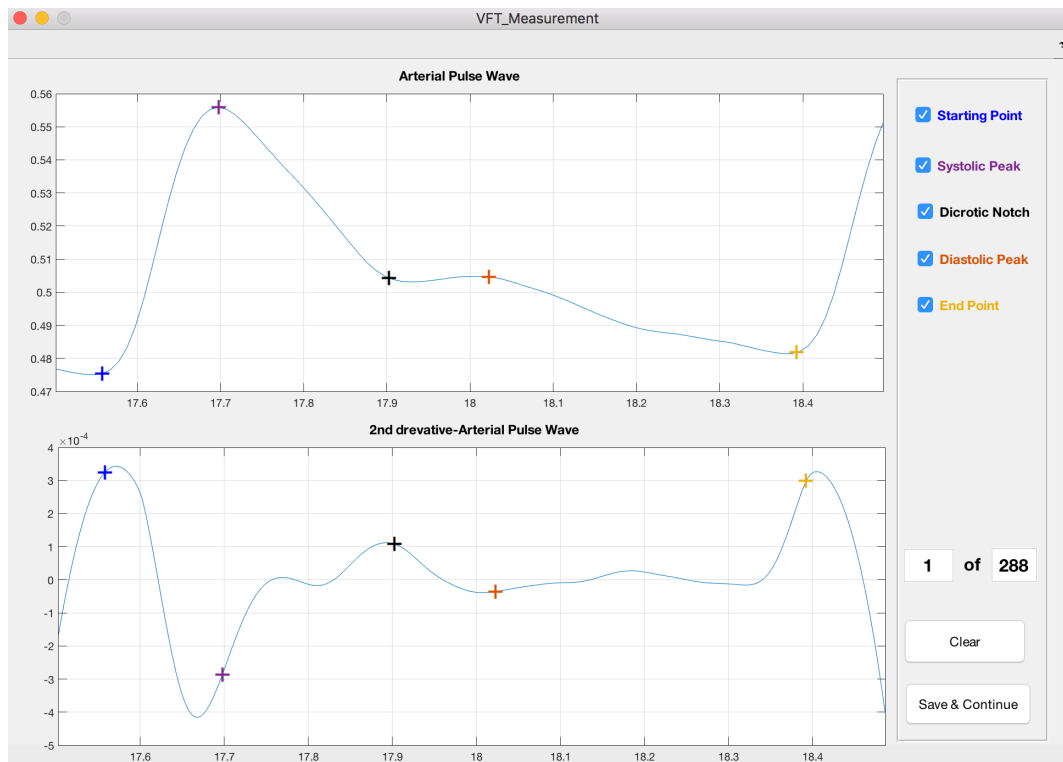
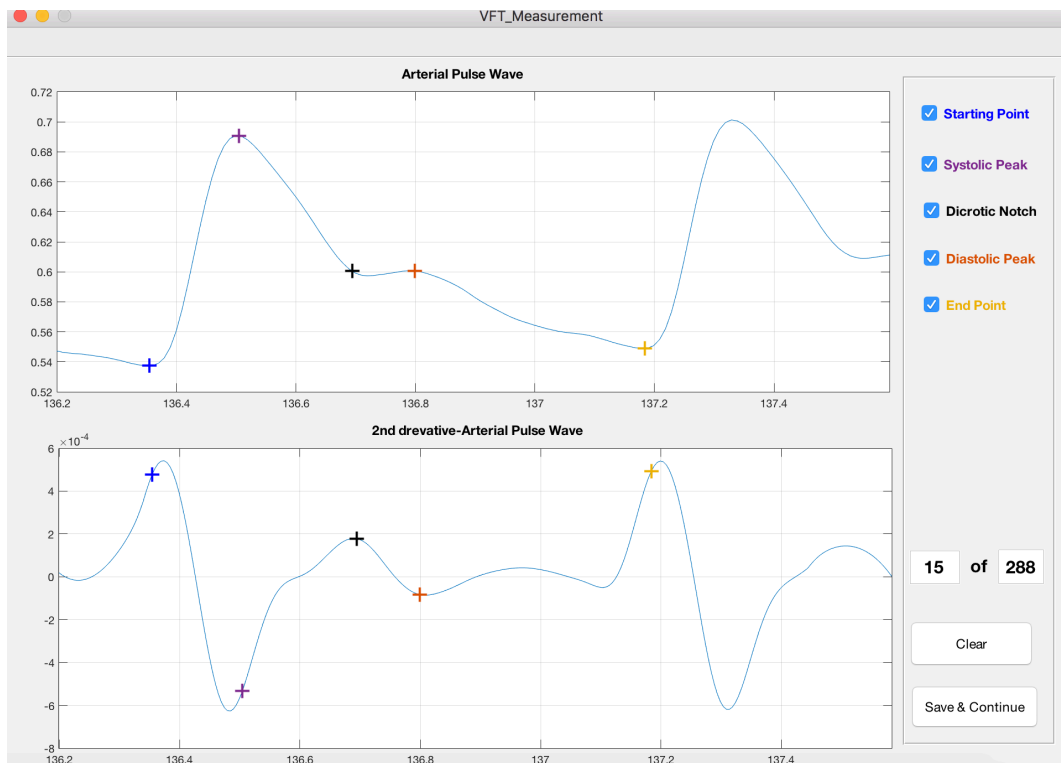
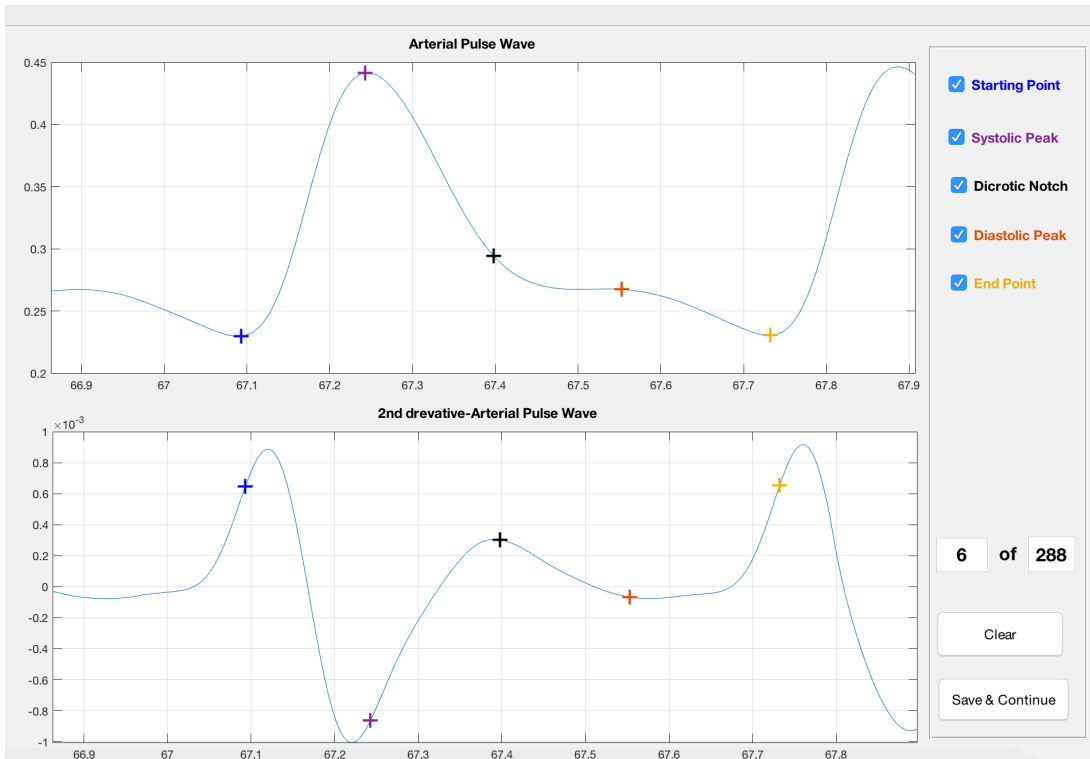


Figure A.8. APW GUI opened. User selected starting point, systolic peak, dicrotic notch, diastolic peak and end point are marked with blue, purple, black, red and yellow crosses.

- Once the data annotation is complete, all information will be automatically saved as APW\_DB.mat in the same folder where the APW GUI is saved.
- The GUI window can be closed before completing annotation of all data. In this case, when the GUI is reopened, the annotation will resume from the data at which the annotation was stopped.
- Examples of APW annotation are presented in Figure A.8.



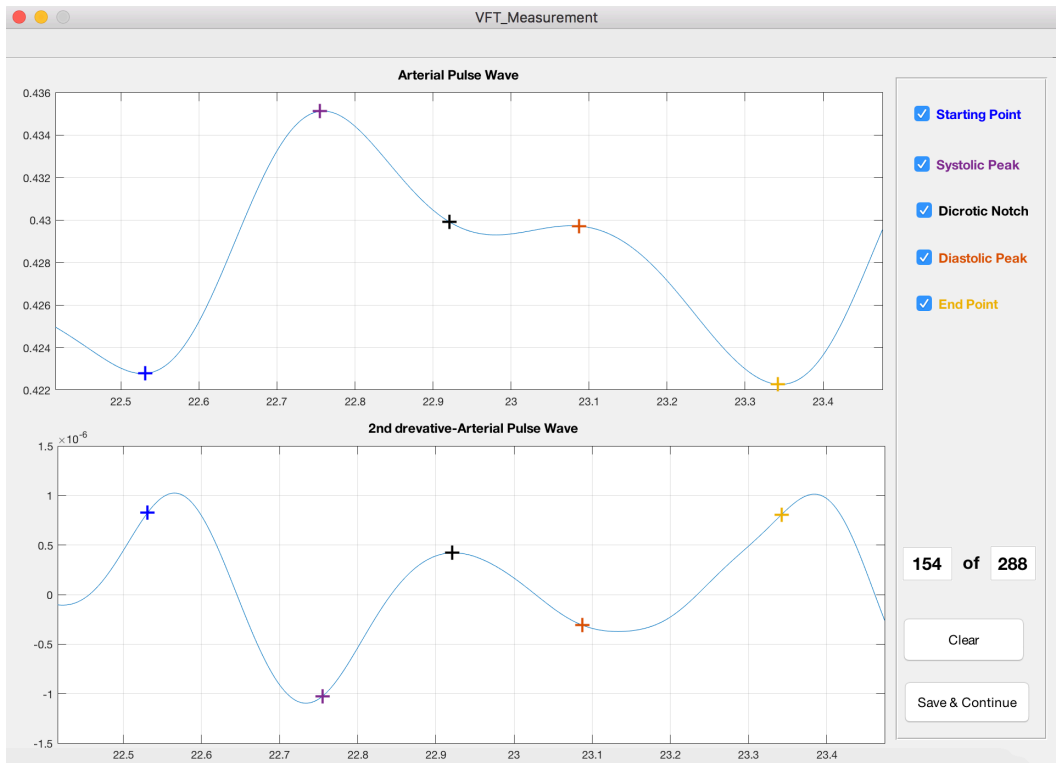
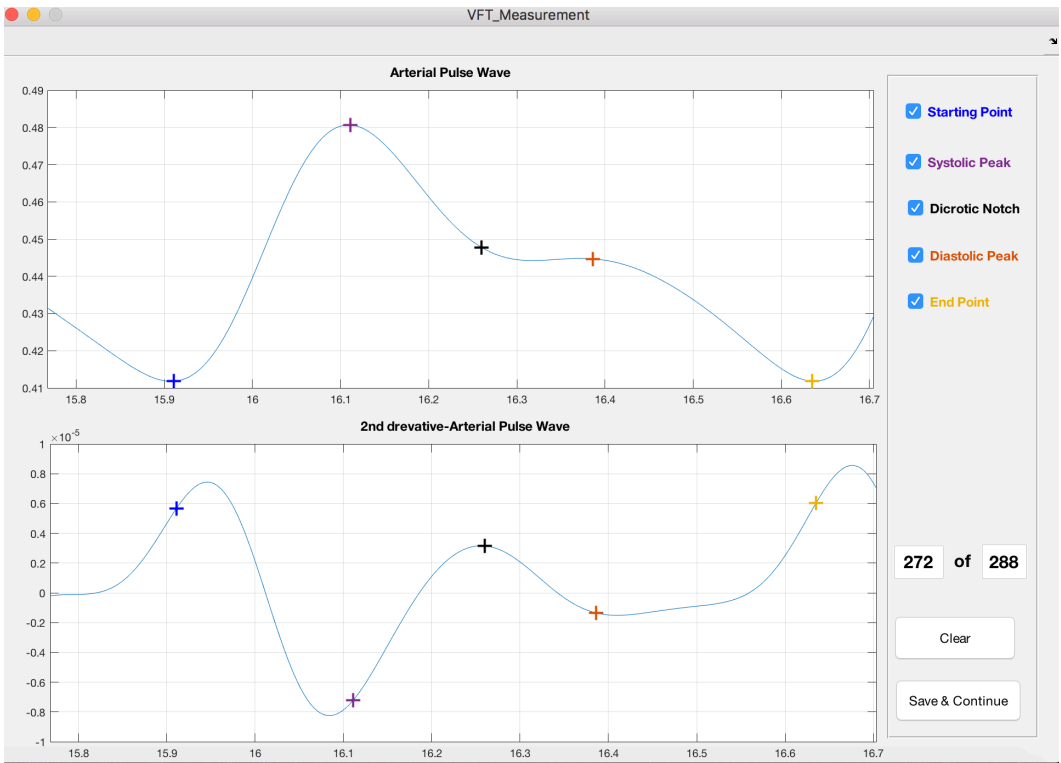


Figure A.9. Examples of APW annotation.

## A.3 Venous Filling Time Annotation Graphical User Interface

```
function varargout = VFT_Measurement(varargin)
% VFT_MEASUREMENT MATLAB code for VFT_Measurement.fig
%     VFT_MEASUREMENT, by itself, creates a new VFT_MEASUREMENT or raises
the existing
%     singleton*.
%
%     H = VFT_MEASUREMENT returns the handle to a new VFT_MEASUREMENT or
the handle to
%     the existing singleton*.
%
%     VFT_MEASUREMENT('CALLBACK', hObject,eventData,handles,...) calls the
local
%     function named CALLBACK in VFT_MEASUREMENT.M with the given input
arguments.
%
%     VFT_MEASUREMENT('Property','Value',...) creates a new
VFT_MEASUREMENT or raises the
%     existing singleton*. Starting from the left, property value pairs
are
%     applied to the GUI before VFT_Measurement_OpeningFcn gets called.
An
%     unrecognized property name or invalid value makes property
application
%     stop. All inputs are passed to VFT_Measurement_OpeningFcn via
varargin.
%
%     *See GUI Options on GUIDE's Tools menu. Choose "GUI allows only one
instance to run (singleton)".
%
% See also: GUIDE, GUIDATA, GUIHANDLES

% Edit the above text to modify the response to help VFT_Measurement

% Last Modified by GUIDE v2.5 03-Mar-2018 22:36:07

% Begin initialization code - DO NOT EDIT
gui_Singleton = 1;
gui_State = struct('gui_Name',       mfilename, ...
                  'gui_Singleton',   gui_Singleton, ...
                  'gui_OpeningFcn', @VFT_Measurement_OpeningFcn, ...
                  'gui_OutputFcn',  @VFT_Measurement_OutputFcn, ...
                  'gui_LayoutFcn',   [], ...
                  'gui_Callback',    []);
if nargin && ischar(varargin{1})
    gui_State.gui_Callback = str2func(varargin{1});
end

if nargout
    [varargout{1:nargout}] = gui_mainfcn(gui_State, varargin{:});
else
    gui_mainfcn(gui_State, varargin{:});
end
% End initialization code - DO NOT EDIT
```

```

% --- Executes just before VFT_Measurement is made visible.
function VFT_Measurement_OpeningFcn(hObject, eventdata, handles, varargin)
% This function has no output args, see OutputFcn.
% hObject    handle to figure
% eventdata  reserved - to be defined in a future version of MATLAB
% handles    structure with handles and user data (see GUIDATA)
% varargin   command line arguments to VFT_Measurement (see VARARGIN)
global Images index FileName PathName Hemo point;

% Choose default command line output for VFT_Measurement
handles.output = hObject;

% Update handles structure
guidata(hObject, handles);

% UIWAIT makes VFT_Measurement wait for user response (see UIRESUME)
% uiwait(handles.figure1);

%load('/Users/elhamshabanvanki/Desktop/untitled folder/LRR_VFT_DB.mat');
PathName=pwd;
FileName='LRR_VFT_DB';

load([PathName, '/', FileName], 'Hemo', 'Images', 'index', 'point');
set(handles.edit3, 'string', num2str(index));
set(handles.edit4, 'string', num2str(length(Images)+length(Hemo)));
plot_data(handles)
setpoint(handles)

% --- Outputs from this function are returned to the command line.
function varargout = VFT_Measurement_OutputFcn(hObject, eventdata, handles)
% varargout  cell array for returning output args (see VARARGOUT);
% hObject    handle to figure
% eventdata  reserved - to be defined in a future version of MATLAB
% handles    structure with handles and user data (see GUIDATA)

% Get default command line output from handles structure
varargout{1} = handles.output;

% --- Executes on button press in setpoint.
function setpoint(handles)
% handles    structure with handles and user data (see GUIDATA)

global point index Images

hold on
[point(index).X1,point(index).Y1]=ginput(1);

plot(point(index).X1,point(index).Y1, 'b+', 'LineWidth',2, 'MarkerSize',12)

[point(index).X2,point(index).Y2]=ginput(1);

plot(point(index).X2,point(index).Y2, 'b+', 'LineWidth',2, 'MarkerSize',12)

```

```

hold off

xpixel=[point(index).X1,point(index).X2];
if index<=length(Images)
xpixel_time=(xpixel/length(cell2mat(Images(index))))*90;
point(index).X1=xpixel_time(1);
point(index).X2=xpixel_time(2);
else
xpixel_time=xpixel;
end
point(index).VFT=xpixel_time(2)-xpixel_time(1);
set(handles.edit1,'string',num2str(point(index).VFT));

% --- Executes on button press in next.
function next_Callback(hObject, eventdata, handles)
% hObject    handle to next (see GCBO)
% eventdata  reserved - to be defined in a future version of MATLAB
% handles    structure with handles and user data (see GUIDATA)
global index Images point FileName PathName Hemo
set(handles.edit1,'string','');

if index<length(Images)+length(Hemo)
    index=index+1;
    plot_data(handles);

    set(handles.edit3,'string',num2str(index));
    setpoint(handles)
    save([PathName,'/',FileName],'point','index','-append');

end

% --- Executes on button press in clear.
function clear_Callback(hObject, eventdata, handles)
% hObject    handle to clear (see GCBO)
% eventdata  reserved - to be defined in a future version of MATLAB
% handles    structure with handles and user data (see GUIDATA)
plot_data(handles)
set(handles.edit1,'string','');
setpoint(handles)

% --- Executes during object creation, after setting all properties.
function edit1_CreateFcn(hObject, eventdata, handles)
% hObject    handle to edit1 (see GCBO)
% eventdata  reserved - to be defined in a future version of MATLAB
% handles    empty - handles not created until after all CreateFcns called

% Hint: edit controls usually have a white background on Windows.
%       See ISPC and COMPUTER.
if ispc && isequal(get(hObject,'BackgroundColor'),
get(0,'defaultUicontrolBackgroundColor'))
    set(hObject,'BackgroundColor','white');
end

```

```

% --- This function is called by other functions to plot LRR and HeMo
datad.
function plot_data(handles)

global index Images Hemo

axes(handles.axes1)
if index<=length(Images)

matlabImage = Images{index};
image(matlabImage)
axis off
axis image

else
    plot(Hemo(index-length(Images)).Time,Hemo(index-length(Images)).Data)
    grid on
end

% --- Executes during object creation, after setting all properties.
function edit3_CreateFcn(hObject, eventdata, handles)
% hObject    handle to edit3 (see GCBO)
% eventdata  reserved - to be defined in a future version of MATLAB
% handles    empty - handles not created until after all CreateFcns called

% Hint: edit controls usually have a white background on Windows.
%         See ISPC and COMPUTER.
if ispc && isequal(get(hObject,'BackgroundColor'),
get(0,'defaultUicontrolBackgroundColor'))
    set(hObject,'BackgroundColor','white');
end

% --- Executes during object creation, after setting all properties.
function edit4_CreateFcn(hObject, eventdata, handles)
% hObject    handle to edit4 (see GCBO)
% eventdata  reserved - to be defined in a future version of MATLAB
% handles    empty - handles not created until after all CreateFcns called

% Hint: edit controls usually have a white background on Windows.
%         See ISPC and COMPUTER.
if ispc && isequal(get(hObject,'BackgroundColor'),
get(0,'defaultUicontrolBackgroundColor'))
    set(hObject,'BackgroundColor','white');
end

```

## A.4 Arterial Pulse Wave Annotation Graphic User Interface

```
function varargout = APW_annotation(varargin)
% APW_annotation MATLAB code for APW_annotation.fig
%     APW_annotation, by itself, creates a new APW_annotation or raises
the existing
%     singleton*.
%
%     H = APW_annotation returns the handle to a new APW_annotation or the
handle to
%     the existing singleton*.
%
%     APW_annotation('CALLBACK', hObject,eventData,handles,...) calls the
local
%     function named CALLBACK in APW_annotation.M with the given input
arguments.
%
%     APW_annotation('Property','Value',...) creates a new APW_annotation
or raises the
%     existing singleton*. Starting from the left, property value pairs
are
%     applied to the GUI before APW_annotation_OpeningFcn gets called. An
%     unrecognized property name or invalid value makes property
application
%     stop. All inputs are passed to APW_annotation_OpeningFcn via
varargin.
%
%     *See GUI Options on GUIDE's Tools menu. Choose "GUI allows only one
%     instance to run (singleton)".
%
% See also: GUIDE, GUIDATA, GUIHANDLES

% Edit the above text to modify the response to help APW_annotation

% Last Modified by GUIDE v2.5 02-Jul-2018 10:25:16

% Begin initialization code - DO NOT EDIT
gui_Singleton = 1;
gui_State = struct('gui_Name',       mfilename, ...
                  'gui_Singleton',   gui_Singleton, ...
                  'gui_OpeningFcn', @APW_annotation_OpeningFcn, ...
                  'gui_OutputFcn',  @APW_annotation_OutputFcn, ...
                  'gui_LayoutFcn',  [], ...
                  'gui_Callback',    []);
if nargin && ischar(varargin{1})
    gui_State.gui_Callback = str2func(varargin{1});
end

if nargout
    [varargout{1:nargout}] = gui_mainfcn(gui_State, varargin{:});
else
    gui_mainfcn(gui_State, varargin{:});
end
% End initialization code - DO NOT EDIT
```

```

% --- Executes just before APW_annotation is made visible.
function APW_annotation_OpeningFcn(hObject, eventdata, handles, varargin)
% This function has no output args, see OutputFcn.
% hObject    handle to figure
% eventdata  reserved - to be defined in a future version of MATLAB
% handles     structure with handles and user data (see GUIDATA)
% varargin   command line arguments to APW_annotation (see VARARGIN)
global Hemo_list index FileName PathName PPG_list point counter CASE ;

% Choose default command line output for APW_annotation
handles.output = hObject;

% Update handles structure
guidata(hObject, handles);

PathName=pwd;
FileName='APW_DB';

load([PathName, '/', FileName]);
set(handles.edit3, 'string', num2str(counter));
set(handles.edit4, 'string', num2str((length(Hemo_list)+length(PPG_list))*3))
;
plot_data(handles)
setpoint(handles)

% --- Outputs from this function are returned to the command line.
function varargout = APW_annotation_OutputFcn(hObject, eventdata, handles)
% varargout  cell array for returning output args (see VARARGOUT);
% hObject    handle to figure
% eventdata  reserved - to be defined in a future version of MATLAB
% handles     structure with handles and user data (see GUIDATA)

% Get default command line output from handles structure
varargout{1} = handles.output;

% --- Executes on button press in setpoint.
function setpoint(handles)
% handles     structure with handles and user data (see GUIDATA)

global point index CASE TIME DATA DATA_2driv

% X1 Start point
[temp_x,~]=ginput(1);
[~,temp_index]=min(abs(TIME-temp_x));
point(index).X1(CASE)=TIME(temp_index);
point(index).Y1(CASE)=DATA(temp_index);
axes(handles.axes1)
hold on
plot(point(index).X1(CASE),point(index).Y1(CASE), 'b+', 'LineWidth',2, 'Marker
Size',12)
axes(handles.axes4)
hold on
plot(point(index).X1(CASE),DATA_2driv(temp_index), 'b+', 'LineWidth',2, 'Marke
rSize',12)

```

```

set(handles.checkbox1, 'value', 1)

%X2 Systolic Peak
[temp_x, ~]=ginput(1);
[~, temp_index]=min(abs(TIME-temp_x));
point(index).X2(CASE)=TIME(temp_index);
point(index).Y2(CASE)=DATA(temp_index);
axes(handles.axes1)
hold on
f=plot(point(index).X2(CASE), point(index).Y2(CASE), '+', 'LineWidth', 2, 'MarkerSize', 12)
f.Color=[0.49, 0.18, 0.56]
axes(handles.axes4)
hold on
f=plot(point(index).X2(CASE), DATA_2driv(temp_index), '+', 'LineWidth', 2, 'MarkerSize', 12)
f.Color=[0.49, 0.18, 0.56]
set(handles.checkbox2, 'value', 1)

%X3 Dicrotic Notch
[temp_x, ~]=ginput(1);
[~, temp_index]=min(abs(TIME-temp_x));
point(index).X3(CASE)=TIME(temp_index);
point(index).Y3(CASE)=DATA(temp_index);
axes(handles.axes1)
hold on
plot(point(index).X3(CASE), point(index).Y3(CASE), 'k+', 'LineWidth', 2, 'MarkerSize', 12)
axes(handles.axes4)
hold on
plot(point(index).X3(CASE), DATA_2driv(temp_index), 'k+', 'LineWidth', 2, 'MarkerSize', 12)
set(handles.checkbox3, 'value', 1)

%X4 Diastolic Peak
[temp_x, ~]=ginput(1);
[~, temp_index]=min(abs(TIME-temp_x));
point(index).X4(CASE)=TIME(temp_index);
point(index).Y4(CASE)=DATA(temp_index);
axes(handles.axes1)
hold on
f=plot(point(index).X4(CASE), point(index).Y4(CASE), 'b+', 'LineWidth', 2, 'MarkerSize', 12)
f.Color=[0.85, 0.33, 0.10]
axes(handles.axes4)
hold on
f=plot(point(index).X4(CASE), DATA_2driv(temp_index), 'b+', 'LineWidth', 2, 'MarkerSize', 12)
f.Color=[0.85, 0.33, 0.10]
set(handles.checkbox4, 'value', 1)

%X5 End point
[temp_x, ~]=ginput(1);
[~, temp_index]=min(abs(TIME-temp_x));
point(index).X5(CASE)=TIME(temp_index);
point(index).Y5(CASE)=DATA(temp_index);
axes(handles.axes1)
hold on

```

```

f=plot(point(index).X5(CASE),point(index).Y5(CASE),'b+','LineWidth',2,'MarkerSize',12)
f.Color=[0.93,0.69,0.13]
hold off
axes(handles.axes4)
hold on
f=plot(point(index).X5(CASE),DATA_2driv(temp_index),'b+','LineWidth',2,'MarkerSize',12)
f.Color=[0.93,0.69,0.13]
hold off
set(handles.checkbox5,'value',1)

% --- Executes on button press in next.
function next_Callback(hObject, eventdata, handles)
% hObject    handle to next (see GCBO)
% eventdata  reserved - to be defined in a future version of MATLAB
% handles    structure with handles and user data (see GUIDATA)
global index PPG_list point FileName PathName Hemo_list counter CASE

set(handles.checkbox1,'value',0)
set(handles.checkbox2,'value',0)
set(handles.checkbox3,'value',0)
set(handles.checkbox4,'value',0)
set(handles.checkbox5,'value',0)

if index<=(length(PPG_list)+length(Hemo_list))
    counter=counter+1;
    CASE=CASE+1;

if CASE>3
    CASE=1;
    index=index+1;
end
    save([PathName,'/',FileName],'point','index','counter','CASE','-append');

if counter<=(length(PPG_list)+length(Hemo_list))*3
    plot_data(handles);
    set(handles.edit3,'string',num2str(counter));
    setpoint(handles)
end
end

% --- Executes on button press in clear.
function clear_Callback(hObject, eventdata, handles)
% hObject    handle to clear (see GCBO)
% eventdata  reserved - to be defined in a future version of MATLAB
% handles    structure with handles and user data (see GUIDATA)
set(handles.checkbox1,'value',0)
set(handles.checkbox2,'value',0)
set(handles.checkbox3,'value',0)
set(handles.checkbox4,'value',0)
set(handles.checkbox5,'value',0)

plot_data(handles)

setpoint(handles)

```

```

% --- Executes during object creation, after setting all properties.
function edit1_CreateFcn(hObject, eventdata, handles)
% hObject    handle to edit1 (see GCBO)
% eventdata  reserved - to be defined in a future version of MATLAB
% handles    empty - handles not created until after all CreateFcns called

% Hint: edit controls usually have a white background on Windows.
%         See ISPC and COMPUTER.
if ispc && isequal(get(hObject,'BackgroundColor'),
get(0,'defaultUicontrolBackgroundColor'))
    set(hObject,'BackgroundColor','white');
end

% --- This function is called by other functions to plot PPG and HeMo data.

function plot_data(handles)

global index PPG_list Hemo_list CASE TIME DATA DATA_2driv
% if index>length(PPG_list)+length(Hemo_list)
%     return;
% end

if index<=length(PPG_list)

switch CASE
    case 1
        TIME=PPG_list(index).Time1;
        DATA=PPG_list(index).Data1;

    case 2
        TIME=PPG_list(index).Time2;
        DATA=PPG_list(index).Data2;

    case 3
        TIME=PPG_list(index).Time3;
        DATA=PPG_list(index).Data3;
end

axes(handles.axes4)
DATA_2driv=smooth(diff(diff(DATA)),0.20,'loess');
plot(TIME(1:end-2),DATA_2driv);
yl=ylim(handles.axes4);
axis(handles.axes4,'tight')
ylim(handles.axes4,yl);

grid on

else
switch CASE
    case 1
        TIME=Hemo_list(index-length(PPG_list)).Time1;
        DATA=Hemo_list(index-length(PPG_list)).Data1;
    case 2
        TIME=Hemo_list(index-length(PPG_list)).Time2;

```

```

        DATA=Hemo_list(index-length(PPG_list)).Data2;

    case 3
        TIME=Hemo_list(index-length(PPG_list)).Time3;
        DATA=Hemo_list(index-length(PPG_list)).Data3;

    end
    axes(handles.axes4)
    DATA_2driv=diff(diff(DATA));
    plot(TIME(1:end-2),DATA_2driv);
    yl=ylim(handles.axes4);
    axis(handles.axes4,'tight')
    ylim(handles.axes4,yl)
    grid on

end
axes(handles.axes1)
plot(TIME,DATA);
yl=ylim(handles.axes1);
axis(handles.axes1,'tight')
ylim(handles.axes1,yl)
grid on

% --- Executes during object creation, after setting all properties.
function edit3_CreateFcn(hObject, eventdata, handles)
% hObject    handle to edit3 (see GCBO)
% eventdata  reserved - to be defined in a future version of MATLAB
% handles    empty - handles not created until after all CreateFcns called

% Hint: edit controls usually have a white background on Windows.
% See ISPC and COMPUTER.
if ispc && isequal(get(hObject,'BackgroundColor'),
get(0,'defaultUicontrolBackgroundColor'))
    set(hObject,'BackgroundColor','white');
end

% --- Executes during object creation, after setting all properties.
function edit4_CreateFcn(hObject, eventdata, handles)
% hObject    handle to edit4 (see GCBO)
% eventdata  reserved - to be defined in a future version of MATLAB
% handles    empty - handles not created until after all CreateFcns called

% Hint: edit controls usually have a white background on Windows.
% See ISPC and COMPUTER.
if ispc && isequal(get(hObject,'BackgroundColor'),
get(0,'defaultUicontrolBackgroundColor'))
    set(hObject,'BackgroundColor','white');
end

```